

Elemental Analysis of Mosses and Lichens from the Western Cape (South Africa) using INAA and ICP-MS

by

Ntombizikhona Beaulah Ndlovu



*Dissertation presented for the degree of Doctorate of
Philosophy in Physics in the Faculty of Science at
Stellenbosch University*

Supervisors:

Prof. Richard T. Newman
Prof. Marina V. Frontasyeva
Dr. Peane P. Maleka

December 2016

Declaration

By submitting this dissertation electronically, I declare that the entirety of the work contained therein is my own, original work, that I am the sole author thereof (save to the extent explicitly otherwise stated), that reproduction and publication thereof by Stellenbosch University will not infringe any third party rights and that I have not previously in its entirety or in part submitted it for obtaining any qualification.

Copyright © 2016 Stellenbosch University
All rights reserved.

Abstract

Elemental Analysis of Mosses and Lichens from the Western Cape (South Africa) using INAA and ICP-MS

N.B. Ndlovu

*Department of Physics,
Stellenbosch University,
Private Bag X1, Matieland 7602,
South Africa.*

Dissertation: PhD

December 2016

Mosses and lichens, analyzed by nuclear and related techniques, have been extensively used as biomonitors in the European countries to provide information about air quality, but not in South Africa. The aim of this project was to infer air pollution levels in the Western Cape, South Africa by collecting and analysing mosses and lichens for chemical content using nuclear and related techniques. Since they lack a root system, which causes them to trap chemicals from air only through wet and dry deposition, mosses and lichens serve as good biomonitors of air pollution. These plants possess efficient accumulation capacity for many air pollutants (heavy metals and other trace elements). Three major causes of atmospheric pollution are industrialisation, urban growth and the wide-spread use of vehicles. Studying air pollution with plants, instead of the commercial air filters is a simple but effective method to estimate levels of air pollutants. Biomonitoring can be performed using naturally growing (indigenous) biomonitors collected in the area under investigation. This is known as passive biomonitoring. The steady global increase in the use of active biomonitoring, whereby biomonitors are collected from relatively pristine habitats and transplanted to different environments, is due to the scarcity or total absence of native biomonitors in certain environments e.g. large cities with heavy technogenic load and industrial regions as well as in arid areas. Hence active biomonitoring was also used in this study to assess ele-

mental content of atmospheric pollution due to urbanisation, industrialisation and vehicle use, in selected areas of the Western Cape, South Africa.

In this study, the collected samples were analysed by the multi-elemental non-destructive technique called instrumental neutron activation analysis (INAA) as well as the ion-coupled mass spectrometry (ICP-MS), thus facilitating an intercomparison of the results obtained by both techniques. From both passive and active biomonitoring techniques, the intercomparison of INAA and ICP-MS results showed major and essential elements (i.e. Na, Ca, Mg, K, Mn, Sr, Al, V, Ba, Zn) to have good linear correlations, $R \geq 80\%$. In order to facilitate the identification and characterization of different pollution sources from the collected sample element content, descriptive statistics were generated and correlation analyses were done using the StatisticaTM package. Our passive biomonitoring results showed the concentration levels for halogens (Cl, I, Br) to be elevated in areas closest to the ocean. The moss-sampling areas closest to the ocean, in relation to Stellenbosch, were False Bay and Betty's Bay. Signal Hill was the lichen-sampling area closest to the ocean, in relation to Stellenbosch, Coetzenburg Mountain and Franschoek. High concentrations of elements associated with vehicular emission (i.e. Pb, V, Zn, Cd, Cr, Cu, Ni, As, Ba, Sn) were observed for Stellenbosch samples that were collected adjacent to roads (Marais Road and Victoria Street). The active biomonitoring results showed Stellenbosch to have higher concentration levels of Al, V, Ba, Cr, Cu, Ti and Zn. These indicate emissions from soil and vehicles. The fingerprints for a combination of potential air pollution sources (oil rig facility, steel plant, heavy mineral plant, galvanising plant and the oil storage facility as well as sea-salt emissions) were identified in the Vredenburg results. The elements associated with these fingerprints are Fe, Al, Hg, As, Cd, Pb, Ba and Na. The Huguenot tunnel results revealed high concentrations of elements associated with the fingerprints for vehicle emissions. These are Zn, V, Ba, Cr, Pb, Ni, Cu, Al and Sb. In general, mosses showed the highest bioaccumulation capacity for metals and presented a more linear element accumulation trend than lichens. Due to their differences in metal uptake and retention, it is advisable to use mosses and lichens concurrently, since the respective results will be complementary.

Uittreksel

Elementele Ontleding van Mos en Ligene van die Wes-Kaap (Suid-Afrika) met behulp van INAA en IGMS

N.B. Ndlovu

*Fisika Departement,
University van Stellenbosch,
Privaatsak X1, Matieland 7602,
Suid Afrika.*

Proefskrif: PhD

Desember 2016

Die analise van die chemiese samestelling van mos en ligene deur middel van onder andere tegnieke in kernfisika kan gebruik word om lugkwaliteit te monitor. Hierdie gebruik van mos en ligene as biomonitors word wyd toegepas in Europa, maar is tot op hede nog nie wyd in Suid-Afrika in gebruik nie. Hierdie studie het ten doel om biomonitoring te gebruik om die vlakke van lugbesoedeling in die Wes-Kaap, Suid Afrika, te bepaal. Die gebrek aan 'n wortelstelsel verseker dat mos en ligene as ideale lugbesoedeling biomonitors optree aangesien slegs chemikalieë uit die atmosfeer versamel kan word. Swaar metale en spoor elemente in die atmosfeer word effektief versamel deur nat en droë neerslag prosesse. Drie belangrike oorsake van lugbesoedeling sluit in industrialisasie, verstedeliking en wydverspreide voertuig gebruik. Die gebruik van biologiese materiaal in plaas van kommersiële lug filters word beskou as 'n eenvoudige en koste effektiewe metode om die vlakke van lugbesoedeling te bepaal. Passiewe biomonitoring verwys na die gebruik van mos en ligene wat natuurlik voorkom in die omgewing wat bestudeer word. In teenstelling hiermee behels aktiewe biomonitoring die verplasing van biomateriaal vanaf ongerepte habitat na die omgewing wat bestudeer word. Aktiewe biomonitoring is aan die toeneem wêreldwyd as gevolg van die afwesigheid van mos en ligene in streke wat gebuk gaan onder menslike impak, omgewings met swaar industriële asook droë gebiede. Daar is in hierdie studie van beide aktiewe en passiewe biomonitoring gebruik gemaak om vas te stel watter elemente deel

uitmaak van atmosferiese besoedeling in die Wes-Kaap, Suid Afrika, spesifiek as gevolg van verstedeliking, industrialisering en voertuig gebruik.

Verskeie monsters is versamel en die resultate van twee verskillende analitiese metodes, naamlik die nie-vernietigende instrumentele neutron aktivering (INA) en ioon- gekoppelde massa spektrometrie (IGMS), is gebruik om die verskillende biomonitoring resultate te vergelyk. Beide analitiese metodes toon 'n sterk lineêre korrelasie ($R \geq 80\%$) tussen die teenwoordigheid van die algemene elemente (Na, Ca, Mg, K, Mn, Sr, Al, V, Ba, Zn) in aktiewe en passiewe biomonitoring monsters. Beskrywende statistiese en korrelasie data is met behulp van die StatisticaTM pakket gegeneer ten einde verskillende besoedelingsbronne te kan identifiseer en karakteriseer. In kusgebiede, soos Valsbaai en Bettiesbaai is bevind dat passiewe biomonitoring met behulp van mos monsters 'n verhoogde konsentrasie van halogene (Cl, I, Br) aandui. Dit is in teenstelling met gebiede soos Stellenbosch (Victoria straat) en Coetzenburg (berg). Soortgelyke resultate is verkry deur ligee monsters te analiseer wat versamel is op Seinheuwel (kusgebied), in teenstelling met binnelandse monsters versamel by Franshoek en Stellenbosch. Hoë konsentrasies van elemente wat gepaard gaan met voertuig uitlaatgasse (soos bv. Pb, V, Zn, Cd, Cr, Cu, Ni, As, Ba, Sn) is waargeneem in passiewe monitoring monsters afkomstig van gebiede langs paaie in Stellenbosch (Victoria en Marais Strate). Die resultate verkry deur aktiewe biomonitoring toon daarteenoor hoër vlakke van Al, V, Ba, Cr, Cu, Ti en Zn. Beide resultate dui op 'n mengsel van voertuig uitlaatgasse en gesuspendeerde grond partikels. Die karakter eienskappe van industriële lugbesoedeling afkomstig van bronne soos olietorings, staal industrië, galvaniserings-en oliebergingsfasiliteite, vermeng met elemente geassosieer met die nabyheid van die see, is waargeneem in die Vredenburg resultate. Dit sluit elemente in soos Fe, Al, Hg, As, Cd, Pb, Ba en Na. Daarteenoor is die elemente waargeneem in die resultate van die Hugenote tunnel, naamlik Zn, V, Ba, Cr, Pb, Ni, Cu, Al en Sb, tipies geassosieer met voertuig uitlaatgasse. Dit blyk uit hierdie studie dat mos 'n beter vermoë het om as bio- akkumulator op te tree as ligee aangesien die opname van elemente teen 'n meer konstante tempo geskied. Ten spyte hiervan is dit steeds belangrik om van beide mos en ligee gebruik te maak aangesien die opname en behoud van metale verskillend is, en die resultate dus as aanvullend beskou kan word.

Acknowledgements

This thesis is the result of experiences I encountered with amazing individuals whom I wish to acknowledge. Firstly, I am greatly indebted to my supervisors;

Prof. Richard T. Newman for guidance and advice he has provided throughout my time as his student. I have been lucky to have a supervisor who cared about my work, my well-being as well as my success.

Prof. Marina V. Frontasyeva for being supportive to me, not only academically but also emotionally, by giving me the moral support I needed in order to move on through the rough path that led me into finishing this thesis. I also thank her for introducing me to Eiliv Steinnes and William Purvis, whose comments on aspects of my work were very helpful.

Dr. Peane P. Maleka for constant support, encouragement, patience, constructive criticism and for being an inspiration on how to always keep a positive attitude in all life situations.

I would like to thank the Department of Physics at Stellenbosch University for financial support and to all its staff members, who have been helpful in many significant ways, especially Christine Ruperti for the emotional support. I am thankful to Ryno Botha, Siyabulela Tshingana and Amany Kamblawe for helping me with collection and cleaning of samples for this study. I am also thankful to David Pool, Eben Shields and Stanley February for helping me with the designing, building and installing of the stands for deploying samples for this study.

I am grateful to Wilfrid Ndebeka for helping me with Latex lessons in preparation for writing up this thesis and to Dr. Retief Neveling for translating my English abstract to Afrikaans.

I am thankful to the people I met at the Frank Laboratory of Neutron Physics (FLNP), Joint Institute of Nuclear Research (JINR), Dubna, Russia. I thank everyone in the department of neutron activation analysis for extending helping hands whenever needed. I am grateful to have built lifetime friendships with Inga Zinicovscaia, Gery Hristozova, Sasha Kzavtsova and Zoya Goryainova.

I would like to thank the Western Cape Nature Conservation Board for the permission to collect samples for this study (permit No. AAA008-00104-0028). I am grateful to the South African National Roads Agency Ltd (SANRAL) and

Murray & Roberts Construction (Pty) Ltd for permission to deploy samples in Huguenot tunnel. I am thankful to Jacques Bezuidenhout for introducing me to Hennie Smit. I am also thankful to Hennie Smit for allowing me to deploy some my sample for this study in his home.

I am also thankful to iThemba LABS and the National Research Foundation (NRF) for providing me with funding to undertake this research, while giving me multiple opportunities to attend academic conferences nationally and abroad.

Lastly, a special feeling of gratitude goes to the following people to whom I am also thankful; my mentors, Dr. Noel Mkaza and Dr. Rudolph for being good examples of excellence as mentors, managers and role models.

My mother, Buyiswa Ndlovu, and my sisters, Andiswa Ndlovu and Ntombizandile Ndlovu whose love and emotional support have never left my side throughout my life. Their words of encouragement, motivation and inspiration have kept me pushing through the sleepless night of my life as a PhD student.

My son, Lisoletu Ndlovu for the continuous love and understanding whenever I had to abandon him while busy with my studies.

My friends, Akhona Mbande, Liza Coni, Anelisa Dumse, Bomikazi Somadlangathi, Zodwa Magidigidi, Ziyanda Magwentshu and Viwe Ngunge for the desirable form of escape from my studies whenever needed. Thank you for constantly reminding me that through prayer, patience and persistence, success is guaranteed.

My iThemba LABS family (everyone from the Department of Nuclear Physics), especially; Ntombi Kheswa, Tshepo Dinoko, Thobeka Lamula, Avuyile Bulala and Hombakazi Wanana for the continuous emotional support. Thank you for always encouraging me to not give up on my studies even when I felt like I could not do it anymore.

My love, Goodman Ndabeni. Thank you for being such an amazing partner and father; caring, thoughtful, joyful and full of love. I appreciate every little effort of support you gave me during my PhD studies.

Dedications

I dedicate this work to my late father, Mziwomntu Ndlovu whose words of encouragement and push for persistence still remain in my head. You might not be around in your physical form but I know your spirit is always around, watching and rejoicing with me in my success. I still feel like you left too soon.

Contents

Declaration	i
Abstract	ii
Uittreksel	iv
Acknowledgements	vi
Dedications	viii
Contents	ix
List of Figures	xi
List of Tables	xvii
1 Introduction	1
1.1 Overview of the Study	1
1.2 Motivation for this study	6
1.3 Aims and Objectives of this study	13
1.4 Outline of this thesis	13
2 Review of Relevant Literature	15
2.1 Neutron Physics Theory	15
2.2 Interaction of Gamma-rays with Matter	23
2.3 Biomonitoring of Air Pollution	28
2.4 Biomonitoring of Air Pollution	31
2.5 Analytical Techniques Used in Air Pollution Biomonitoring	36
2.6 Advantages and Disadvantages of INAA and ICP-MS	45
2.7 Uncertainties Associated with Biomonitoring of Air Pollution	48
3 Experimental Methods	50
3.1 Sampling	50
3.2 Sample Preparation for Analysis	61
3.3 INAA Experimental Setup	64

<i>CONTENTS</i>	x
4 Data Analysis	73
4.1 Gamma-ray Spectrometry related	73
4.2 Calculating Elemental Concentrations	94
5 Results and Discussion	98
5.1 Biomonitoring Results: Passive	98
5.2 Active Biomonitoring Results	120
5.3 General discussion of results	137
6 Conclusion and Recommendations for Further Work	144
Appendices	147
A Sample data	148
A.1 Sampling, sample preparation, irradiation and counting data . .	148
B Standard reference material (SRM) elemental concentrations: certified and measured (analysis of passive biomonitors)	160
C Descriptive statistics: passive biomonitoring	162
C.1 Moss Data	162
C.2 Lichen Data	169
D Standard reference material (SRM) elemental concentrations: certified and measured (analysis of active biomonitors)	175
E Elemental concentrations in Montagu (pristine) samples	177
F Descriptive statistics: active biomonitoring	180
F.1 Moss Data	180
F.2 Lichen Data	187
G Sample elemental concentrations (measured by INAA and ICP-MS)	194
G.1 Passive biomonitoring	194
G.2 Active biomonitoring	199
List of References	208

List of Figures

1.1	Diagram showing neutron capture by the stable (target) nucleus followed by emission of γ -ray by the unstable (radioactive) nucleus. PGNAA means for prompt gamma neutron activation analysis and DGNAA means delayed gamma neutron activation analysis.	2
1.2	Schematic representation of processes in ICP-MS from sample introduction to mass analysis.	4
1.3	Periodic table of elements.	8
1.4	Types of air pollution sources.	12
1.5	Equipment for monitoring air quality in the Western Cape.	12
2.1	Typical neutron flux spectrum in a nuclear reactor.	17
2.2	Relationship between total neutron cross section and neutron energy.	19
2.3	Possible significant nuclear reactions for Al after neutron capture.	19
2.4	Cross-section plots for the ^{27}Al neutron capture reactions.	20
2.5	Major processes involved when gamma radiation interacts with matter.	23
2.6	Schematic diagram of a NaI(Tl) scintillation detector and photomultiplier assembly.	26
2.7	Schematic cross-sectional view of a Ge detector.	26
2.8	Comparative pulse height spectra recorded using NaI(Tl) and Ge detectors.	28
2.9	Relationship between passive and active biomonitoring.	29
2.10	Microscopic image of <i>Leptodon smithii</i>	34
2.11	Microscopic image of <i>Pterogonium gracile</i>	34
2.12	Typical lichen thallus cross section.	35
2.13	<i>Usnea subfloridana</i> and <i>Parmotrema perlatum</i> on a tree.	36
2.14	Common demarcations in quantitative analysis.	38
2.15	Elements comparatively determined by INAA (\square) and ICP-MS (\circ) when using mosses.	40
2.16	Typical PGNAA setup.	41
2.17	DGNAA activity/time graph; showing irradiation time (t_{irr}), decay time (t_d) and counting (measurement) time (t_c).	41
2.18	An ICP-MS spectrum showing relative abundances of elemental constituents.	44

2.19	Reaction cross-section plots showing the under-estimated interferences of nuclear reactions during NAA measurements.	47
3.1	Western Cape location in South Africa.	51
3.2	Passive biomonitoring sampling sites around the Western Cape province.	52
3.3	Passive biomonitoring sampling sites in Stellenbosch.	52
3.4	Illustration of the sampling grid at Jan-Marais Nature Reserve. . .	53
3.5	Stellenbosch sampling image.	54
3.6	Coetzenburg sampling image.	54
3.7	Signal Hill sampling image.	54
3.8	Franschhoek sampling image.	54
3.9	Betty's Bay sampling image.	54
3.10	False Bay sampling image.	54
3.11	Active biomonitoring sampling site and the monitored areas.	55
3.12	Weighing mosses before packing.	56
3.13	Mesh bags for packing samples.	56
3.14	Packed lichen- and moss- bags.	56
3.15	Exposed samples at Stellenbosch.	58
3.16	Exposed samples inside Huguenot Tunnel.	58
3.17	Vredenburg sample deployment.	58
3.18	Stellenbosch University area showing the location where the active biomonitoring samples were deployed.	59
3.19	Part of the Western Cape map showing the Huguenot tunnel.	60
3.20	Potential air pollution sources around Vredenburg.	61
3.21	ICP-MS sample preparation process.	62
3.22	INAA Sample preparation process	63
3.23	INAA stages. SRM refers to standard reference material.	64
3.24	Schematic layout of the IBR-2 reactor.	65
3.25	Schematic layout of the IBR-2 pulsed fast reactor, showing the spectrometer complex, and radioanalytical complex REGATA.	66
3.26	Experimental facility-REGATA at IBR-2 reactor.	67
3.27	Picture of a "hot-cell".	67
3.28	REGATA neutron energy spectra and irradiation channels.	68
3.29	Schematic drawing of a Polyethylene transportation capsule.	69
3.30	Pictures of both aluminium and Polyethylene capsules.	69
3.31	Canberra HPGe detector set-up at REGATA.	71
3.32	Diagram of gamma-ray spectrometer system at the radioanalytical complex REGATA at IBR-2 reactor of the JINR in Dubna, Russia.	72
3.33	Typical detector shield image.	72
4.1	Graphical representation of reaction cross-sections for $^{27}\text{Al}(n,\gamma)^{28}\text{Al}$, $^{28}\text{Si}(n,p)^{28}\text{Al}$ and $^{29}\text{Si}(n,p)^{29}\text{Al}$	76
4.2	Diagram ^{239}U daughter nuclide formation reaction.	76

4.3	Diagram showing ^{232}Th daughter nuclide formation reaction.	77
4.4	Graphical representation of reaction cross-sections for $^{232}\text{Th}(n,\gamma)^{233}\text{Th} \rightarrow (\beta^-)^{233}\text{Pa}$ and $^{238}\text{U}(n,\gamma)^{239}\text{U}(\beta^-)^{239}\text{Np}$	77
4.5	The spectrum measured for a point source containing ^{152}Eu and ^{133}Ba (used for energy and efficiency calibration in this study).	78
4.6	The energy calibration curve generated with the Genie 2000 software in this study using the ^{152}Eu - ^{133}Ba point source (sample ID: 6000599).	79
4.7	Efficiency calibration curve of HPGe Canberra coaxial detector number 6 (D6) using ^{152}Eu - ^{133}Ba point source.	79
4.8	The list of steps and the data required for evaluating gamma-ray spectra, calculating activities and elemental content.	81
4.9	Genie-2000 window for fitting the peaks interactively.	82
4.10	Short-lived isotopes spectrum \rightarrow (0 - 1000) MeV energy region.	85
4.11	Short-lived isotopes spectrum \rightarrow (1000 - 2000) MeV energy region.	86
4.12	Short-lived isotopes spectrum \rightarrow (2000 - 3000) MeV energy region.	87
4.13	Long-lived 1 isotopes spectrum \rightarrow (0 - 1000) MeV energy region.	88
4.14	Long-lived 1 isotopes spectrum \rightarrow (1000 - 2000) MeV energy region.	89
4.15	Long-lived 1 isotopes spectrum \rightarrow (2000 - 3000) MeV energy region.	90
4.16	Long-lived 2 isotopes spectrum \rightarrow (0 - 1000) MeV energy region.	91
4.17	Long-lived 2 isotopes spectrum \rightarrow (1000 - 2000) MeV energy region.	92
4.18	Long-lived 2 isotopes spectrum \rightarrow (1800 - 3000) MeV energy region.	93
4.19	Concentration program flowchart.	95
5.1	Linear correlation coefficients graph for elements determined by INAA and ICP-MS for both mosses and lichens (passive biomonitoring).	100
5.2	Na correlations.	101
5.3	K correlations.	101
5.4	Ca correlations.	101
5.5	Mn correlations.	101
5.6	Zn correlations.	101
5.7	Sr correlations.	101
5.8	Al correlations.	102
5.9	Mg correlations.	102
5.10	V correlations.	102
5.11	Cr correlations.	102
5.12	Fe correlations.	102
5.13	Co correlations.	102
5.14	As correlations.	103
5.15	Se correlations.	103
5.16	Ba correlations.	103
5.17	Major elements for Stellenbosch (INAA).	106
5.18	Major elements for Coetzenburg mountain (INAA).	106

5.19	Essential elements for Stellenbosch (INAA)).	106
5.20	Essential elements for Coetzenburg mountain (INAA).	107
5.21	Rare earth elements for Stellenbosch (INAA).	107
5.22	Rare earth elements for Coetzenburg mountain (INAA).	107
5.23	Potentially toxic elements for Stellenbosch (INAA).	108
5.24	Potentially toxic elements for Coetzenburg mountain (INAA).	108
5.25	Stellenbosch town halogen concentrations in mosses vs. lichens . . .	109
5.26	Coetzenburg mountain halogen concentrations in mosses vs. lichens	109
5.27	Major elements in mosses (INAA).	110
5.28	Major elements in mosses (ICP-MS).	110
5.29	Essential elements in mosses (INAA).	110
5.30	Essential elements in mosses (ICP-MS).	111
5.31	Potentially toxic elements in mosses (INAA).	111
5.32	Potentially toxic elements in mosses (ICP-MS).	111
5.33	Rare earth elements in mosses (INAA).	112
5.34	Toxic elements in mosses (ICP-MS).	112
5.35	Major elements in lichens (INAA).	113
5.36	Major elements in lichens (ICP-MS).	113
5.37	Essential elements in lichens (INAA).	113
5.38	Essential elements in lichens (ICP-MS).	114
5.39	Potentially toxic elements in lichens (INAA).	114
5.40	Potentially toxic elements in lichens (ICP-MS).	114
5.41	Rare earth elements in lichens (INAA).	115
5.42	Toxic elements in lichens (ICP-MS).	115
5.43	Concentrations of Pb, Cd, Cu and Ni plotted against the distance from Marais Road (lichen samples)	116
5.44	Concentrations of Sn, V, Zn, As, Ba and Cr plotted against the distance from Marais Road (lichen samples)	117
5.45	Google earth map showing locations of collected moss samples. . . .	118
5.46	Google earth map showing locations of collected lichen samples. . .	119
5.47	Halogens concentrations in mosses (INAA data).	119
5.48	Halogens concentrations in lichens (INAA data).	119
5.49	Elements identified from active biomonitoring	120
5.50	Linear correlation coefficients graph for elements determined by INAA and ICP-MS from both mosses and lichens (active biomoni- toring results)	121
5.51	Na correlations.	121
5.52	Mg correlations.	121
5.53	Al correlations.	121
5.54	V correlations.	121
5.55	Mn correlations.	122
5.56	Sr correlations.	122
5.57	Ba correlations.	122
5.58	K correlations.	122

5.59	Ca correlations.	122
5.60	Cr correlations.	122
5.61	Fe correlations.	123
5.62	Co correlations.	123
5.63	Fe correlations.	123
5.64	Co correlations.	123
5.65	Zn correlations.	123
5.66	As correlations.	123
5.67	Se correlations.	124
5.68	Ti correlations.	124
5.69	Mo correlations.	124
5.70	Sb correlations.	124
5.71	Accumulation of elements in <i>Usnea subfloridana</i> after 12 days of exposure.	128
5.72	Accumulation of elements in <i>P. perlatum</i> after 12 days of exposure.	128
5.73	Accumulation of elements in a mixture of two moss species (<i>L. smithii</i> and <i>P. gracile</i>) over different exposure times.	128
5.74	B concentrations in <i>L. smithii</i> , <i>P. gracile</i> and <i>U. subflorida</i> ; respectively	129
5.75	Ca concentrations in <i>L. smithii</i> , <i>P. gracile</i> and <i>U. subflorida</i> ; respectively	130
5.76	Mg concentrations in <i>L. smithii</i> , <i>P. gracile</i> and <i>U. subflorida</i> ; respectively	131
5.77	Na concentrations in <i>L. smithii</i> , <i>P. gracile</i> and <i>U. subflorida</i> ; respectively	132
5.78	Pb concentrations in <i>L. smithii</i> , <i>P. gracile</i> and <i>U. subflorida</i> ; respectively	133
5.79	Zn concentrations in <i>L. smithii</i> , <i>P. gracile</i> and <i>U. subflorida</i> ; respectively	134
5.80	Sb concentrations in the samples from Stellenbosch, Vredenburg and Huguenot tunnel; respectively	135
5.81	Comparison of the Stellenbosch University campus ICP-MS results with the Limpopo University campus results.	138
5.82	Comparison of the ICP-MS results from an industrial area in Pretoria with the results from Vredenburg.	138
5.83	Comparison of the ICP-MS results from a high traffic center in Pretoria with the results from Huguenot tunnel.	138
5.84	Concentrations of elements from moss samples exposed in tunnels (Stellenbosch (ICP-MS data) and Vienna (ICP-AES) data).	139
5.85	Concentrations of elements from moss samples collected along the roads (Stellenbosch data vs. Vienna data) for 1 month exposure.	140
5.86	Comparing median concentrations of Al, As, Cd, Cr, Cu, Fe, Hg, Ni in moss from the Western Cape, South Africa with corresponding European data.	140

5.87 Comparing median concentrations of Pb, Sb in moss from the Western Cape, South Africa with corresponding European data	141
G.1 Concentrations of Na, Mg, Al, K.	195
G.2 Concentrations of Ca, V, Cr, Mn.	196
G.3 Concentrations of Fe, Co, Zn, As.	197
G.4 Concentrations of Se, Sr, Ba.	198
G.5 Concentrations of Al and Ca.	199
G.6 Concentrations of Fe and K.	200
G.7 Concentrations of Mg and Na.	201
G.8 Concentrations of Ti and V.	202
G.9 Concentrations of Cr and Mn.	203
G.10 Concentrations of Co and Zn.	204
G.11 Concentrations of As and Se.	205
G.12 Concentrations of Sr and Mo.	206
G.13 Concentrations of Sb and Ba.	207

List of Tables

1.1	South African National Standards (SANS) for the classic pollutants in the ambient air, measured at standard temperature (25°C) and pressure (101.3 kPa).	10
2.1	Typical classification of neutrons.	16
2.2	Advantages and disadvantages of active biomonitoring.	31
2.3	Applicability of analytical techniques in biomonitoring heavy-metal air pollution.	37
2.4	INAA and ICP-MS comparison for the determination of elements.	38
2.5	List of approximate sensitivities for determination of elements, assuming interference-free spectra and irradiation in a reactor neutron flux of $1 \times 10^{13} n.cm^{-2}.s^{-1}$	46
3.1	A summary of sampling locations for passive biomonitoring performed in 2012.	53
3.2	Summary of prepared sample bags for active biomonitoring.	57
3.3	Details of the stations and exposure time for active biomonitoring.	57
3.4	Neutron flux in REGATA irradiation channels.	68
3.5	Typical REGATA sample irradiation conditions.	70
3.6	REGATA gamma-spectrometers.	71
4.1	List of elements determined by INAA	73
4.2	Additional list of elements determined by INAA.	75
4.3	List of NIST/NBS SRMs used for elemental concentration calculations in this study.	95
5.1	Comparison of sample k02 for concentrations calculated manually with the results from the automated concentration program for the INAA measurements and the ICP-MS results.	99
5.2	Comparison of sample k23 for concentrations calculated manually with the results from the automated concentration program for the INAA measurements.	99
5.3	Classification of elements determined in this study	104
5.4	Group patterns for elemental concentration (passive biomonitoring results).	105

5.5	Deployment and collection dates for lichen and moss bags	126
5.6	Matrix of Varimax normalised factor loadings for n=64, 37 elements and factor loadings 55	142
A.1	Passive biomonitoring sample preparation data.	148
A.2	Passive biomonitoring sample irradiation data (duration given in seconds).	150
A.3	Passive biomonitoring counting data for short-lived isotopes (dura- tion given in seconds).	151
A.4	Passive biomonitoring counting data for the 1 st long-lived isotopes (duration given in seconds).	152
A.5	Passive biomonitoring counting data for the 2 nd long-lived isotopes (duration given in seconds).	153
A.6	Active biomonitoring sample preparation data.	154
A.7	Active biomonitoring sample irradiation data for short-lived iso- topes (duration given in seconds).	155
A.8	Active biomonitoring sample irradiation data for the 1 st and 2 nd long-lived isotopes (duration given in seconds).	156
A.9	Active biomonitoring counting data for short-lived isotopes (dura- tion given in seconds).	157
A.10	Active biomonitoring counting data for the 1 st long-lived isotopes (duration given in seconds).	158
A.11	Active biomonitoring counting data for the 2 nd long-lived isotopes (duration given in seconds).	159
B.1	Comparison of the SRM measured values with values listed in the certificates (short-lived isotopes).	160
B.2	Comparison of the SRM measured values with values listed in the certificates (long-lived 1 isotopes).	161
B.3	Comparison of the SRM measured values with values listed in the certificates (long-lived 2 isotopes).	161
C.1	Descriptive statistical analysis for passive biomonitoring moss data.	162
C.2	Descriptive statistical analysis for passive biomonitoring lichen data.	169
D.1	Comparison of the SRM measured values with values listed in the certificates (short-lived isotopes).	175
D.2	Comparison of the SRM measured values with values listed in the certificates (long-lived 1 isotopes).	176
D.3	Comparison of the SRM measured values with values listed in the certificates (long-lived 2 isotopes).	176
E.1	Concentrations (in $\mu\text{g/g}$) of elements in biomonitors (1 sample per species) collected from Montagu (INAA data)	177

*LIST OF TABLES***xix**

E.2	Concentrations (in $\mu\text{g/g}$) of elements in biomonitors (1 sample per species) collected from Montagu (ICP-MS data)	178
F.1	Descriptive statistical analysis for active biomonitoring moss data. .	180
F.2	Descriptive statistical analysis for active biomonitoring lichen data.	187

Chapter 1

Introduction

An effective approach to monitoring air pollution includes assessing toxic trace elements content in air [1, 2]. Nowadays, nuclear physics is widely used in a variety of applications including monitoring of the environmental quality through the analysis of trace element content in environmental samples [3]. This includes the elemental analysis of biological samples in order to identify and quantify toxic trace elements in air. Like any other technique, nuclear physics techniques also have limitations. During practical applications of these techniques, other classical analytical techniques are used to overcome specific limitations inherent to nuclear techniques.

1.1 Overview of the Study

The monitoring of environmental quality through the analysis of trace element content of environmental samples can be done using neutron-induced reactions by investigating reaction products and measuring their activities [3]. Neutron activation analysis (NAA) is a nuclear physics technique that offers the most effective way of identifying as well as quantifying toxic trace elements in air by studying nuclear reactions that occur between neutrons and target nuclei (neutron-induced reactions) [4, 5]. In NAA, elements are determined via nuclear reactions through a conversion of stable nuclei of atoms in a sample into radioactive nuclei by bombarding samples with neutrons, followed by measurements of characteristic radiation (i.e. γ -rays) that the radioactive nuclei emit [4]. In this study, primary measurements were performed using NAA and secondary measurements were performed using inductively coupled plasma-mass spectrometry (ICP-MS).

1.1.1 Neutron Activation Analysis: an overview

In 1936, George de Hevesy and Hilde Levi (the two NAA pioneers) discovered NAA when they noticed that samples containing certain rare earth elements

became highly radioactive when exposed to a source of neutrons [6, 7]. Nowadays, neutrons used to perform NAA investigations could be from a neutron source in a reactor, or a particle accelerator, or a fast neutron generator. These nuclear reactions are caused by bombarding the target nucleus with neutrons of kinetic energies [thermal (slow), epithermal and fast], resulting in a compound nucleus. The compound nucleus then de-excites by instantaneously emitting characteristic prompt γ -rays (high-energy photons). This leads to the formation of a more stable configuration, which is generally a radioactive nucleus with a certain half-life ($t_{1/2}$), and this radioactive nucleus continues to decay into a more stable product nucleus by emitting a characteristic delayed gamma ray (γ -ray) or a cascade of delayed γ -rays as illustrated in Figure 1.1 [5, 8–12].

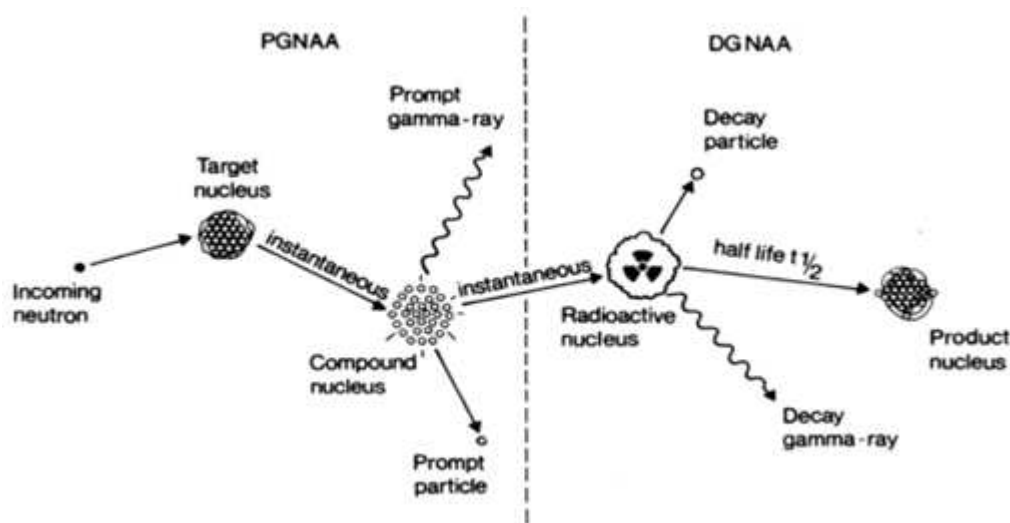


Figure 1.1: Diagram showing neutron capture by the stable (target) nucleus followed by emission of γ -ray by the unstable (radioactive) nucleus. PGNA means for prompt gamma neutron activation analysis and DGNA means delayed gamma neutron activation analysis [13].

Three necessities required to perform NAA include; a source of neutrons, a sample to be analysed and a suitable γ -ray detector, e.g. HPGe (high-purity germanium) detector. The procedure followed in INAA (Instrumental Neutron Activation Analysis) mainly comprises the following steps [4, 10]:

- (i) sample preparation for irradiation,
- (ii) selection of optimum nuclear reaction (by choosing relevant neutron flux),
- (iii) sample activation or irradiation with neutrons,
- (iv) γ -radiation measurements after one or more decay times, and
- (v) counting of the irradiated sample and interpretation of the resulting γ -ray spectra in terms of elements and concentrations.

1.1.1.1 Applications of NAA

Applications of NAA are so widespread that the estimated number of samples undergoing NAA is approximately 100,000 samples each year [12]. Amongst possible applications of NAA, including the environmental monitoring application used in this study, NAA is routinely utilised in the following fields [8, 12];

(i) **Nuclear Industry** → NAA was used in a project to develop radiotracers that are used to determine the fates of hazardous elements during gasification in support of the use of gasification as a way of decomposing, stabilizing and reducing the volume of hazardous mixed wastes including radioactive wastes resulting from the nuclear weapons program. As a result of this project, radiotracers were developed and are used to monitor the fates of arsenic, strontium, cadmium, cesium, mercury, uranium, thorium, neptunium and protactinium, chlorine (as an organochloride) and phosphorus (as organophosphorus surrogates for military wastes).

(ii) **Archaeology** → NAA is used to characterize archaeological specimens (e.g. pottery, obsidian, ceramic utensils, teeth, bones) and in identifying the chemical elements present. The obtained information helps archaeologists reconstruct the habits of prehistoric peoples. NAA is an approximately 100 percent successful method in "fingerprinting" obsidian (volcanic glass or rock) artifacts for determining prehistoric trade routes since sources of obsidian are easily differentiated from one another through their chemical compositions.

(iii) **Geology** → NAA is used by geochemists in research to analyse rock specimens and the processes involved in the formation of different rocks through the analysis of the rare earth elements (REEs) and other trace elements.

(iv) **Materials science** → NAA is used to measure trace- and ultra-trace-element concentrations of impurities and/or dopants in semiconductors and other high-purity materials.

(v) **Soil Sciences** → NAA allows soil scientists to quantify the distribution of agricultural chemicals under a wide variety of environmental and land use influences through the analysis of stable tracers which are capable of being activated, such as bromide.

(vi) **Medicine** → NAA is used in the analysis of boron taken up by cells in a rheumatoid arthritis treatment. To test for thyroid cancer, NAA is also used to measure iodine in nails where nails are characterized as biologic monitors for iodine.

1.1.2 Inductively Coupled Plasma Mass Spectrometry: an overview

ICP-MS was developed in the early 1980s as a commercial analytical technique and has become the most widely used detection technique in the determination of trace, minor and major elements for both routine analyses and research in a variety of areas [14, 15]. As shown by Figure 1.2 an ICP-MS combines excitation of elements at a high-temperature (of the order of 10,000 K) inductively coupled plasma (ICP) of argon source with detection by a mass spectrometer (MS). The process includes the ionisation of the atoms of elements in the sample by the ICP source, followed by separation and detection of the ions by the mass spectrometer [14, 16]. According to Ammann [17], this high temperature in ICP as well as the high ion density provide an ideal atomizer and element ionizer for all types of samples and matrices introduced by a variety of specialized devices.

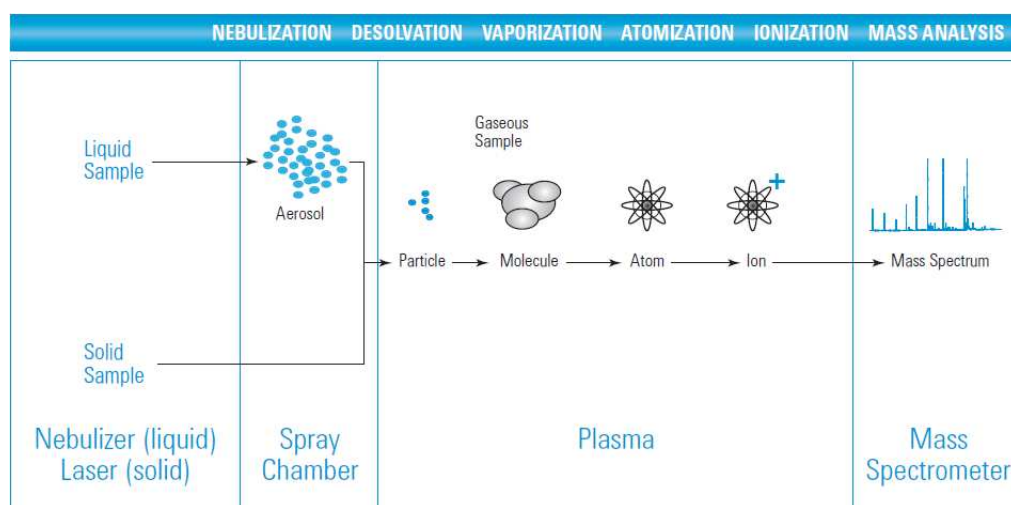


Figure 1.2: Schematic representation of processes in ICP-MS from sample introduction to mass analysis [14].

1.1.2.1 Applications of ICP-MS

ICP-MS is routinely deployed in diverse fields such as the following [14, 17, 18];

- industries (such as; nuclear, semiconductor, food and agriculture, chemical and petrochemical);
- environmental and life sciences;
- geology and geochemistry;
- forensic science;
- archaeology; and
- clinical and pharmaceutical sciences.

1.1.3 Air Pollution

Many parts of the world are faced with the challenging issue of air pollution. Air pollution affects people and the economy of countries, leading to forest decline, loss in agricultural production and diminished status of the population [19]. A wide array of substances including greenhouse gases, organic dust, and particulate matter are the cause of polluted air. Developing and developed countries continue to face a challenge of experiencing a variety of human health problems and environmental degradation caused by exposure to polluted air [1, 2]. The long term result of this environmental degradation is a prospective cause of our planet's struggle to sustain life. Hence it is crucial for modern society to protect the environment by striving towards maintaining the existence of clean air, pure water and an unpolluted earth. The main strategy towards achieving this goal is to identify sources of air pollution, determine concentrations of available toxicants in air, assess risks involved, integrate economical aspects and reduce the spreading of major toxicants [1, 20]. Consistent industrial growth, emissions from auto-mobiles and urbanisation are the primary and major causes of air pollution which account for environmental degradation and specifically a large deterioration of air quality [1].

The key in ensuring the improvement of air quality lies in vigorous control of air pollution, cleaner technologies and cleaner production practices [21]. As an industrialised nation, the Republic of South Africa (SA) carries a burden of industrial air pollution in addition to the common need of managing the bioaccumulative toxic elements. This industrial air pollution includes trace elements (e.g. heavy metals) and anthropogenic organic pollutants, which contribute to high levels of air pollution and waste in SA [22]. According to the World Health Organization (WHO)[2], exposure to any type of air pollutant leads to adverse effects on human health. Hence, one of the basic necessities for the existence and normal growth of all living organisms is to minimize air pollution levels. This indicates the necessity for authorities of all nations to come up with a science-based approach which provides guidelines intended to manage air quality. Increasing demand for experimental methods to study the environment was due to the growing concerns about constant rising levels of environmental pollution. This led to the development of the biomonitoring technique; to obtain information on levels, availability, as well as pathways of a variety of pollutants in the environment [23].

1.1.4 Biomonitoring Technique

The biomonitoring technique was initially introduced in the form of passive biomonitoring by Rühling and Tyler [24, 25] in 1968 through collection and analysis of mosses. Their aim was to monitor heavy metal deposition from the atmosphere. Rühling and Tyler [24, 25] recognised that high cost and difficulty of carrying out sampling using power-driven equipment was a limitation

in air pollution studies [26]. It was then that they decided to use biological material (plants) in order to acquire certain information about conditions of the environment. Since plants show an integrated response to air pollution and are independent of any form of external power source during exposure period, biomonitoring seemed to provide a better indication of the level of pollution and relatively cheaper than any direct physical and chemical methods would. Biological monitoring of trace element pollution with plants was therefore considered suitable and an effective way to estimate levels of air pollutants and their impact on humans and animals [1, 25, 27–29]. In 1971, Goodman and Roberts [30] originally introduced active biomonitoring which was later modified and put into action by Little and Martin in 1974 [31]. Active biomonitoring is performed, for example, through moss transplants enclosed in nylon mesh bags. This was done by collecting biomonitors in a pristine area and exposing them in a polluted area under investigation in order to monitor air quality. From their findings, Little and Martin [31] established active biomonitoring to be an appropriate and a convenient method of locating emission sources as well as integration of local metal burdens over weeks or even months. Hence, two types of biomonitoring are in use; passive biomonitoring (involves "in situ" monitoring using native biomonitors) and active biomonitoring (involves the use of "transplanted" biomonitors) [32–34].

1.2 Motivation for this study

A greater part of any biological material consists of H, C, N, O, and S. Moreover; Na, Mg, P, Cl, K, and Ca, which are essential for functioning of all cells are also found in biological material. H, C, N, O and S elements are found in larger quantities in biological material and as such, they are referred to as bulk elements and expressed in concentrations of g/kg. Na, Mg, P, Cl, K, and Ca also occur in concentrations of g/kg and hence these are referred to as macrominerals. Bulk elements as well as macrominerals are required by human bodies in gram amounts per day. Besides bulk elements and macrominerals, other elements occur in matter at much lower concentrations of $\text{mg}\cdot\text{kg}^{-1}$ (ppm) or $\mu\text{g}\cdot\text{kg}^{-1}$ (ppb). Due to their much smaller concentrations in matter, these elements were not easily quantified by the early analytical methods. Hence, they were given the name "trace" and "ultra-trace" elements. Trace elements are defined as the chemical elements that occur in small amounts of $100\ \mu\text{g}\cdot\text{g}^{-1}$ (100 ppm) or less in organisms and may be essential for many physiological and biochemical processes e.g. Fe, Zn, I, Co, Se, Mn, and Cu [35]. Ultra-trace elements are defined as the chemical elements that normally occur in very small amounts of less than $1\ \mu\text{g}\cdot\text{g}^{-1}$ in organisms, which may also play significant roles in the organisms metabolism. These include; Cd, As, B, Si, Pb, Ni, V, Br, Li, F, Hg, Cr, Se, Sn [36].

Some trace elements; e.g. Fe, Zn, I play an important role in the effective and proper functioning of biological systems sustaining a variety of biochemical processes. Other trace elements, whose proof of essentiality in living organisms is non-existent, are known as toxic trace elements e.g. Pb, Cd, Ba, etc. However, even the essential trace elements can be potentially toxic in concentrations above the acceptable levels required for optimal nutrition [1, 27, 37–40].

Environmental degradation caused by air pollution due to toxic trace elements is a serious environmental health problem that has harmful effects on the quality of human health and environment. This is one of the World Health Organisation (WHO) concerns. Effects of these air pollutants on people include, headaches, cancer, cardiovascular disease, heart and kidney failures, etc. In severe cases, air pollution due to toxic trace elements can lead to death [2]. Human activities such as waste disposals, coal and waste burning, generation and use of energy, motorized traffic, production and use of consumer goods steadily affect our environmental health by emission of toxic trace elements polluting the air, the most toxic of these being heavy metals.

According to Tangahu *et al.* [41], a conventional definition of a heavy metal is any elements with metallic properties and an atomic number >20 , where according to Appenroth [42], the most common heavy metal contaminants are Cd, Cr, Cu, Hg, Pb, and Zn. Appenroth [42] goes on to suggest three groups from the periodic table (see Figure 1.3) that should be considered heavy metals. These are;

- (1) transition elements (i.e. Ti, Zr, Hf, Rf, V, Nb, Ta, Cr, Mo, W, Mn, Tc, Re, Fe, Ru, Os and Zn),
- (2) rare earth elements; which are subdivided into the lanthanide series (including La) and the actinide series (including Ac), and
- (3) some elements from the p-group that are either metals (Al, Ga, In, Tl, Sn, Pb, Sb, Bi and Po) or metalloids, including Ge, As and Te.

Due to high toxicity in heavy metals present in air, there is a need for necessary approaches acceptable to give balance between accommodating modernisation for mankind worldwide as well as protecting the environment [1, 2]. In SA, air pollution data on atmospheric metal deposition is particularly scarce. This study focuses on the application of both passive and active biomonitoring of trace elements in the Western Cape Province using mosses and lichens. Mosses and lichens were found suitable to monitor atmospheric deposition of heavy metals and other trace elements. This is due to their enhanced ability to trap, accumulate and retain air pollutants [27, 43]. Mosses and lichens will be used as natural air filters to trap the toxic trace elements in air. These will then be analysed by non-destructive INAA as well as the ICP-MS, in order to determine trace element concentrations. Moreover, INAA will be used as the main technique of this study. This is because INAA is

Periodic Table of Elements

		1	2	3	4	5	6	7	8	9	10	11	12	13	14	15	16	17	18													
1	Atomic #																															
	Symbol																															
		<div style="display: flex; justify-content: space-between; align-items: center;"> <div style="border: 1px solid black; padding: 2px;">C Solid</div> <div style="border: 1px solid black; padding: 2px;">H Liquid</div> <div style="border: 1px solid black; padding: 2px;">G Gas</div> <div style="border: 1px solid black; padding: 2px;">Rf Unknown</div> </div>										Metals		Nonmetals																		
		Alkali metals		Alkaline earth metals		Lanthanoids		Actinoids		Transition metals		Poor metals		Other nonmetals		Noble gases																
1	H	2	He															10	Ne	18	Ar	36	Kr	54	Xe	86	Rn	118	Uuo			
2	Li	Be											13	Al	14	Si	15	P	16	S	17	Cl	18	Ar	36	Kr	54	Xe	86	Rn	118	Uuo
3	Na	Mg											13	Al	14	Si	15	P	16	S	17	Cl	18	Ar	36	Kr	54	Xe	86	Rn	118	Uuo
4	K	Ca	Sc	Ti	V	Cr	Mn	Fe	Co	Ni	Cu	Zn	Ga	Ge	As	Se	Br	Kr	54	Xe	86	Rn	118	Uuo								
5	Rb	Sr	Y	Zr	Nb	Mo	Tc	Ru	Rh	Pd	Ag	Cd	In	Sn	Sb	Te	I	Xe	86	Rn	118	Uuo										
6	Cs	Ba	57-71	Hf	Ta	W	Re	Os	Ir	Pt	Au	Hg	Tl	Pb	Bi	Po	At	Rn	118	Uuo												
7	Fr	Ra	89-103	Rf	Db	Sg	Bh	Hs	Mt	Ds	Rg	Cn	Uut	Fu	Uup	Uuq	Uur	Uus	Uuo	118	Uuo											

For elements with no stable isotopes, the mass number of the isotope with the longest half-life is in parentheses.

Periodic Table Design and Interface Copyright © 1997 Michael Dayah. <http://www.ptable.com/> Last updated: May 9, 2013

57	La	58	Ce	59	Pr	60	Nd	61	Pm	62	Sm	63	Eu	64	Gd	65	Tb	66	Dy	67	Ho	68	Er	69	Tm	70	Yb	71	Lu
89	Ac	90	Th	91	Pa	92	U	93	Np	94	Pu	95	Am	96	Cm	97	Bk	98	Cf	99	Es	100	Fm	101	Md	102	No	103	Lr

Michael Dayah For a fully interactive experience, visit www.ptable.com. michael@dayah.com

Figure 1.3: Periodic table of elements [42].

considered to be a highly sensitive developed analytical technique used to perform both qualitative and quantitative multi-element analysis of major, minor, trace and rare-earth elements in samples from almost every conceivable scientific or technical field [4, 9, 44].

NAA was established as the powerful primary method of measurement to determine the International System of Units (SI) traceable values of element content in complex samples and this is due to its potential for a superior accuracy and reliability over competing non-nuclear techniques (ICP-MS, AAS (atomic absorption spectrometry), ICP-AES (inductively coupled plasma - atomic emission spectrometry), etc.) in providing quantification of trace elements at ultralow detection limits in multielemental environmental, biological and geological studies [12, 44–46]. Passive biomonitoring (using native biomonitors) will be used to infer average levels of the air quality in selected areas around the Western Cape, South Africa. This will be achieved by assessing trace element concentrations in the collected native biomonitors. However, active biomonitoring (using transplanted biomonitors) will be used to assess atmospheric pollution in areas where mosses and lichens do not grow e.g. in a tunnel. Active biomonitoring provides an opportunity to evaluate and compare different capacities of biomonitors in accumulating different trace elements in air. The defined exposure time involved in active biomonitoring will also allow an opportunity to investigate the uptake rate of trace elements by the de-

ployed biomonitors. Samples will be analysed using INAA and ICP-MS, thus facilitating an intercomparison of the results obtained by INAA and ICP-MS [1]. Factor analysis will be applied on the results in order to reveal geochemically bound elements as well as pollution emitting sources associated with the determined elements.

1.2.1 International Air Pollution Monitoring

The conventional and internationally utilised method of assessing air pollution levels involves the use of ordinary air filters, pumps and analysers. This method has been used extensively in SA and will be discussed further in subsection 1.2.2. Another simple and effective air pollution monitoring system is called biomonitoring. Researchers from Russia [1], Norway [43], Italy [47], Bulgaria [48], UK [49], etc. have been using biomonitoring of air pollution for almost four decades. This internationally recognised method is based on the use of plants to accumulate and retain trace elements from the air instead of using air filters. These plants are then analysed with nuclear physics-based as well as classical analytical techniques in order to perform both quantitative and qualitative analysis of trace elements in air [1]. Analytical techniques are chosen based on their suitability and sensitivity to assess concentrations of the elements and compounds to be monitored in the sample [47]. A list of analytical techniques routinely used in conjunction with the biomonitoring technique is provided in section 2.5 of Chapter 2.

The biomonitoring method estimates levels of toxic trace elements in air. This technique will be discussed fully in Chapter 2. In general, biomonitoring may simply be defined as the use of any biological material (e.g. plants, animals, etc) to acquire certain information about conditions of the environment [46]. In the case of plants, biomonitoring can be performed firstly by sampling them *in situ* and this is known as passive biomonitoring. Alternatively, plants can be trans-located or transplanted to a different targeted area of interest, for a specific period, and this is called active biomonitoring (e.g. the use of moss-bags) [1, 34, 50]. Both passive and active biomonitoring techniques have not been used extensively in SA. Apart from being an easily-performed operation, the main advantages of air pollution biomonitoring is its cost-effectiveness regarding sample collection for both passive and active approaches. Moreover, biomonitoring techniques (excluding sample analysis) does not require any electricity supply or maintenance.

1.2.2 Air Pollution Monitoring in SA

According to the SA government [51], "everyone has the right to an environment that is not harmful to his or her health or well-being". Therefore, the levels of air pollutants in air have to be kept low at all times. SA air pollution

levels are monitored according to the Air Quality Act, No. 39 of 2004, stated in a government gazette [21] and was published in 2005. This act serves as a guide to be followed by all SA provinces in managing and minimizing pollution from sources, minimizing waste, remediation and monitoring pollution. Its aim is to enforce an environment with less polluted ambient air, that is not harmful to human health and well-being, by improving ambient air quality. However, these air quality standards mainly focus on minimizing levels of classical pollutants as opposed to heavy metals and other trace elements. SA ambient air quality standards were set out for the following air pollutants; sulphur dioxide (SO₂), nitrogen dioxide (NO₂), particulate matter (PM₁₀), ozone (O₃), benzene (C₆H₆)¹, lead (Pb) and carbon monoxide (CO) as shown in Table 1.1. The maximum concentration standards for these classical pollutants were set at a standardised temperature of 25°C and a pressure of 101.3 kPa [52].

Table 1.1: South African National Standards (SANS) for the usual pollutants in the ambient air, measured at a standard temperature (25°C) and pressure (101.3 kPa) [52].

Pollutant	10 minutes average	1 hour average	8 hours average	24 hour average	1 year average
SO ₂	500 $\mu\text{g}\cdot\text{m}^{-3}$ (191 ppb)	350 $\mu\text{g}\cdot\text{m}^{-3}$ (134 ppb)		125 $\mu\text{g}\cdot\text{m}^{-3}$ (48 ppb)	50 $\mu\text{g}\cdot\text{m}^{-3}$ (19 ppb)
NO ₂		200 $\mu\text{g}\cdot\text{m}^{-3}$ (106 ppb)			40 $\mu\text{g}\cdot\text{m}^{-3}$ (21 ppb)
CO		30 $\text{mg}\cdot\text{m}^{-3}$ (26 ppm)	10 $\text{mg}\cdot\text{m}^{-3}$ (8.7 ppm)		
PM-10				75 $\mu\text{g}\cdot\text{m}^{-3}$	40 $\mu\text{g}\cdot\text{m}^{-3}$
O ₃			120 $\mu\text{g}\cdot\text{m}^{-3}$ (61 ppb)		
Pb					0.5 $\mu\text{g}\cdot\text{m}^{-3}$
C ₆ H ₆					5 $\mu\text{g}\cdot\text{m}^{-3}$

Since the establishment of the air quality standards, SA air pollution studies have focused mainly on assessing the concentrations of the above mentioned classical pollutants. Concentrations of trace elements (heavy metals and other trace elements) in ambient air have not yet been given deserving attention. Nonetheless, heavy metals are still identified as the most active toxicants that have adverse effects on living organisms [1]. Hence an effective approach of monitoring air pollution has to also include the assessment of heavy metals and other trace elements.

The literature survey shows that little is being done by the SA government on air monitoring of heavy metals and other trace elements except for Pb

¹There are no safe levels for benzene

[53–61]. The inclusion of Pb might have been motivated by the previous use of leaded gasoline in the country. However, a number of studies aimed at determining levels of most heavy metals and other trace elements in air have been conducted in a lot of countries, especially in Europe [1, 62]. In these studies, plants (biomonitors) as well as nuclear physics and related techniques (e.g. NAA, ICP-MS, XRF (X-ray fluorescence analysis), etc.) are used to measure the fallout of these elements from the atmosphere. So far, three studies have been published on trace element biomonitoring in South Africa [63–65]. Two of the studies are related to data acquired in the Pretoria region (Gauteng Province) [63, 64] and other one in the mining industrial area of the North West Province [65].

1.2.3 Air Pollution Monitoring in the Western Cape, South Africa

The air pollution management directorate of the Department of Environmental Affairs and Development Planning (DEADP) in the Western Cape Province has done a lot in managing air pollution and controlling air quality in the Western Cape, South Africa. Air quality monitoring in the Western Cape is managed at both provincial and local government levels. The DEADP continuously monitors classical pollutants in order to evaluate them against those national standards reported in Table 1.1. Based on the acquired results from analysed data, the status of the air quality within the province is then described and compiled into daily, monthly and annual reports. Furthermore, informed decisions regarding atmospheric dispersion modelling are also made [57]. According to Linde [58, 59], Western Cape air quality monitoring processes are conducted via emissions inventory projects and passive sampling projects across the province. The aim of compiling an emissions inventory is to collect, collate and store information consistently about relevant emission parameters. Moreover, emission inventories may be compiled for specific pollutants at different scales e.g. for a country, suburbs or industries [60].

Generally (only considering the classical pollutants) the quality of air in the Western Cape is good, relative to other provinces in SA, with the exception of localised urbanised and industrial areas [57]. These areas include the City of Cape Town, Saldanha Bay and Mossel Bay where air quality degradation results from a combination of mostly emissions from vehicles and industrial emissions. Other areas that tend to further deteriorate the quality of air in the WC include; low-income residential areas, as well as agricultural areas. In these areas, the quality of air is compromised by a number of activities including unpaved roads, use of wood and fuel for cooking, refuse and tyre burning, refuse burning, as well as crop spraying. In general, types of air pollution sources are divided into three, namely; area sources, point sources and mobile sources as shown in Figure 1.4 [55, 57].

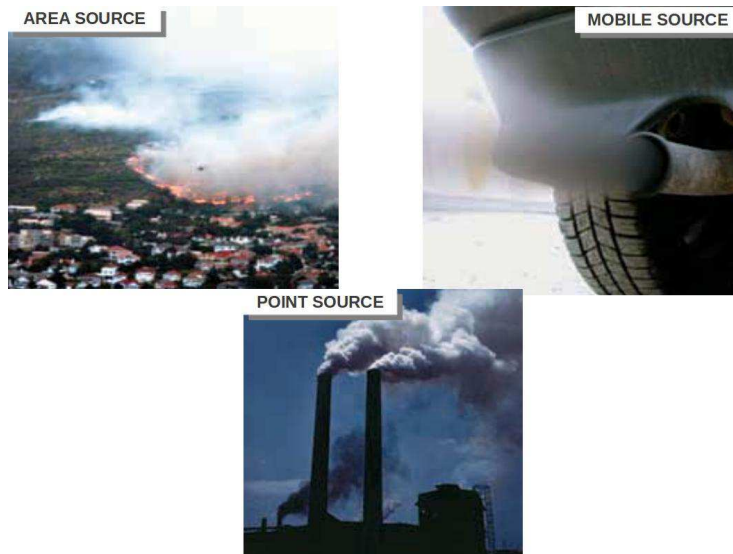


Figure 1.4: *Types of air pollution sources [55, 57].*

The Western Cape ambient air quality monitoring stations consist of mobile units containing equipment like; pumps, air samplers with filter papers, analysers, instrumentation logging devices as well as maintenance tools for analysers (see Figure 1.5 [66]). Even though the DEAPD has achieved a significant level of competence in improving the quality of air in the WC, more work still needs to be done. This is due to the continuous industrial growth, urbanisation, as well as the automobile traffic increase in the province.

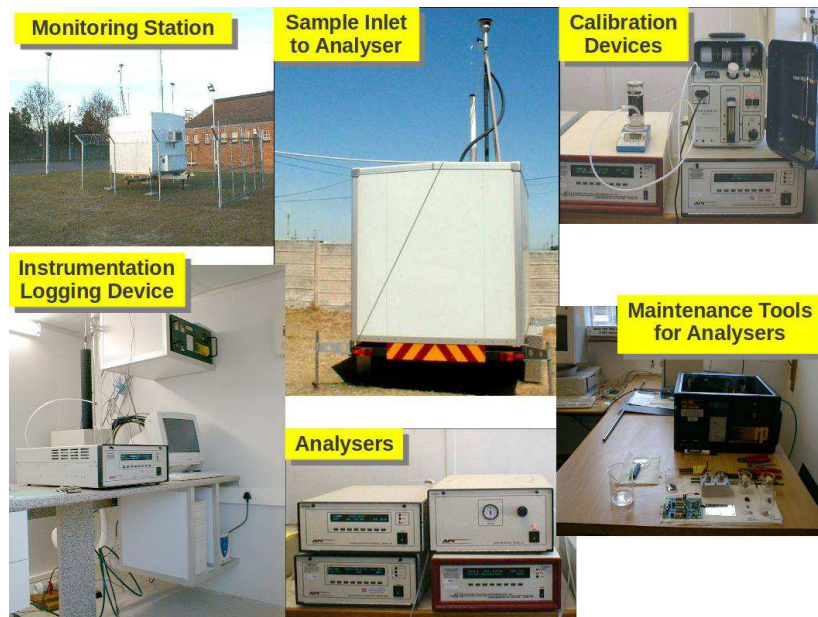


Figure 1.5: *Equipment for monitoring air quality in the Western Cape [66].*

1.3 Aims and Objectives of this study

The main aim of this study is:

- to "bridge a gap" by assessing and providing data about concentration levels of heavy metals and other trace elements in the Western Cape air using INAA and ICP-MS.

The objectives of this study in order to achieve our aim are the following:

1. to use native biomonitors (passive biomonitoring) to assess atmospheric pollution across the Western Cape;
2. to use active biomonitoring (mosses and lichens) to assess atmospheric pollution around Stellenbosch, and Saldanha Bay, as well as inside the Huguenot Tunnel;
3. to evaluate and compare accumulation of heavy metals and other trace elements by different lichen and moss species; and
4. to investigate the uptake of heavy metals and other trace elements (from vehicle emissions, industrial and urban emissions) by biomonitors as a function of time.

1.4 Outline of this thesis

This study presents a multifaceted analysis of mosses and lichens in order to quantify their elemental content using complementary multi-elemental techniques, namely; INAA and ICP-MS.

In Chapter 2, an overview of relevant theory or literature on which this study is based, is given. Since neutrons were used to irradiate samples, neutrons as well as their properties are discussed. This is followed by a discussion on the theory related to the interaction of γ -rays with matter. This is included since the measurement of γ -rays from the irradiated samples are used to determine the elemental concentrations in samples. Different kinds of biomonitors that are generally used in biomonitoring of air pollution are also reviewed, with more attention given to mosses and lichens (biomonitors used in this study). This section is then followed by a discussion of the biomonitoring technique based on both passive and active biomonitoring of air pollution. Furthermore, various nuclear physics and related techniques that are routinely used in biomonitoring studies are reviewed, with discussion more focused on INAA (main technique of the study) and to some degree on ICP-MS (secondary technique). The last section of this chapter focusses on a discussion of the uncertainties associated with air pollution biomonitoring technique.

In Chapter 3, the experimental methods used to collect samples from different areas of interest as well as the rationale behind the selection of those areas are explained. In the case of active biomonitoring, a step by step procedure on how moss- and lichen- bags were prepared, deployed and collected from different sites is discussed. This includes the manner in which samples were

exposed, the dates of exposure as well as collection. The procedures used to prepare samples for both INAA and ICP-MS analysis are also discussed. The experimental setup of INAA which includes; the REGATA irradiation facility at the IBR-2 reactor of the Joint Institute of Nuclear Research (JINR) in Dubna Russia, the equipment and all procedures used for sample transportation, sample irradiation and sample counting (using the γ -ray detectors) are discussed in detail.

In Chapter 4, the INAA data analysis is discussed. This is based on a γ -ray spectra analysis procedure using Genie-2000 Canberra software. Prior to discussing how the spectra were evaluated; the energy and efficiency calibration for gamma-ray detectors are discussed. Subsequent to the discussion of spectra evaluation, the background radiation and how it was accounted for is discussed. Then, the procedure for calculating final concentrations using a 'concentration program' developed at the Frank Laboratory of Neutron Physics (FLNP) of the JINR in Dubna, Russia is discussed.

In Chapter 5, the results of active and passive biomonitoring obtained from both INAA and ICP-MS are presented and discussed. A summary of this study, as well as its conclusions and recommendations for further work are found in Chapter 6.

Chapter 2

Review of Relevant Literature

In this chapter, a review of literature relevant to this study is provided. NAA is first discussed starting from neutrons (as the starting particle), all the way to the detection and analysis of γ -rays (emitted from reaction products). Different types of biomonitors used in air pollution studies as well as the two types of biomonitoring technique are discussed. Various analytical techniques suitable for air pollution biomonitoring are reviewed. Finally, the uncertainties associated with air pollution biomonitoring are discussed.

2.1 Neutron Physics Theory

Neutrons are subatomic particles found in all nuclei of chemical elements and their isotopes, including hydrogen isotopes: deuterium (^2H) and tritium (^3H) but not in protium (^1H). Neutrons are neutral subatomic particles with high penetrating power. Due to their charge-free character as well as their size (1.0086654 a.m.u. or 1.6749×10^{-27} kg), neutrons can deeply penetrate almost any material and interact with the atomic nucleus rather with than the electrons around the nucleus [67, 68]. The first indication of the existence of neutrons was detected by Bothe and Becker when they observed that a very penetrating radiation was released when beryllium (Be) was bombarded with α (^4He) particles as shown by Equation (2.1.1) below;



Since neutrons had not yet been discovered then, Bothe and Becker thought that the penetrating radiation was high energy photons (γ -rays). In 1932, Curie and Joliot noticed that this kind of penetrating radiation was able to remove protons from a hydrogen-rich material. The discovery of neutrons was made by Chadwick in 1932 [67] through an experiment conducted at the Cavendish Laboratory in Cambridge.

Chadwick showed that protons ejected from a hydrogen-rich material had collided with neutral particles with a mass closer to that of a proton (1.0072766 a.m.u. or 1.6726×10^{-27} kg) [3, 67, 68]. Since neutrons have no charge, they can approach a target nucleus without being affected by the Coulomb force. Once they are outside the nucleus, neutrons have an average life-time of 886.7 s (± 1.9 s) and they decay via β^- decay as shown by Equation (2.1.2) below [3, 69];



The β^- decay is a process whereby a neutron (n) is transformed into a proton (p) and in the process, emitting leptons (an electron (e^-) and an anti-neutrino ($\bar{\nu}_e$)) [3, 67, 68].

2.1.1 Production of Neutrons

Neutrons and protons inside the nuclei of atoms are bound up by strong nuclear forces that holds the nucleus together. A number of processes can be used to produce neutrons (i.e. release neutrons from the nucleus of any target material). A significant source of neutrons are nuclear reactors [4]. In nuclear reactors, neutrons are produced via induced fission of usually ^{235}U or ^{239}Pu with a neutron and this leads to the production of neutrons with a wide range of energies [70, 71]; e.g. $n + ^{235}\text{U} \rightarrow ^{174}\text{La} + ^{81}\text{Br} + 2n \dots \bar{E}_n \sim 2 \text{ MeV}$.

A nuclear research reactor was used in this study to produce neutrons, hence only the process of producing neutrons by a nuclear reactor will be discussed here. Fission reactors are discussed in more detail in Subsection 2.1.2.2. Depending on their kinetic energies; neutrons produced are generally classified as thermal neutrons, slow neutrons, epithermal neutrons and fast neutrons as shown in Table 2.1 [6, 12, 72, 73].

Table 2.1: *Typical classification of neutrons [6, 12, 72, 73].*

Thermal Neutrons	Slow Neutrons	Epithermal Neutrons	Fast Neutrons
$E_n \approx 0.025 \text{ eV}$	$E_n < 0.5 \text{ eV}$	$0.025 \text{ eV} < E_n \leq 0.5 \text{ MeV}$	$E_n > 0.5 \text{ MeV}$

Thermal neutrons are the neutrons in thermal equilibrium with the atoms of the moderator e.g. D_2O [4] and they are characterised by very low energies. At room temperatures (293 K), their energy spectrum is best described by a Maxwellian distribution with the maximum value corresponding to the neutron kinetic energy $E = 3/2kT$ (where k is the Boltzmann constant equals to 1.38×10^{-23} J/K, and T is the room temperature in Kelvin) [46]. In this region, the most probable neutron speed, v_p , is $2200 \text{ m}\cdot\text{s}^{-1}$, corresponding to a mean

energy of 0.025 eV [4, 6]. The root mean square speed of the neutron speed can be calculated using Equation (2.1.3) [74].

$$v_{\text{rms}} = \sqrt{\frac{3kT}{m}}, \quad (2.1.3)$$

where; T = temperature in Kelvin, m = neutron mass (1.66×10^{-27} kg), and k = Boltzmann constant (1.38×10^{-23} K $^{-1}$ ·kg·m 2 ·s $^{-2}$). A Cd foil of 1 mm thickness in a reactor cuts-off all thermal neutrons but allows epithermal and fast neutrons, with energies greater than 0.5 eV, to pass through. This is due to the large absorption cross section for thermal neutrons by Cd [4, 6]. Epithermal neutrons are the neutrons which are in the process of slowing down by colliding with nuclei of the moderator. Fast neutrons are the neutrons with energies greater than 0.5 MeV. In a reactor, fast neutrons are usually released in the fission of ^{235}U or ^{239}Pu and slowed down by interaction with a moderator, thus increasing the probability of causing ^{235}U or ^{239}Pu fission chain reactions [4, 6]. According to Hassan [10] and Peetermans [11], nuclear reactions are dependent on the neutron flux, energy spectrum and reaction cross section. Determined by the rate of flow of neutrons, the *neutron flux* is defined as a measure of the intensity of neutron radiation. Neutron flux value, measured in neutrons.(cm $^{-2}$.sec-1), is the product of neutron density (n) and neutron velocity (v), where n is the number of neutrons per cubic centimetre (expressed as neutrons.cm $^{-3}$) and v is the distance the neutrons travel in 1 second (expressed in centimetres per second, or cm.s $^{-1}$) [75]. Neutron fluxes vary according to the source of neutrons used. Figure 2.1 shows a typical neutron flux spectrum of a nuclear reactor with slow, thermal, epithermal and fast neutrons (which are discussed above).

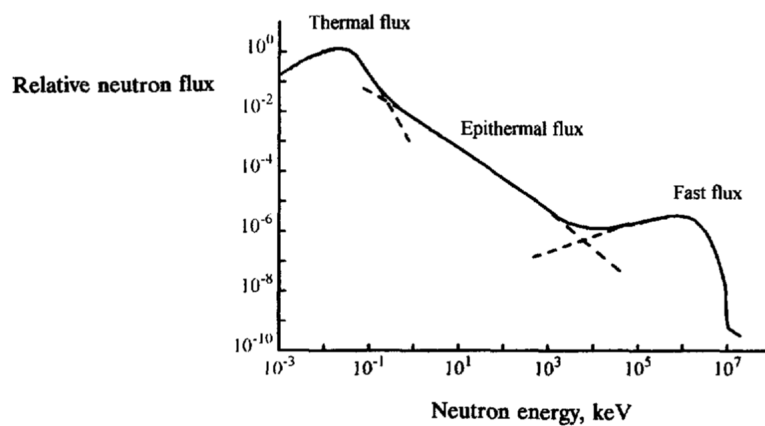


Figure 2.1: Typical neutron flux spectrum in a nuclear reactor [13].

As shown by Figure 2.1 above, thermal neutrons always have the highest flux, whereas, epithermal and fast neutrons' flux mainly depend on the type of the moderator used [4].

2.1.2 Interaction of Neutrons with Matter and Possible NAA Reactions

Neutrons interact with nuclei via strong nuclear reactions, however, in order for these interactions to occur, a neutrons has to pass close to a nucleus [70]. The strong nuclear force, which dominates and characterizes the neutron interactions with matter, has an interaction range of the order of $\leq (10^{-14})$ m [71]. As neutrons interact with matter, a number of reactions (producing radioactive nuclides with measurable radiations) can take place. These include: elastic scattering (n, n); inelastic scattering (n,n'); radiative capture (n, γ); particle producing reactions (n, α), (n,p), and (n,2n); as well as fission reaction (n,f) [46, 69]. The cross section is related to the probability for a specific reaction (e.g., absorption, scattering, or fission) to take place between a given atomic nucleus or subatomic particle and a certain incident particle. Thermal neutrons provide cross sections, of the order of (0.1 to 100) barn², for (n, γ), (n, n) and (n, f) reaction types, while fast neutrons favour (n, p), (n, α), (n, n'), and (n, 2n) reaction types, with cross sections that are two to three orders of magnitude lower. For thermal neutrons, the cross section is often inversely proportional to the neutron velocity, while the neutron cross-section can be very high for discrete energy neutrons in the epithermal region (see Figure 2.2) [4, 46].

In NAA, the most common reaction is (n, γ) [4]. To determine trace elements in biological materials by NAA, (n, γ) reactions are preferred and mostly utilised because of the generally higher sensitivity achieved as compared to other reactions [76]. According to Filby [76], the type of nuclear reaction to take place during NAA depends on the target nucleus and neutron energy. For example, Figure 2.3 is an illustration of significant nuclear reaction channels possible for Al after neutron capture, where [²⁸Al*] is the compound nucleus (excited nuclear state of ²⁸Al) resulting from neutron capture with a very short half-life (less than 10^{-13} s). Figure 2.4 shows cross-section plots for all those possible channels, as well as which reactions are dominant in which energy regions.

Figure 2.4 also shows that in the neutron region energy range between 1×10^{-10} MeV and 1 MeV, ²⁸Al(n, γ) reaction is the dominating reaction amongst all the reactions illustrated in Figure 2.3. The reaction cross-section data for ²⁸Al(n, γ) shows a resonance range between 0.08 MeV and 0.95 MeV. On the other hand,(n,n'), (n, α), (n,p), and (n,2n) reactions mainly take place as com-

²1 barn = 10^{-28} m² or 10^{-24} cm²

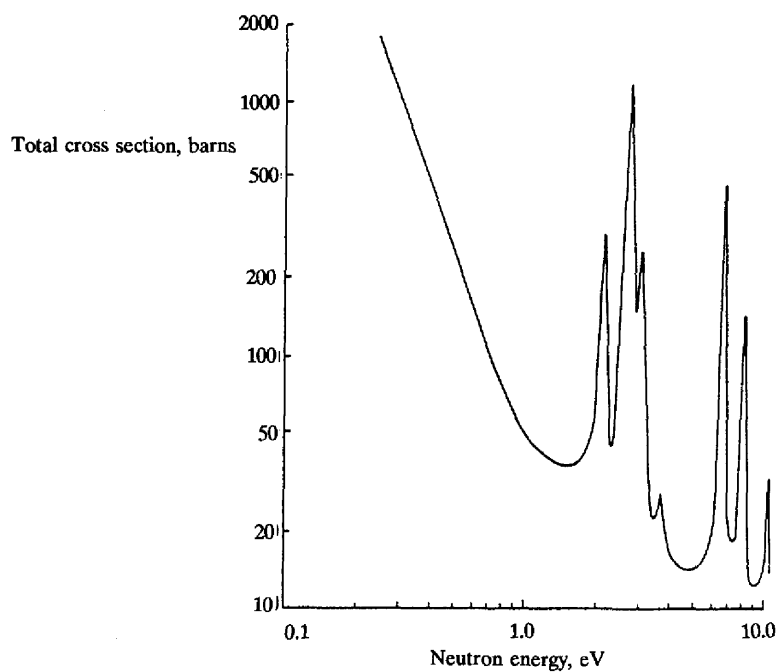


Figure 2.2: Relationship between total neutron cross section and neutron energy [4].

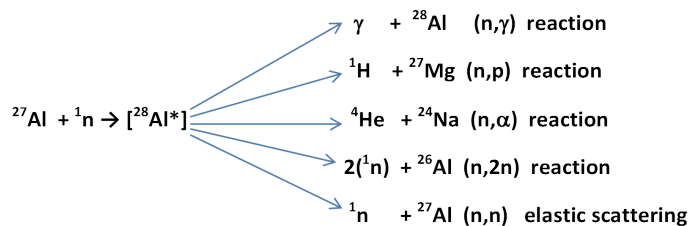


Figure 2.3: Possible significant nuclear reactions for Al after neutron capture [46].

peting reactions between 0.95 MeV and 14 MeV. Induced fission reactions (n,f), for fissionable elements (U, Pu, Th), and inelastic scattering reactions (n,n'), in which the isomeric state of target nuclide is measured, are limited in NAA [76].

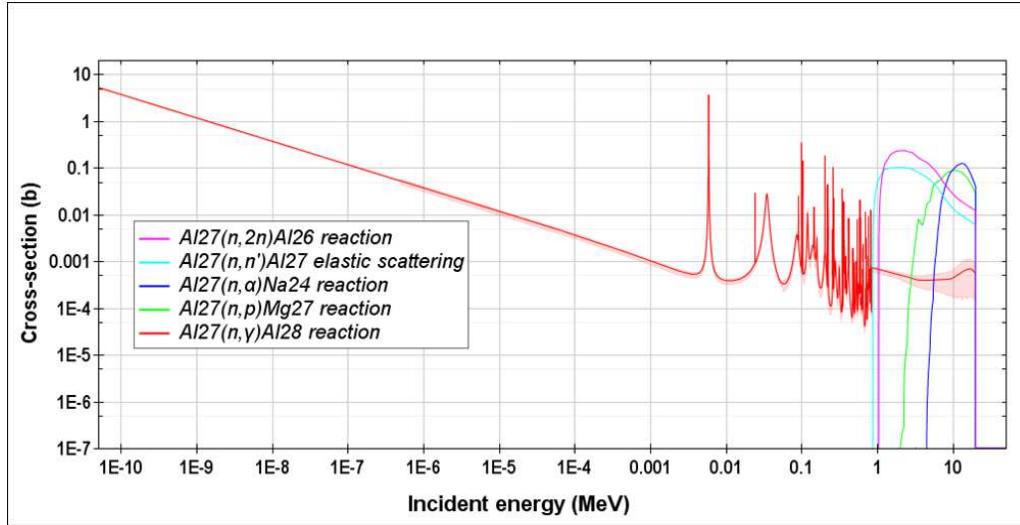


Figure 2.4: Cross-section plots for ^{27}Al neutron capture reactions [77].

2.1.2.1 Nuclear Reaction Rate

The way in which activation cross section and neutron flux depend on the neutron energy is taken into account in the reaction rate (R) per nucleus capturing a neutron (given by Equation (2.1.4)) by dividing the neutron spectrum into thermal and epithermal regions [4]. The division is made at the so-called cadmium cut-off energy, $E_n = 0.55$ MeV.

$$R = \int_0^{\infty} n(v)v\sigma(v)dv, \quad (2.1.4)$$

where;

v = neutron speed (in $\text{m}\cdot\text{s}^{-1}$),

$\sigma(v)$ = neutron cross section (in m^2 : 1 barn = 10^{-28} m^2) for neutrons with speed v , and

$n(v)dv$ = number density (m^{-3}) of neutrons with speeds between $v+dv$ (considered to be constant in time).

Dividing Equation (2.1.4) into thermal and epithermal regions, the integral can be re-written as follows (see Equation (2.1.5));

$$R = \int_0^{v_{Cd}} n(v)v\sigma(v)dv + \int_{v_{Cd}}^{\infty} n(v)v\sigma(v)dv, \quad (2.1.5)$$

where;

v_{Cd} = neutron speed (in $\text{m}\cdot\text{s}^{-1}$) at the Cd cut-off,

From Equation (2.1.5) above, the first term is for the thermal region and can

be integrated as follows (see Equation (2.1.6));

$$\int_0^{v_{Cd}} n(v)v\sigma(v)dv = v_0\sigma_0 \int_{v_{Cd}}^{\infty} n(v)dv = nv_0\sigma_0, \quad (2.1.6)$$

where; σ_0 = the thermal neutron activation cross section (m^2) at 0.025 eV (i.e. E_n for thermal neutrons)

v_0 = the most probable neutron speed at 20 °C: 2200 ms^{-1} .

The second term of Equation (2.1.5) is for the epithermal region. This part of the integral can be re-formulated in terms of neutron energy rather than neutron velocity. In this region, another effective cross section called the infinite dilution resonance integral, I_0 , is also introduced (see Equation (2.1.7));

$$\int_{v_{Cd}}^{\infty} n(v)v\sigma(v)dv = \Phi_{epi} \int_{E_{Cd}}^{E_{max}} \frac{\sigma(E_n)dE_n}{E_n} = \Phi_{epi}I_0, \quad (2.1.7)$$

where;

$$I_0 = \int_{E_{Cd}}^{E_{max}} \frac{\sigma(E_n)dE_n}{E_n}, \quad (2.1.8)$$

in which Φ_{epi} is the 'conventional' epithermal neutron flux per unit energy interval, at 1 eV. This implies that I_0 is proportional to $1/E_n$. In practice, the epithermal neutron flux (Φ_{epi}) in nuclear reactors does not precisely follow the inverse proportionality to the neutron energy. This small deviation can be accounted for through introducing an epithermal flux distribution parameter, α (see Equation (2.1.9) [4];

$$I_0\alpha = \alpha \int_{E_{Cd}}^{E_{max}} \frac{\sigma(E_n)dE_n}{E_n}. \quad (2.1.9)$$

Using Equations (2.1.6) - (2.1.9), the expression for the reaction rate can then be re-written as follows (see Equation (2.1.10));

$$R = \Phi_{th}\sigma_0 + \Phi_{epi}I_0\alpha, \quad (2.1.10)$$

where $\Phi_{th} = nv_0$,

Φ_{th} is the 'conventional' thermal neutron flux ($n.m^{-2}.s^{-1}$) for energies up to the Cd cut-off energy of 0.55 eV.

Using the ratio of thermal neutron flux and epithermal neutron flux, expressed as $f = \Phi_{th}/\Phi_{epi}$, and the ratio of the resonance integral and the thermal

activation cross section, expressed as $Q_0(\alpha) = I_0(\alpha)/\sigma_0$, an effective cross section can be defined as follows (see Equation (2.1.11));

$$\sigma_{eff} = \sigma_0 \left(1 + \frac{Q_0(\alpha)}{f}\right). \quad (2.1.11)$$

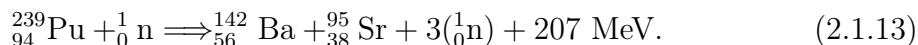
Equation (2.1.11) simplifies Equation (2.1.7) for the reaction rate (see Equation (2.1.12));

$$R = \Phi_{th} \sigma_{eff}. \quad (2.1.12)$$

2.1.2.2 Nuclear Fission Reactors

Nuclear fission is a process whereby an incident neutron enters a heavy target nucleus (e.g. ^{235}U and ^{239}Pu), causing the nucleus to "split" (fission) into two or more large fragments, during which energy and further neutrons are released [78–80]. Nuclear fission reactors are mostly based on the induced fission reactions of ^{235}U and ^{239}Pu to yield 2 to 3 neutrons per fission with kinetic energies of approximately 2 MeV.

In this study, the induced fission of ^{239}Pu was used to produce neutrons for irradiation. One of the reactions through which ^{239}Pu can undergo fission is shown in Equation (2.1.13) below [81];



The types of neutron produced during fission reactions are fast neutrons. These fast neutrons are slowed down to epithermal and thermal neutrons by colliding with matter with low proton number (Z) e.g. heavy water (D_2O) or normal water (H_2O), usually used both as moderator and coolant. After they have been slowed down, neutrons are reflected back into the reactor core by reflectors (D_2O , Be, graphite) to maintain the core critical through chain reactions. A reflector blanket (also low Z material) surrounding the reactor core is used to minimize neutron leakage. After each fission event, two types of fission neutrons are produced. The first type of fission neutrons, called prompt neutrons, appears instantaneously. This comprises more than 90% of the overall produced neutrons. However, a small fraction of about less than 1% of the neutrons get delayed and appear after a subsequent decay of radioactive fission products. These delayed neutrons effectively control the process of the nuclear chain reaction by "slowing" the transient kinetics and then play a vital role in the operation of nuclear reactors. A nuclear reactor would respond quickly and be uncontrollable without the delayed neutrons [81–84].

2.2 Interaction of Gamma-rays with Matter

There are several types of radiation emitted after activation during NAA, of which gamma-radiation offers the best characteristics for selective and simultaneous detection of radionuclides and elements [5]. These γ -rays are the high energy photons of the electromagnetic spectrum. Gamma-ray spectroscopy allows one to measure electromagnetic radiation emitted from radioactive nuclei by counting and measuring the energy and intensity of individual photons [85]. From those measurements, the measured full-energy peak of a γ -ray is characteristic of a given de-exciting radionuclide. The analysis in gamma-ray spectrometry entails an optimum separation of peaks, the γ -ray line identification as well as the peak area determination in the γ -ray spectrum [4]. Like neutrons, gamma rays have no mass and no charge and so, they need an indirect way to transfer energy. Unlike charged particles (electrons and protons), the penetrating power of gamma rays is very high [3, 73]. As shown in Figure 2.5, the interaction of gamma radiation with matter causes ionization in matter via three major processes; (i) photo-electric effect, (ii) Compton scattering, and (iii) pair production [86, 87].

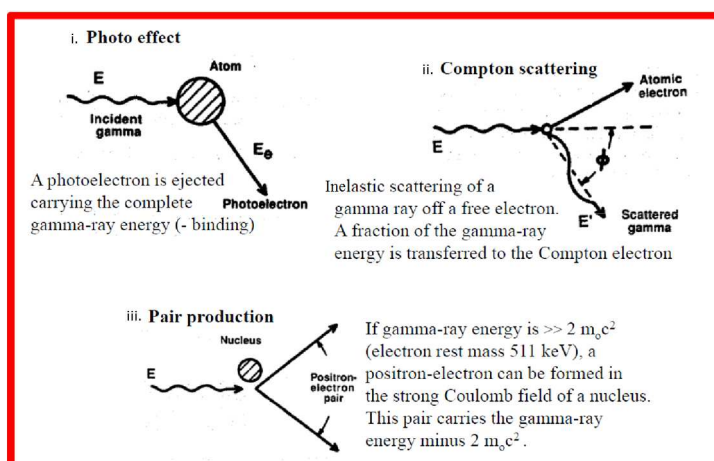


Figure 2.5: Major processes involved when gamma radiation interacts with matter [87].

2.2.1 The photoelectric effect

This is a process which predominantly takes place with orbital shells close to the nucleus whereby an incident γ -ray photon interacts with the orbital electron of the atom of the detector crystal, e.g. Ge. It also predominantly occurs when low energy gammas interact with high atomic weight atoms and rarely occurs with gammas having an energy greater than 1 MeV [84]. During this process, the energy of the photon is completely transferred to the electron in a single step. The electron overcomes the ionization potential by utilizing

part of the transferred energy, and gets ejected with a kinetic energy given by equation (2.2.1) [73, 86]:

$$E_e = E_\gamma - E_b, \quad (2.2.1)$$

where; E_γ is the photon energy and E_b , the electron binding energy (the energy required to remove an electron from the atom) in its original shell [3, 68]. The photoelectric absorption occurs if the incident photon energy is greater than or equal to the binding energy of the ejected electron [88]. An electron falling from the next higher shell occupies the vacancy created by the ionized electron and in the process, characteristic X-rays of the detector material are simultaneously emitted. Hence, characteristic X-rays of the detector material are also emitted during photoelectric interaction [86].

2.2.2 Compton scattering

Compton scattering usually takes place at the outer orbital shells, whereby an inelastic collision occurs between the incident γ -ray and the outer orbital electron. Here, only part of the γ energy gets transferred to the recoil electron. The remaining energy is emitted as a lower energy γ -ray (scattered inelastically) so that the total energy and momentum are conserved. If a maximum amount of energy is transferred, this results in a head-on collision whereby a secondary γ -ray is emitted at 180° to the first. The secondary γ photon can itself interact by further Compton or photoelectric interactions. Nevertheless, it is possible that this secondary γ -ray might escape from the detector, with the photon energy of the outgoing photon related to the scattering angle ϕ and given by equation (2.2.2) [73]:

$$E_{\gamma'} = \frac{E_\gamma}{1 + \frac{E_\gamma}{m_0c^2}(1 - \cos\phi)}, \quad (2.2.2)$$

where; E_γ is the incident photon energy, $m_0c^2 = 511$ keV, the rest mass energy of an electron. In this case, the detected event for the recoil energy of the electron (E_e) therefore corresponds to the full energy of the incident photon less that of the Compton escape γ -ray (see equation (2.2.3)) [73].

$$E_e = E_\gamma - E_{\gamma'}. \quad (2.2.3)$$

Compton scattering is the main cause of the high background continuum below the energies of principal gamma photopeaks recorded on the gamma-ray detectors [86].

2.2.3 Pair production

This is a process whereby an interaction of the incident γ -ray in the strong Coulomb field surrounding the nucleus results in complete transmutation of γ photon energy into an electron-positron pair. Formation of the electron-positron pair requires an energy twice the rest rest mass of the electron m_0c^2 , hence the pair production interaction becomes significant when the incident γ -ray energies exceed 1.022 MeV. The excess energy given by the photon energy minus 1.022 MeV (2×511 keV), is then shared between electron and positron as kinetic energy. The positrons are very short lived and they lose their kinetic energy very quickly by further collision with the electrons of the detector, followed by the spontaneous annihilation of a positron and an electron to generate two 511 keV γ -rays. In most cases, the two photons are most likely to be emitted at almost 180° to one another. However, the angle between electron-positron pair might be smaller due to the residual energies of the positronium mass at the time of annihilation. If the detector absorbs both annihilation gamma rays, their interaction contributes to the full-energy peak in the measured spectrum. However, if one of the annihilation gamma rays escapes from the detector, the interaction contributes to the single-escape peak located 511 keV below the full-energy peak. Moreover, if both gamma rays escape, the interaction contributes to the double-escape peak located 1.022 MeV below the full-energy peak [89, 90].

2.2.4 Gamma-ray Detection

In NAA measurements, nuclear radiations emanating from the irradiated material produce ionization in the detector medium by means of charged particle products of their interactions and the nuclear radiation detector converts the energy of nuclear radiation into an electrical signal. Gamma-ray detectors typically used for γ -ray detection gamma are categorized into three categories:

- (i) scintillators : e.g. NaI(Tl), CsF, CsI(Tl), ZnS(Ag),
- (ii) semiconductors : e.g. Si, HPGe, CdTe, GaAs, and
- (iii) gas filled: e.g. He, Air, H₂, N₂.

However the energy discrimination capacity of semiconductors and scintillators are better than that of the gas-filled detectors [86]. A brief comparison of certain semiconductors and scintillators will be given, but gas-filled detectors will not be discussed here.

Scintillation detectors are radiation sensitive crystals that produce low-energy flashes of light via a scintillation process when struck by ionizing radiation (e.g. gamma) [87]. As shown in Figure 2.6, scintillation detector consists of a phosphor, photocathode, photomultiplier and a charge collector. In these detectors, the phosphor converts the energy deposited by the gamma rays into light pulses. When these light photons strike the photocathode, it consequently emits photoelectrons. Then, the photomultiplier tube accelerates (by means

of high voltage) and multiplies these photoelectrons. The negative charge collected is presented as an electrical signal, which is proportional to the energy of the incident radiation [69, 85, 86].

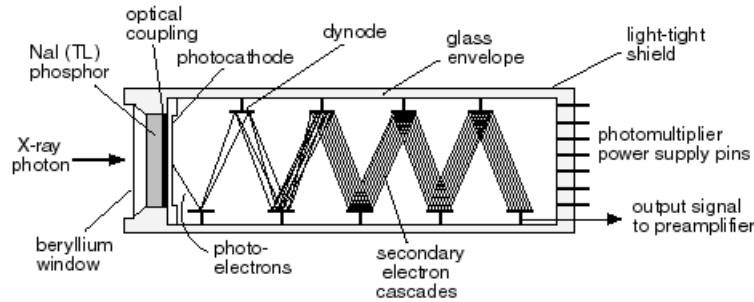


Figure 2.6: Schematic diagram of a NaI(Tl) scintillation detector and photomultiplier assembly [91].

Semiconductor detectors contain detector crystals, devoid of any charge carriers at liquid nitrogen temperature (77 Kelvin). When a high voltage is applied on the opposite sides of the detector crystal, an electric field is established. In these detectors; the incident nuclear radiation ionizes the detector crystal, creating electrons (negative charge) and holes (positive charge). Due to the created electric field, the charge carriers get attracted to the electrodes of opposite polarity. Thus, the charge collected at the electrodes is proportional to the energy lost by the incident radiation. Energy resolution varies with gamma-ray energies and also the size of the detector, where the energy resolution decreases with increasing gamma-ray energy and size of the Ge crystal [69, 85, 86]. A schematic diagram showing the cross sectional view of a Ge detector is shown in Figure 2.7.

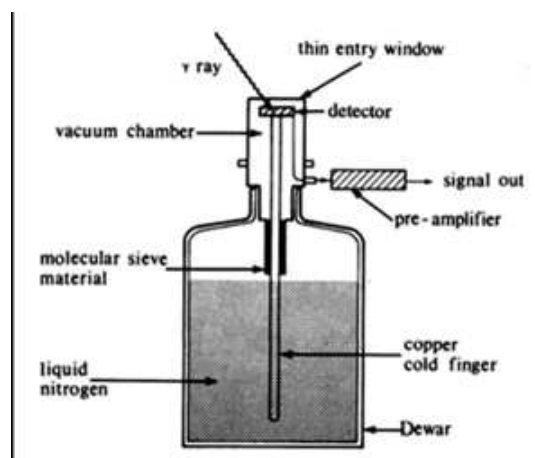


Figure 2.7: Schematic cross-sectional view of a Ge detector [69].

Ge semi-conductor detectors; i.e. lithium (Li) and high purity (HP), have good sensitivity and excellent energy resolution for γ -ray detection. However, Ge(Li) detectors are unstable at room temperature. This is due to lithium drifting into the intrinsic region, which is not reversible through cooling and in effect destroys the detector [69]. Nowadays, High Purity Germanium (HPGe), stand out as the most commonly used semiconductor material detectors in NAA and since it has been used in this study, more details pertaining this type of detectors are discussed here. The detection of high energy gamma rays requires the detector to have a depletion depth of at least 10 mm in order to absorb the energies [88]. This depth can be best achieved by Ge crystals but they must have a level of impurity of 10^{10} atoms/cm³ in order to reach a high enough resistance. It is due to this extremely low impurity level, that the detector owes its name of high purity germanium detector. When in use, HPGe semiconductor detectors are kept cooled at 77 K with liquid nitrogen and this is done to alleviate the risk of excessive leakage current at higher temperatures. However, the leakage current issue only applies during operation. Therefore when not in use, HPGe detectors can be stored at room temperatures as long as there is no contamination on the Ge from residual vapours [85, 86, 88].

The consideration to use a certain detector is usually based on its energy resolution, detection efficiency, peak shape, peak-to-Compton ratio, shape and price. The detector's ability to separate closely spaced peaks in a spectrum is known as its resolution, specified in terms of the full-width-at-half-maximum (FWHM). This energy resolution is expressed in keV or MeV, typically provided by the width of the gamma-ray peak at half of its height. On the other hand, the efficiency of a detector depends on type, size and geometry of the detecting medium, and the incident gamma-ray energies. Germanium (Ge) crystals are generally known to provide excellent energy resolution for gamma-ray energies. To produce an electron-hole pair in Ge crystals, the average energy required is only 2.98 eV as compared to 40 eV for gas detectors and 300 eV for scintillation detectors. Therefore, the signal from a Ge detector is 10-100 times bigger, and hence their resolution is better [69, 86]. The efficiency values of any detector also depend on the type of reference source from which they were derived [92].

According to Bode [4], detectors best suitable for NAA application are germanium semiconductor radiation detectors and this is due to their best energy resolution, which varies typically from approximately 1 keV for photons of approximately 100 keV to approximately 2 keV for photons of approximately 1.5 MeV. The best detector efficiency is important in INAA measurements because it offers an opportunity to detect low-intensity peaks above the continuum caused by Compton scattering [93]. The total energy resolution for gamma-ray spectrometer system depends on detector (i.e. the type of the detector used) and electronics (e.g. the pre-amplifiers, amplifiers, multi-channel

analysers (MCA), etc.) and is given by equation (2.2.4) [86, 93].

$$(\text{System Resolution})_{\text{total}} = \sqrt{R(d)^2 + R(E)^2} \quad (2.2.4)$$

where $R(d)$ is the detector resolution and $R(E)$ is the electronics resolution. As shown by Figure 2.8, the better resolution is given by HPGe detectors as compared to NaI(Tl). This can be deduced from the much narrower peaks measured by HPGe detectors [70]. Furthermore, HPGe detectors also offer an enhanced ability to see a photopeak above the Compton distribution [93].

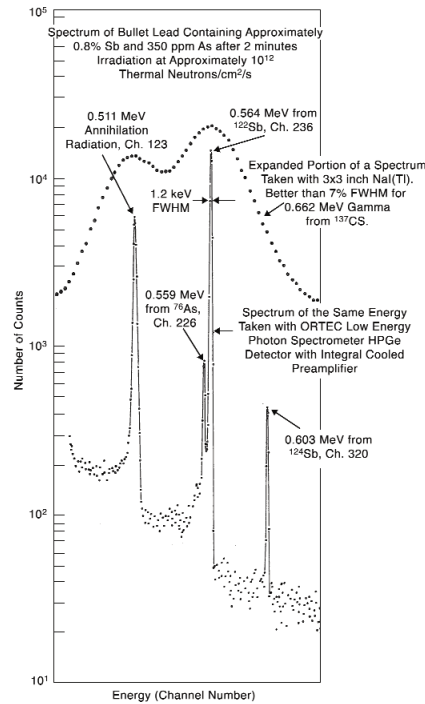


Figure 2.8: Comparative pulse height spectra recorded using NaI(Tl) and Ge detectors [93].

2.3 Biomonitoring of Air Pollution

Biomonitoring is generally defined as the use of living organisms to obtain information on certain characteristics of the atmosphere, lithosphere and/or hydrosphere by monitoring the response of those living organisms to changes in their environment [94–97]. It is a suitable and accepted quantitative tool for assessing heavy metals and other trace elements air pollution resulting from both dry and wet atmospheric deposition [20, 97, 98]. The use of biomonitoring cannot be justified in cases whereby direct physical and chemical methods

(e.g. use of aerosol filters) are able to produce comparable results quicker and cheaper. However in the case of air pollution related to heavy metals and other trace elements, concentrations of elements are often low in the atmosphere or a very extensive sampling network is desired. According to Basile *et al.* [99], air pollution can now be studied effectively using biomonitoring techniques. This is because biomonitors have the ability to absorb and retain trace elements from the atmosphere and then reflect their ambient conditions quantitatively [97]. The observed changes in biomonitor's behavior (e.g. composition, physiological performance, morphology, etc.) as well as measured elemental concentrations in the biomonitor's tissue provide the relevant information in biomonitoring [97]. Hence biomonitoring has emerged effectively as a more economical approach of measuring ambient air quality [94]. Although not extensively utilised in SA, biomonitoring of air pollution is a well-established technique in Europe and is widely used to investigate atmospheric deposition of trace elements related to both local pollution sources (e.g. regional studies) as well as large scale studies (e.g. national studies) [29, 100]. This study focuses on the application of both passive and active biomonitoring of atmospheric pollution in the Western Cape province. A clear summary of the relationship between active and passive biomonitoring is shown in Figure 2.9, with the information given by Frontasyeva, Steinnes, as well as Steinnes *et al.* [1, 33, 34].

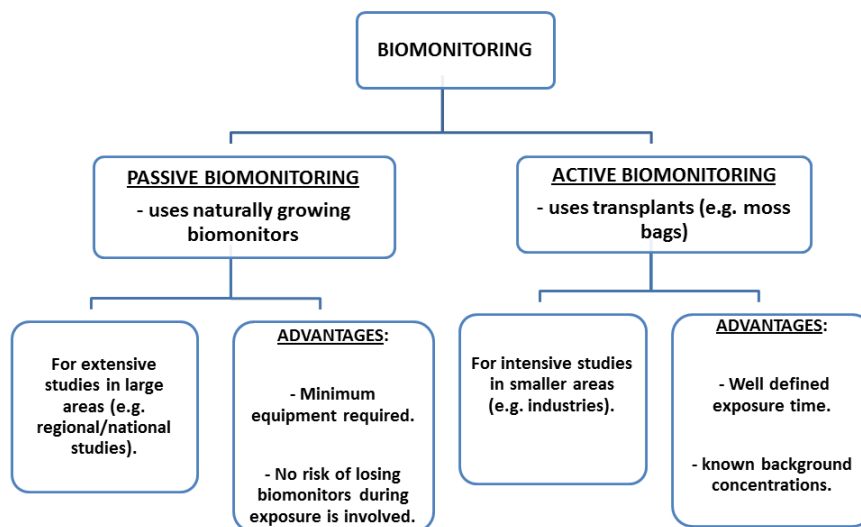


Figure 2.9: Relationship between passive and active biomonitoring [1, 33, 34].

2.3.1 Passive Biomonitoring

Passive biomonitoring is when chemical analysis or observation of biomonitors is performed on naturally growing (indigenous) biomonitors collected in the area under investigation [101]. The only major steps involved in passive biomonitoring involve sample collection and analysis. Passive biomonitoring offers an advantage over active biomonitoring as it is often used for extensive studies (e.g. regional or national studies) to cover large areas [102]. Since passive biomonitoring does not require any installation of a sampler or measuring instrument at each measuring point and thus no maintenance is required; it is a cost-effective technique [94, 98]. This type of biomonitoring is more popular in biomonitoring studies as it requires no additional deployment of samples.

2.3.2 Active Biomonitoring

Active biomonitoring is an alternative and a valuable tool of evaluating air pollution levels in large cities with heavy technogenic load and industrial regions as well as in arid areas where mosses or lichen do not grow [46, 99]. As stated earlier, active biomonitoring is performed by collecting biomonitors in a pristine area and then intentionally exposing them in a polluted area under investigation in order to monitor air quality [32, 103–105]. Moreover, active biomonitoring is said to be especially suitable to monitor urban areas, also known as "lichen or moss desert" areas, as well as any sites with relatively high pollutant levels [32, 106]. In order to ensure an efficient accumulation of elements and adequate replicability of results, the minimum exposure period of 30 days for samples is proposed [50]. In case of mosses, active biomonitoring can be done using both dry and wet moss bags. The aim of using wet bags is to avoid drying out of moss bags as well as the presumed physiological stress in moss tissue caused by change of environment [26, 107]. However, the main challenge in the use of wet bags is the need to constantly irrigate mosses throughout the exposure period, more especially if the investigated area is too far or if the investigated areas are too scattered. Another important factor to note in active biomonitoring is the use of inert material (e.g. nylon, plastic, glass fibre) to pack and suspend the biomonitors during exposure. This is to avoid any contaminants which may be released by the used material or equipment. Moreover, the space in-between moss or lichens bags should be big enough to prevent screening or dripping from one bag to another [50]. A list of some advantages that distinguish active biomonitoring from passive biomonitoring is given in Table 2.2 [26, 29, 106].

Active biomonitoring does not have any enabled standardised protocol [50]. According to Saitanis *et al.* [105], active biomonitoring needs to be used cautiously as there are few elements which might be vulnerable to leaching and/or volatilization over time. Therefore, timing and duration of the sample exposure must be taken into consideration when interpreting the results. Moreover, the

Table 2.2: *Advantages and disadvantages of active biomonitoring [26, 29, 106].*

Advantages	Disadvantages
well-defined exposure time under controlled conditions	unknown collection efficiency for different contaminants in different biomonitors
known background concentration of elements in the biomonitor	the impossibility to standardize the exposure time for the exact species in bags for urban, industrial or other source of pollution
flexibility in site selection as well as the number of stations that can be chosen	deciding on the choice of a biomonitor to be used because different biomonitors differ in ecophysiology and mechanism of element accumulation
uniformity of entrapment surface	lack of data with respect to the comparative accumulation capacity of two or more types of organisms

efficiency of moss and/or lichen bags in retaining metals may vary depending on the environmental conditions they are exposed to [26]. Even though this method has been applied for over 40 years to monitor air quality, its applications have been limited to scientific research. It has not yet been implemented by public authorities in air quality management [50].

2.4 Biomonitors of Air Pollution

The use of biomonitors analysed with analytical techniques that provide information on concentrations of multiple elements has become a powerful tool for detecting and identifying air pollutants as well as revealing air pollution sources [23]. Basile *et al.* [99] define biomonitors as organisms which quantify environmental quality and whose parameters change in response to pollution. These authors [23, 99] go on to explain that since biomonitors are able to record the effects of environmental changes in time, they can then be employed as air pollution "data integrators". According to Conti and Cecchetti [108], biomonitors of air pollution are mainly used to quantitatively determine air contaminants and can be classified as being sensitive and/or accumulative. Plants are immobile and so they more readily reflect local conditions of the environment they inhabit. However, different plants show diverse response to air pollution [109]. As a result, the main criteria for selecting a suitable biomonitoring material is as follows [28, 94, 98, 108, 110];

1. common occurrence in the area of interest;
2. availability during all sampling seasons with relative ease of collection;
3. the biomonitor should be tolerant of pollutants at the relevant levels;
4. element uptake should be relatively independent of local conditions;
5. the biomonitor should have low background concentrations of elements;

6. the accumulated concentration levels must be measurable by routine analytical techniques;
7. the biomonitor should have little or no significant amounts of element uptake from sources other than the atmosphere;
8. physiological mechanisms for uptake of elements should be known to facilitate interpretation of the results;
9. the biomonitor should average the elemental concentrations over a period of time as a result of integrated exposure; and
10. sample collection and analysis should be simple and quick.

Biomonitors include mosses, lichens, ferns, bacteria, pine needles, tree bark and leaves, fungi, as well as human and animal tissue such as feathers, hair and livers [1, 23]. Among these, mosses and lichens are dominantly used as biomonitors of heavy metals and other trace elements in air pollution surveys [19, 107]. This is because mosses and lichens absorb nutrients predominantly from the atmosphere and have high capacities for retaining many ions. Hence they are useful indicators of air pollution [33, 99]. According to Aničić *et al.* [107], mosses and lichens can accumulate elements to a far greater level than is necessary for their physiological needs. Furthermore, these biomonitors can even concentrate toxic substances that may be present in low concentrations in their local environment. Mosses and lichens possess efficient accumulation capacity for many air pollutants (heavy metals and other trace elements) from atmospheric deposition [27, 43]. Although mosses and lichens grow naturally in many terrestrial ecosystems, their growth and existence is largely affected by anthropogenic factors. According to Bates [111], lichens may be found and sampled on trees, rocks, tiles, etc., while mosses grow on stones, soil, tree-stumps and branches. Mosses and lichen fall under two completely unrelated groups of cryptogamic (seedless plants and plantlike) organisms. However, they still have some features in common [99]. One of them being their lack of a root system which causes them to gain water and most nutrients directly from air via both wet and dry deposition. Therefore, their uptake of the nutrients from the substrate is insignificant. These plants rely largely on atmospheric deposition for nourishment. Furthermore, mosses and lichens have no cuticle and have thin leaves which allow easy uptake from the atmosphere. Unlike higher plants (e.g. trees), these biomonitors do not shed plant parts as easily. As a result, they accumulate persistent atmospheric pollutants to concentrations far greater than those in air, rain and snow [29, 46, 110, 112, 113].

The application of mosses and lichens as biomonitors, analyzed by nuclear and related techniques, has been extensively used to provide information about air quality. According to Bargagli and Chakraborty [94, 112], trace element accumulation in mosses differs from lichens, thus producing varying results from one place to another. This is due to the fact that mosses accumulate trace elements much better under wet conditions. Moreover, there is no existing distinct evidence showing which biomonitor is a better heavy-metal biomonitor

under all conditions yet. Mosses tend more to clearly express the differences between different parts of the country and locations of emission sources than lichens. This is because mosses are only found in wet and less polluted areas. For this reason, mosses are mostly regarded to be better biomonitors than lichens. However, lichens may be better biomonitors than mosses under arid conditions.

2.4.1 Mosses as Biomonitors

The use of mosses in a biomonitoring network for heavy metals was originally established as a Swedish initiative in 1980 [49]. For the European biomonitoring network, moss surveys are conducted under United Nations Economic Commission for Europe (UNECE) - International Cooperative Programme on Effects of Air Pollution on Natural Vegetation and Crops (ICP Vegetation, formerly known as ICP Crops). UNECE-ICP was established to consider the underlying science for quantifying damage to plants by ozone and other air pollutants [110]. Initially, UNECE-ICP was only covering the region of Europe and North-America. However, it has recently established links with countries outside the Economic Commission for Europe (ECE) region, e.g. South Asia and South Africa [114].

Mosses are bryophytes, i.e. plants that lack vascular tissue [47], with an exceptional ability to intercept, retain and accumulate pollutants [24, 115]. Bryophytes are defined as plants with a differential ability to accumulate a wide range of heavy metals and other trace elements. For this reason, mosses are generally regarded as excellent biomonitors of air pollution [116]. According to Frontasyeva [1], mosses are not just considered to be the best biomonitors of air pollution but they are also believed to be analogues of air filters. One of the essential and distinguishing attributes of mosses is that they are not attacked by micro-organisms. Hence they can be stored for long periods and be sent for inter- or intra-species examination. Furthermore, mosses do not lose any trapped elements during their storage. Hence these plants are said to be precise biomonitors of heavy metals with high sensitivity [116]. Mosses meet all the requirements imposed on them to be biomonitors. On top of that and where mosses are available, sample collection of mosses is simple and much higher sampling density can be achieved than with the conventional precipitation analysis or air sampling [1, 113]. An additional significant advantage of mosses is that they grow almost everywhere, settling successfully in almost every habitat. They survive even in habitats where most other organisms fail to survive. Instead, mosses simply hibernate when extremely dehydrated and then regain their vital functions once rehydrated [47].

When working with mosses, a moss specialist is always needed for determination or identification of species [48]. The two moss species that were exposed for 3 months in active biomonitoring in this study are; *Leptodon smithii* (see

Figure 2.10) [117] and *Pterogonium gracile* (see Figure 2.11) [118].

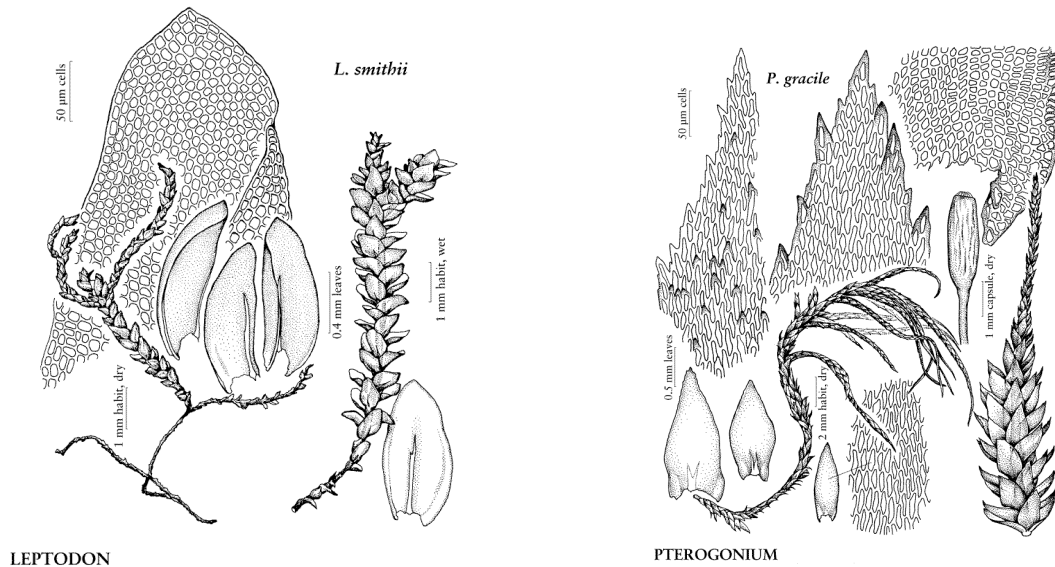


Figure 2.10: Microscopic image of *Leptodon smithii* [117].

Figure 2.11: Microscopic image of *Pterogonium gracile* [118].

2.4.2 Lichens as Biomonitors

For over 30 years, lichens have been used extensively to monitor pollution status or the health of the environment. They have been well utilised in biogeochemical prospecting [119–121]. According to Bettinelli *et al.* lichens are globally used as air pollution biomonitors, and to follow changes in air pollution patterns [122]. This is due to their potential to show metal air pollution through colour change [123], as well as their ability of to accumulate high levels of potentially toxic metals [120]. Lichen symbiosis is a successful example of two or more organisms living together; fungi (mycobiont), algae (photobiont) and/or cyanobacteria (a bacterium with a blue-green photosynthesis pigment) [108, 121, 124]. A cross-section for a typical lichen thallus is shown in Figure 2.12 [125].

Although lichens tend to accumulate air pollutants from both airborne particles as well as dissolved and suspended materials, their mechanisms of element uptake are not very well known [123]. Furthermore, more information is still

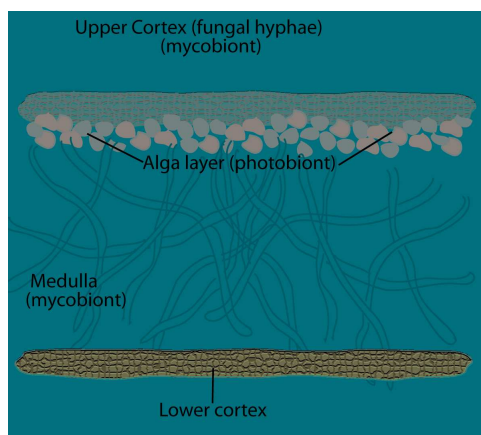


Figure 2.12: Typical lichen thallus cross section [125].

needed on certain aspects of the physiology of lichens, such as elemental distribution within their thalli [126]. Some modern analytical techniques, e.g. Proton Induced X-ray Emission (PIXE), can be used in parallel with Scanning Electron Microscope/electron probe microanalysis to provide opportunities to understand accumulation and the influence of trace and ultra-trace elements on lichens [120, 126, 127]. According to Conti and Cecchetti [108] lichens may accumulate trace element from the atmosphere via a variety of mechanisms. These include; particulate trapping, ion exchange, extracellular electrolyte absorption, hydrolysis, and intracellular uptake. However, the efficiency of element retention by lichens mainly depends on the number and nature of the extracellular binding sites, tissue age, and growth [64]. All these competing factors may significantly influence uptake and release of trace elements [123]. This is because unlike vascular plants, lichens do not have an epidermis, stomata and waxy cuticle and thus are incapable of controlling gas exchange [126]. Moreover, pH levels of the environment and metal bioavailability influence the composition of lichen clusters and play a role in metal fixation and retention on lichens [120].

Lichens are usually used in air pollution studies due to their metal fixation and retention nature as well as their differential sensitivity to environmental disturbances. As a result, the use of lichen to monitor air pollution is becoming mandatory in some European countries (Germany, Italy and Switzerland) [121, 128]. According to Garty [124], trace elements tend to settle in extra- or intra-cellular locations of a lichen and airborne metals get incorporated into lichen thalli by the interception of soluble or particulate matter. Furthermore, lichen species with finely divided thalli (e.g. *Usnea subfloridana*) are assumed to have a greater affinity for air pollutants than those species with undivided thallus (e.g. *Parmotrema perlatum*). Two lichen species that were exposed for 3 months in active biomonitoring in this study are shown in Figure 2.13. These are *Usnea subfloridana* and *Parmotrema perlatum* [129].



Figure 2.13: *Usnea subfloridana* and *Parmotrema perlatum* on a tree [129].

Most lichens remain unharmed by air pollutants, but different lichen species vary in their sensitivity as well as their ability to accumulate air pollutants. Lichen species growing on trees are less affected by the substrate than those growing on rocks. Therefore, lichens growing on trees are more useful and valuable in identifying air pollution sources both regionally and nationally. This is because the analysis of metals in lichens offers the possibility to identify the source of those metals as well as how far are they dispersed, especially if metals are associated with a particular industry [121, 126]. Besides their ability to accumulate mineral elements far above their need, lichens possess an extraordinary capability to grow in abundance in most geographical areas and that ranks them among the best air pollution biomonitors [124]. According to Purvis and Pawlik-Skowrońska [120], lichens survive abundantly even in areas traditionally regarded as highly toxic where few, if any, higher plants survive.

2.5 Analytical Techniques Used in Air Pollution Biomonitoring

Nuclear physics and classical analytical techniques routinely used in biomonitoring studies include INAA, ICP-MS/AES, AAS, XRF, PIXE (charged particle induced X-ray emission analysis), synchrotron radiation analysis, etc. [1, 23, 110, 130, 131]. Since nuclear physics techniques (e.g. INAA) are based on principles fundamentally different from those of other analytical techniques (e.g. ICP-MS), they are distinctly useful in method validation studies as they are less likely to be prone to the same systematic errors. However, their main drawbacks are that they are expensive, difficult to calibrate, and have a relatively low throughput. Furthermore, the main aspects that have to be consid-

ered when selecting a proper analytical method are; multi-element capability, sensitivity, accuracy and precision, analysis costs, sample characteristics, and availability [16, 23, 130]. De Bruin [23] did a comparison of a few analytical techniques that are commonly used in biomonitoring of air pollution. In his work, he mentions that INAA is preferred because of its high accuracy, followed by ICP-MS/AES (provided matrix can be dissolved easily). However; AAS is basically a single-element based technique and that makes it less suited for multi-element analysis, whereas PIXE's micro-beam makes it less suited for accurate bulk analysis. Moreover; XRF offers limited sensitivity due to the surface area of a sample being analysed with a large excitation beam [1, 23, 130, 131]. A comparison of these techniques is shown in Table 2.3, where the "+" refers to capability and/or advantage of the technique and "-" refers to non-capability and/or disadvantage [23].

Table 2.3: *Applicability of analytical techniques in biomonitoring heavy-metal air pollution [23].*

Technique	Aspects				
	Multi-element capability	Sensitivity	Accuracy & precision	Costs & Availability	Sample features
INAA	+	+	+	+/-	+
ICP-MS	+	+	+	+	+/-
ICP-AES	+	+	+	+	+/-
PIXE	+	+/-	+/-	- & +/-	+
AAS	-	+	+	+	+/-
XRF	+	-	+	+	+

Nuclear physics techniques are generally found to be more sensitive than any other method. This is because they provide very low detection limits (down to the 10^{-15} g.g⁻¹ (ppt) level) [1, 130]. Very low detection limits are very important when determining trace elements in biological samples during the multi-element analysis of pollutants in ambient air [130]. This led to the development of nuclear techniques with analytical capabilities to perform accurate measurements of heavy metals in environmental matrices. These nuclear techniques were developed in order to assess compliance with legislative limits that equate to element mass fractions of 10^{-10} g.g⁻¹ (0.1 ppb) and below. This is a requirement mainly driven by international legislations on reducing the allowable concentration of pollutants in the atmosphere to ultra-trace levels [130]. Some common detection limits in quantitative analysis of element are dramatically shown in Figure 2.14; where INAA's detection limits range between

$10^{-12} \text{ g.g}^{-1}$ and $10^{-15} \text{ g.g}^{-1}$, while ICP-MS's detection limits are between $10^{-10} \text{ g.g}^{-1}$ and $10^{-13} \text{ g.g}^{-1}$.

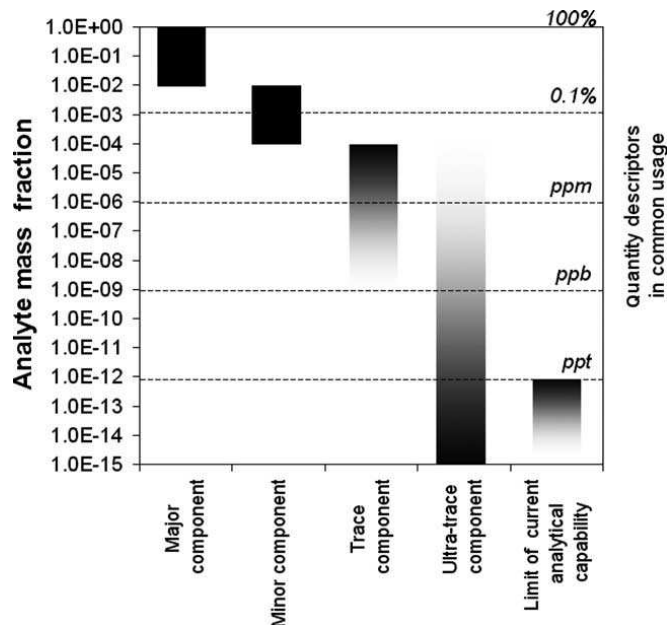


Figure 2.14: Common demarcations in quantitative analysis [130].

Air pollution studies require a multi-element analysis over a wide range of concentrations from a potentially large number of samples and not all analytical techniques are well suited for them. However, INAA and ICP-MS appear to be commonly used for mineral pollutants from the mines [16, 132]. Even though these techniques differ greatly in their operating principle, they both offer well accepted sensitivity for the determination of multiple elements and isotopes [16, 23, 110]. According to Brown [130], "a single method is no method at all". Hence, INAA and ICP-MS were both used in this study. Thus, further and detailed discussions on INAA and ICP-MS will follow. Note also that INAA was considered the main technique of this study, hence in-depth discussion on this method will be given. Table 2.4 gives a more concise comparison of INAA and ICP-MS for the determination of elements in biological samples [16].

Table 2.4: INAA and ICP-MS comparison for the determination of elements [16].

Elements	Method	Comments
Li, B, Y, Nb, Tl Pb, Gd, Ho, Er, Tm	ICP-MS	INAA not applicable.
Mg, Al, Ti, V, Dy	INAA and ICP-MS	Short time irradiation required for INAA.
Continued on next page		

Table 2.4 –continued from previous page		
Elements	Method	Comments
		Oxide dissolution (Al_2O_3) difficult for ICP-MS.
Ca	INAA and ICP-MS	Poor sensitivity by INAA: γ -ray at 1297 keV. Interferes with the γ -rays of ^{59}Fe , ^{60}Co , ^{182}Ta .
Sc	INAA	Ca and Ti concentrations conceal Sc concentrations in ICP-MS. γ -ray at 889.3 keV very selective in INAA.
Cr, Fe	INAA and ICP-MS	Oxide dissolution difficult and mass interference for ICP-MS.
Ni	ICP-MS	Poor sensitivity using (n, γ) reaction. Better results obtained by (n,p) reaction which requires a special irradiation.
Cu	ICP-MS	Poor sensitivity in INAA. radiochemical separation required.
Zn	INAA and ICP-MS	Blank value difficult to control in ICP-MS.
As	INAA and ICP-MS	Loss risks during the dissolution in ICP-MS.
Rb, Ag, Th	INAA and ICP-MS	
Sr	ICP-MS	Poor selectivity of 514 keV γ -ray in INAA.
Zr	INAA	Interference risk with uranium fission in INAA. Oxide dissolution (ZrO_2) difficult in ICP-MS.
Mo	ICP-MS	Interference with uranium fission and poor sensitivity in INAA.
Cd	INAA and ICP-MS	Poor sensitivity in INAA.
Sn	ICP-MS	Poor sensitivity in INAA.
Co, Sb, Cs, Au, Sm	INAA	Determination accurate and sensitive by INAA.
Continued on next page		

Elements	Method	Comments
Eu, Tb, Yb, Lu		
Ba	INAA and ICP-MS	Poor selectivity of 496 keV γ -ray in INAA
Hf, Ta	INAA	Oxide dissolution difficult for ICP-MS.
W, Pr	INAA and ICP-MS	INAA not convenient for samples having high sodium concentration.
U	INAA and ICP-MS	Possibility to use delayed neutrons to increase the INAA sensitivity.
La, Ce	INAA and ICP-MS	Interference risk with U fission in INAA.
Nd	INAA and ICP-MS	Poor selectivity of 531 keV γ -ray in INAA.

Additionally, Figure 2.15 shows a number of elements which are comparatively determined by INAA and ICP-MS when mosses are used as biomonitors.

H																				He
◦Li	◦Be												◦B	C	N	O	F			Ne
◦Na	◦Mg												◦Al	Si	P	S	Cl			Ar
◦K	◦Ca	◦Sc	◦Ti	◦V	◦Cr	◦Mn	◦Fe	◦Co	◦Ni	◦Cu	◦Zn	◦Ga	Ge	◦As	◦Se	Br				Kr
◦Rb	◦Sr	◦Y	Zr	◦Nb	◦Mo	Tc	Ru	Rh	Pd	◦Ag	◦Cd	In	◦Sn	◦Sb	◦Te	I				Xe
◦Cs	◦Ba	◦La	◦Hf	◦Ta	◦W	Re	Os	Ir	Pt	◦Au	◦Hg	◦Tl	◦Pb	◦Bi	Po	At				Rn
Fr	Ra	Ac												Rf	Db	Sg	Bh			Hs
		◦Ce	◦Pr	◦Nd	Pm	Sm	Eu	◦Gd	Tb	◦Dy	◦Ho	◦Er	◦Tm	Yb	Lu					
		◦Th	Pa	◦U	Np	Pu	Am	Cm	Bk	Cf	Es	Fm	Md	No	Lw					

Figure 2.15: Elements comparatively determined by INAA (◻) and ICP-MS (◦) when using mosses. Closed symbols (◼ and ◐) indicate the preferred method for the element in question [133].

2.5.1 Neutron Activation Analysis

NAA can be defined as a sensitive multi-element analytical technique used to perform the qualitative and quantitative analysis of major, minor, trace and rare elements in samples from almost every conceivable field of scientific or technical interest. As mentioned earlier, the activation of elements by neutrons during NAA is followed by detection of the gamma radiation emitted during the decay of these radioactive nuclei [5, 11, 12, 67]. NAA comprises of two categories: prompt gamma-ray neutron activation analysis (PGNAA) and delayed gamma-ray neutron activation analysis (DGNAA), which are characterised by the time of decay [6]. In PGNAA, measurement of γ -rays takes place during irradiation as shown in Figure 2.16. In DGNAA, irradiated samples are first allowed to undergo radioactive decay before γ -ray measurements can take place (see Figure 2.17).

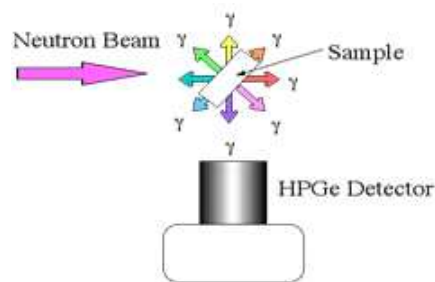


Figure 2.16: Typical PGNAA setup [134].

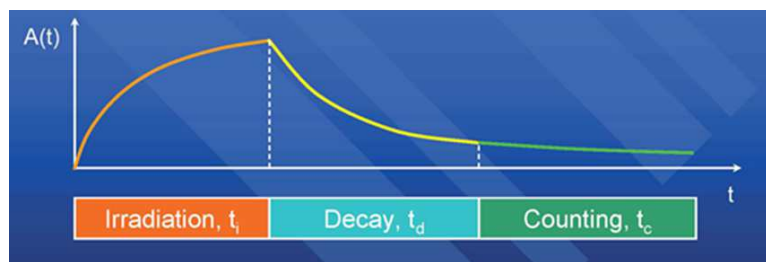


Figure 2.17: DGNAA activity/time graph; showing irradiation time (t_{irr}), decay time (t_d) and counting (measurement) time (t_c) [6].

In NAA, activated samples can be analysed either by a destructive (radiochemical) neutron activation analysis (RNAA) or by a non-destructive (instrumental) neutron activation analysis (INAA). In RNAA, the resulting radioactive sample is chemically decomposed and the elements are chemically separated, whereas in INAA (used in this study), the resulting radioactive sample is kept intact, and the radionuclides are determined by taking advantage of their different decay rates via measurements at different decay intervals using γ -ray detector with high energy resolution [5].

When radioactive nuclei decay from excited states to more stable states, a list of possible decay modes include: [5, 86]

- (i) β -decay (β^+), (β^-),
- (ii) proton, neutron emission,
- (iii) α -decay,
- (iv) fission (e.g. $^{242}\text{Cm} \rightarrow ^{148}\text{Ce} + ^{92}\text{Sr} + 2\text{n}$),
- (v) electron capture,
- (vi) internal conversion, and
- (vii) emission of gamma-rays (mass-less high energy electromagnetic radiation called photons).

By measuring the number of nuclear decays per time, generally known as the activity, nuclei changes can be studied and the formula for activity is given by equation (2.5.1) below [5, 86].

$$A = N\sigma\phi[1 - e^{-\lambda t_{irr}}], \quad (2.5.1)$$

where; A is the activity or the decay rate (in decays/s),
 $N \rightarrow$ the number of atoms of the target isotope,
 $\lambda \rightarrow$ the decay constant,
 $\phi \rightarrow$ the neutron flux ($\text{n.cm}^{-2}.\text{sec}^{-1}$),
 $\sigma \rightarrow$ the activation cross-section, (cm^2) and
 $t_{irr} \rightarrow$ the irradiation time (s).

However, after a delay time t_d activity is given by equation (2.5.2).

$$A = N\sigma\phi[1 - e^{-\lambda t_{irr}}]e^{-\lambda t_d}. \quad (2.5.2)$$

And for counting time t_c , the activity is given by equation (2.5.3).

$$A = N\sigma\phi[1 - e^{-\lambda t_{irr}}]e^{-\lambda t_d}[1 - e^{-\lambda t_c}]. \quad (2.5.3)$$

Furthermore by comparing the activity induced in a standard of known weight (in g) to that of the unknown, the weight of the elements in the unknown sample can determined using equation (2.5.4) below [70]:

$$\frac{\text{Weight}_{standard}}{\text{Weight}_{unknown}} = \frac{A_{standard}}{A_{unknown}}, \quad (2.5.4)$$

where; $A_{standard}$ is the activity of an isotope of an element in the standard, and $A_{unknown}$ is the activity of the isotope of the same element in the measured sample.

2.5.2 Inductively Coupled Plasma-Mass Spectrometry

ICP-MS is defined as an accurate analytical technique for simultaneous determination of almost all elements in a single sample with very low detection limits for most elements [132] (also see subsection 1.1.2 and Chapter 1). This works as an advantage in reducing the sample analysis time. Even though ICP-AES and AAS have been used instead of ICP-MS in a number of studies; AAS does not provide simultaneous multi-elemental detection, and ICP-AES has been found to be generally less sensitive than ICP-MS. Furthermore, ICP-MS is capable of performing a rapid multi-element scanning over a wide range of masses across the periodic table with lower detection limits which are 100 to 1000 times superior to those achieved by AAS and ICP-AES. The mass spectra of chemical elements makes ICP-MS a quick tool for automated qualitative and quantitative analysis with extremely low detection limits ranging from parts per billion (ppb) to parts per trillion (ppt) for most elements [15, 135]. The detection limits generally depend on the element, sample matrix, sample preparation, and the instrumental conditions used for analysis [135]. However, ICP-MS can be used in a large variety of environmental samples. ICP-MS strengths include the following [14, 16];

- dynamic range (constant change of levels from ppm levels to percentage levels in the same analytical run) and elemental coverage,
- performance (high sensitivity and low background signals),
- fast analysis time (speed),
- isotopic information, and
- easy access and high sample throughput.

During ICP-MS measurements, the sample is typically introduced into the ICP as an aerosol, produced either by passing a liquid or dissolved solid sample into a nebulizer or by using a laser to directly convert solid samples into an aerosol. Once the sample aerosol is introduced into the ICP torch, it is completely desolvated (subjected to desolvation) and the elements in the aerosol are vaporised and converted first into gaseous atoms and then ionized towards the end of the plasma. After the conversion of elements in the sample into positively charged ions, the ions are brought into the mass spectrometer via a pair of interface cones (the sampler and the skimmer); which are metal plates with central orifices through which the ions pass. Since the ions coming from the system are positively charged, electrostatic lenses (also positively charged) keep the ions focused in a compact ion beam as they pass through the vacuum system to the final chamber, where the mass spectrometer and detector are housed. Ion lenses also separate the ions from the photons and residual neutral material. Once the ions enter the mass spectrometer, they are separated according to their mass-to-charge (m/z) ratios by a quadrupole mass filter. In a quadrupole mass filter, alternating AC and DC voltages are applied to opposite pairs of the rods. The ratio of the DC and AC electrical fields is fixed but the voltages can be switched at a very rapid rate. For a given voltage setting, only

one m/z is stable, therefore; the electrostatic filter allows ions of a single m/z ratio to sequentially pass through the rods to the detector at a given instant in time. Each ion is then detected by the electron multiplier as it exits the quadrupole. The total signal for each mass (m/z) is then counted and stored by the detector electronics, creating a mass spectrum which provides a simple and accurate qualitative representation of the sample as shown in Figure 2.18. The enlargement in the figure shows isotopes of lead (Pb), present at 10 ppb [14]. Each peak magnitude is directly proportional to the concentration of an element in a sample and quantitative results are produced by comparing signal intensities to those generated by calibration standards. Since the plasma produces almost exclusively singly-charged ions, the m/z ratio is equal to the mass of the ion, making the spectrum very simple to interpret. The use of high resolution or magnetic sector mass spectrometers allows the elimination or reduction of the interference effects due to mass overlap [14, 17, 18].

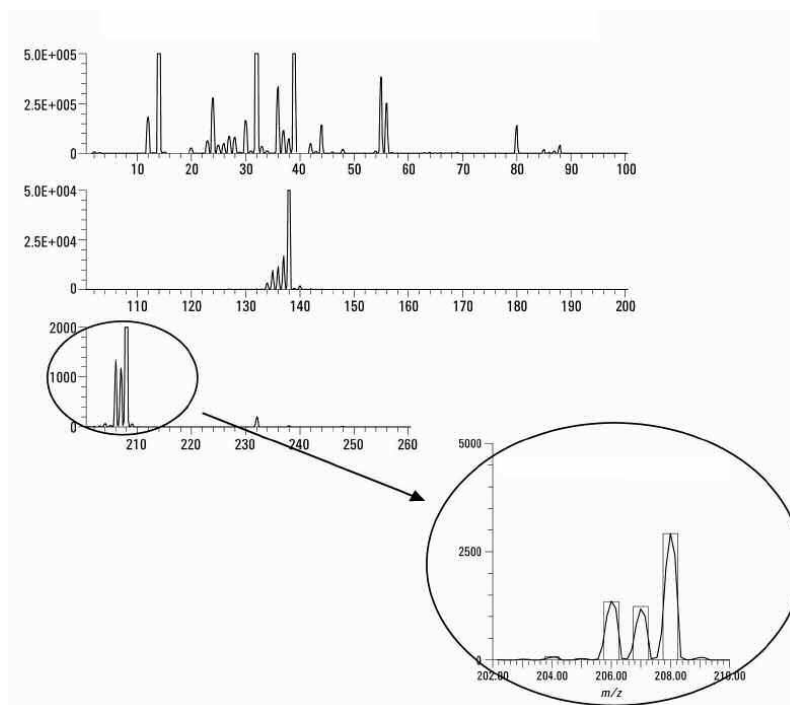


Figure 2.18: An ICP-MS spectrum showing relative abundances of elemental constituents. [14].

2.6 Advantages and Disadvantages of INAA and ICP-MS

Nuclear and related physics techniques are found to be the most sensitive techniques to analyse biological and environmental samples and they are currently preferred over classical methods of analytical chemistry [1]. Some of these techniques are listed in section 2.5. Since INAA and ICP-MS were used in the analysis of samples in this study, their major advantages as well as their disadvantages (merits and limitations) are listed in the next subsections.

2.6.1 Merits and Limitations of INAA

INAA is the most effective method in multi-element analysis of a great deal of samples and determination of elemental concentrations of the order of ppm ($10^{-6}g.g^{-1}$). The major limitation of INAA is the limited availability of nuclear reactors or accelerators; which are required for sample irradiation [132]. INAA merits that make it a preferred method of choice are listed below [1, 4, 69].

- (i) The non-destructive nature. Samples are not converted into solutions prior to analysis. No risk of sample contamination with reagents or their incomplete dissolution.
- (ii) Easy sample preparation procedure for analysis. No sample pre-treatment steps involved.
- (iii) Nuclear technique. Final results are not influenced by chemical or physical state of the elements because the method focuses in the nuclei of the elements.
- (iv) Involves utilisation of gamma rays, which are highly energetic compared to X-rays and are less readily absorbed. This makes it possible to eliminate systematic errors and minimize the effect of the sample type (e.g. soil, plant, water, etc.) due to self-absorption.
- (v) Good accuracy, about $(15 \pm 5)\%$, high precision and sensitivity.
- (vi) Ease of preparation of standards for comparison.
- (vii) Obtainable detection limits for many elements are in ppm to ppb range.

2.6.1.1 Sensitivity of INAA

Sensitivity in INAA determines the level of smallest degree to which a particular element can be detected in a specific sample of interest [69, 70]. Depending upon the experimental procedure, more than 30 elements can be simultaneously detected by INAA and given INAA's excellent sensitivity, the analysis of up to 70 elements is possible [69, 70]. According to Glascock, [12], INAA provides sensitivities that are on the order of parts per million (ppm) to parts per billion (ppb) and even better, depending on the element under investigation. Furthermore, INAA sensitivity is dependent upon the following factors: 1. irradiation parameters (neutron flux, irradiation time and decay time),

2. measurement conditions (measurement time and detector efficiency), and
3. nuclear parameters of the elements being measured (isotope abundance, neutron cross-section, half-life, and gamma-ray branching ratios).

Heavy elements have a higher sensitivity to INAA because they have larger nuclei and thus have larger neutron capture cross-section [69]. Table 2.5 gives the list of approximate sensitivities for determination of different elements [12].

Table 2.5: *List of approximate sensitivities for determination of elements, assuming interference free spectra and irradiation in a reactor neutron flux of $1 \times 10^{13} n.cm^{-2}.s^{-1}$ [12].*

Sensitivity (picograms)	Elements
10^0	Dy, Eu
$10^0 - 10^1$	In, Lu, Mn
$10^1 - 10^2$	Au, Ho, Ir, Re, Sm, W
$10^2 - 10^3$	Ag, Ar, As, Br, Cl, Co, Cs, Cu, Er, Ga, Hf, I, La, Sb, Sc, Se, Ta, Tb, Th, Tm, U, V, Yb
$10^3 - 10^4$	Al, Ba, Cd, Ce, Cr, Hg, Kr, Gd, Ge, Mo, Na, Nd, Ni, Os, Pd, Rb, Rh, Ru, Sr, Te, Zn, Zr
$10^4 - 10^5$	Bi, Ca, K, Mg, P, Pt, Si, Sn, Ti, Tl, Xe, Y
$10^5 - 10^6$	F, Fe, Nb, Ne
10^7	Pb, S

2.6.1.2 Accuracy in INAA

Accuracy is defined as the measure of how close the measured value is to the true value, which is determined by measuring certified reference materials (CRMs) or standard reference materials (SRM) [86]. In determining elements concentration using INAA method, the accuracy usually ranges between 10 to 20 percent of the reported value [12]. According to Bode [4]; the quality of the catalogue of gamma-ray energies, the gamma-ray intensity ratios and the knowledge of nuclear transformations involved in radionuclide production governs the qualitative accuracy (i.e. identification of elements) in INAA. This qualitative accuracy may be affected by the following factors:

- (i) peak assignments to erroneous radionuclides, which is due to instrumental drift of the spectrometer from calibration conditions,
- (ii) gamma-ray spectrum interferences (e.g. narrowly spaced peak, and sum peaks and self-absorption phenomena), and
- (iii) under-estimated interferences of nuclear reactions, e.g., $^{27}\text{Al}(n,\gamma)^{28}\text{Al}$; $^{28}\text{Si}(n,p)^{28}\text{Al}$, $^{31}\text{P}(n,\alpha)^{28}\text{Al}$ or $^{26}\text{Mg}(n,\gamma)^{27}\text{Mg}$ and $^{27}\text{Al}(n,p)^{27}\text{Mg}$ [13]. Cross-section data versus the neutron energies for these interfering reactions is plotted in Figure 2.19.

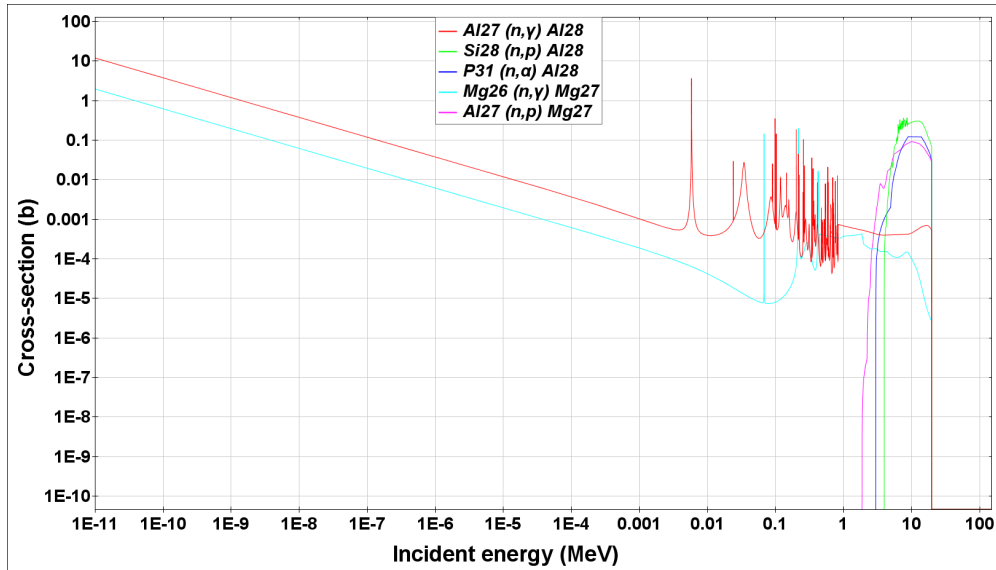


Figure 2.19: Reaction cross-section plots showing the under-estimated interferences of nuclear reactions during NAA measurements [77].

However by taking into consideration the half-lives of radio-nuclides, the effects of the above factors can be minimised or even reduced to zero for a number of nuclides for which such situations may occur. Due to the fact that the analytical results are estimates of the true values, uncertainties have to be included in the results. The additional advantage that adds to the INAA's accuracy is that the principle is based on effects taking place inside the nucleus therefore, the results are not affected by the chemical or physical state of the elements. Furthermore, when processing small samples in INAA, errors due to neutron and gamma-ray self-absorption as well as neutron self-thermalization can be neglected [4]. According to IAEA [136], INAA's estimate of the accuracy can be obtained by comparing the results of an analysis of certified reference materials with the data in the certificates. That accuracy is expressed as a standardized difference 'z', as shown in equation (2.6.1), thus taking into account the uncertainties of the obtained result and the uncertainty in the certified value:

$$z_i = \frac{C_i - C_{ref,i}}{\sqrt{\sigma_i^2 + \sigma_{ref,i}^2}}, \quad (2.6.1)$$

where; C_i , σ_i = the observed concentration and uncertainty (standard deviation), respectively.

$C_{ref,i}$, $\sigma_{ref,i}$ = the reference material concentration and uncertainty, respectively.

However if the element under consideration is one of a few elements that have no reference materials available with certified concentrations, indication of the

degree of accuracy may be obtained by participation in laboratory intercomparison rounds or proficiency testing [4].

2.6.2 Merits and Limitations of ICP-MS

Apart from the simultaneous determination of almost all elements in a single sample and thus greatly reducing the sample analysis time, ICP-MS does not require any nuclear facilities and there is no handling of radioactive waste required after the analysis. Furthermore, ICP-MS can determine some environmentally meaningful elements, such as Pb, Cd, Cu, etc. that could not be routinely determined by INAA [1, 16, 132, 137–139]. The non-compatibility of INAA for some elements is possible due to the following [1, 16];

1. if the elements produce no usable radionuclides after irradiation (i.e. if the produced γ -ray intensities are too low);
2. if the (n,γ) products do not emit γ -rays (e.g., ^{49}Ca);
3. if the half-lives of the reaction-products are too short or excessively long for accurate and sensitive measurements;
4. if the element produces too many isotopes, or if the element produces stable isotopes;
5. if the cross section for the (n,γ) reaction is too small;
6. if the element is likely to go through volatilization during sample irradiation e.g. Hg.

However, ICP-MS appears to be less accurate than INAA and this is due to contamination risks from the reagents during digestion (sample preparation) with strong acids. This is a crucial step for total element concentration measurements. Furthermore, ICP-MS is subject to mineral matrix effects and formation of polyatomic ions which lead to isobaric interferences [16, 132]. Examples of interferences include the following; $^{35}\text{Cl}^{16}\text{O}^+$ on $^{51}\text{V}^+$, $^{40}\text{Ar}^{12}\text{C}^+$ on $^{52}\text{Cr}^+$, $^{23}\text{Na}^{40}\text{Ar}^+$ on $^{63}\text{Cu}^+$, $^{40}\text{Ar}^{35}\text{Cl}^+$ on $^{75}\text{As}^+$, $^{40}\text{Ar}^{16}\text{O}^+$ on $^{56}\text{Fe}^+$, $^{40}\text{Ar}^{38}\text{Ar}^+$ on $^{78}\text{Se}^+$, etc. These interferences can be reduced by adding a collision gas, such helium (He), to the small internal volume cell containing an octupole reaction system and mounted on-axis to the quadrupole for high ion transmission. This is because the interaction between polyatomic ions and the cell gas leads to the removal of interference from the mass spectrum, thereby improving the resolution.

2.7 Uncertainties Associated with Biomonitoring of Air Pollution

For any experimental results, it is important to express the extent to which the results can be relied on for the purpose at hand. This is done by understanding and indicating relevant uncertainties or errors associated with the results. In

biomonitoring, uncertainties may arise from environmental conditions, sampling, uncertainties of masses and volumetric equipment, matrix effects and interferences during the experiment, reference values, approximations and assumptions incorporated in the measurement method and procedure, as well as from data collection and analysis. Uncertainties associated with sampling due to human or natural irregularities cannot be eliminated. The quality of the experimental data depends on how precise and accurate the measurements have been conducted. Precision is a measure of how reproducible/repeatable the measurement is, and accuracy is a measure of how close the measured value is to the true/accepted value [140, 141].

In general, the types of errors associated with air pollution biomonitoring techniques can be divided into two [1, 44, 140–142]:

1. systematic uncertainties - these are not easy to detect. They mainly arise from built-in errors in the instrument (in design or calibration), systematic changes caused by inadequate control of experimental conditions, contamination of samples, moisture content in samples and errors in determination of concentrations of elements in the standard. During NAA measurements, systematic errors also arise from self shielding of neutrons by the sample, thermalization of neutrons in the sample due to occurrence of light elements in its matrix, variation in detector photopeak detection efficiency, background radiation, absorption of γ -rays in the sample, as well as errors in determination of time intervals in the analysis. These errors may also arise from difference in neutron flux at irradiation of samples and the standard, γ -ray counting rate, difference in γ -ray flux at measurement of samples and the standard, inhomogeneity of the sample, and the difference in matrix between samples and the standard.

2. random uncertainties - these may arise from fluctuations in physical parameters due to the statistical character of a particular phenomenon of the experiment (e.g. variations in scale readings).

Some of these errors can be eliminated, e.g. human errors which may arise from sampling, the misreading of scales and handling of spectra. However, some errors like changes in composition of samples while they are being prepared for analysis and dried as well as errors involved in determination of all samples cannot be eliminated. These include the evaporation of some volatile elements and the contamination of sample with alien elements during the experiments.

Chapter 3

Experimental Methods

Two types of biomonitoring (passive and active) were performed for different areas in the Western Cape Province of South Africa. This chapter describes the procedures and methods used to collect data for both INAA and ICP-MS measurements in this study. It also gives a detailed description of the experimental setup that was used to perform INAA measurements (main technique for this study). For ICP-MS measurements (secondary measurements), samples were sent to the ICP-MS Laboratory of the Central Analytical Facilities (CAF) at Stellenbosch University. The author of this thesis was involved in the sample preparation as well as results interpretation and discussion processes. The customized maps for this study were created using Google Earth mapping program (software version: 7.1.5.1557) [143].

3.1 Sampling

Mosses and lichens were collected from seven areas around the province and analysed by both INAA and ICP-MS. Where possible, sampling was performed in accordance with the guidelines specified in the monitoring manual for atmospheric deposition of heavy metal deposition using bryophytes, prepared by UNECE-ICP on Effects of Air Pollution on Natural Vegetation and Crops [110]. Some of these guidelines are listed below.

1. Mosses should be collected in moist areas as they are hard to find in dry areas. Moreover, mosses are said to accumulate and retain the highest number of pollutants under wet conditions [1, 110].
2. Sampling points should be at least 300 m away from main roads, industries and villages and at least 100 m away from minor roads.
3. Sampling must not be done on slopes with running water.
4. Where possible, sampling below large-leafed trees must be avoided in order to reduce through-fall effects from forest canopy.
5. Sampling dates, the names of sampling locations as well as the geographic co-ordinates of sampling points should be recorded.

6. Photographs of sampling points as well as the samples should be taken.
7. To collect mosses and lichens, disposable (non-powdered) plastic gloves were used.
8. For moss and lichen storage, both plastic and paper bags should be used.
9. To detach biomonitors which were too fixed on their substrates, plastic knives (in order to avoid metal contamination from stainless steel knives) were used.
10. Samples should be air-dried and stored at room temperatures until the analysis.

3.1.1 Sample Collection - study area and sample collection

Situated in the south-western part of SA (as shown in Figure 3.1 [144]), Western Cape is the fourth largest of the nine SA provinces in terms of area and the third largest in terms of population [145].



Figure 3.1: *Western Cape location in South Africa, Western Cape represented in red. [144].*

The Western Cape exhibits diverse climatological conditions influenced by both the Indian (warm water) and Atlantic (cold water) oceans. The part of the Western Cape province where this study was conducted is considered to have a Mediterranean climate with cool and wet winters as well as warm and dry summers. The Western Cape province weather starts cooling down with light rain in March (beginning of autumn season), making way for rainy winter season (from June until August). After that, it starts warming up in September (beginning of spring season), followed by a much warmer summer which goes on until the end of February. The Western Cape is also famous for its fynbos which is rich in species diversity, with Table Mountain providing more plant species than the entire United Kingdom (UK) [145].

3.1.1.1 Site Description for Passive Biomonitoring

As shown in Figures 3.2 and 3.3, sampling sites for passive biomonitoring in this study comprised of; urban (Stellenbosch town), suburban (Franschhoek), coastal (False Bay) and mountainous areas (Coetzenburg Mountain) as well as nature reserves (e.g. Jan Marais local nature reserve in Stellenbosch). Assuming Marais Road is the area source of pollution due to vehicle emission, samples at Jan Marais local nature reserve were collected from different trees in order to check the effect of distance from the road. The illustration of how the trees were distributed is shown in Figure 3.4.

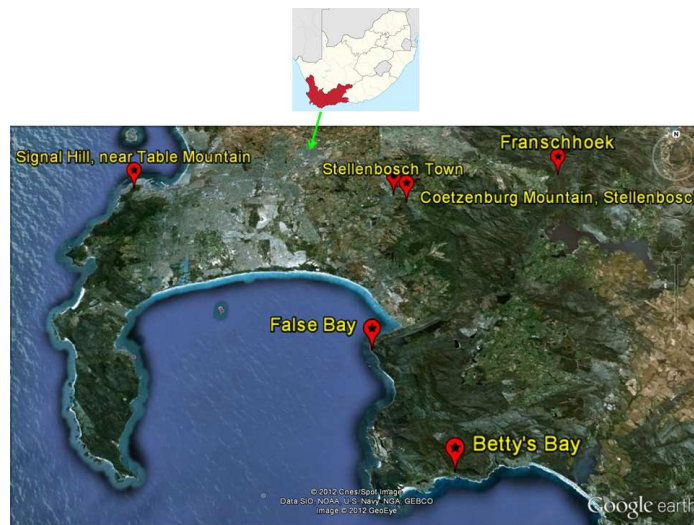


Figure 3.2: *Passive biomonitoring sampling sites around the Western Cape province.*



Figure 3.3: *Passive biomonitoring sampling sites in Stellenbosch.*

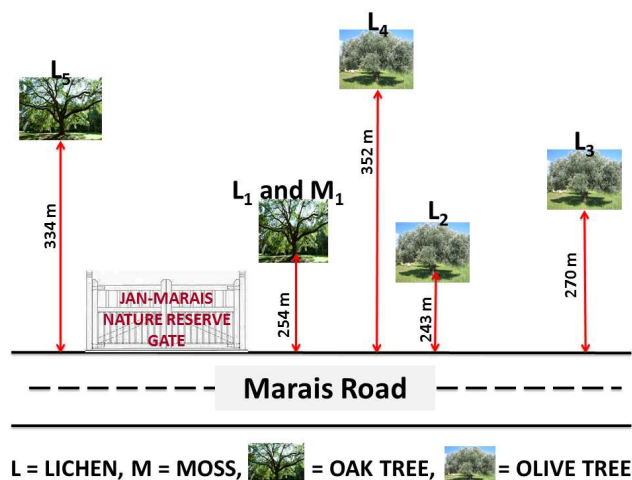


Figure 3.4: Illustration of the sampling grid at Jan-Marais nature reserve.

Samples of mosses and lichens for passive biomonitoring were collected during March-April 2012. The rationale behind the selection of sampling sites was to get samples from diverse potential pollution sites; i.e. urban, suburban, coastal and mountainous. A summary of sampling locations for passive biomonitoring in 2012 is given by Table 3.1. More details on the samples collected are given in Appendix A.

Table 3.1: A summary of sampling locations for passive biomonitoring performed in 2012.

Location	Collection Date	Collected Samples
Stellenbosch Town (i.e. Victoria Street and Jan Marais Nature Reserve)	14 March	5 mosses 7 lichens
Coetzenburg Mountain	28 March	7 mosses 4 lichens
Signal Hill	02 April	2 lichens
Franschhoek	03 April	1 moss 1 lichen
Betty's Bay	05 April	3 mosses 1 lichen
False Bay	05 April	1 moss 1 lichen

Some of the sampling photos for each sampling location are shown in Figures 3.5 - 3.10.



Figure 3.5: *Stellenbosch sampling.*



Figure 3.6: *Coetzenburg sampling.*



Figure 3.7: *Signal Hill sampling.*

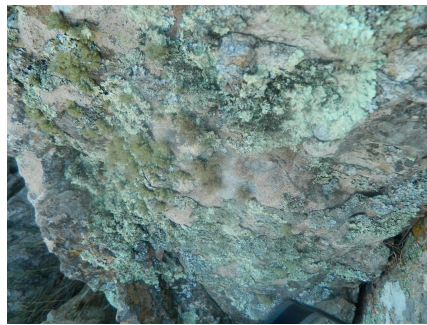


Figure 3.8: *Franschhoek sampling.*



Figure 3.9: *Betty's Bay sampling.*



Figure 3.10: *False Bay sampling.*

3.1.1.2 Site Description for Active Biomonitoring

For active biomonitoring in this study, two moss species (*Pterogonium gracile* and *Leptodon smithii*) as well as two lichen species (*Usnea subfloridana* and *Parmotrema perlatum*) were used. The two moss species that were exposed for 3 months in active biomonitoring in this study were identified by a bryologist in the department of botany, University of Cape Town [146]. Those species were chosen because they were the only species that could be found in abundance in one of the pristine areas in the Western Cape. Mosses and lichens were collected from the pristine area close to Montagu. Figure 3.11 shows our active biomonitoring sampling site (Montagu, South Africa), as well as the sites where samples were deployed for monitoring purposes (Stellenbosch University, Huguenot Tunnel and Vredenburg). More details on the samples collected are given in Appendix E.



Figure 3.11: Active biomonitoring sampling site and the monitored areas.

3.1.2 Preparation and Deployment of Moss- and Lichen-Bags for Active Biomonitoring

Collected moss and lichen samples were taken to the laboratory where they were air-dried and cleaned from soil and/or external plant material. Moreover, samples were manually homogenised by stirring the collected material. Moss-

and lichen-bags were prepared by weighing about 3 g dry weight (Figure 3.12), and loosely packing it in nylon nets of about 10 cm × 10 cm with mesh area of 1 mm² (Figure 3.13).



Figure 3.12: Weighing mosses before packing.



Figure 3.13: Mesh bags for packing samples.

Nine bags of each species i.e. *Leptodon smithii*, *Pterogonium gracile*, *Usnea subfloridana* and *Parmotrema perlatum*, were prepared for deployment in the Huguenot tunnel (36 bags in total). However, only 3 species i.e. *Leptodon smithii*, *Pterogonium gracile* and *Usnea subfloridana* were prepared for Stellenbosch and Vredenburg (27 bags in total for each site). Enough *Parmotrema perlatum* could not be found for deployment at all three sites. Figure 3.14 shows examples of the prepared moss- and lichen-bags.



Figure 3.14: Packed lichen- and moss- bags.

Prepared moss and lichen-bags were deployed for three months on the roof-top of one of the Stellenbosch University buildings (33° 55' 57.8028" S, 18° 51' 55.3674" E) and on the roof-top of a private home at Vredenburg (32° 55' 29.12" S, 17° 58' 24.74" E), as well as at about 3 m above the ground inside Huguenot tunnel (33° 44' 2" S, 19° 5' 47" E). Inside the tunnel, samples were deployed at the first vehicle cross cutting (VCC1), which is about 1 km from the western entrance (in the direction Cape Town to Worcester) of the tunnel. Table 3.2 shows a summary of prepared sample bags for active biomonitoring.

Table 3.2: Summary of prepared sample bags for active biomonitoring.

Biomonitor	Species	Deployment Station	No. of Bags
Moss	<i>Leptodon smithii</i>	Stellenbosch	9 bags
		Huguenot Tunnel	9 bags
		Vredenburg	9 bags
Moss	<i>Pterogonium gracile</i>	Stellenbosch	9 bags
		Huguenot Tunnel	9 bags
		Vredenburg	9 bags
Lichen	<i>Usnea subfloridana</i>	Stellenbosch	9 bags
		Huguenot Tunnel	9 bags
		Vredenburg	9 bags
Lichen	<i>Parmotrema perlatum</i>	Huguenot Tunnel	9 bags

All bags at Stellenbosch and Vredenburg were deployed in such a way that the moss and lichen samples were totally exposed to wind and precipitation. While the ones in the Huguenot tunnel were deployed in such a way that the moss and lichen samples were totally exposed to traffic emissions. The exposure period for samples in Stellenbosch, Vredenburg and Huguenot tunnel were August 2013 - November 2013, September 2013 - December 2013 and October 2013 - January 2013; respectively (see Table 3.3).

Table 3.3: Details of the stations and exposure time for active biomonitoring.

Station	Deployed	1 st Collection	2 nd Collection	3 rd Collection
Stellenbosch	19/08/2013	19/09/2013	19/10/2013	19/11/2013
Vredenburg	18/09/2013	22/10/2013	19/11/2013	18/12/2013
Tunnel	11/10/2013	11/11/2013	13/12/2013	15/01/2014

The designed structures that were used to hang the bags are shown in Figures 3.15 - 3.17. Three bags of each species of biomonitor were collected after each month of exposure.



Figure 3.15: *Exposed samples at Stellenbosch.*



Figure 3.16: *Exposed samples inside Huguenot Tunnel.*



Figure 3.17: *Vredenburg sample deployment.*

3.1.2.1 Site Description: Stellenbosch

Stellenbosch University is dispersed throughout Stellenbosch town and a large part of the town is occupied by University buildings (see Figure 3.18). Choosing Stellenbosch University building as one of our deployment sites was motivated by our interest in monitoring emissions from urban sources around town. These sources include; vehicle emissions due to traffic, factory exhausts, waste burning, etc.



Figure 3.18: *Stellenbosch University* area showing the location where the active biomonitoring samples were deployed.

3.1.2.2 Site Description: Huguenot Tunnel

Huguenot Tunnel was selected solely as the source of vehicle emissions as it is a confined place where at least 12 000 vehicles; including both light and heavy-duty vehicles using both diesel and petrol, pass through daily. Huguenot tunnel is about 4 kilometres long. It is an extension of the national road (N1) through the Du Toitskloof mountains that separate Paarl from Worcester (about 80 km from Cape Town, Western Cape Province, South Africa) see Figure 3.19. The tunnel is maintained by a subsidiary of the Murray & Roberts construction company called Tolcon (Pty) Ltd. It currently provides one lane of traffic in each direction [147]. The ventilation system of the tunnel is made up of ventilation fans, allowing air flow inside the tunnel [148].

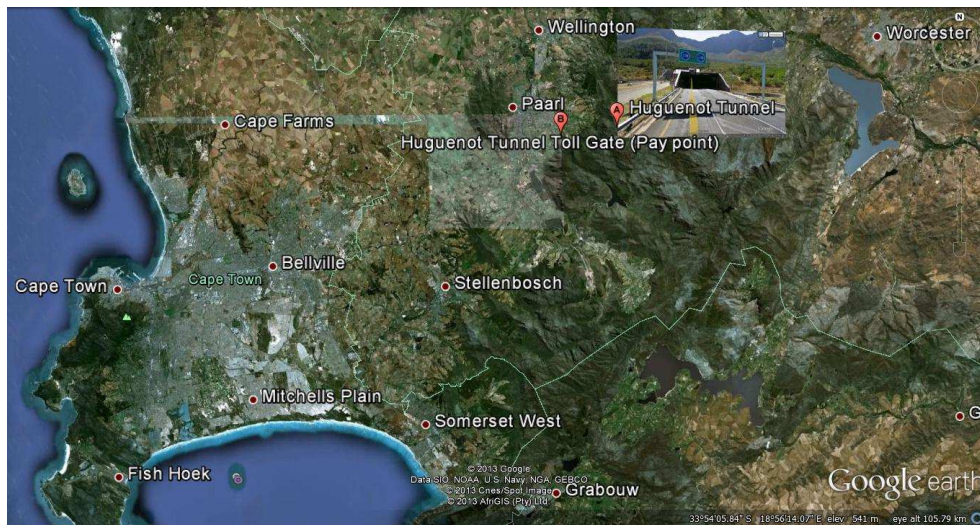


Figure 3.19: Part of the Western Cape map showing the Huguenot tunnel.

3.1.2.3 Site Description: Vredenburg

Vredenburg was selected based on the number of industrial sources of air pollution situated in its surrounding. Situated along the West Coast in the Western Cape, *Vredenburg* has an unobstructed and wide view over Saldanha Bay, where most of our sources of interest are situated (see Figure 3.20).



Figure 3.20: *Potential air pollution sources around Vredenburg.*

3.2 Sample Preparation for Analysis

Since INAA is a non-destructive technique (samples require no chemical separation) measurements and ICP-MS (chemical separation involved), samples were prepared differently. The procedures followed in preparing samples for both INAA and ICP-MS measurements are given in sections 3.2.1 and 3.2.2. More details on the preparation of the samples are given in Appendix A.

3.2.1 ICP-MS Sample Preparation

For ICP-MS measurements, samples were prepared at the environmental analysis laboratory of the Central Analytical Facilities (CAF), Stellenbosch University, Stellenbosch. ICP-MS measurements were then performed at the ICP-MS laboratory of the CAF, using an Agilent 7700× ICP-MS with Octupole Reaction System. Samples were dried at 40°C in a laboratory oven for 3 days. After the drying process, samples were cleaned by hand of all external plant material and soil contamination (but not washed). Then, samples were milled in IKA A10 analytical mill. About 0.5 g of each sample was then weighed and transferred into a microwave vessel and about 10 ml HNO₃ was added into each vessel. Samples were left to stand open for 20 minutes to predigest before the vessels were sealed after which microwave heating and digestion process commenced. About 40 ml of deionised water was weighed and added in a sample bottle that was cleaned in 1% HNO₃ and then added to the digest sample in the microwave vessel to make up 50 ml. Samples were stirred in the microwave vessel, transferred to the sample bottle and then subjected to ICP-MS.

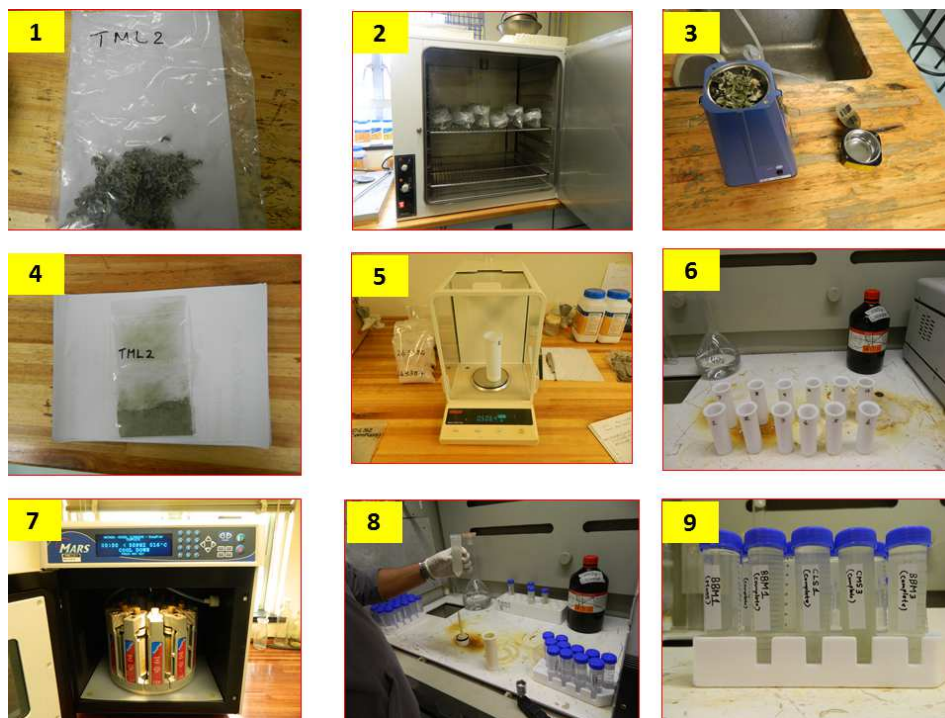


Figure 3.21: ICP-MS sample preparation process.

The following descriptions relate to the ICP-MS sample preparation process as shown by images in Figure 3.21;

1. the collected sample,
2. drying of samples in an oven,

3. sample placed in an analytical mill,
4. milled sample,
5. about 0.5 of the sample being weighed,
6. 10 ml of HNO_3 added to the sample in a microwave vessel,
7. samples placed in a microwave for heating and digestion process,
8. 40 ml of deionised water added into the digested sample, and
9. prepared samples ready for ICP-MS analysis.

3.2.2 INAA Sample Preparation

Samples of mosses and lichens were prepared for irradiation at the chemical laboratory of the Frank Laboratory of Neutron Physics (FLNP) according to the following procedures.

1. Samples were cleaned by hand of all external plant material and soil contamination (but not washed).
2. Mosses/lichen samples of about 0.3 g were put in a vial and then sealed.
3. The vial was put in a press machine, to pelletize the sample.
4. Each sample pellet was weighed to approximately 0.3 g dry-weight and their masses were recorded.
5. For short-term irradiation; samples were heat-sealed in polyethylene bags and for long-term irradiation; they were packed in aluminium foil cups.
6. Samples were then transported to the reactor for irradiation.



Figure 3.22: INAA Sample preparation process

The following descriptions relate to the INAA sample preparation process as shown by images in Figure 3.22.

1. about 0.3 g of the sample being weighed,
2. the weighed sample placed in a vial,
3. vial placed in a manual press to pelletise the sample,
4. pressing of samples,
5. the pelletised samples,
6. samples re-weighed while being covered for irradiation,
7. small aluminium cups (for long irradiation) and small plastic bags (for short irradiation),
8. the prepared samples ready for irradiation, and
9. containers used to pack samples for irradiation in the reactor (aluminium cup -for long irradiation and polyethylene cup - for short irradiation).

3.3 INAA Experimental Setup

The INAA stages that were followed in these experiments are shown in Figure 3.23 below.

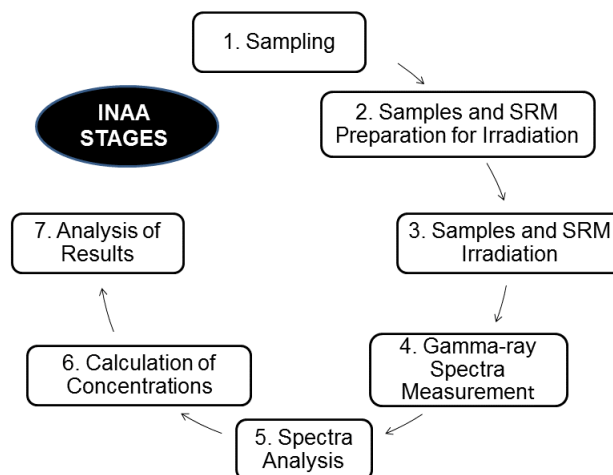


Figure 3.23: *INAA stages [7]. SRM refers to standard reference material.*

INAA experiments were performed at the Sector of Neutron Activation Analysis and Applied Research, Division of Nuclear Physics of the Frank Laboratory of Neutron Physics (FLNP) at the Joint Institute of Nuclear Research (JINR), Dubna(Russia). Measurements were performed using REGATA ("Russian-European Gateway To Asia") experimental facility at IBR-2 reactor. The IBR-2 reactor is a fast-burst reactor type that operates at a normal power of 2

MW (with the maximum power of 2.5 MW) and uses plutonium oxide (PuO_2) as a fuel [149]. It operates as a neutron source for investigations in the field of condensed matter physics, biology, chemistry and materials science. It is a periodic-pulse neutron reactor that generates a power pulse of approximately 1.8 GW of 200 μs duration with a frequency of 5 Hz. It is the only world-class modern neutron source for condensed matter research in Russia with the world's largest pulsed neutron flux of 10^{13} n.cm $^{-2}$.s $^{-1}$ (time-averaged) to 10^{16} n.cm $^{-2}$.s $^{-1}$ (maximum) available at a research reactor [149–151].

According to Pavlov [7], the first pulsed reactor at JINR with average thermal power of 1 kW was constructed in the Laboratory of Neutron Physics (LNP) in 1960. Then, the second one with average thermal power 30 kW was constructed at 1969. However, IBR-2 began to operate for physical experiments in 1984 and the REGATA setup began to operate simultaneously with IBR-2. IBR-2 mainly differs from other reactors due to its mechanical modulation of reactivity with a movable reflector, a complicated mechanical system with a total mass of 60 tonnes (Mg), providing the two parts that perform reactivity modulation - the main movable reflector and additional movable reflector (see Figure 3.24). The rotors of both reflectors rotate with different rotating speeds against each other [151].

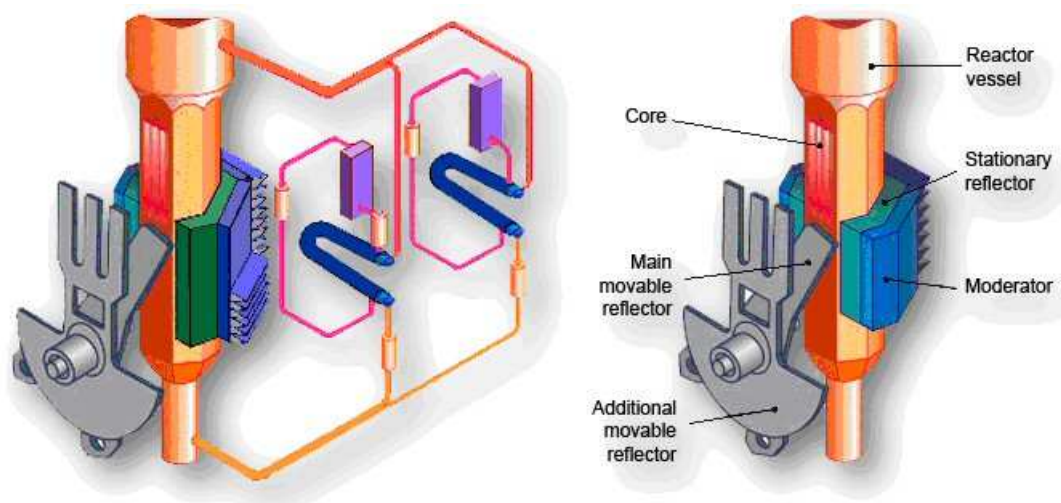


Figure 3.24: Schematic layout of the IBR-2 reactor [151].

The IBR-2 reflectors are rotated by an asynchronous engine and when they coincide near the core, the power pulse is generated. The reflectors are located inside a helium-filled thin-wall pressurized casing. The cooling system has three circuits with two loops, where the heat-transfer agent in the first and second circuits is liquid sodium and the third one is just air. Liquid sodium circulation is maintained by electromagnetic pumps. After operating for more than 20 years, IBR-2 has undergone a number of modifications including the

development of a unique spectrometer complex (11 spectrometres) at its neutron beams (see Figure 3.25) [151, 152].

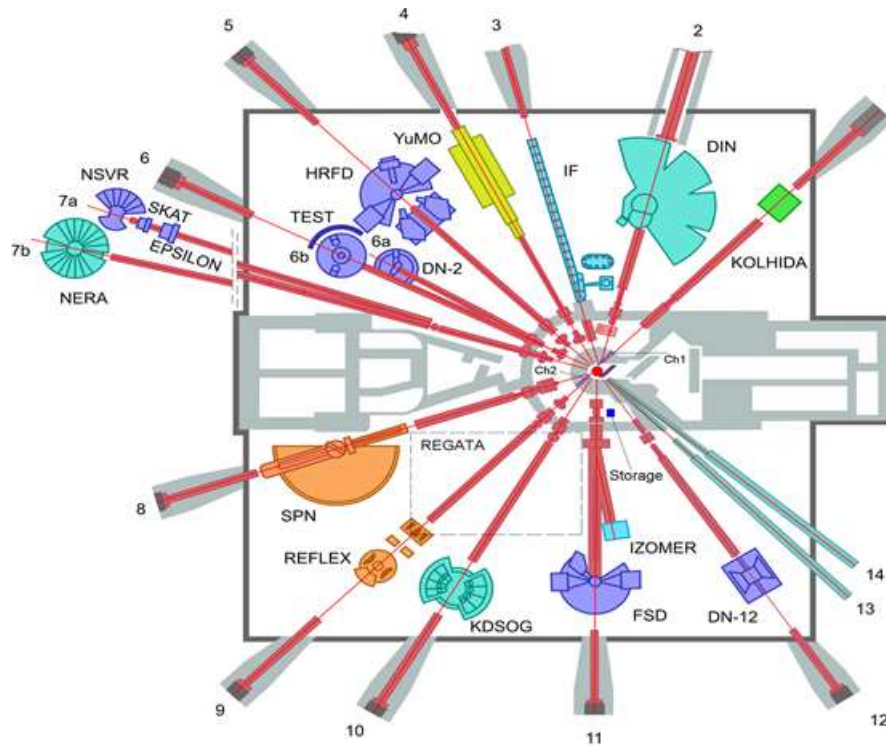


Figure 3.25: Schematic layout of the IBR-2 pulsed fast reactor, showing the spectrometer complex, and radioanalytical complex REGATA. [152].

3.3.1 REGATA Irradiation Facility for INAA

Beside the spectrometer complex in the IBR-2, the radioanalytical facility-REGATA (see Figure 3.26) of the IBR-2 reactor is equipped with a pneumatic transportation system (PTS) REGATA. The PST of REGATA and three "hot-cells" like the one shown in Figure 3.27 are used for conducting neutron activation analysis (NAA) and radiation research [150].

The following describes the experimental facility (REGATA) for neutron activation at IBR-2 reactor as shown by images in Figure 3.26; Ch1-Ch4 → irradiation channels, S → intermediate storage, DCV → directional control valves, L → loading unit, RCB → radiochemical glove-cell, U → unloading unit, SU → separate unit, SM → storage magazine, R → repacking unit, D → detector, CB → control board, R1-R3 → the rooms where the system is located.

The REGATA irradiation channels have exceptional feature of low temperatures at the irradiation position (no higher than (60-70)°C as compared to

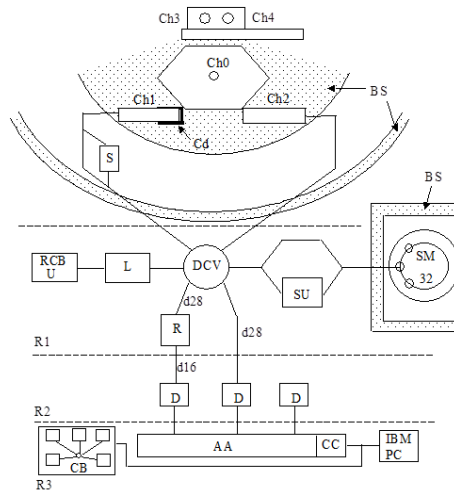


Figure 3.26: *Experimental facility- REGATA at IBR-2 reactor [153].*

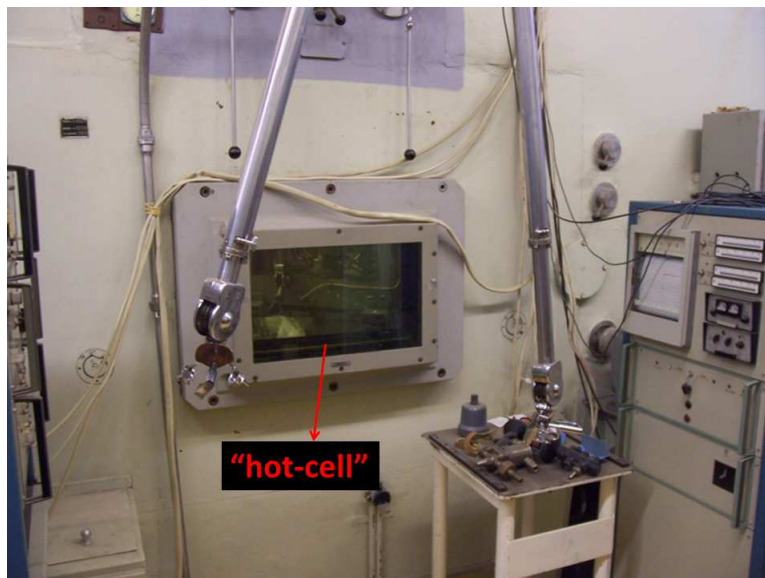


Figure 3.27: *Picture of a "hot-cell" [150].*

that of $(300-400)^{\circ}\text{C}$ at conventional reactors). Due to this exceptional feature, biological matrices can be analyzed without any destruction caused in them. Out of the four irradiation channels of the reactor, REGATA is allocated two irradiation channels. The first one has a cadmium shield for irradiation with epithermal and fast neutrons (see Figure 3.28 and Table 3.4) [13, 150] and the second one allows irradiation with the full neutron spectrum. This makes it possible to optimize the irradiation conditions for samples of different elemental composition [153].

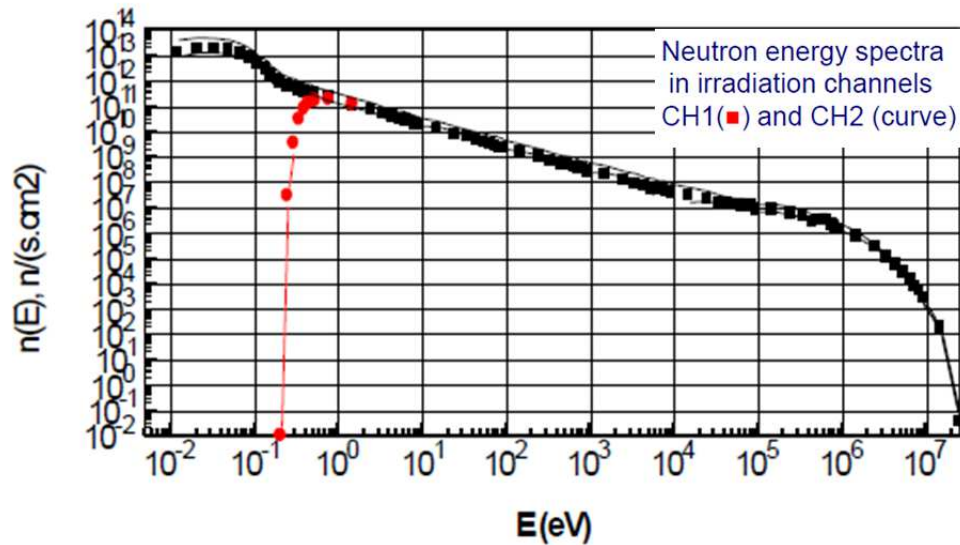


Figure 3.28: REGATA neutron energy spectra and irradiation channels [13].

Table 3.4: Neutron flux in REGATA irradiation channels [150].

	Ch1 ($\text{n.cm}^{-2}.\text{s}^{-1}$) Cd-coated			Ch2 ($\text{n/cm}^{-2}.\text{s}^{-1}$)		
	Channel diameter 28 mm Channel length 260 mm			Channel diameter 28 mm Channel length 260 mm		
	Thermal	Resonance	Fast	Thermal	Resonance	Fast
Experimental value	Cd-coated i.e. N/A	3.6E11	5.5E11	1.5E12	1.8E11	2.7E11

3.3.2 REGATA Transport System

To transport samples for irradiation, three types of capsules are used; i.e. *Polyethylene*, *Polytetrafluoroethylene* (PTFE) generally called Teflon, and *aluminium* capsules. Figures 3.29 and 3.30 respectively show a schematic drawing of the a transportation capsule and the pictures of both aluminium and polyethylene capsules. Polyethylene containers can only sustain irradiation for 40 minutes, otherwise radiation heat will cause them to melt inside the system. On the other hand, Teflon containers can survive up to 5 hours. For longer irradiation, aluminium containers are appropriate.

The principal characteristics of the REGATA transport system are as follows [7];

- distance between irradiation and measurement position: 60 m (Ch2) and 70 m (Ch1);
- PTS air pressure: (3 to 7) bar;
- transportation capsule types for short irradiation: polyethylene/Teflon;
- transportation capsule types for long irradiation: aluminium;

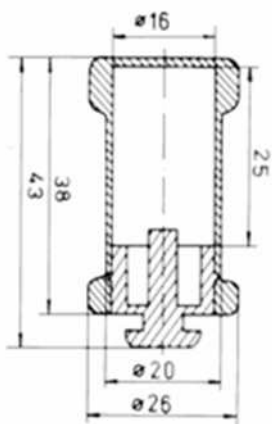


Figure 3.29: Schematic drawing of a Polyethylene transportation capsule [150].



Figure 3.30: Pictures of both aluminium and Polyethylene capsules [150].

- internal transportation capsule volume: (3.5 to 5) cm³;
- maximum irradiation time with 2.0 MW power for capsule: 40 minutes for Polyethylene and 5 hours for Teflon; and
- transportation time for capsule: (7 to 30) s for Polyethylene, (3 to 10) s for Teflon and (3 to 6) s for aluminium.

3.3.3 Sample Irradiation and Counting

The irradiation conditions for samples are given in Table 3.5;

More details on the irradiation of the samples are given in Appendix A.

The counting of samples was performed using Canberra HPGe gamma-ray detectors. A typical gamma-ray spectrometer system for measuring activity of an irradiated material consists of the following components [86];

- detector;
- preamplifier and Amplifier;
- Analog to Digital Converter (ADC);
- multi-Channel Analyser (MCA);
- computer with data acquisition and reduction software; and
- NIM Bin, high voltage unit and other peripherals.

The detector set-up at REGATA with some of the HPGe detectors that were used for this work is shown by Figure 3.31.

Gamma-ray spectrometers available and used for counting at the REGATA set-up are given in Table 3.6. Figure 3.32 illustrates the gamma-ray spectrometer system at REGATA, where detectors (D1, D5, D6 and D7) were used to analyse our samples.

Table 3.5: Typical REGATA sample irradiation conditions [150].

Isotopes to be Used	Types of Capsule Used	Irradiation Channel	Irradiation Time	Decay Time (min)	Counting Time
Short-lived	Polyethylene (3 samples per capsule)	Ch.2 (Full neutron spectrum)	3 min.	5 min	5 min. for 1 st measurements and 15 min. for 2 nd measurements
Long-lived	aluminium (10 to 15 samples per capsule)	Ch.1 (Cd-screen) epithermal and fast neutrons	4 days	4 days	30 min. for 1 st measurements (immediately after repackaging and) 1.5 hours for 2 nd measurements (after another cooling time of 20 days)

More details on the counting of the samples are given in Appendix A.

3.3.3.1 Background Radiation

During NAA measurements, the existing background (both natural and due to activation) as well as cosmic radiation contributes to the observed spectrum and the relative size of this background signal depends on the detector type and size. However, this spectral background can be improved by shielding [4, 92]. On the other hand, contamination within the shielding material also contributes to the background signal, thus it is suggested that the materials used must be pure or at least with a low inherent activity. This signal can be reduced when the appropriate choice of shielding is used. Two materials often used as shielding are lead (Pb) and copper (Cu). Typical arrangement of a detector shielding is shown in Figure 3.33, where the typical thickness is 10 cm thick lead castle fitted with a copper inner lining (usually 1.5 mm to 2.0 mm thick) in order to reduce the background in the sample spectra [154]. The background radiation from the surrounding environment where the detection system is placed is generally detected and measured before introducing the sample to the detector [70].

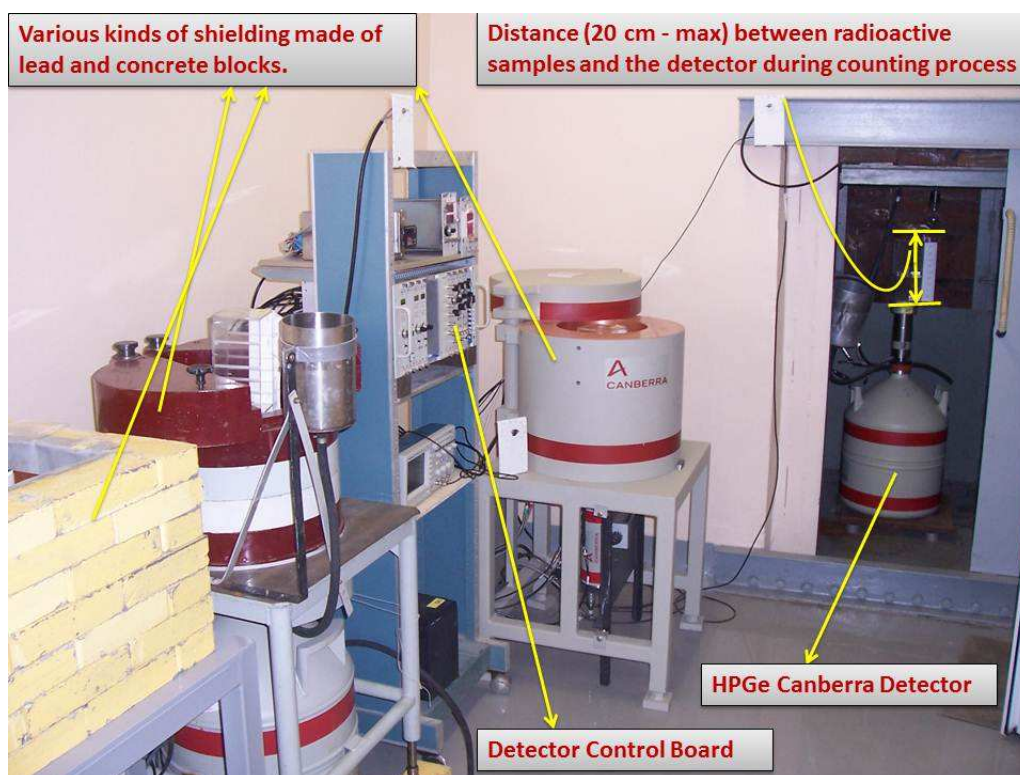


Figure 3.31: Canberra HPGe detector set-up at REGATA.

Table 3.6: REGATA gamma-spectrometers [150].

Detector Type	Model	Efficiency/ Resolu- tion	Start- up Date	HV Power Sup- ply	Amplifier	ADC	Pro- gram
HPGE (D1)	GC1020-7500SL	11.2%/ 1.78 keV	2000	2861A Can- berra	2022 Can- berra	AccuSpec A Card Can- berra	Genie 2000
HPGE (D5)	GC4019-7500SL	41.8%/ 1.74 keV	2007	3106D Can- berra	2026 Can- berra	Multiport II	Genie 2000
HPGE (D6)	GX4020-CRIO-JT	42.6%/ 1.81 keV	2009	3106D Can- berra	2026 Can- berra	Multiport II A	Genie 2000
HPGE (D7)	GC3018-7500SL	30.3%/ 1.74 keV	2011	Incorp- orated		DSA- 1000	Genie 2000

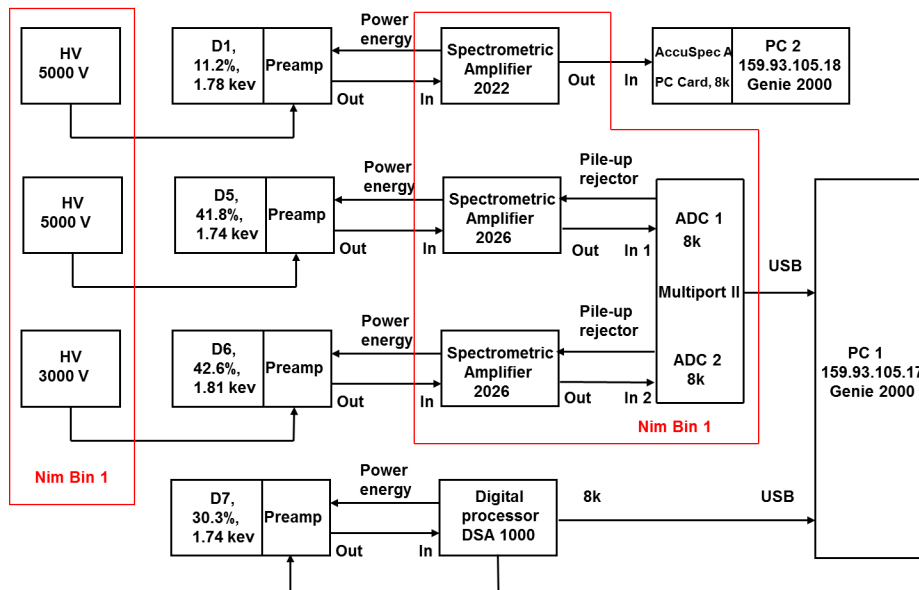


Figure 3.32: Diagram of gamma-ray spectrometer system at the radioanalytical complex REGATA at IBR-2 reactor of the JINR in Dubna, Russia [150].



Figure 3.33: Typical detector shield image [154].

Chapter 4

Data Analysis

This chapter describes the process used to identify and quantify elements present in moss and lichen samples. This follows after the samples have been irradiated with neutrons in the IBR-2 reactor.

4.1 Gamma-ray Spectrometry related

Table 4.1 shows a list of elements identified by INAA and the reactions through which they were identified using γ -ray spectrometry. With the exception of Th and U, the rest of the elements were determined solely from radionuclides formed in (n,γ) reactions. This is because reactors used for neutron irradiation general have larger abundance of thermal and epithermal neutrons than fast neutrons. These thermal and epithermal neutrons with $E_n \approx 0.025$ eV and $0.025 < E_n \leq 0.5$ MeV, respectively, have relatively higher (n,γ) reaction cross-sections as compared to (n,p) (n,α) and $(n,2n)$ reactions, which usually occur with fast neutrons. Hence (n,γ) reactions have higher analytical sensitivity for most target nuclides [76].

Table 4.1: *List of elements determined by INAA [77].*

Element	Isotope Abundance (%)	Reaction	Principal γ -line (keV) (%)	Half-life	Type
Na	^{23}Na (100)	$(n,\gamma)^{24}\text{Na}$	1368.6(100), 2754.1(99.9)	15.0 hrs	LLI1
Mg	^{26}Mg (11.0)	$(n,\gamma)^{27}\text{Mg}$	843.8(71.8), 1014.4(28.0)	9.5 mins	SLI
Al	^{27}Al (100)	$(n,\gamma)^{28}\text{Al}$	1778.8(100)	2.2 mins	SLI
Si	^{28}Si (92.2)	$(n,p)^{28}\text{Al}$	1778.8(100)	2.2 mins	SLI

Continued on next page

Table 4.1 –continued from previous page					
Element	Isotope Abundance (%)	Reaction	Principal γ -line (keV) (%)	Half-life	Type
Si	²⁹ Si (4.7)	(n,p) ²⁹ Al	1273.0(91.0), 2.42(5.7)	6.5 mins	SLI
Cl	³⁷ Cl (24.2)	(n, γ) ³⁸ Cl	1642.7(31.0), 2167.7(42.0)	37.2 mins	SLI
K	⁴¹ K (6.7)	(n, γ) ⁴² K	1524.6(18.0)	12.4 hrs	LLI1
Ca	⁴⁸ Ca (0.2)	(n, γ) ⁴⁹ Ca	3084.4(91.7)	8.7 mins	SLI
Sc	⁴⁵ Sc (100)	(n, γ) ⁴⁶ Sc	889.3(100), 1120.5(100)	83.8 days	LLI2
Ti	⁵⁰ Ti (5.2)	(n, γ) ⁵¹ Ti	320.1(93.1)	5.8 mins	SLI
V	⁵¹ V (99.8)	(n, γ) ⁵² V	1434.1(100)	3.7 mins	SLI
Cr	⁵⁰ Cr (4.4)	(n, γ) ⁵¹ Cr	320.1.4(10.1)	27.7 days	LLI2
Mn	⁵⁵ Mn (100)	(n, γ) ⁵⁶ Mn	846.8(98.9), 1810.7(27.2)	2.6 hrs	SLI
Fe	⁵⁸ Fe (0.3)	(n, γ) ⁵⁹ Fe	1099.3(56.5), 1291.6(43.2)	44.5 days	LLI2
Zn	⁶⁴ Zn (48.6)	(n, γ) ⁶⁵ Zn	1115.5(50.7)	244.1 days	LLI2
Ni	⁵⁸ Ni (68.1)	(n,p) ⁵⁸ Co	810.8(99.5)	70.9 d	LLI2
Co	⁵⁹ Co (100)	(n, γ) ⁶⁰ Co	1173.2(99.9), 1332.5(100)	5.3 y	LLI2
As	⁷⁵ As (100)	(n, γ) ⁷⁶ As	559.1(45.0)	1.1 d	LLI1
Se	⁷⁴ Se (0.9)	(n, γ) ⁷⁵ Se	264.7(58.5), 279.5(24.8)	119.8 d	LLI2
Br	⁸¹ Br (49.3)	(n, γ) ⁸² Br	554.3(70.8), 776.5(83.5)	1.48 d	LLI1
Rb	⁸⁵ Rb (72.2)	(n, γ) ⁸⁶ Rb	1076.6(8.6)	18.6 d	LLI2
Sr	⁸⁴ Sr (0.6)	(n, γ) ⁸⁵ Sr	514.0(96.0)	64.9 d	LLI2
Sb	¹²³ Sb (42.8)	(n, γ) ¹²⁴ Sb	602.7(97.8), 1691.0(47.3)	60.2 d	LLI2
I	¹²⁷ I (100)	(n, γ) ¹²⁸ I	442.9(16.9)	25.0 m	SLI
Cs	¹³³ Sr (100)	(n, γ) ¹³⁴ Cs	604.7(97.6), 795.8(85.4)	2.1 y	LLI2
Ba	¹³⁰ Ba (0.1)	(n, γ) ¹³¹ Ba	216.1(19.9), 496.3(44.0)	11.5 d	LLI2
La	¹³⁹ La (99.9)	(n, γ) ¹⁴⁰ La	487.0(44.3), 1596.2(95.4)	1.7 d	LLI1
Ce	¹⁴⁰ Ce (88.5)	(n, γ) ¹⁴¹ Ce	145.4(48.2)	32.5 d	LLI2

Continued on next page

Table 4.1 –continued from previous page					
Element	Isotope Abundance (%)	Reaction	Principal γ -line (keV) (%)	Half-life	Type
Nd	^{146}Nd (17.2)	$(n,\gamma)^{147}\text{Nd}$	121.8(28.4), 531.0(13.1)	11.0 d	LLI2
Sm	^{152}Sm (26.8)	$(n,\gamma)^{153}\text{Sm}$	103.2(31.4)	1.9 d	LLI1
Tb	^{159}Tb (100)	$(n,\gamma)^{160}\text{Tb}$	298.6(28.9), 879.4(32.9)	72.3 d	LLI2
Hf	^{180}Hf (35.1)	$(n,\gamma)^{181}\text{Hf}$	133.0(43.3), 482.2(80.5)	42.4 d	LLI2
Ta	^{181}Ta (100)	$(n,\gamma)^{182}\text{Ta}$	1189.1(16.2), 1221.4(27.0)	114.4 d	LLI2
W	^{186}W (28.4)	$(n,\gamma)^{187}\text{W}$	479.6(21.8), 685.7(27.3)	23.7 h	LLI1
Th	^{232}Th (100)	$(n,\gamma)^{233}\text{Th}$ $(\beta^-)\rightarrow^{233}\text{Pa}$	312.2(38.6)	27.0 d	LLI2
U	^{238}U (0.6)	$(n,\gamma)^{239}\text{U}$ $(\beta^-)\rightarrow^{239}\text{Np}$	106.1(22.9)	2.4 d	LLI1

INAA reactions through which elements from active biomonitoring were identified are similar to those from which passive biomonitoring results were obtained (see Table 4.1). Gd, Zr, Tm and Mo were additionally identified from active biomonitoring samples, whereas Ta was only identified from passive biomonitoring samples. INAA reactions through which Gd, Zr, Tm and Mo were formed are showed in Table 4.2.

Table 4.2: Additional list of elements determined by INAA.

Element	Isotope (Abundance(%))	Reaction	Principal γ -line (keV)(%)	Half-life	Isotope Type
Gd	^{152}Gd (20.0)	$(n,\gamma)^{153}\text{Gd}$	103(21.4)	241,6 days	LLI2
Zr	^{94}Zr (17.4)	$(n,\gamma)^{95}\text{Zr}$ $(\beta^-)\rightarrow^{95}\text{Nb}$	724.2(43.00), 756.7(54.60), 765.8(99.00)	65.5 days	LLI2
Tm	^{169}Tm (100)	$(n,\gamma)^{170}\text{Tm}$	84.0(3.26)	128.6 days	LLI2
Mo	^{98}Mo (23.8)	$(n,\gamma)^{99}\text{Mo}$ $(\beta^-)\rightarrow^{99}\text{Tc}^m$	140.5(18.3), 181.1(7.0)	66.0 hrs	LLI1

Al can be identified from; $^{27}\text{Al}(n,\gamma)^{28}\text{Al}$, $^{28}\text{Si}(n,p)^{28}\text{Al}$ and $^{29}\text{Si}(n,p)^{29}\text{Al}$ reactions. Even though ^{28}Al can be formed from $^{27}\text{Al}(n,\gamma)^{28}\text{Al}$ and $^{28}\text{Si}(n,p)^{28}\text{Al}$,

$E_{threshold}$ of the incident neutron for this $^{27}\text{Al}(n, \gamma)^{28}\text{Al}$ reaction is in the thermal region, ≈ 0.025 eV (refer to Figure 2.1). However, about 4 MeV neutron kinetic energy is required for the $^{28}\text{Si}(n,p)^{28}\text{Al}$ reaction to occur. Hence, the $^{27}\text{Al}(n, \gamma)^{28}\text{Al}$ reaction is more likely in this study. Figure 4.1 show graphical representation of the reaction cross-sections for Al formation. On the other hand, Th and U were measured using their daughter nuclides as shown and explained in Figures 4.2 and 4.3, respectively [155, 156]. A graphical representation of the reaction cross-sections for $^{232}\text{Th}(n, \gamma)^{233}\text{Th} \rightarrow (\beta^-)^{233}\text{Pa}$ and $^{238}\text{U}(n, \gamma)^{239}\text{U}(\beta^-)^{239}\text{Np}$ reactions is shown in Figure 4.4.

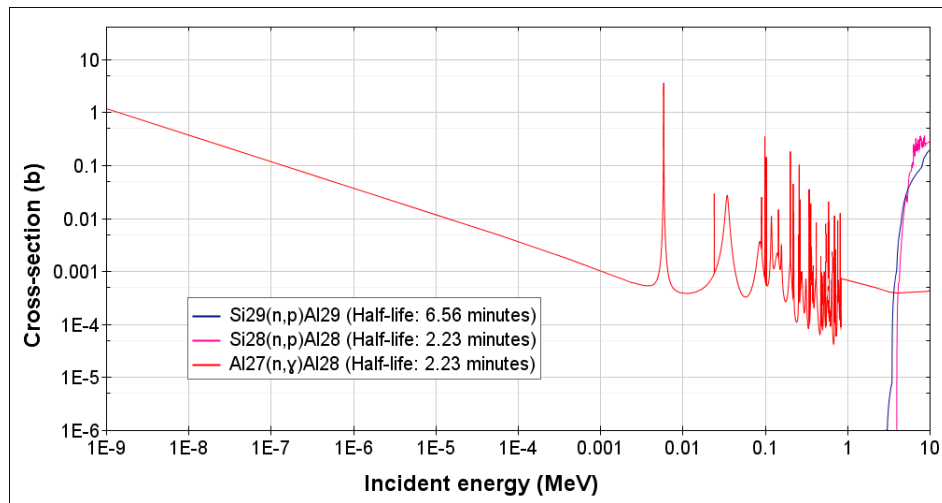


Figure 4.1: Graphical representation of reaction cross-sections for $^{27}\text{Al}(n, \gamma)^{28}\text{Al}$, $^{28}\text{Si}(n, p)^{28}\text{Al}$ and $^{29}\text{Si}(n, p)^{29}\text{Al}$ [77].

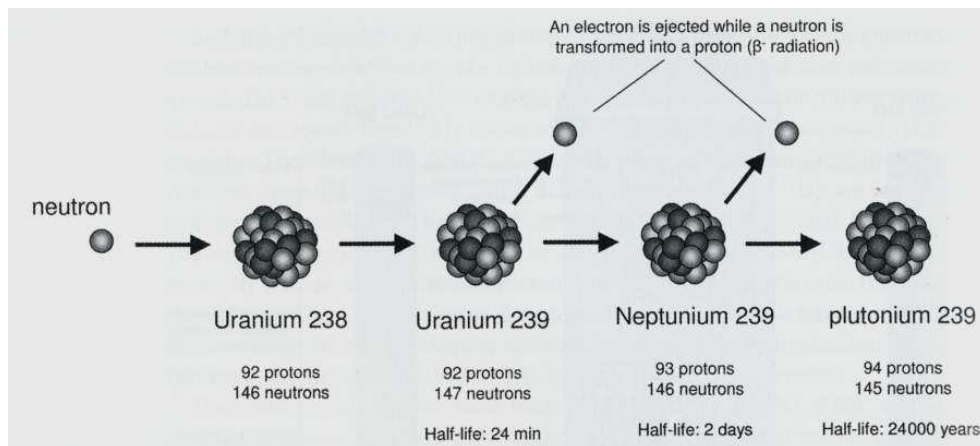


Figure 4.2: Diagram ^{239}U daughter nuclide formation reaction [156].

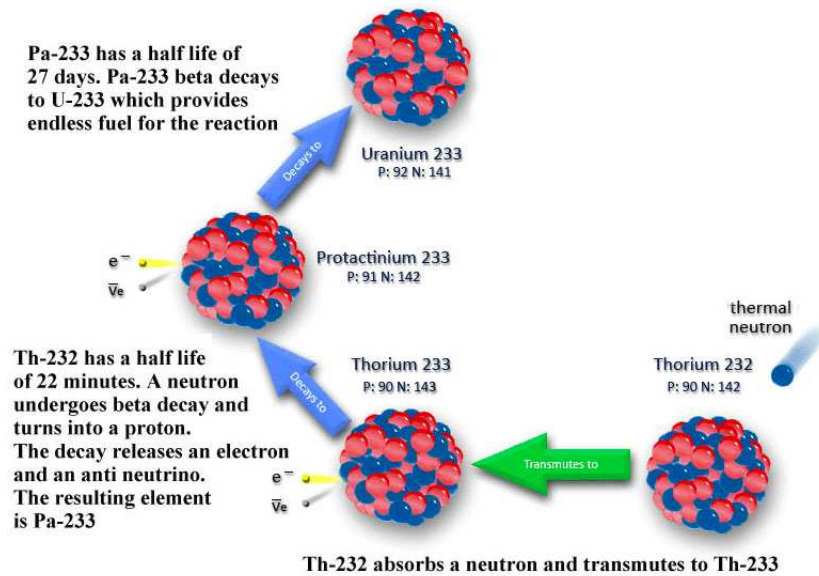


Figure 4.3: Diagram showing ^{232}Th daughter nuclide formation reaction [155].

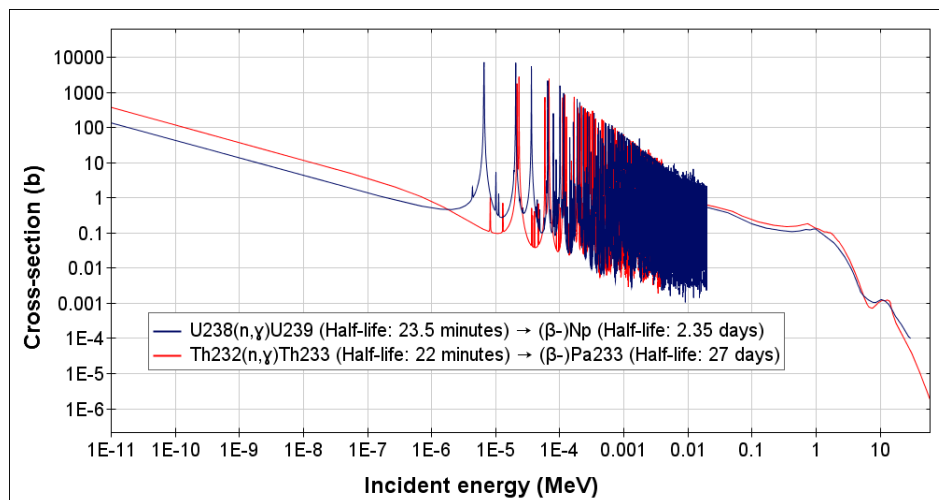


Figure 4.4: Graphical representation of reaction cross-sections for $^{232}\text{Th}(n,\gamma)^{233}\text{Th} \rightarrow (\beta^-)^{233}\text{Pa}$ and $^{238}\text{U}(n,\gamma)^{239}\text{U} \rightarrow (\beta^-)^{239}\text{Np}$ [77].

The identification of Tm and Gd was determined through (n, γ) reactions, whereas Zr and Mo were measured through the use of their daughter nuclides. The mechanisms through which Zr and Mo were identified is similar to the ones explained above for Th and U (see Figures 4.2 - 4.3).

Prior to counting the irradiated samples on the gamma-ray detector system, energy calibration was performed for our system and channel numbers were converted to energies. Essential steps during spectra analysis involves a proper calibration of both energy (to identify radionuclides) as well as the γ -ray detection efficiency (needed to determine activity concentrations).

4.1.0.2 Energy and Efficiency Calibration

Calibration is the process used to verify the functioning of a detector and its performance within certain specifications, using reference material values. Prior to conducting NAA measurements, the detection system was first be calibrated using standard reference materials as shown in Figures; 4.5, 4.6, 4.7.

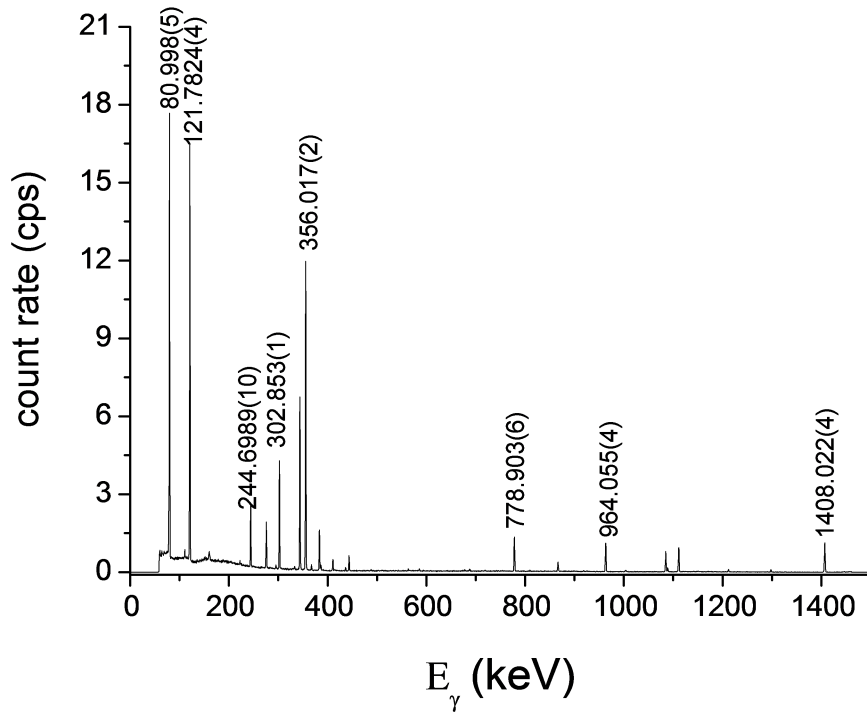


Figure 4.5: The spectrum measured for a point source containing ^{152}Eu and ^{133}Ba (used for energy and efficiency calibration in this study). The labelled photopeaks of ^{133}Ba are at 81 keV, 303 keV and 356 keV. The other labelled photopeaks are from ^{152}Eu .

For this study, energy calibration was done using gamma-emitting standard sources; ^{152}Eu and ^{133}Ba . As shown in Equation (4.1.1), energy calibration involves the experimental determination of a function (usually a 1st or 2nd degree polynomial) that describes the energy dependence of the channel number in the spectrum [157, 158]. The functional form used for the energy calibration in this study was as follows:

$$E_{\gamma} = a + b \cdot \text{Ch}, \quad (4.1.1)$$

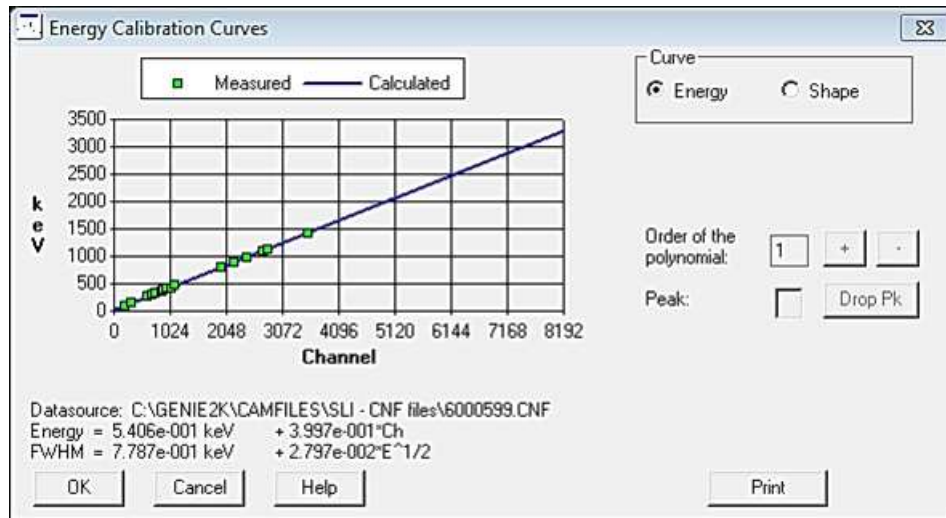


Figure 4.6: The energy calibration curve generated with the Genie 2000 software in this study using the ^{152}Eu - ^{133}Ba point sources (sample ID: 6000599).

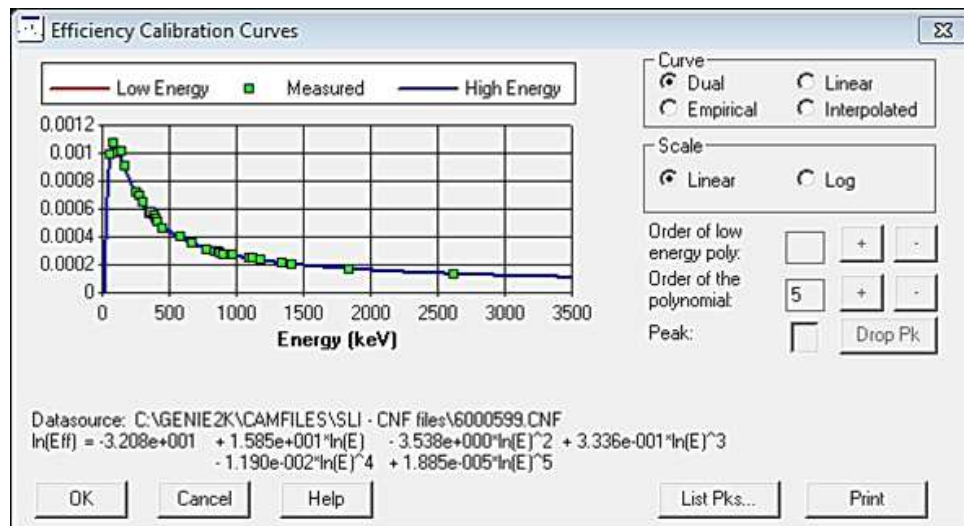


Figure 4.7: Efficiency calibration curve of HPGe Canberra coaxial detector number 6 (D6) using ^{152}Eu - ^{133}Ba point source.

where; a and b are coefficients determined by curve fitting and Ch is the channel number.

The energy calibration curve of an HPGe system that was obtained using certified spectrometric multi-gamma ray source, ^{152}Eu and is shown in Figure 4.5. In-order to determine the activity of radionuclides in our samples, a full energy peak (FEP) efficiency calibration was also carried out after energy calibration of the detector system. FEP efficiency $\mathcal{E}_\gamma(E)$ is defined the ratio of the number of counts or events ($N(E)$) detected when the complete energy $E(N(E))$ was deposited in the detector to the number of photons ($P(E)$) of that

energy emitted from the source at time t (see Equation (4.1.2))[154, 158, 159].

$$\mathcal{E}_\gamma(E) = \frac{N(E)}{A \cdot I_\gamma \cdot t} \cdot K, \quad (4.1.2)$$

where; $N(E)$ is the the net peak area of a γ -ray peak with centroid at energy, E ,

$I_\gamma \rightarrow$ the branching ratio or the γ -ray emission probability,

$A \rightarrow$ the reference activity of the radionuclide emitting the γ -ray of energy, E ,

$t \rightarrow$ the spectrum collection time (live time),

$K \rightarrow$ decay-correction factor ($e^{-\lambda t_1} - e^{-\lambda t_2}$ for $t_1 =$ reference date and $t_2 =$ counting date), and

$\lambda \rightarrow$ the decay constant.

The FEP efficiency calibrations were carried out using the same multi-gamma ray sources, ^{152}Eu and ^{133}Ba , with certificates containing gamma emissions and corresponding activity. As ^{152}Eu and ^{133}Ba cover a wide energy range, emit several gamma rays and are longer lived, they are often preferred for the FEP efficiency calibrations in a variety of experiments[159]. Efficiency is energy dependent and described by the function given by Equation (4.1.3) [158].

$$\ln \mathcal{E}(E) = a_0 + a_1 \cdot \ln E + a_2 \cdot (\ln E)^2 + \dots, \quad (4.1.3)$$

where; $\mathcal{E} \rightarrow$ efficiency, $E \rightarrow$ energy, and $a_0, a_1, a_2 \rightarrow$ the coefficients of the fitting curve.

The FEP efficiencies recalled during the analysis were acquired by counting point sources of standard ^{152}Eu and ^{133}Ba at different geometries between 2.5 cm and 25 cm (within 2.5 cm intervals) between the detector end-cap and the source sample. To avoid uncertainties in the efficiency curves due to coincidence summing, larger distance are usually favoured for calibrations with multi γ -ray sources. Moreover, the counting of the samples has to be done for a sufficiently long time so as to minimise the statistical uncertainties [160]. The Eu-Ba efficiency curves for this study were fitted by a fifth order of linear polynomial curve by a dual fitting (see Figure 4.6).

4.1.0.3 Evaluation of Gamma-spectra

During INAA investigations, the critical part of data analysis process involves fitting of gamma-ray spectra. This is where the gamma-ray peaks in the spectrum are associated with decay of particular radionuclides based on the gamma-ray energy [160]. In order to identify elements from irradiated and counted samples in this study, the spectra obtained from HPGe measurements were analyzed using the PC-based gamma spectroscopy software, Genie 2000

(CANBERRA). Thereafter, concentrations of the identified elements were calculated based on the decay rates (activities) calculated during spectral analysis and reflected on the generated reports [161]. A survey of steps as well as the information/data required for the evaluation of γ -ray spectra and finally calculating elemental concentrations is given by Figure 4.8 [153, 162].

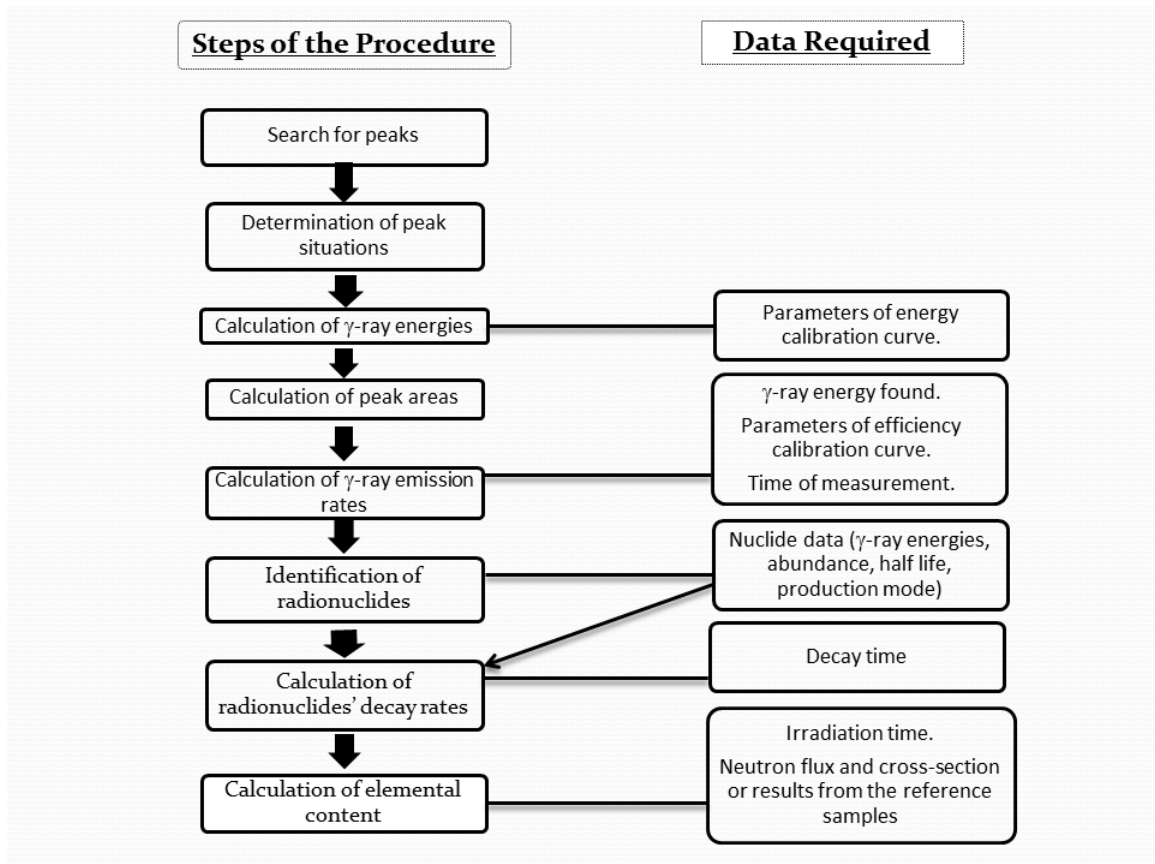


Figure 4.8: The list of steps and the data required for evaluating gamma-ray spectra, calculating activities and elemental content [153, 162].

Before using the peak search algorithm during γ -ray spectra evaluation, sample information was checked to confirm detector calibration (if the detector was not calculated, sample information will not be available in the spectra). This is where the appropriate efficiency calibration file can be recalled and loaded, based on a particular detector and geometry that were used to acquire the spectrum to be analysed. For the purpose of searching for peaks as well as calculating γ -ray energies, the 'Unidentified 2nd Diff' algorithm available in Genie 2000 was selected. For applications whereby the contents of the spectrum are not known in advance, the 'Unidentified 2nd Diff' algorithm is the best choice. For this algorithm, Genie 2000 program automatically determines the expected peak width value based on the shape calibration data for

the spectrum to be analysed. The coefficients are then recalculated every 100 channels to make sure that the peak locate algorithm is appropriate for the types of peaks expected. Furthermore, the 'Unidentified 2nd Diff' peak locate algorithm contains a test for each peak shape. During the test, peak regions for which the sign of the second derivative remains unchanged are classified as Compton continuum features and so are rejected as real peaks [163].

After locating the peaks, the algorithm that was selected for calculating peak areas was the 'Sum/Non-Linear LSQ Fit Peak Area' algorithm. This algorithm includes calculations for defining peak region limits, and also calculating peak areas as well as their uncertainties for either singlets or multiplets. When the 'Unidentified 2nd Diff.' algorithm is used for locating peaks, then regions of interest (ROI) limits are determined automatically before executing the peak-area calculation algorithms. This automatic method of determining the ROI limits also determines whether adjacent peaks are going to be analyzed as two singlets or as a multiplet [163]. Peak areas were also adjusted interactively by manually editing, adding and deleting peaks, as well as peak regions of a spectrum which has been calibrated for energy and shape e.g. (see Figure 4.9). The Interactive Peak Fit (IPF) option offers an advantage to examine the peak analysis results included in the active spectrum to see whether individual peak areas are multiplet peaks, real peaks which have not been found to be statistically significant, or found peaks which are not relevant to specific needs, etc. [164].

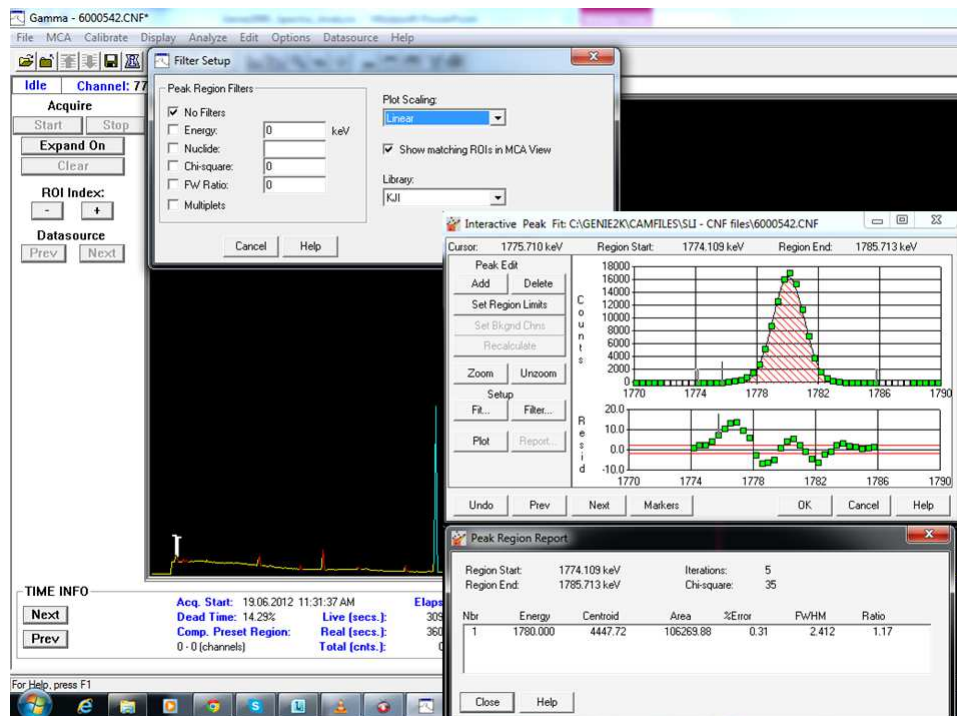


Figure 4.9: Genie 2000 window for fitting the peaks interactively.

During sample spectra analysis of long-lived isotopes, there should be background data of all net peak areas from a separate analysis performed on background radiation. When all the peaks were checked and fitted interactively, the background spectra contribution was subtracted from the spectra by choosing a relevant background spectrum file acquired from a specific detector used. This was done by choosing 'Area Correction' from the 'Analyze' drop-down menu, followed by selecting 'Std. Bkg. Subtract'. This algorithm allows one to subtract background peak areas from the matching peak areas in the current data source (spectrum) [163, 165].

After the background subtraction, efficiency correction was performed using the 'Standard' option, followed by the 'Dual' function efficiency correction. The option of selecting the 'Standard' efficiency correction uses the efficiency calibration that was previously established and loaded to calculate and apply respective efficiencies to the calculated net areas of each found peak [165]. The 'Dual' function efficiency correction was chosen because two separate models supported by two curves; one for the low energy region (using ^{133}Ba calibration curve) and one for the high energy region (using ^{152}Eu calibration), were used for efficiency correction.

After the background subtraction and performing detector efficiency correction, nuclides were identified by respectively executing two algorithms for Nuclide Identification (NID); i.e. 'Tentative NID' and 'NID with Interference Correction'. The tentative NID algorithm generates a tentative nuclide identification by looking at each of the peaks established by the Peak Area step of the analysis, and attempts to find a match in the specified nuclide library. After that, the algorithm uses the specified tolerance to perform a search. Then, all the nuclides satisfying that tolerance are recorded for reporting with the nearest match reported first and followed by any other 'more distant' matches available. The 'NID with Interference Correction' algorithm identifies the nuclides in the spectrum and automatically performs an interference correction as well as the weighted mean activity calculation on the identified nuclides [165].

When all radionuclides in a spectrum were identified, their decay rates (minimum detectable activities (MDAs)) were calculated using 'Currie MDA' algorithm. The MDA algorithm calculates MDA values for both the radionuclides which have not been found in the spectrum, as well as for those that have been found. Currie's method incorporates two concepts; a 'Critical Level' (L_C), i.e. below which a net signal cannot reliably be detected, as well as a 'Detection Limit' (L_D), i.e. the smallest net signal that can reliably be quantified [163]. For each spectrum, when all the analysis steps were executed, the final step was to generate a final customised (e.g. SLI for short-lived isotopes or LLI for long-lived isotopes) text-file appropriate report. These are the reports that were saved and used to calculate the final concentrations in $\mu\text{g/g}$. Figures;

4.10 → 4.18 show examples of spectra for the short-lived, long-lived 1 and long-lived 2 isotopes. Each set (i.e. SLI, LLI1 and LLI2) is divided into three regions in order to clearly show the peaks of interest. In each of the spectra below for a moss sample, the spectra for irradiated reference material is also plotted. These spectra were saved after spectral analysis and the customised final analysis reports served as input to the JINR computer program that automatically calculates elemental concentrations.

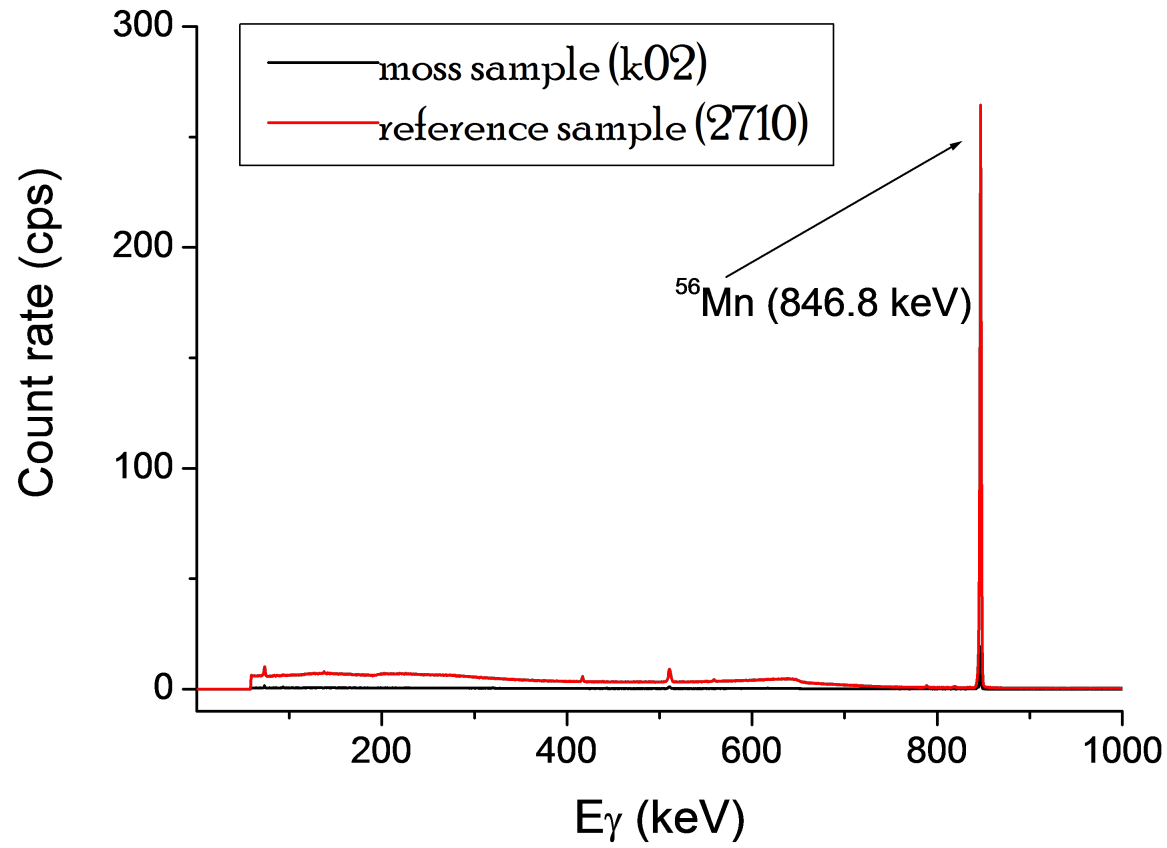


Figure 4.10: Short-lived isotopes spectrum → (0 - 1000) MeV energy region.

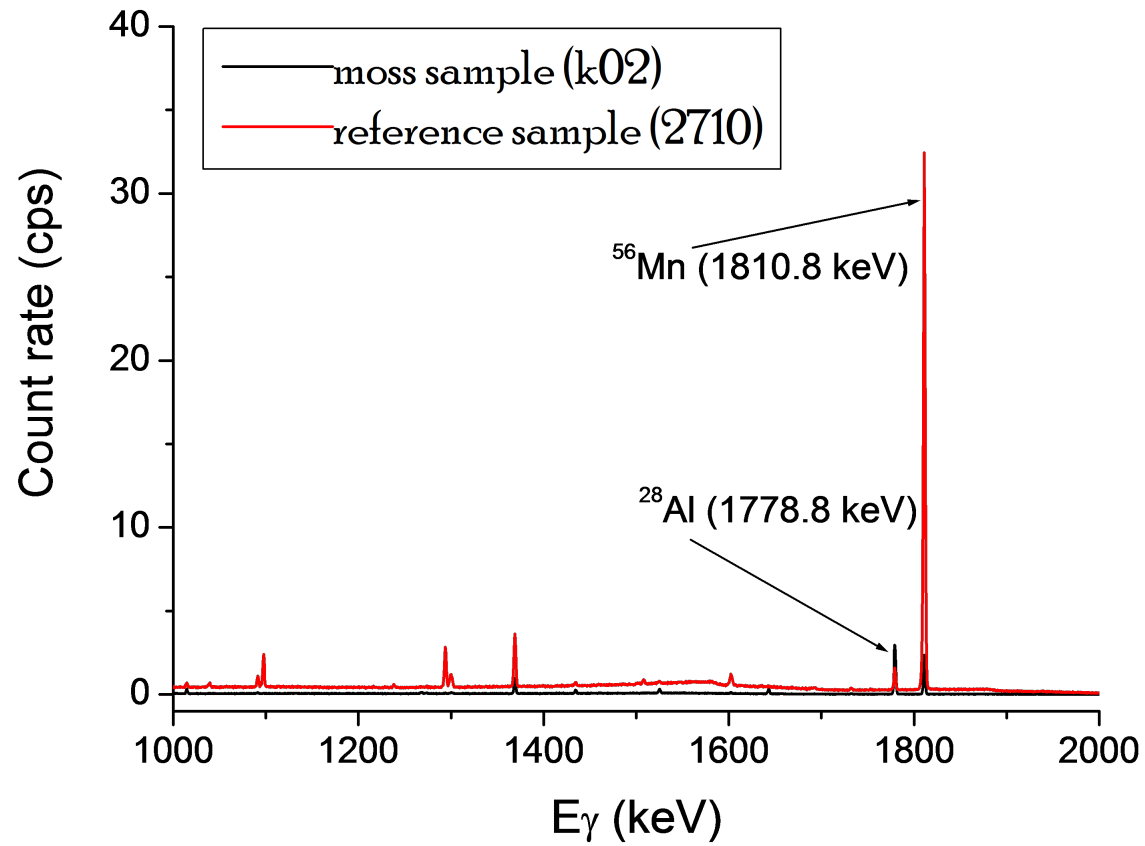


Figure 4.11: Short-lived isotopes spectrum → (1000 - 2000) MeV energy region.

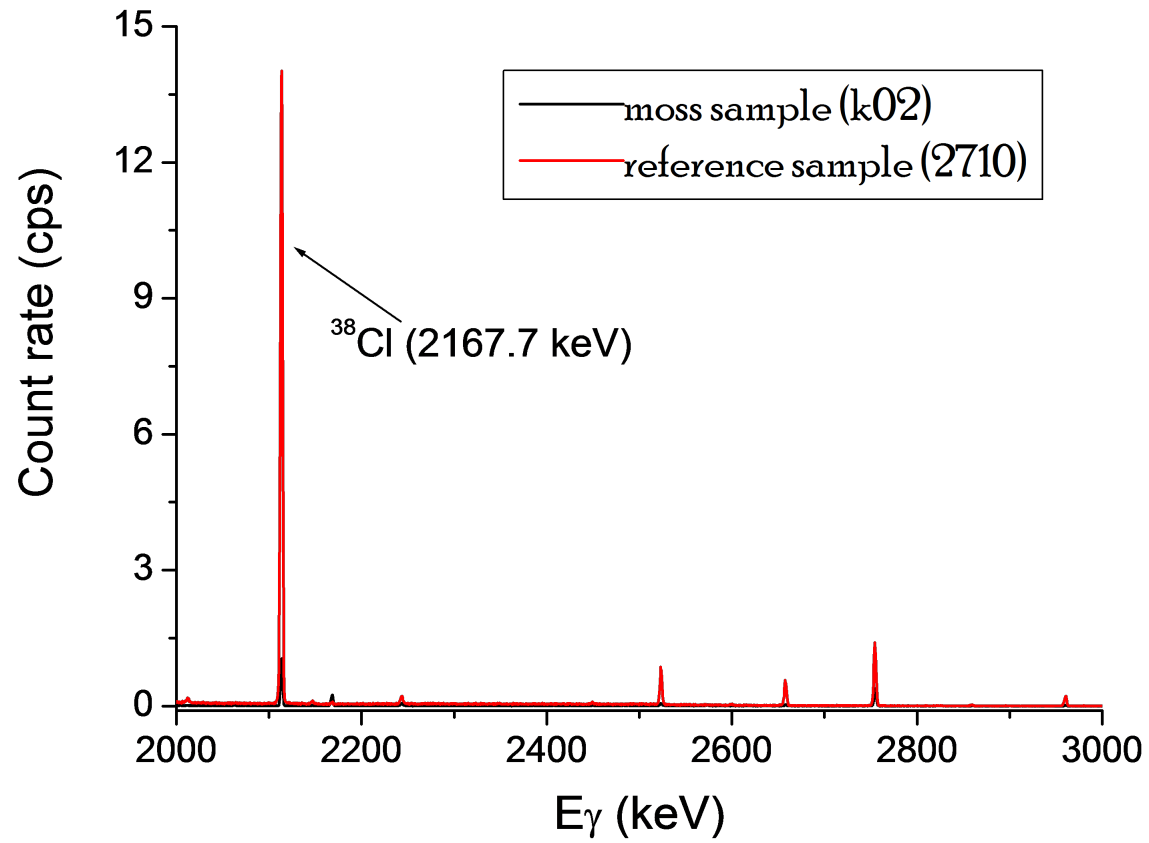


Figure 4.12: Short-lived isotopes spectrum → (2000 - 3000) MeV energy region.

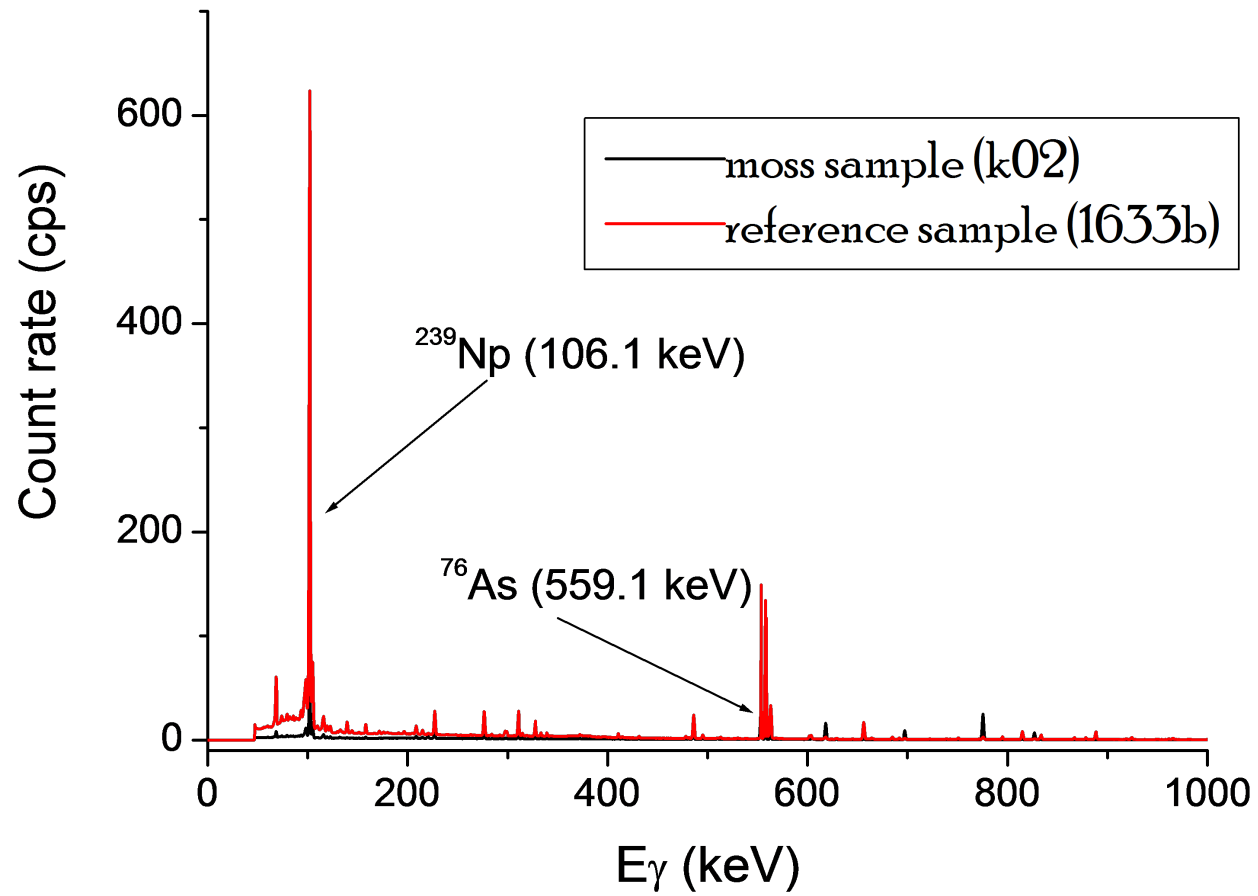


Figure 4.13: Long-lived 1 isotopes spectrum → (0 - 1000) MeV energy region.

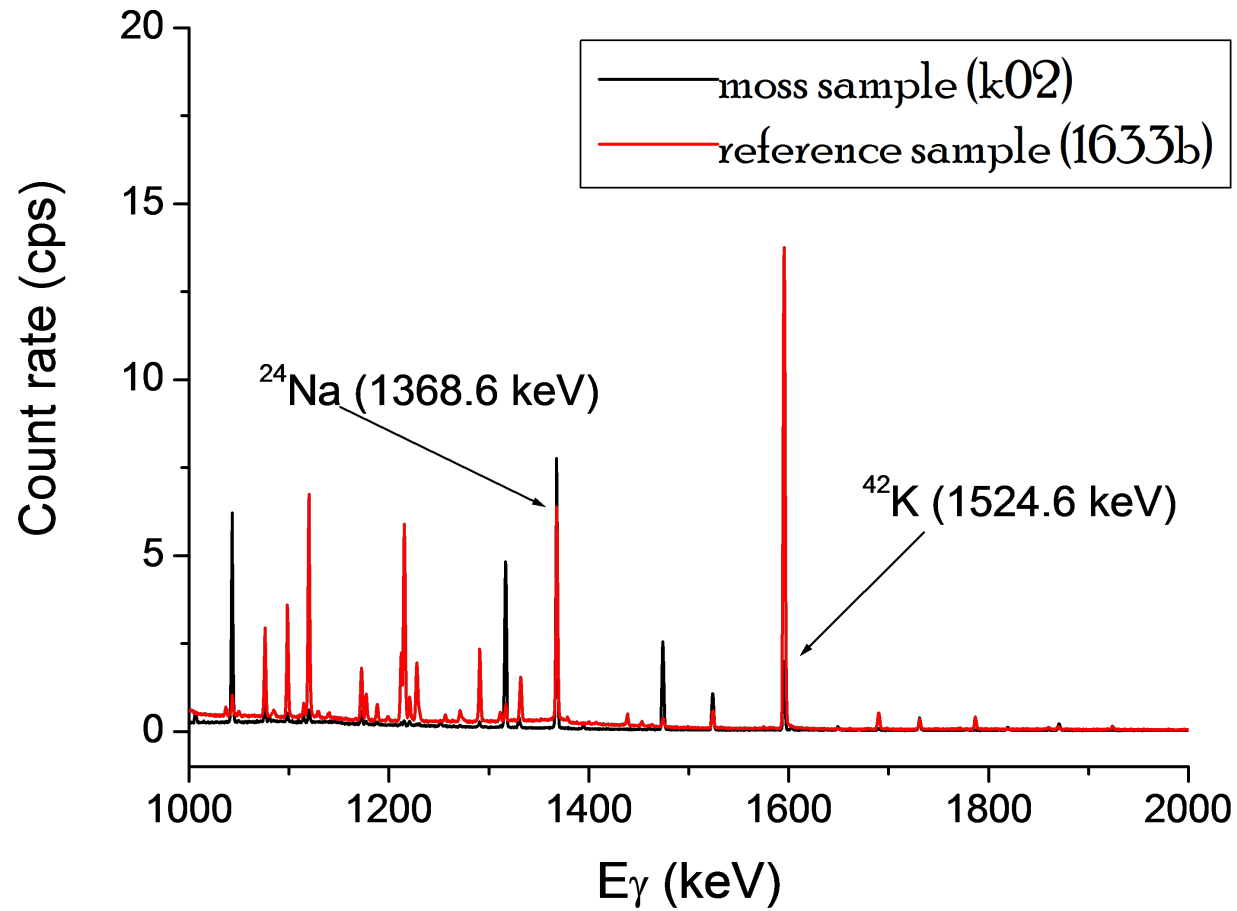


Figure 4.14: Long-lived 1 isotopes spectrum \rightarrow (1000 - 2000) MeV energy region.

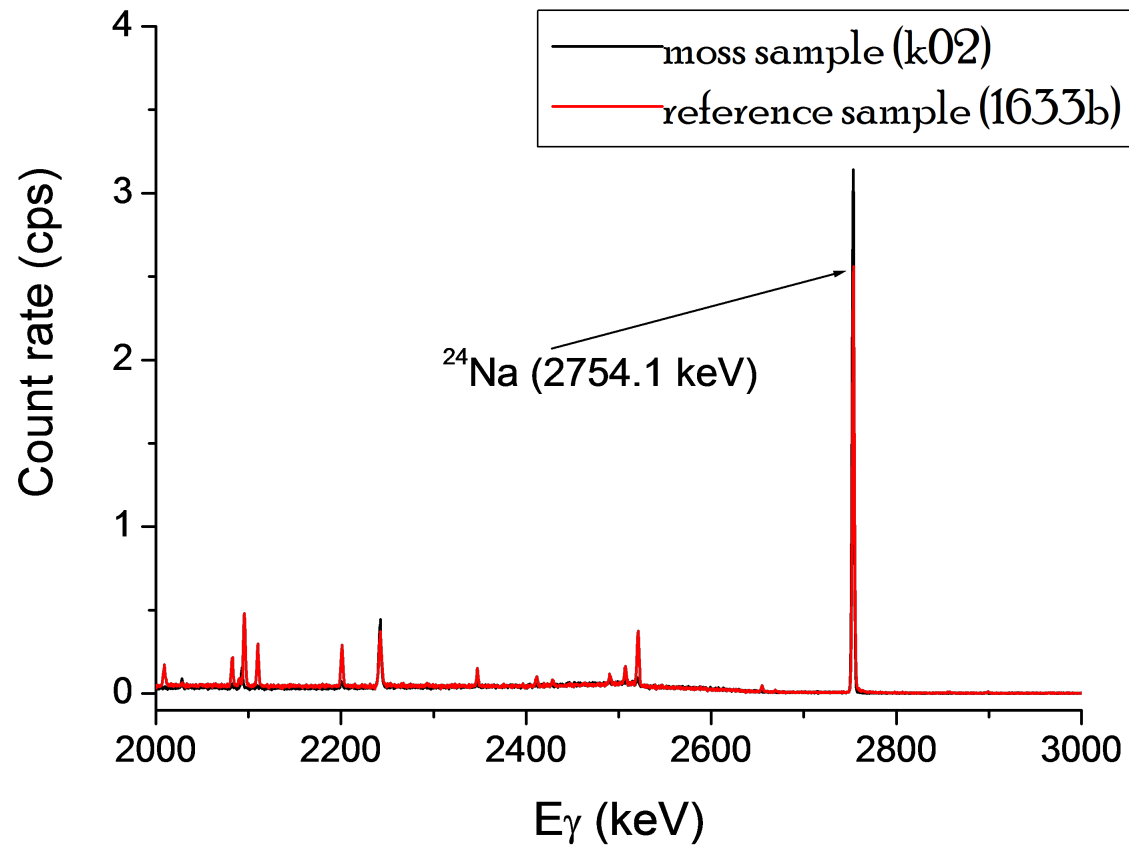


Figure 4.15: Long-lived 1 isotopes spectrum \rightarrow (2000 - 3000) MeV energy region.

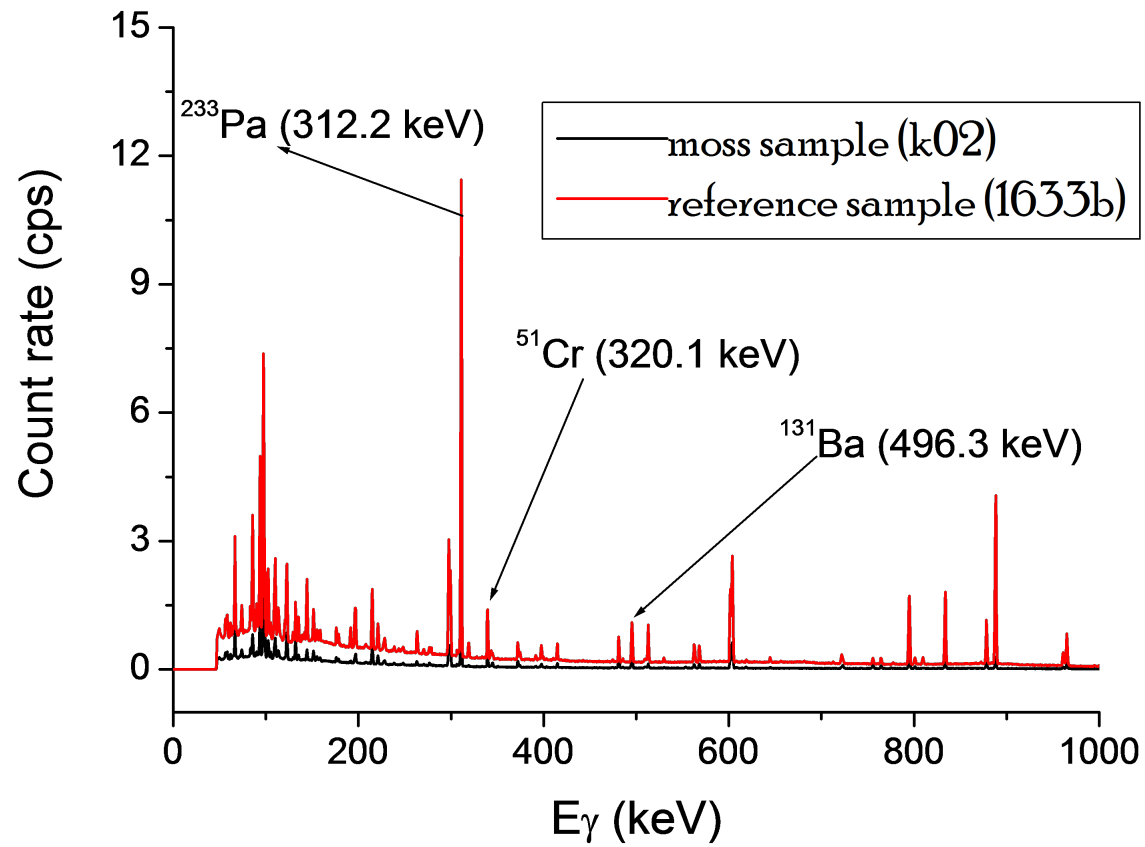


Figure 4.16: Long-lived β isotopes spectrum \rightarrow (0 - 1000) MeV energy region.

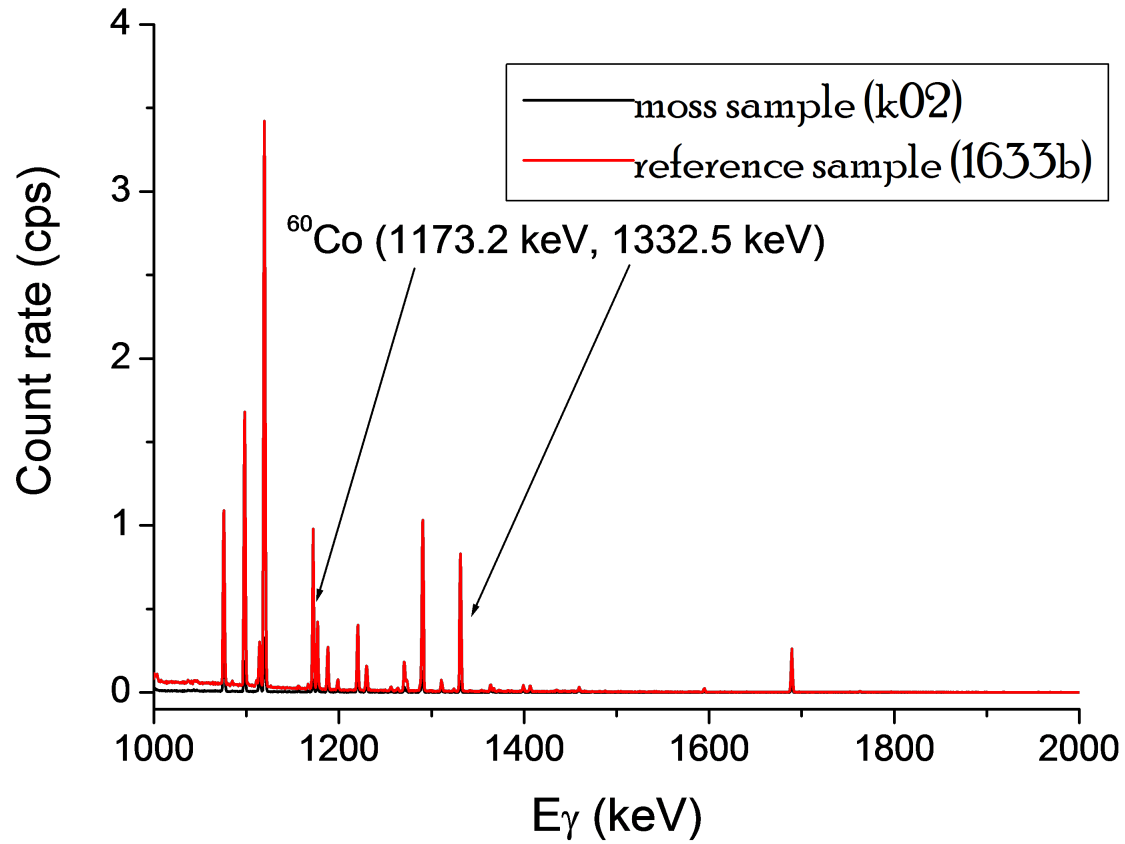


Figure 4.17: Long-lived 2 isotopes spectrum \rightarrow (1000 - 2000) MeV energy region.

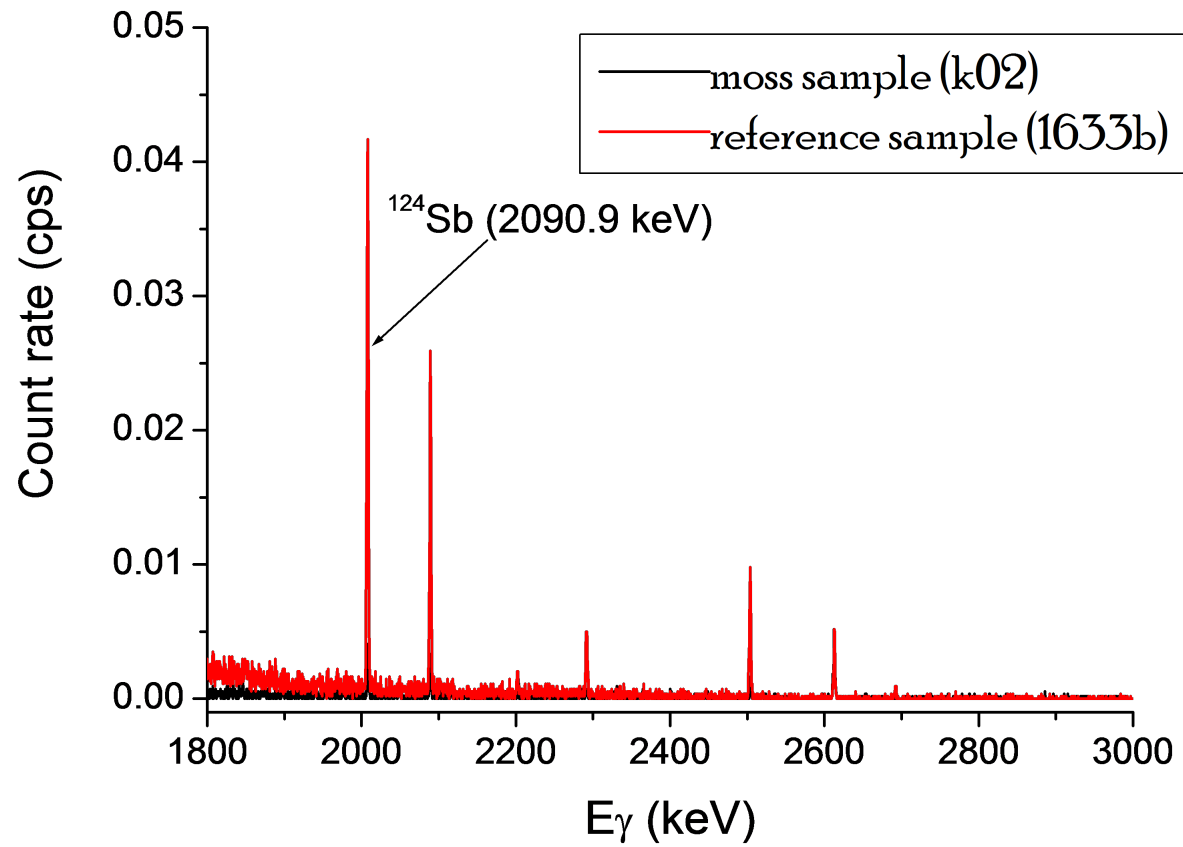


Figure 4.18: Long-lived 2 isotopes spectrum → (1800 - 3000) MeV energy region.

4.2 Calculating Elemental Concentrations

Elemental content in samples for this study was determined quantitatively using an automated 'concentration program' that was developed for NAA studies at the IBR-2 Reactor. This concentration program was created using the Visual Studio programming environment. The concentration program is based on the NAA comparative technique. This is where the analyzed samples and the standard reference material (SRM), with known and certified concentration values of elements, are simultaneously irradiated. Thereafter, concentrations of elements in the samples are calculated using isotope activities recorded in output files from Genie 2000 analysis of the spectra (associated with samples, standards, and the neutron flux monitors). The concentration program is based on a proportional comparison of activities of the same isotopes in the sample as well as in the standard. If the analyzed samples and standards were irradiated at different times or measured at different times and/or different positions in the irradiation channel, the program takes into account the differences in neutron fluxes. For this purpose, neutron flux monitors (one being the base monitor) are irradiated together with standard samples. Then, the activities of the isotopes in standard samples corresponding to other monitors are recalculated (corrected) to correspond to the base flux using Equation 4.2.1 [161].

$$A_{\text{std. corr.}} = A_{\text{std.}} \frac{A_{\text{base mon. std.}}}{A_{\text{mon. std.}}}, \quad (4.2.1)$$

where; $A_{\text{std. corr.}}$ is corrected isotope activity in the standard,
 $A_{\text{std.}}$ is the initial isotope activity in the standard,
 $A_{\text{base mon. std.}}$ is the activity of the base standard monitor, and
 $A_{\text{mon. std.}}$ is the activity in the standard monitor.

Moreover, the program analyzes the results to reveal possible random errors. The scheme followed by the concentration program in calculating final concentrations of elements in the analysed samples is presented in Figure 4.19 [161]. Table 4.3 gives a list of standard reference materials (SRM) certified by the National Institute for Standards and Technology (NIST) in the USA, formerly known as the National Bureau of Standards (NBS), that were used in this study.

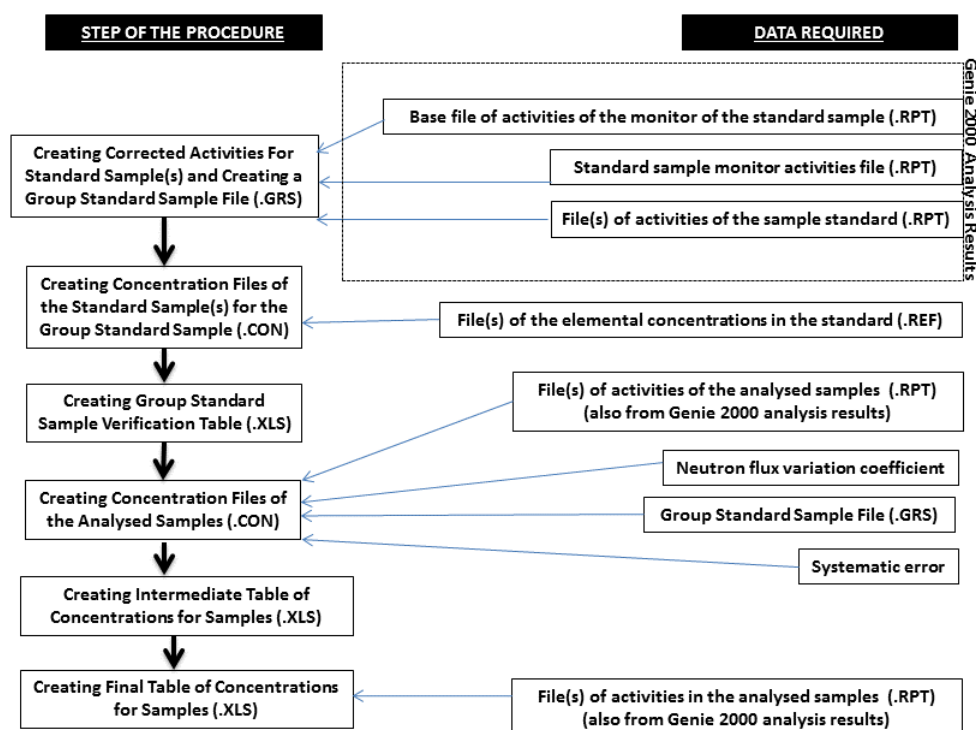


Figure 4.19: Concentration program flowchart [161].

Table 4.3: List of NIST/NBS SRMs used for elemental concentration calculations in this study.

SRM No.	SRM Name	Isotope Type Used for
1515	Apple Leaves	SLI
1575a	Pine Needles	SLI
1571	Orchard Leaves	SLI
1547	Peach Leaves	SLI
1568a	Rice Flour	SLI
2711	Montana Soil	SLI
2709	San Joaquin Soil	SLI
1632c	Bituminous Coal	SLI
1549	Non-Fat Milk Powder	SLI
1572	Citrus Leaves	SLI
1633b	Coal Fly Ash	LLI 1 & 2
2710	Montana Soil	LLI 1 & 2
1633c	Coal Fly Ash	LLI 1 & 2

Using the concentration program discussed above, elemental concentrations in the samples for this study (C_{sample} in $\mu\text{g/g}$) were calculated based on Equation 4.2.2.

$$C_{\text{sample}} = C_{\text{std.cert.}} \frac{A_{\text{sample}}}{A_{\text{GSS}}} \quad (4.2.2)$$

where;

$C_{\text{std.cert.}}$ is the certified (rated) concentration of the element in the standard reference material,

A_{sample} is the isotope activity in the analyzed sample, and

A_{GSS} is the isotope activity in the group standard (comprising a combination of reference materials).

Thereafter, uncertainties in elemental concentrations in samples ($\sigma_{C_{\text{sample}}}$ in %) were calculated using Equation 4.2.3.

$$\sigma_{C_{\text{samp}}} = 100 \times \sqrt{\left(\frac{\Delta A_{\text{samp}}}{A_{\text{samp}}}\right)^2 + \left(\frac{\sigma_{C_{\text{std.cert.}}}}{100}\right)^2 + \left(\frac{\Delta A_{\text{std}}}{A_{\text{std}}}\right)^2 + \left(\frac{\sigma_{SE}}{100}\right)^2} \quad (4.2.3)$$

where; ΔA_{sample} is the uncertainty of the isotope activity in the sample,

$\sigma_{C_{\text{std.cert.}}}$ is the certified uncertainty of the element concentration in the standard reference material (in %),

ΔA_{std} is the uncertainty of isotope activity in the standard reference material,

$A_{\text{std.}}$ is the calculated isotope activity in the standard reference material, and σ_{SE} is the systematic error in percent.

In order to assess the accuracy of the JINR 'concentration program', γ -ray spectra acquired for various irradiated reference materials were analysed and the results were compared with the certified values. The results from these investigations are shown in Appendices B and D.

As an alternative way of verifying the results produced using the automatic program, manual calculations of the concentrations of elements were also performed using Equation 4.2.4.

$$C_{\text{samp}} (\text{ppm}) = \frac{N_{\text{samp}}}{N_{\text{std}}} \times \frac{(t_{\text{cD}} \mathfrak{R} m)_{\text{std}}}{(t_{\text{cD}} \mathfrak{R} m)_{\text{samp}}} \times C_{\text{std}} (\text{ppm}) \quad (4.2.4)$$

where; C_{samp} is concentration of the element in the sample,

N is the γ -ray net peak area of the isotope γ -ray photopeak in the sample or in the standard reference material,

D is the decay factor = $\exp(-\lambda t_{\text{d}})$,

t_{d} is the delay time,

\mathfrak{R} is the counting factor = $[1 - \exp(-\lambda t_{\text{c}})] / \lambda t_{\text{c}}$,

t_{c} is the counting time

λ is the decay constant $=\ln 2/t_{1/2}$,

m is the mass of the sample or the standard reference material, and

C_{std} is concentration of the element in the standard reference material.

The uncertainties associated with calculated elemental concentrations were calculated using Equation 4.2.5

$$\sigma_{C_{\text{samp}}} (\text{ppm}) = C_{\text{samp}} \times \sqrt{\left(\frac{\sigma_1}{N_{\text{samp}}}\right)^2 + \left(\frac{\sigma_2}{N_{\text{std}}}\right)^2 + \left(\frac{\sigma_3}{C_{\text{std}}}\right)^2} \quad (4.2.5)$$

where; σ_1 is the uncertainty in the γ -ray net peak area of the isotope in the sample,

σ_2 is the uncertainty in the γ -ray net peak area of the isotope in the standard reference material, and

σ_3 is the uncertainty in the concentration of the element in the standard reference material.

The relative method of INAA is considered more accurate than the absolute method. This is because the main formula for the absolute method involves more quantities (see Equation 4.2.6) which might contribute to the total error [142].

$$C_{\text{samp}} (\text{ppm}) = A_{\text{p}} \frac{\lambda \cdot W}{(1-e^{-\lambda t_{\text{irr}}}) \cdot e^{-\lambda t_{\text{D}}} \cdot (1-e^{-\lambda t_{\text{C}}}) \cdot \Phi \cdot \sigma \cdot \Gamma \cdot \varepsilon \cdot I_{\text{a}} \cdot \theta \cdot N_{\text{Av}}} \quad (4.2.6)$$

where; A_{p} is the γ -ray net peak area of the isotope photopeak in the sample,

λ is the decay constant,

W is the atomic mass of the element,

t_{irr} is the irradiation time,

t_{D} is the delay time (between irradiation and start of counting),

t_{C} is the counting time,

Φ is the neutron flux,

σ is the reaction cross-section,

Γ is the gamma-ray branching ratio (i.e. the probability of the disintegrating nucleus emitting a photon of E_{γ}),

ε is the photopeak detection efficiency (function of γ -ray energy),

I_{a} is the absolute intensity,

θ is the isotopic abundance of the target isotope, and

N_{Av} is Avogadro's number.

Continuous calibration of the measuring system is recommended during the analysis. This includes; neutron flux monitoring, detector efficiency determination, as well as energy calibration of the spectrometric channels [1, 4].

Chapter 5

Results and Discussion

This discussion of results is separated into two sections, i.e. for passive biomonitoring (performed in 2012) and active biomonitoring (performed from 2013 till 2014).

5.1 Biomonitoring Results: Passive

In passive biomonitoring, 44 elements were identified and their concentrations determined using INAA and ICP-MS. INAA allowed determination of 33 elements (Na, Mg, Al, Cl, K, Ca, Sc, Ti, V, Cr, Mn, Fe, Co, Zn, As, Se, Br, Rb, Sr, Sb, I, Cs, Ba, La, Ce, Nd, Sm, Tb, Hf, Ta, W, Th, U), while ICP-MS allowed determination of 26 elements (Al, V, Cr, Mn, Co, Ni, Cu, Zn, As, Se, Sr, Mo, Cd, Sn, Ba, Hg, Pb, B, Ca, Fe, K, Li, Mg, Na, P, Si).

As part of confirming concentration results from the INAA measurements, equations 4.2.4 and 4.2.5 were respectively used to perform manual calculations of elemental concentrations as well as their uncertainties. Some of the obtained results using moss samples Stellenbosch (k02) and from Franschoek (k23) are demonstrated in Tables 5.1 and 5.2, respectively. The first sample (k02) was measured with both INAA and ICP-MS, while k23 was only measured with INAA. In both cases, INAA manual and automated results are in agreement with each other. Hence, the preferred results from the overall results were on the whole the ones provided by INAA. Moreover, INAA was confirmed as a powerful reference method for measurement to determine SI traceable values of element content in complex samples [1, 12, 44, 45]. This is because, INAA offers improved sensitivity for most elements [1, 12, 44–46, 166–168].

Table 5.1: Comparison of sample k02 for concentrations calculated manually with the results from the automated concentration program for the INAA measurements and the ICP-MS results.

Element	INAA data		ICP-MS Data
	C, ppm (manual)	C, ppm (automated)	C, ppm
Elements identified from short-lived isotopes			
Al	6700 ± 170	6200 ± 160	5200 ± 170
Mn	152 ± 5	158.3 ± 1.8	132.3 ± 1.5
V	5.6 ± 1.3	5.2 ± 0.4	6.2 ± 0.1
Elements identified from long-lived isotopes 1			
Na	656 ± 18	653 ± 19	270 ± 20
As	2.01 ± 0.04	1.8 ± 0.1	1.35 ± 0.01
K	7800 ± 200	7300 ± 500	5700 ± 500
Elements identified from long-lived isotopes 2			
Ba	88 ± 4	85 ± 4	53.3 ± 0.7
Co	2.1 ± 0.1	2.1 ± 0.1	1.9 ± 0.1
Cr	5.3 ± 0.5	5.1 ± 1.4	146.3 ± 1.4

Table 5.2: Comparison of sample k23 for concentrations calculated manually with the results from the automated concentration program for the INAA measurements.

Element	C, ppm (manual)	C, ppm (automated)
Elements identified from short-lived isotopes		
Al	16000 ± 200	15000 ± 300
Cl	1800 ± 200	1900 ± 100
V	13.9 ± 1.1	13.2 ± 0.5
Elements identified from long-lived isotopes 1		
Na	1190 ± 30	1190 ± 30
Br	22.7 ± 1.2	24 ± 7
K	4600 ± 200	4400 ± 400
Elements identified from long-lived isotopes 2		
Ba	35 ± 4	32 ± 2
Co	0.7 ± 0.1	0.7 ± 0.1
Zn	27.9 ± 1.8	28.6 ± 1.1

ICP-MS was used to obtain results for other environmentally meaningful elements which could not be determined using INAA (i.e.; Cd, Pb, Cu and Hg) [1]. However, a total of 15 elements (Na, Mg, Al, K, Ca, V, Cr, Mn, Fe, Co, Zn, As, Se, Sr, Ba) were determined by both INAA and ICP-MS. The concentrations for these elements are shown in Appendix G.1. This helped in

facilitating an intercomparison of results from the two techniques in order to check for correlations using R , the square root of the R^2 (coefficient of determination). In Figure 5.1, linear correlation coefficients for all elements that were determined by INAA and ICP-MS are plotted. These linear correlation coefficients indicate strength and direction of the linear relationship between INAA and ICP-MS results for the plotted elements. All those elements with correlation coefficients between 80% and 100% (i.e. $0.8 \leq R \leq 1.0$) are the ones considered to have good correlations.

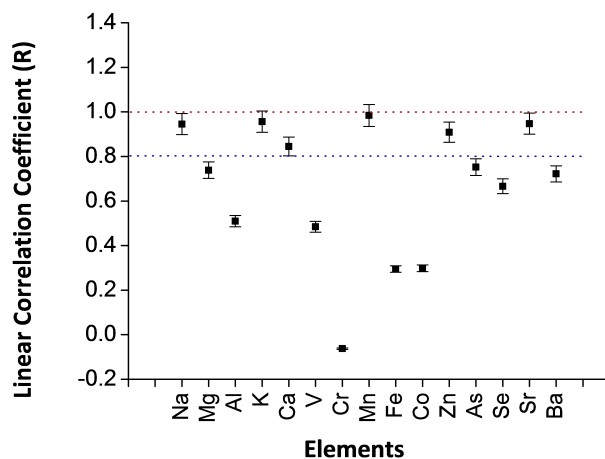


Figure 5.1: *Linear correlation coefficients graph for elements determined by INAA and ICP-MS for both mosses and lichens (passive biomonitoring).*

Out of the 15 elements; Ca, K, Na, Sr, Zn and Mn indicated favourable linear correlation coefficients (i.e. $R \geq 80\%$). Correlation graphs (generated from both moss and lichen data) for Na, K, Ca, Mn, Zn and Sr concentrations (in $\mu\text{g}\cdot\text{g}^{-1}$ or ppm) are shown in Figures 5.2 → 5.7. Correlation graphs for all the other elements with $R \leq 80\%$ are shown in Figures 5.8 → 5.16. Halogens, which are known to be the indicators of emissions from the ocean, as well as rare earth elements (REE) could not be determined by ICP-MS. Moreover, toxic elements (Pb, Cd, Hg) were not determined by INAA due to the reasons mentioned in subsection 2.6.2. Descriptive statistics per element for all passive biomonitoring results are given in Appendix C.

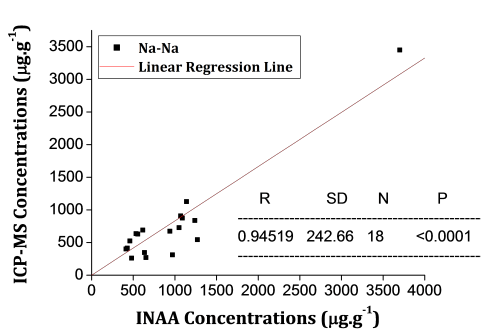


Figure 5.2: Na correlations.

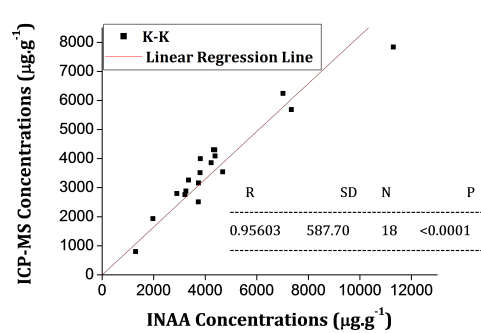


Figure 5.3: K correlations.

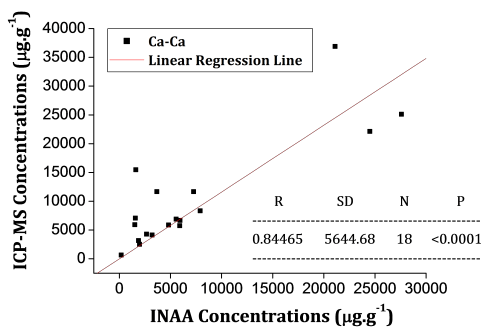


Figure 5.4: Ca correlations.

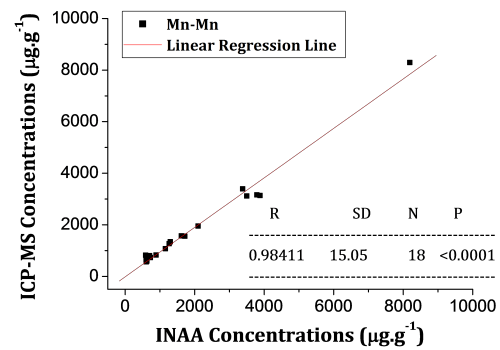


Figure 5.5: Mn correlations.

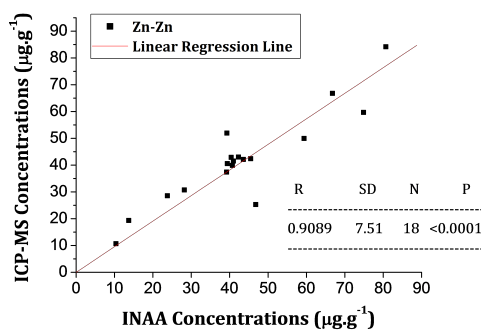


Figure 5.6: Zn correlations.

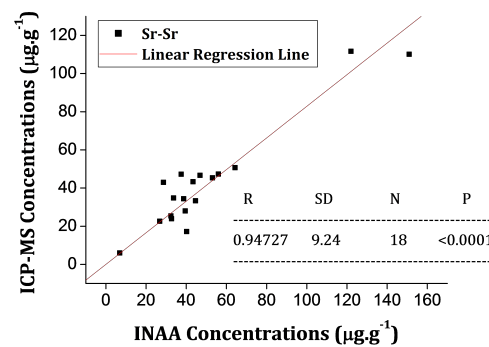


Figure 5.7: Sr correlations.

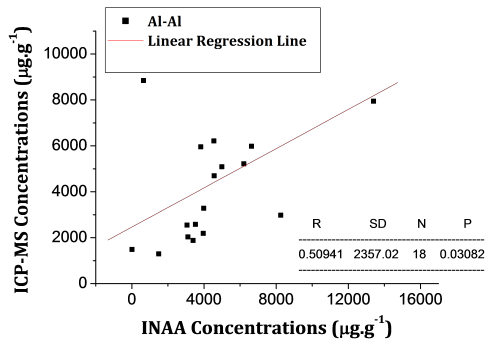


Figure 5.8: *Al* correlations.

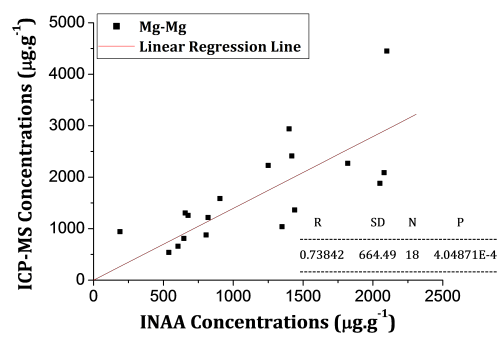


Figure 5.9: *Mg* correlations.

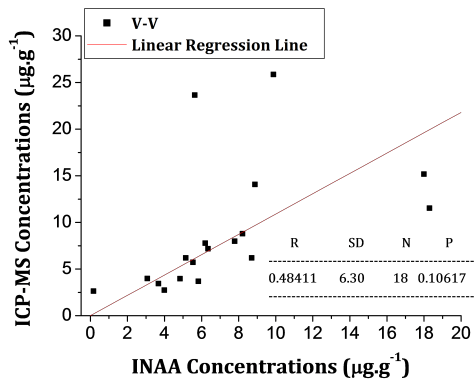


Figure 5.10: *V* correlations.

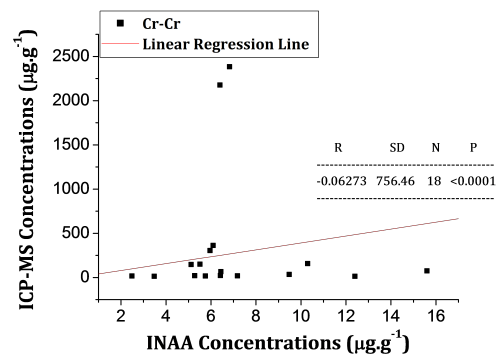


Figure 5.11: *Cr* correlations.

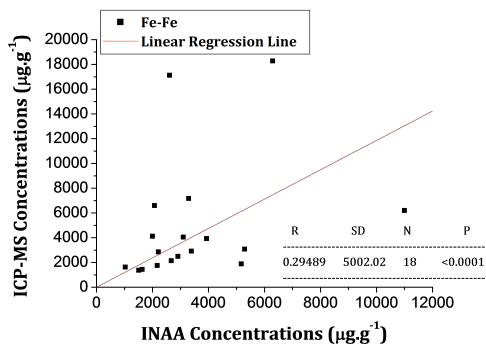


Figure 5.12: *Fe* correlations.

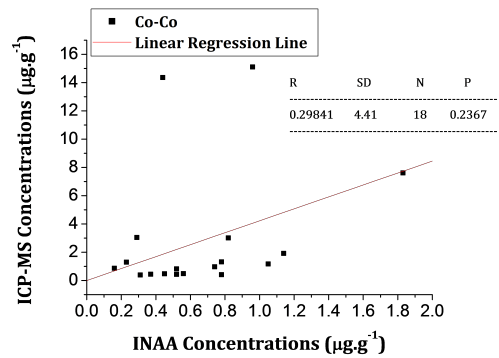


Figure 5.13: *Co* correlations.

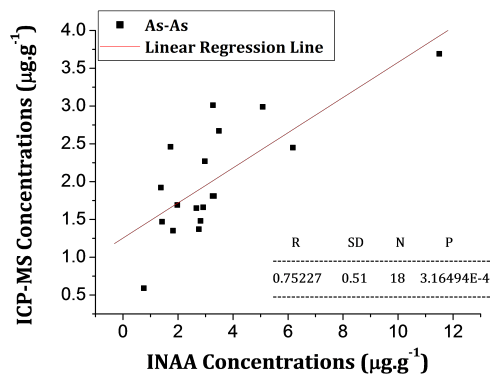


Figure 5.14: *As* correlations.

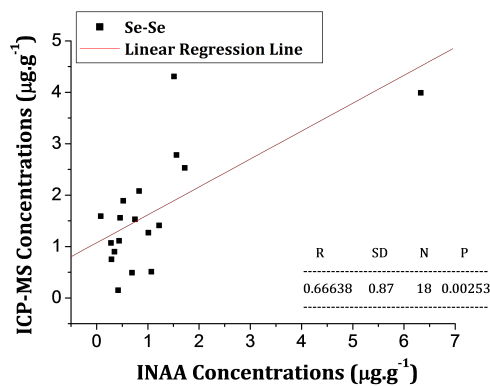


Figure 5.15: *Se* correlations.

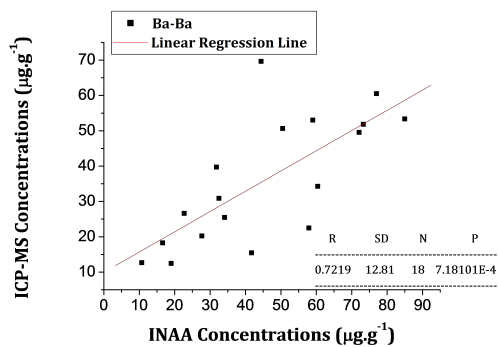


Figure 5.16: *Ba* correlations.

5.1.1 Discussion: Passive

Air pollution monitoring is an important task since trace elements may be generated through a variety of sources. These include natural disasters (e.g. volcanoes), natural weathering of parent rocks, as well as various anthropogenic activities. Therefore, not all elements determined during trace element analysis are potentially toxic or toxic air pollutants. However, determination of these elements is also important due to their vital role in geochemical cycles. These elements, which are not potentially toxic or toxic, can be toxic when their concentrations are too high in the environment. Moreover, their determination is usually just carried out because it does not necessarily require any remarkable extra budget [1, 169]. All the elements determined in this study can be separated into six groups, i.e. major elements, essential (also known as biologically important) trace elements, potentially toxic trace elements, toxic trace elements, rare earth elements (REE), as well as halogens (see Table 5.3) [1, 169, 170]. Dividing elements into separate groups helps in facilitating a meaningful analysis as well as inter-comparison between certain elements of the same group. This is due to the huge differences in elemental concentration values found between different groups of elements, e.g. major elements and toxic trace elements. Table 5.4 gives an overall pattern (based on average values) for elemental concentrations for all groups of elements found in this study, using both by INAA and ICP-MS.

Table 5.3: *Classification of elements determined in this study [1, 169, 170].*

Major Elements	Trace Elements				
	Essential	Potentially Toxic	Toxic	REE	Halogens
Na	Zn	As	Cd	La	Cl
Mg	Se	Ba	Hg	Ce	Br
Al	Co	Co	Pb	Nd	I
Cl	I	Cs		Sm	
K	Cr	Sn		Tb	
Ca	Sr	Li			
Fe	Cu	Se			
P	B	Mo			
Si	Ni	Cu			
	Rb	Ta			
	Mn	Sb			
	V	W			
	Ti	Sc			
	Ba	Hf			
	Mo	Th			
		U			

Table 5.4: Group patterns for elemental concentration (passive biomonitoring results).

Group	Technique	Pattern
Major Elements	INAA	Ca>Al>K>Fe>Na>Cl>Mg
	ICP-MS	Ca>Fe>Al>K>Mg>Na>P>Si
Essential Elements	INAA	Mn>Ti>Ba>Sr>Zn>Rb> I>V>Cr>Se>Co
	ICP-MS	Zn>Cr>Ni>Mn>Ba>Sr> B>Cu>Mo>V>Co>Se
Potentially Toxic Elements	INAA	As>Se>Th>Hf>Sc>Co> U>Cs>Sb>W>Ta
	ICP-MS	Cu>Mo>Co>Li>Se>Sn>As
Rare Earth Elements	INAA	Ce>La>Nd>Sm>Tb
	ICP-MS	-
Halogens	INAA	Cl>Br>I
	ICP-MS	-
Toxic Trace Elements	INAA	-
	ICP-MS	Pb>Cd>Hg

When they are within biologically optimum concentrations, major elements and biologically important elements are required by humans for both good health and longevity. However, at very low or higher concentrations they negatively affect biological functioning of the body. Human beings rarely show any deficiency due to these elements. This is because these elements are needed in the body only in trace concentrations. Even so, major and essential elements are still necessary for the fulfilment of essential functions in the body [171]. The availability and fluctuation in concentrations of major and essential elements in the body is highly influenced by several dietary inhibitors including toxic metals like Cd, Pb and Hg. These toxic elements also lead to physiological and toxicological changes in humans. They have been reported to affect nutritional status of essential micro-nutrients like Fe, Zn and Cu in humans [46, 170, 171].

5.1.1.1 Elemental Concentrations in Mosses and Lichens

Results from passive biomonitoring in this study confirmed the fact that mosses are generally more efficient at concentrating trace and other elements as compared to lichens (see Figures 5.17 → 5.4).

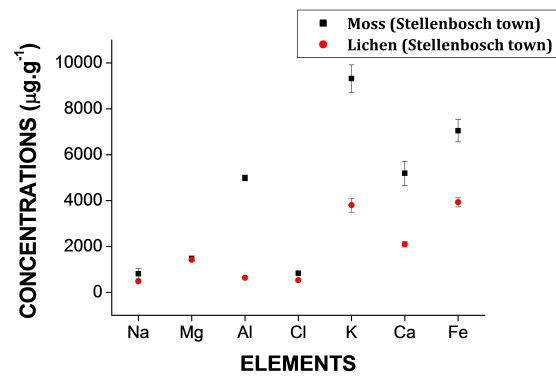


Figure 5.17: Major elements Stellenbosch (INAA)

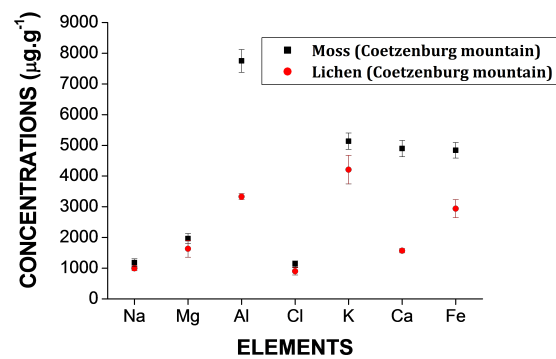


Figure 5.18: Major elements for Coetzenburg mountain (INAA).

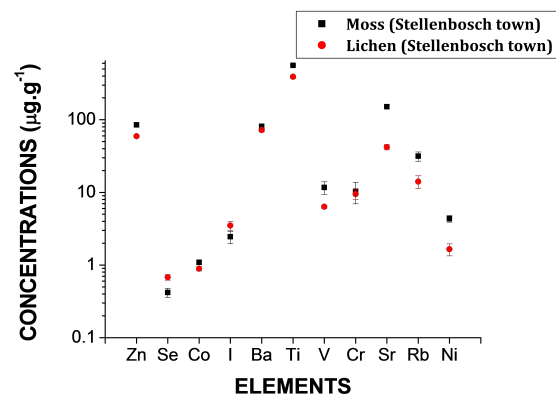


Figure 5.19: Essential elements for Stellenbosch (INAA).

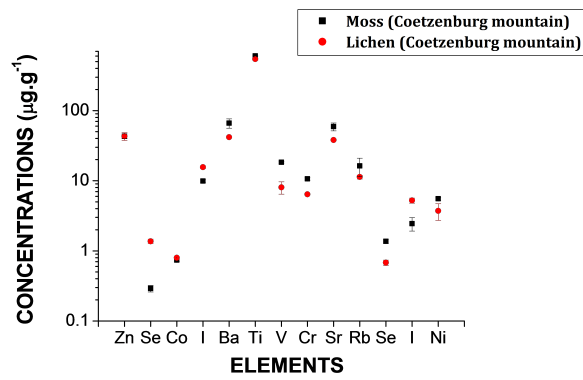


Figure 5.20: Essential elements for Coetzenburg mountain (INAA).

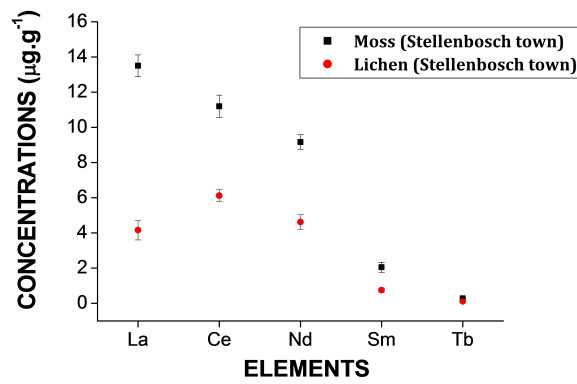


Figure 5.21: Rare earth elements for Stellenbosch (INAA).

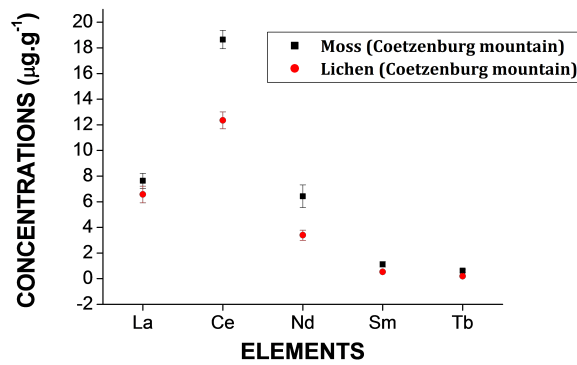


Figure 5.22: Rare earth elements for Coetzenburg mountain (INAA).

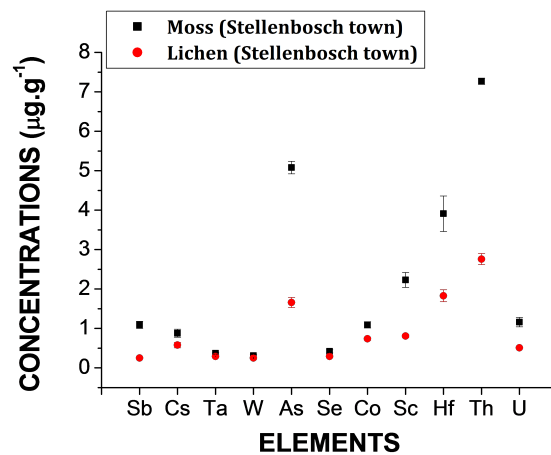


Figure 5.23: Potentially toxic elements for Stellenbosch (INAA).

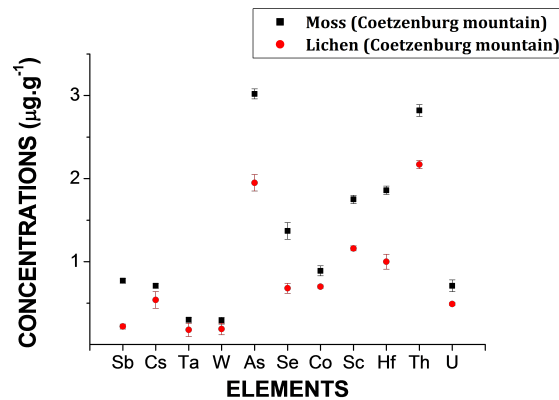


Figure 5.24: Potentially toxic elements for Coetzenburg mountain (INAA).

Our results have shown that lichens concentrations are generally lower than concentrations of mosses. This comparison was based on mosses and lichens that were collected from Victoria Street in Stellenbosch town as well as Coetzenburg mountain. This is because those were the only two locations from which mosses and lichens could be collected from the same point. The presented data above is from INAA (similar trends were observed in the ICP-MS data).

Response patterns to increasing levels of atmospheric pollutants differ from biomonitor to biomonitor and also from species to species. These response patterns vary from relative resistance to high sensitivity [172]. Even with halogens in this study, this variation in response patterns was confirmed. This

is because, halogens behaved differently as compared to other elements. Higher concentrations of halogens were observed in lichens as opposed to mosses. As shown by Figure 5.25 and Figure 5.26, this behavior was observed to be similar in lichen and moss samples collected from both Stellenbosch town and Coetzenburg mountain. In his review of lichens and rocks, specifically looking at the geological application of lichenology, Easton[173] mentioned that lichens are highly sensitive to halogens and sulphur dioxide. This characteristic behavior of lichens has also been recently confirmed by the UK Air Pollution Information System [174].

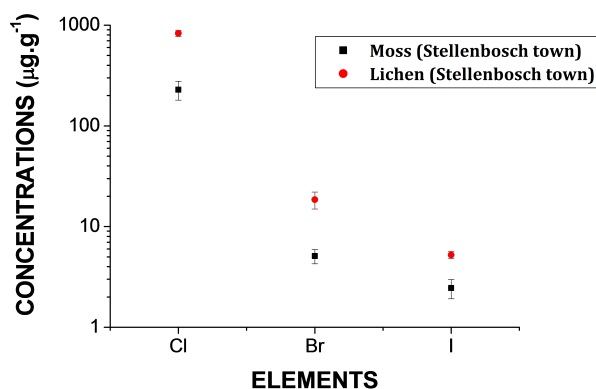


Figure 5.25: Stellenbosch town halogen concentrations in mosses vs. lichens

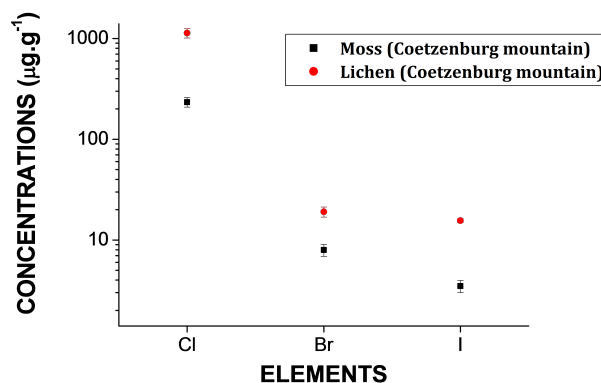


Figure 5.26: Coetzenburg mountain halogen concentrations in mosses vs. lichens

The Figures 5.27 \rightarrow 5.34 represent the average concentrations of elements in the analysed mosses in this study. Low elemental concentrations were generally found for Betty's Bay samples. No clear trend of which area has the highest elemental concentrations was observed.

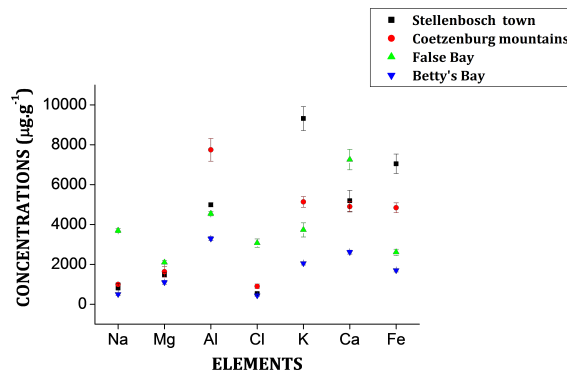


Figure 5.27: Major elements in mosses (INAA).

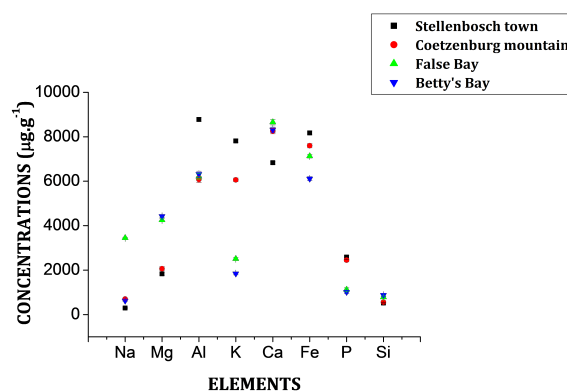


Figure 5.28: Major Elements in Mosses (ICP-MS).

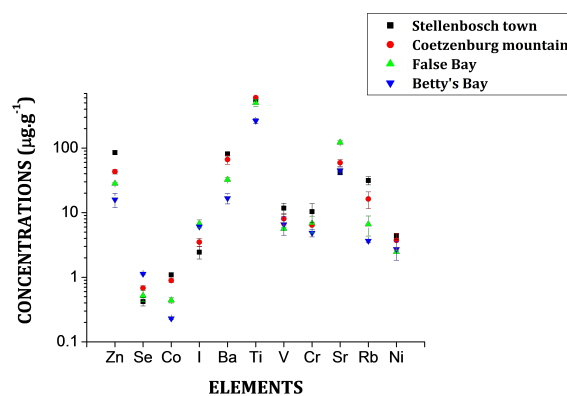


Figure 5.29: Essential elements in mosses (INAA).

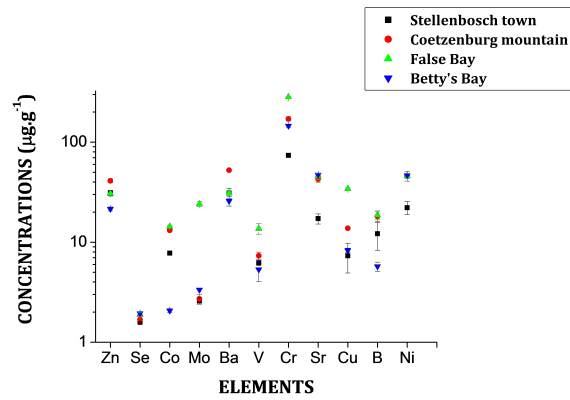


Figure 5.30: *Essential elements in mosses (ICP-MS).*

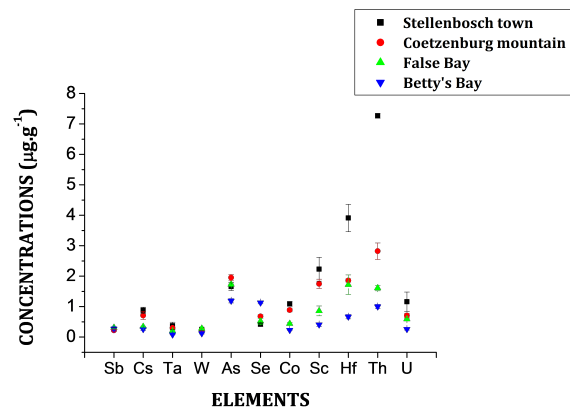


Figure 5.31: *Potentially toxic elements in mosses (INAA).*

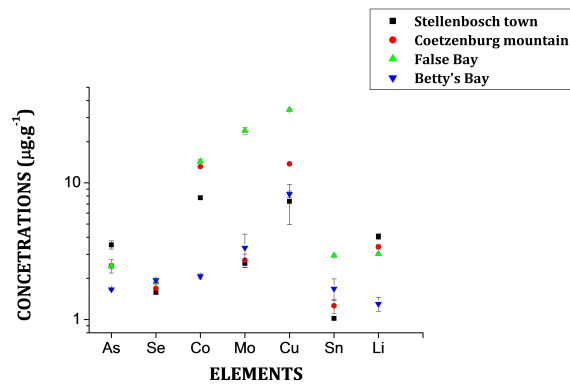


Figure 5.32: *Potentially toxic elements in mosses (ICP-MS).*

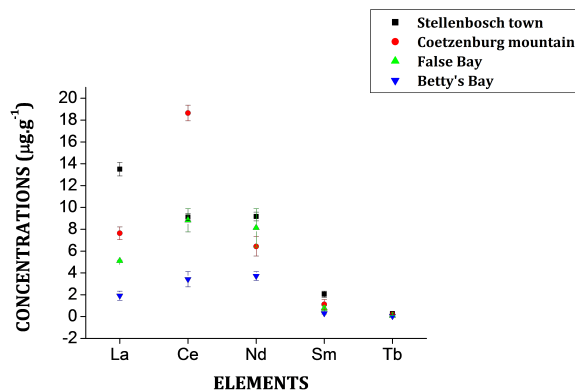


Figure 5.33: Rare earth elements in mosses (INAA).

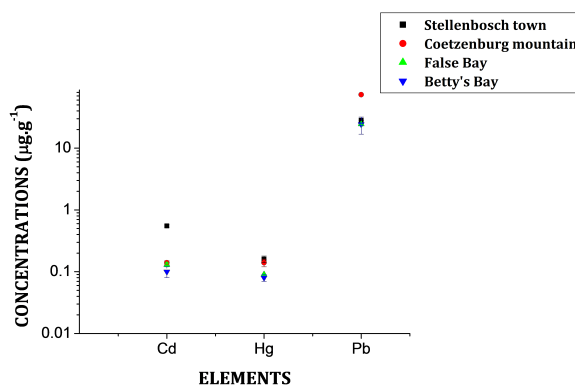


Figure 5.34: Toxic elements in mosses (ICP-MS).

Results of mosses from Stellenbosch town, Coetzenburg mountain, and Betty's Bay showed comparable values. However, there was a correlation found for toxic elements between Stellenbosch town and Coetzenburg mountain as well as between Betty's Bay and False Bay. Stellenbosch town and Coetzenburg mountain had the highest values, while Betty's Bay and False Bay had the lowest values. For lichens, low elemental concentrations were generally found for Franschoek samples. This trend was observed from the major, essential, potentially toxic, and the toxic trace elements (Figures 5.35 → 5.42).

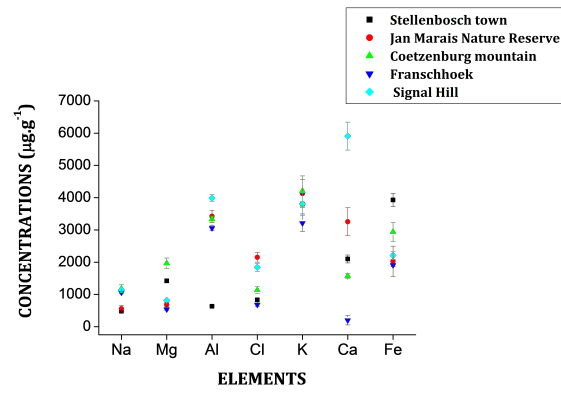


Figure 5.35: Major elements in lichens (INAA).

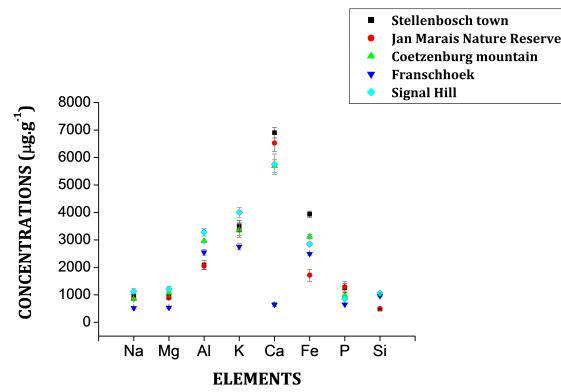


Figure 5.36: Major elements in lichens (ICP-MS).

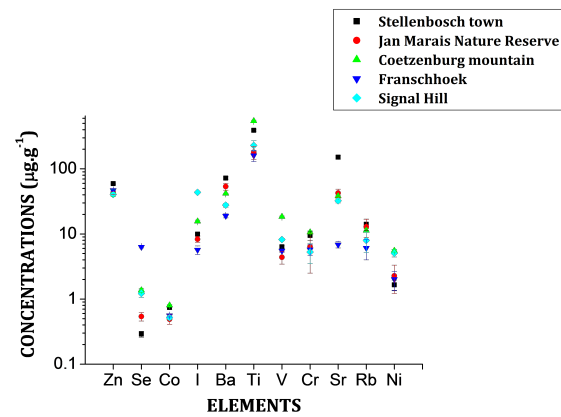


Figure 5.37: Essential elements in lichens (INAA).

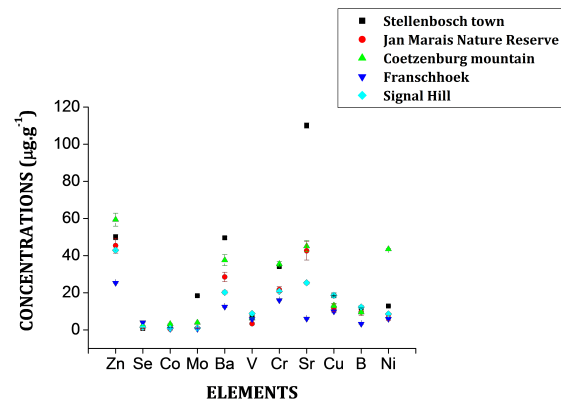


Figure 5.38: *Essential elements in lichens (ICP-MS).*

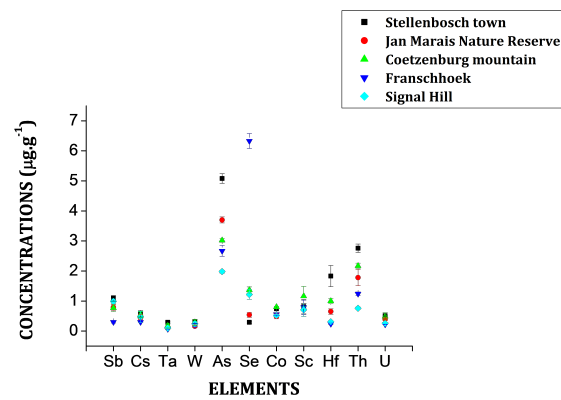


Figure 5.39: *Potentially toxic elements in lichens (INAA).*

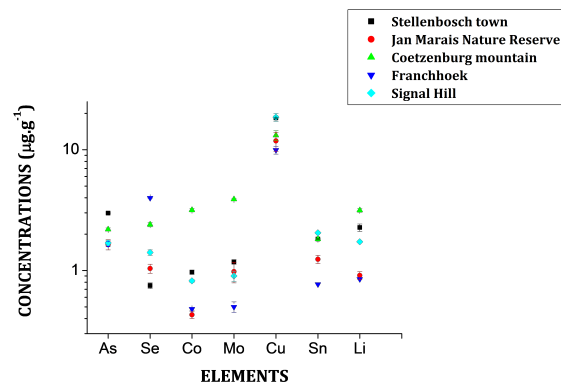


Figure 5.40: *Potentially toxic elements in lichens (ICP-MS).*

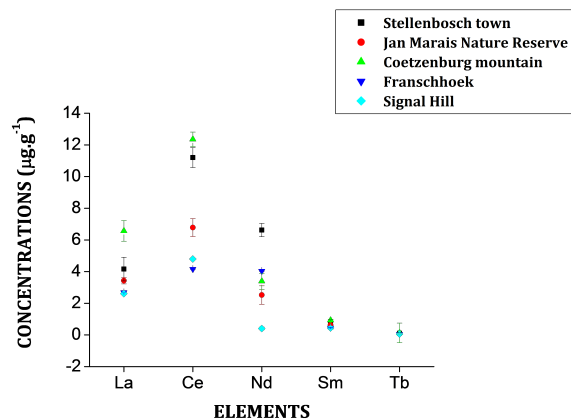


Figure 5.41: Rare earth elements in lichens (INAA).

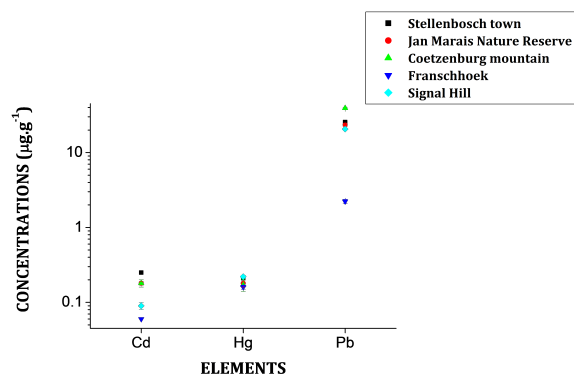


Figure 5.42: Toxic elements in lichens (ICP-MS).

As indicated by these lichen results, REE concentrations were found to be lowest in Signal Hill. As compared to all other stations from which lichens were collected, Signal Hill is closest to the ocean. Previous studies by other authors are in agreement that for coastal regions, REE concentration levels are generally lower than in areas with less effect from marine sediments [137, 175]. With the exception of REE, the second lowest elemental concentrations for the other groups of elements were generally found for Signal Hill samples. Overall, elemental concentrations in both mosses and lichens in this study were found comparable for Stellenbosch town, Coetzenburg mountain, Jan Marais nature reserve and False Bay. However, Stellenbosch concentrations do occasionally exceed those other locations.

5.1.1.2 Vehicle Emission Association with Distances from the Road

The effect of distance from the road on concentration levels of elements generally associated with vehicular emission was examined. This was done using a sampling grid from Jan Marais Nature reserve (shown in Chapter 3, subsection 3.1.1.1). As mentioned earlier in Chapter 3, Marais road was assumed to be the main source of pollution due to air pollutants emitted by vehicles on a daily basis. As indicated by Figures 5.43 - Figure 5.44, 10 elements (Pb, V, Zn, Cd, Cr, Cu, Ni, As, Ba, Sn) which are generally associated with vehicular emission [1, 27, 43, 176–178] showed a clear trend of decreasing concentrations as the distance from the road increases.

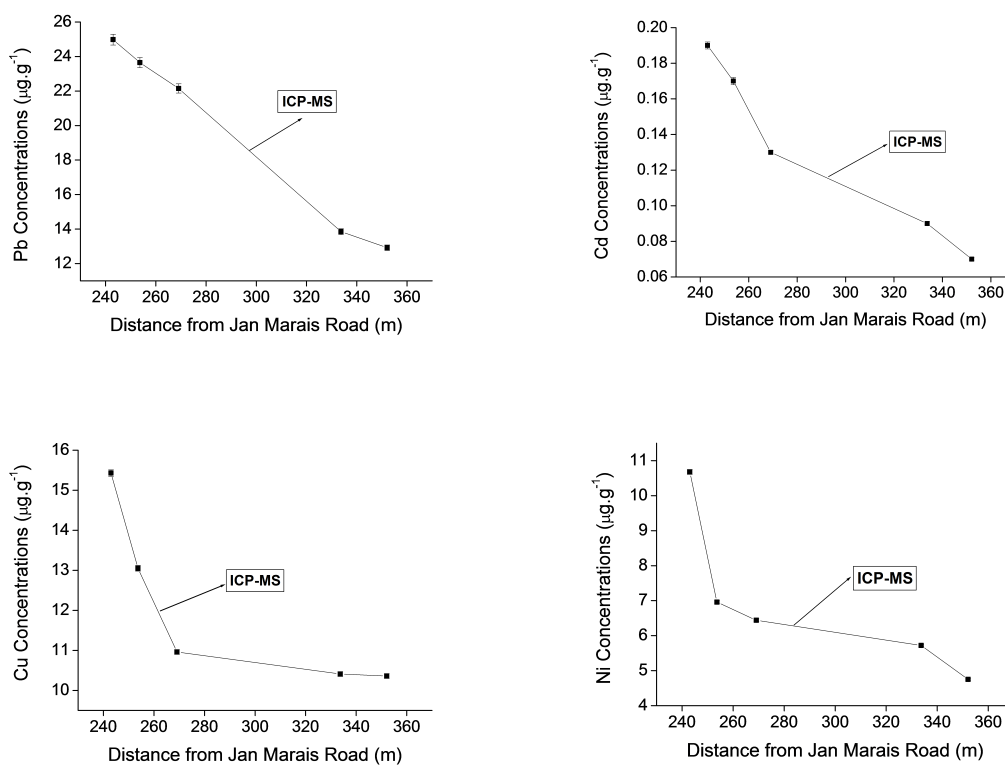


Figure 5.43: Concentrations of Pb, Cd, Cu and Ni plotted against the distance from Marais Road (lichen samples)

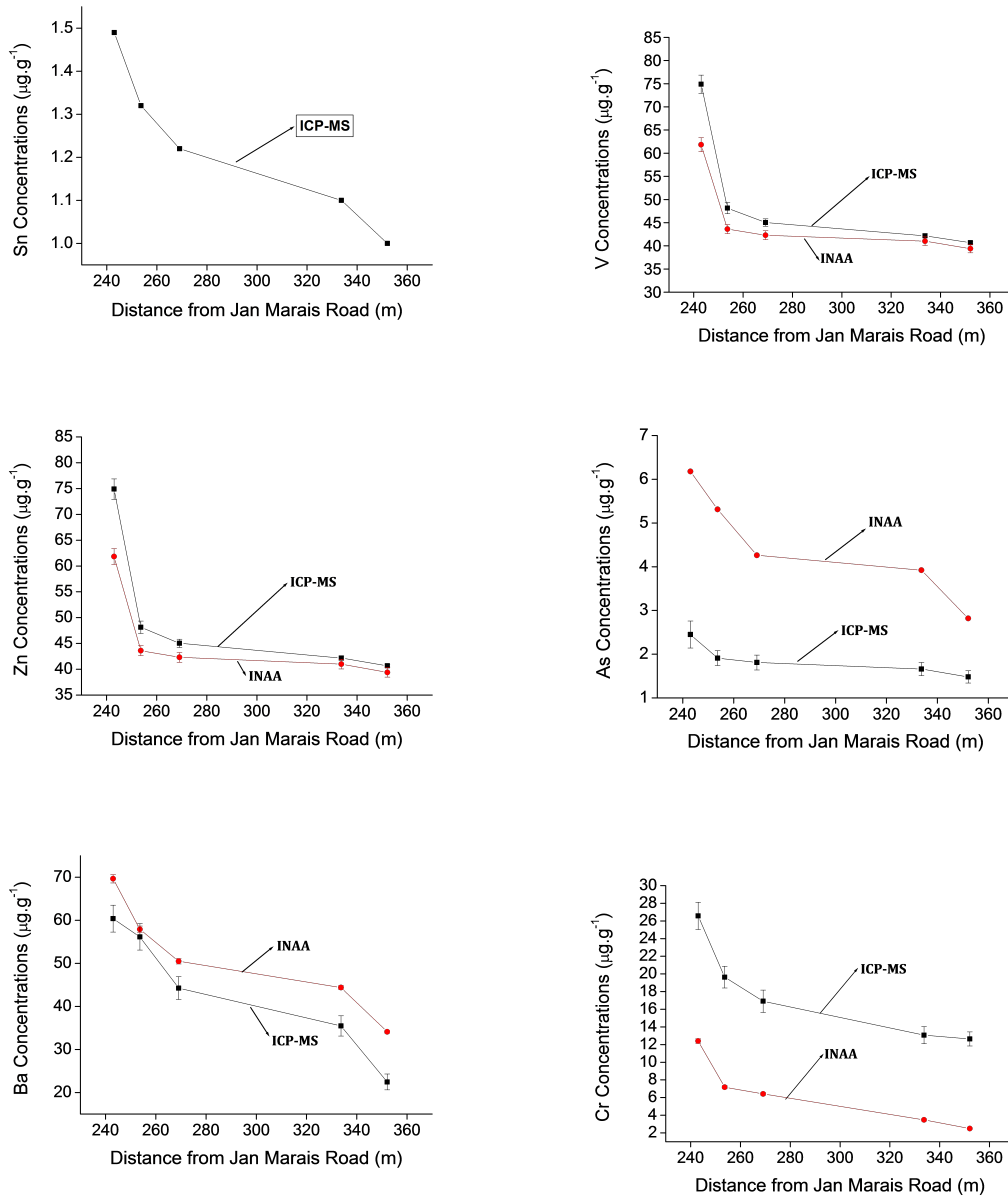


Figure 5.44: Concentrations of Sn, V, Zn, As, Ba and Cr plotted against the distance from Marais Road (lichen samples)

5.1.1.3 Analysis of Halogens

In this study, halogens were given special attention as the study area is in relative close proximity to the ocean, which is known to be a source of halogens [166, 168]. In terms of contributing to overall air pollution levels, halogens are said to be less visible or effectual and direct when compared to other types of air pollutants. Even so, their effect on humans as well as the environment can be harmful at very high concentrations. Just like many other pollutants, human exposure to halogens also comes from air, water as well as the food. However, for these contaminants, a lot of studies demonstrate that about 95 % of them are consumed by humans directly from food and only a small fraction gets inhaled from polluted air [170, 179–182].

The passive biomonitoring results of this study showed halogens to have common trend of having elevated concentrations for samples collected nearest to the ocean. Mosses showed higher halogen concentrations for False Bay and Betty's Bay as compared to Stellenbosch town (Victoria Street) and Coetzenburg mountain, which are further from the ocean. Also, lichens showed elevated halogen concentrations for Signal Hill as compared to Stellenbosch town, Jan Marais nature reserve, Coetzenburg mountain and Franschoek; which was the furthest from the ocean (see Figures 5.45-5.48).

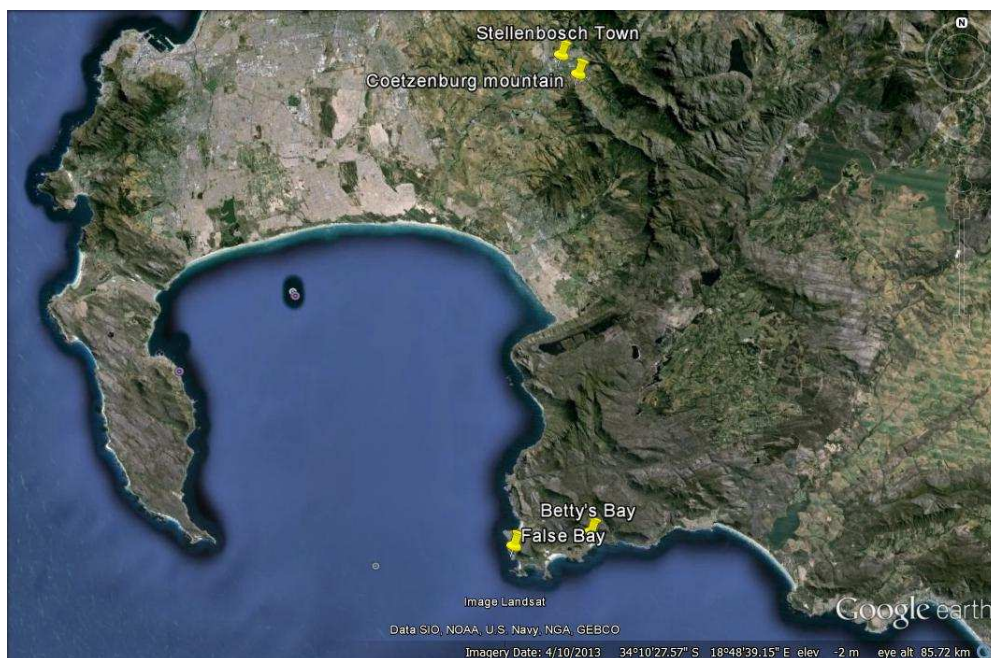


Figure 5.45: Google earth map showing locations of collected moss samples.

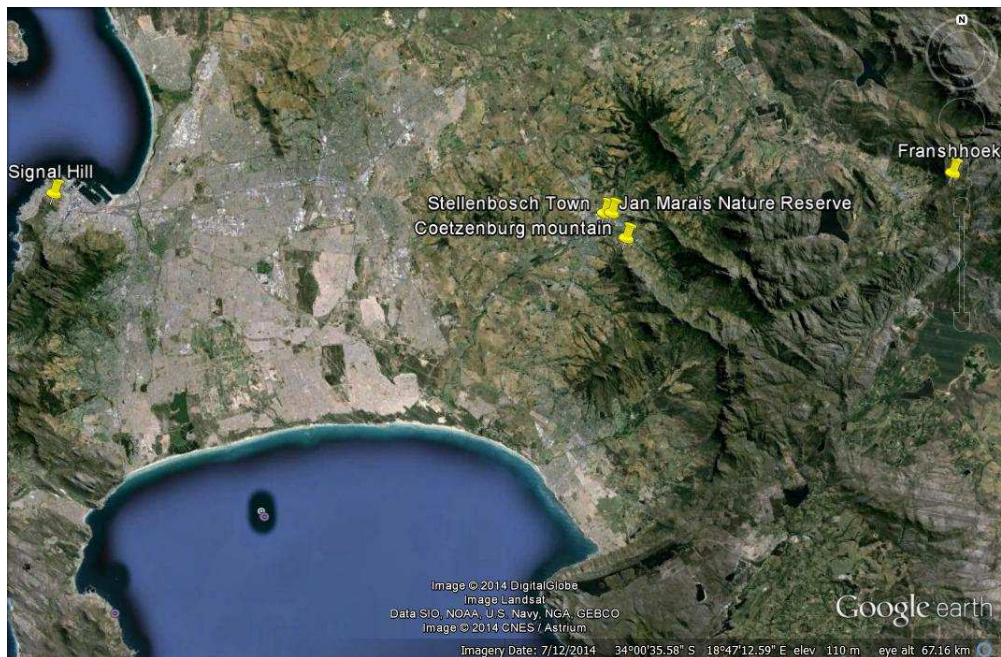


Figure 5.46: Google earth map showing locations of collected lichen samples.

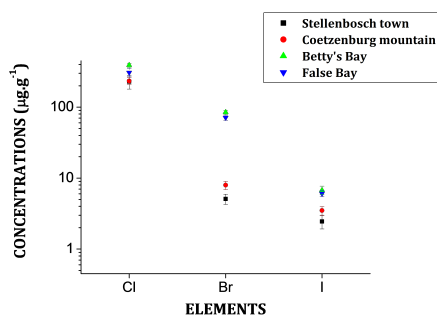


Figure 5.47: Halogens concentrations in mosses (INAA data).

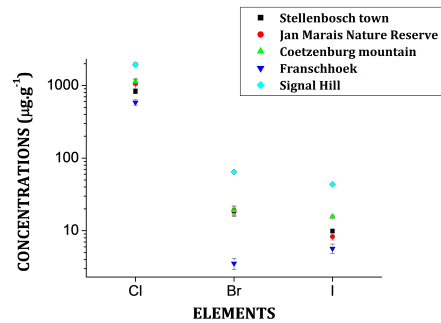


Figure 5.48: Halogens concentrations in lichens (INAA data).

5.2 Active Biomonitoring Results

In active biomonitoring, 47 elements were identified and their concentrations were determined using INAA and ICP-MS. As shown in Figure 5.49, INAA allowed determination of 37 elements (Al, Ca, Fe, K, Mg, Na, Ti, V, Cr, Mn, Co, Zn, As, Se, Sr, Mo, Sb, Ba, Cl, I, Br, La, Sm, W, U, Sc, Rb, Zr, Cs, Ce, Nd, Gd, Tb, Tm, Hf, Th), while ICP-MS allowed determination of 29 elements (Al, B, Ca, Fe, K, Mg, Na, P, Si, Li, Be, Ti, V, Cr, Mn, Co, Ni, Cu, Zn, As, Se, Sr, Mo, Cd, Sn, Sb, Ba, Hg, Pb).

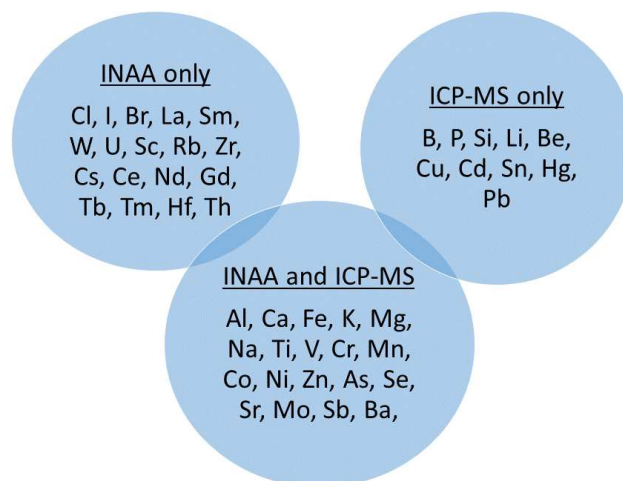


Figure 5.49: Elements identified from active biomonitoring.

In total, 18 elements (see Figure 5.49) were identified by both techniques; INAA and ICP-MS. The concentrations for these elements are shown in Appendix G.2. Using these elements, intercomparison between INAA and ICP-MS techniques was performed to check for correlations between the two techniques. Consequently, linear correlation coefficients for those elements were plotted (see Figure 5.50).

Of the 18 elements, 7 elements (Na, Mg, Al, V, Mn, Sr and Ba) indicated favourable linear correlation coefficients (i.e. $R \geq 80\%$) for INAA and ICP-MS results and their correlation graphs (generated from both moss and lichen data) are shown in Figures 5.51 → 5.57. Also, the correlation graphs for the other elements with $R \leq 80\%$ are shown in Figures 5.58 → 5.72. ICP-MS uniquely allowed determination of 10 additional elements while INAA uniquely allowed determination of 18 more elements (see Figure 5.49). As mentioned earlier in this chapter, some of those elements which are only sensitive to INAA mainly include halogens and REE, whereas, those elements which can only be determined with ICP-MS are mainly toxic elements.

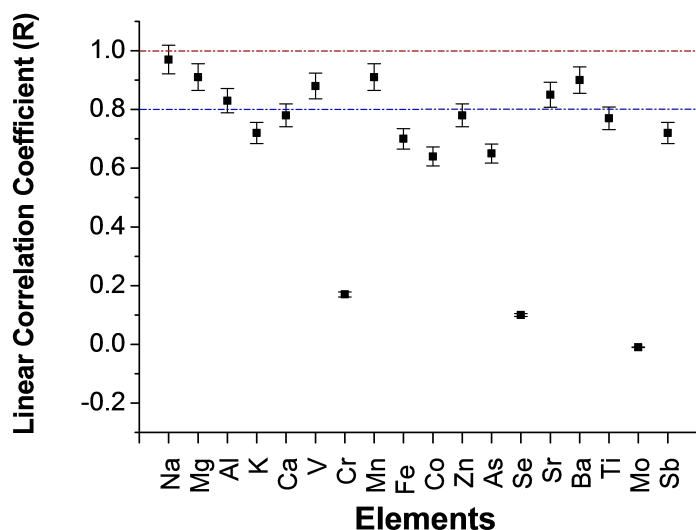


Figure 5.50: Linear correlation coefficients graph for elements determined by INAA and ICP-MS from both mosses and lichens (active biomonitoring results)

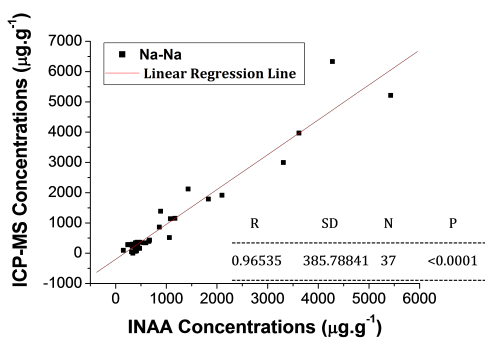


Figure 5.51: Na correlations.

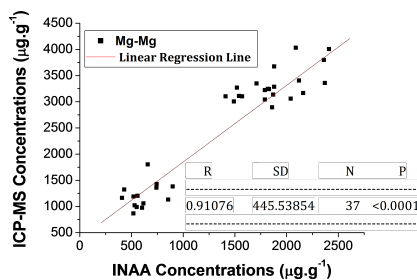


Figure 5.52: Mg correlations.

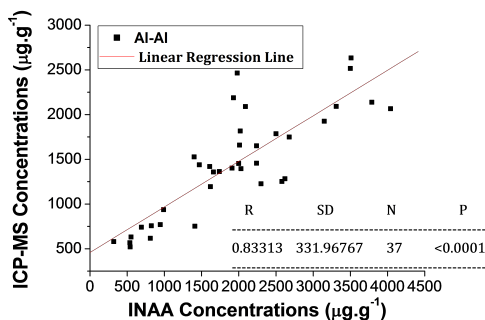


Figure 5.53: Al correlations.

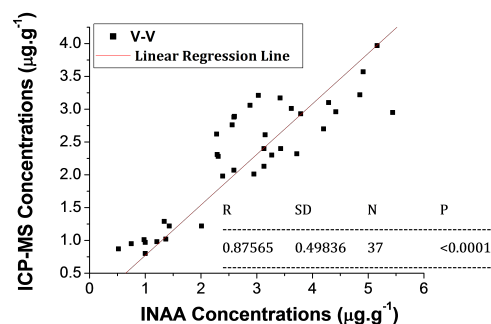


Figure 5.54: V correlations.

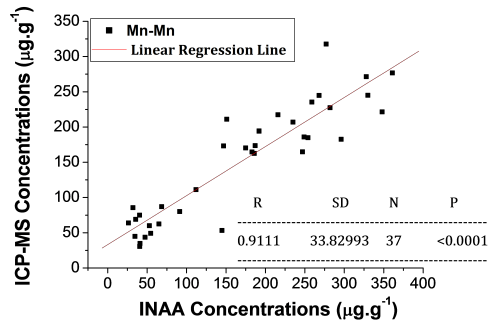


Figure 5.55: *Mn* correlations.

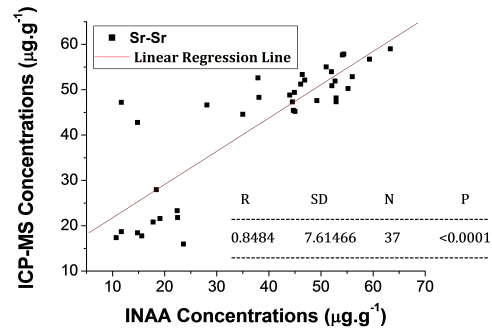


Figure 5.56: *Sr* correlations.

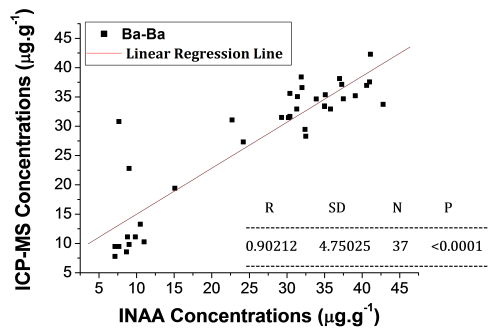


Figure 5.57: *Ba* correlations.

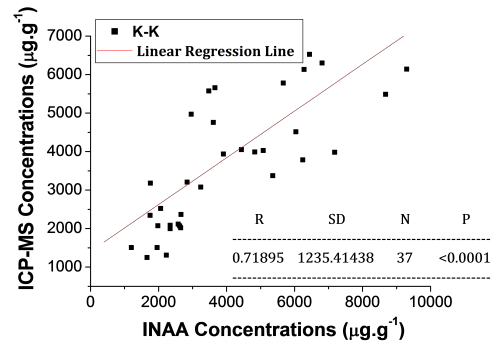


Figure 5.58: *K* correlations.

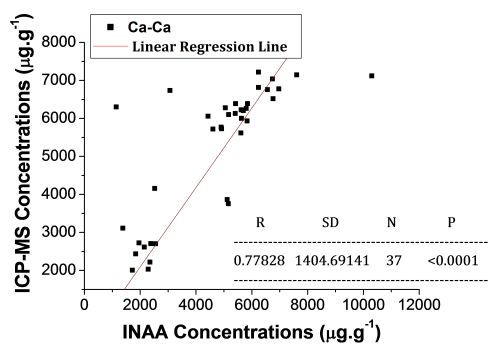


Figure 5.59: *Ca* correlations.

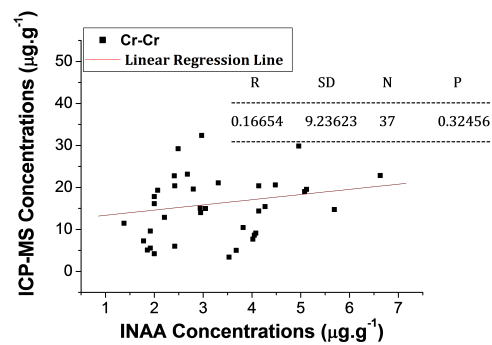


Figure 5.60: *Cr* correlations.

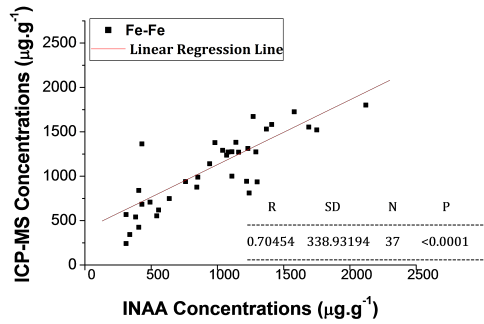


Figure 5.61: *Fe* correlations.

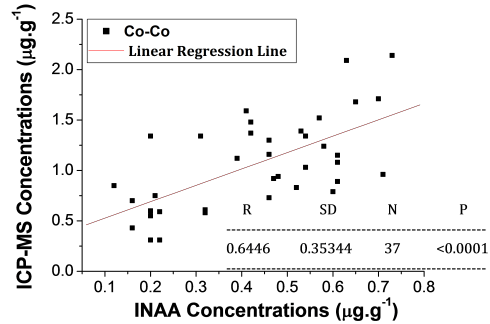


Figure 5.62: *co* Correlations.

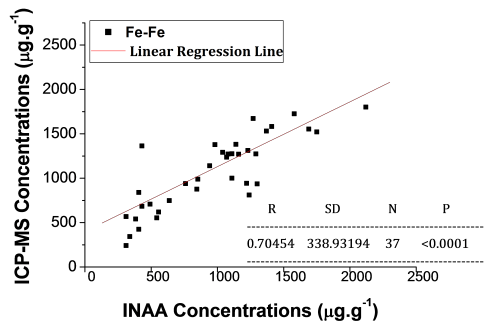


Figure 5.63: *Fe* correlations.

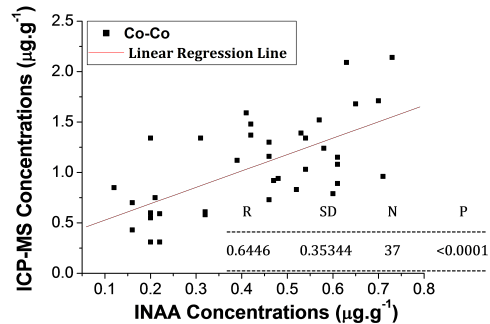


Figure 5.64: *Co* correlations.

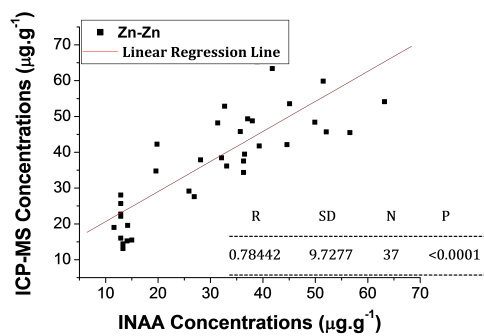


Figure 5.65: *Zn* correlations.

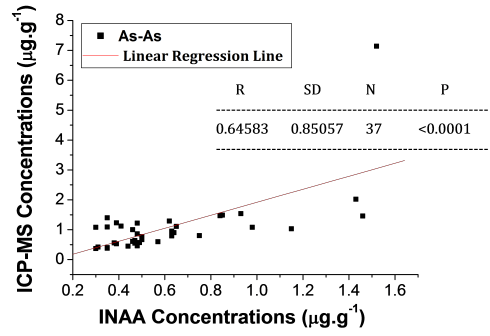


Figure 5.66: *As* correlations.

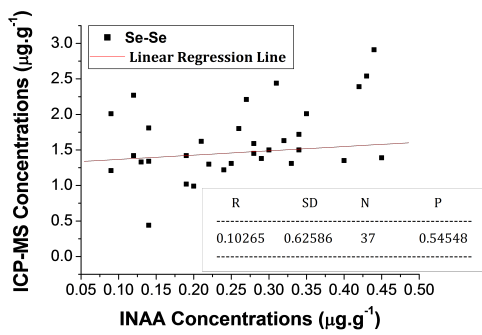


Figure 5.67: *Se* correlations.

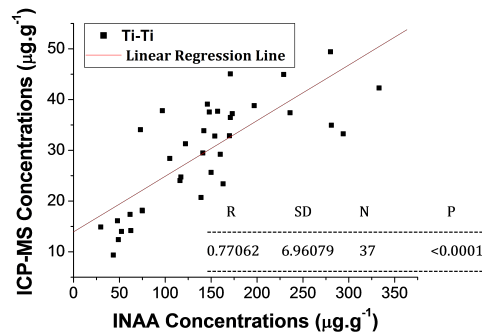


Figure 5.68: *Ti* correlations.

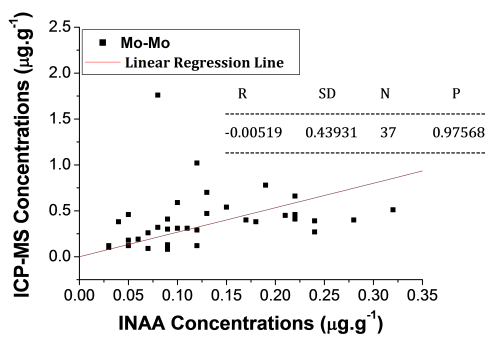


Figure 5.69: *Mo* correlations.

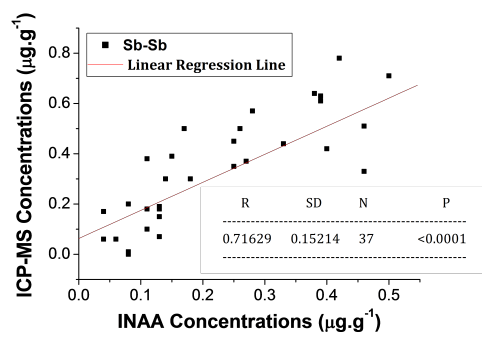


Figure 5.70: *Sb* correlations.

5.2.1 Discussion: Active

High concentrations of trace elements accumulated at all three sites (Stellenbosch, Vredenburg and Huguenot tunnel) over the entire 3 months exposure period were observed. Maximum cumulative element concentrations for most heavy metal were found at Vredenburg for Al, Hg, As, Cd, Fe, Pb and Ba. These are fingerprints of a combination of emission sources from oil combustion, emissions from railway lines, dust re-suspension of soil mixed with traffic-related particles, as well as the vehicle exhaust emissions [1, 26, 183]. This is evidence of a combination of emissions from the potential air pollution sources from Vredenburg mentioned in Chapter 3 and as shown in Figure 3.20. These potential sources of air pollution include; an oil rig facility, steel plant, heavy mineral plant, galvanising plant and the oil storage facility. In general, maximum concentrations of V, Ba, Cr, Cu, Ti and Zn, which are indicators of mostly dust resuspension of soil mixed with traffic related particles [1, 27, 43] were observed from Stellenbosch.

Inside Huguenot tunnel, the observed maximum cumulative metal concentrations were for Sb, Cr, Zn and Al. Even though these are also indicators of vehicle exhaust emissions and dust re-suspension of soil mixed with traffic related particles, the concentrations were not as high as one would expect considering the confined space inside the tunnel. High concentrations of road traffic related air pollutants from a combination of road dust containing traffic-related particles, auto exhausts, oil combustion, diesel emissions, brake wear and tyre wear were expected from the tunnel results. The elements which are similar to those that were obtained in the other three tunnel studies from; Lisbon, Portugal traffic tunnel, Laaer Berg tunnel in Vienna, Austria and a highway tunnel in Houston, USA are Zn, Cr, Pb, V, Ba, Cd, As, Cu, and Sb [176–178]. Of those elements, only Cr and Zn showed higher concentrations in the Huguenot tunnel.

Prior to conducting the deployment of samples for three months in the Huguenot tunnel, a pilot study was conducted in order to monitor vehicle emissions inside the tunnel. During the pilot study, lichen and moss bags were deployed on a railing attached to the inside wall of the tunnel, about 4 m above the ground. Lichen and moss species used in the pilot study were the same as the ones used for the major (3 months) deployment. These were; *L. smithii* (moss), *P. gracile* (moss), *U. subflorida* (lichen), and *P. perlatum* (lichen).

Initially, the lichen bags (2 bags) were deployed on 5th of April 2013 and were both collected on the 17th of April 2013 (12 days exposure time). On collection of lichen bags (17 April 2013), 2 moss bags were deployed. The first moss bag was collected on the 24th of April 2013 (7 days exposure time) and the second one was collected on the 5th of May 2013 (19 days exposure time).

For each deployed (exposed) sample, a non-exposed portion was kept for the

purpose of determining background concentrations of that particular species (i.e. concentrations of elements before exposure). A summary of deployment and collection dates for our lichen and moss bags is given by Table 5.5. For lichens, one bag contained *U. subflorida* and the other one contained *P. perlatum*. For mosses, both bags contained a mixture of *L. smithii* and *P. gracile*. This was before the identification of our moss and lichen species.

Table 5.5: *Deployment and collection dates for lichen and moss bags*

Date	lichen-bags		moss-bags	
5-April-13	2 deployed			
17-April-13		2 collected	2 bags deployed	
24-April-13				1 st collected
5-May-13				2 nd collected

After all exposed samples had been collected, the exposed and non-exposed samples were analysed by ICP-MS. As shown in Equation 5.2.1, the accumulated content of trace elements were evaluated by directly subtracting the concentrations of elements measured before exposure ($C_{\text{non-exposed}}$) from the ones measured after exposure (C_{exposed}).

$$C_{\text{final}} = C_{\text{exposed}} - C_{\text{non-exposed}} \quad (5.2.1)$$

Elemental concentrations in the non-exposed samples (from a pristine area close to Montagu) are given in Appendix E.

Similar to the tunnel studies mentioned above (Lisbon, Portugal traffic tunnel, Laaer Berg tunnel in Vienna, Austria and a highway tunnel in Houston, USA); Zn, V, Ba, Cr, Pb, Ni and Cu, which are linked to vehicular emissions inside traffic tunnels, were identified from our pilot study. All these studies are in agreement that Zn, Ba, Cr and Cu are the major marker elements (fingerprints) for vehicle emissions inside traffic tunnels [176–178, 184]. The results from our pilot study, for the accumulated concentrations of Zn, V, Ba, Cr, Pb, Ni and Cu by our biomonitors inside the tunnel are shown in Figures 5.71 → 5.73 [185].

A combination of our results show that biomonitors tend to release their heavy metal content once they get exposed to highly toxic and unfavourable conditions inside tunnels. This in turn points out one of the short-comings of the biomonitoring technique for highly polluted environments. Therefore, it can be deduced that too much air pollution might damage the biomonitors' cell membranes and thus makes them lose their capacity to accumulate pollutants effectively [27]. Hence the deviation from linearly increasing concentrations for most elements inside the tunnel. It is also possible that the exposed biomonitors inside the tunnel were not distributed in such a way that they give a

true representation of the tunnel pollution. According to Vuković [186], when monitoring air pollution using biomonitors, it is crucial that the deployment of moss- and/or lichen-bags is representative for the particulate load at the sites of interest which depends on the structure of the site and its specific air ventilation.

Comparing the accumulated trace elements content from Stellenbosch, Vredenburg and Huguenot tunnel (ICP-MS results) results, some elements showed common increasing trends. These are B, Ca, Mg, Na, Pb and Zn. Figures 5.74 → 5.79 show accumulated concentrations of these elements for different species over different exposure times and at the different deployment areas.

For all these elements, the used biomonitoring species (*L. smithii*, *P. gracile* and *U. subflorida*), which were common for all three deployment stations, behaved in a similar manner to each other. For B, Ca, Mg, Pb and Zn (except Na), the increase in elemental content of the exposed samples is directly proportional to the length of exposure. However, a different behaviour was observed in Na concentrations. For Stellenbosch, Na concentrations (in all species) only increased for the 1st two months and there was a significant drop in the 3rd month. On the other hand, there was a clear increase in the Na concentrations at Vredenburg throughout the exposure time of three months. The Na concentrations inside the tunnel only increased in the 1st month and then remained constant over the 2nd and 3rd months.

The noticeable increase in Na concentrations in Vredenburg could be accounted for by the sea-salt emissions from the nearby Saldanha Bay. The non-increasing Na concentrations in the tunnel could be due to the fact that the tunnel is a closed space that is not easily accessible to emissions from the ocean. Our results from the pilot study as well the major deployment of 3 months show *U. subflorida* to have the lowest levels of elemental content in both non-exposed and exposed samples. However, comparing the 3 months results for all stations, *U. subflorida* tends to behave in the same manner as *P. gracile* and *L. smithii* for all the elements shown in Figures 5.74 → 5.79. On the other hand, our INAA results indicated a common linearly increasing trend in the Sb content in all exposed species for the entire exposure period (1 month, 2 months and 3 months) and in all deployment stations (Stellenbosch, Vredenburg, Huguenot tunnel). These Sb results are shown in Figure 5.80.

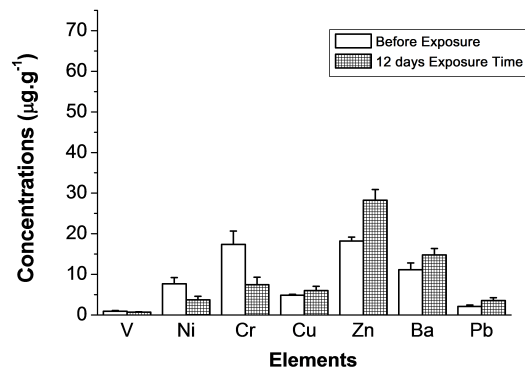


Figure 5.71: Accumulation of elements in *U. subflorida* after 12 days of exposure.

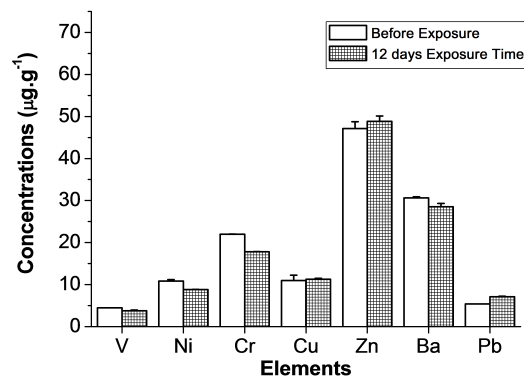


Figure 5.72: Accumulation of elements in *P. perlatum* after 12 days of exposure.

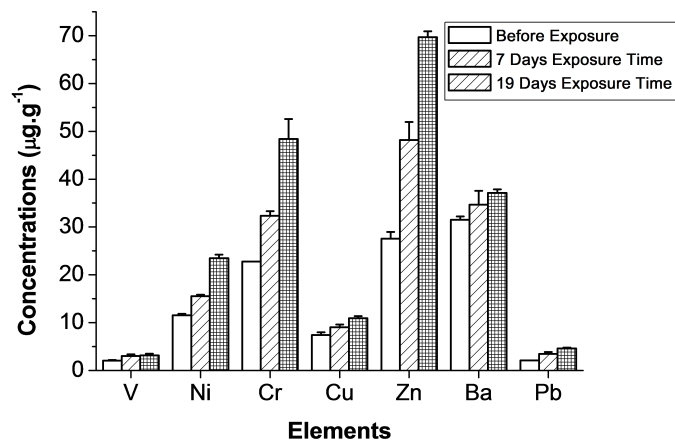


Figure 5.73: Accumulation of elements in a mixture of two moss species (*L. smithii* and *P. gracile*) over different exposure times.

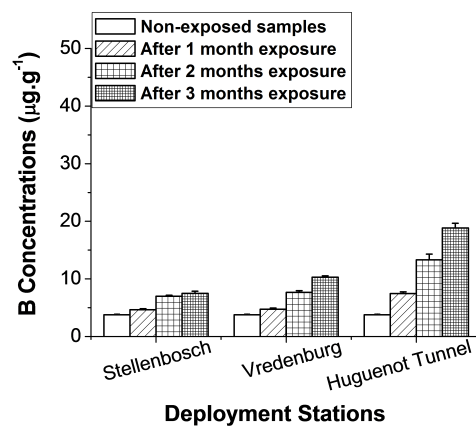
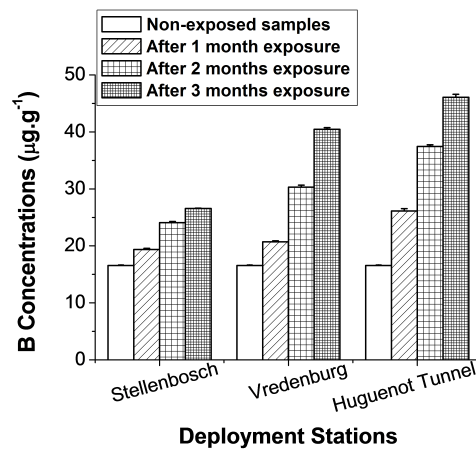
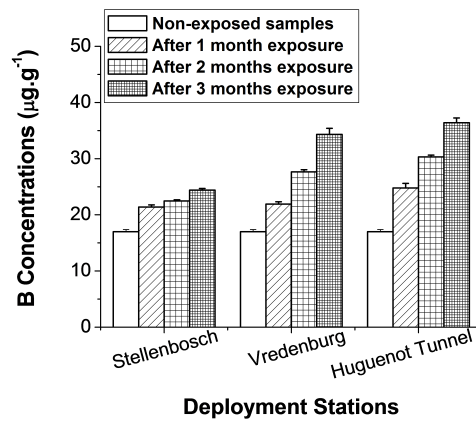


Figure 5.74: *B* concentrations in *L. smithii*, *P. gracile* and *U. subflorida*; respectively

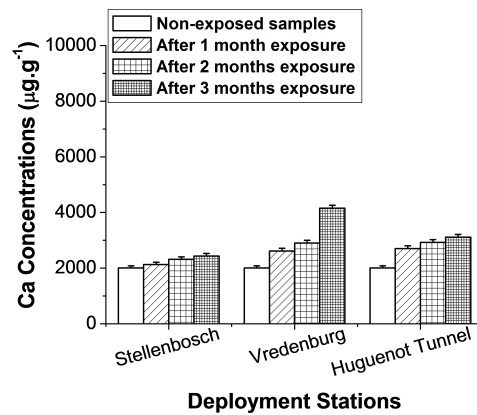
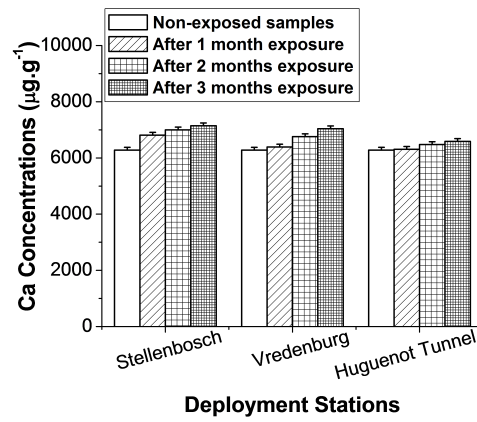
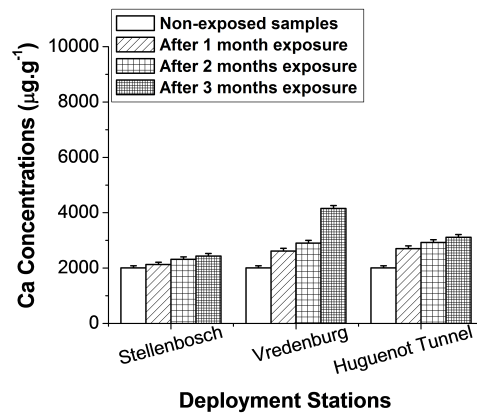


Figure 5.75: *Ca* concentrations in *L. smithii*, *P. gracile* and *U. subflorida*; respectively

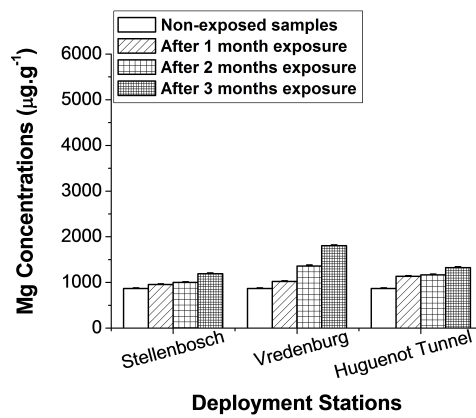
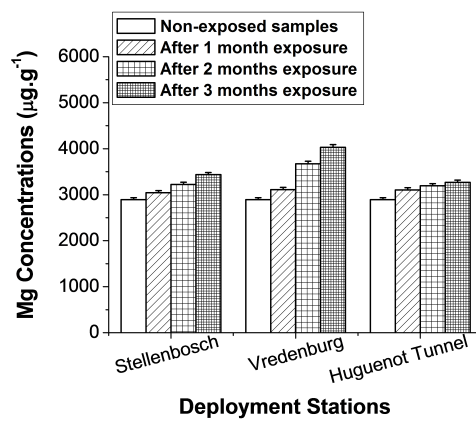
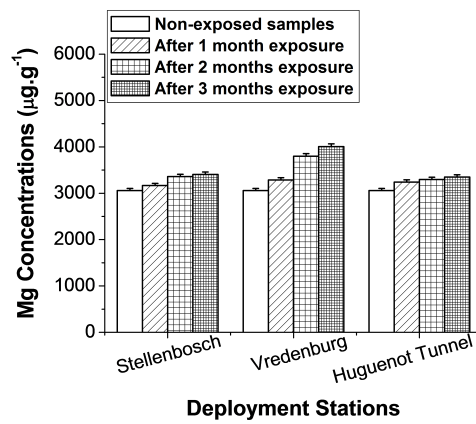


Figure 5.76: Mg concentrations in *L. smithii*, *P. gracile* and *U. subflorida*; respectively

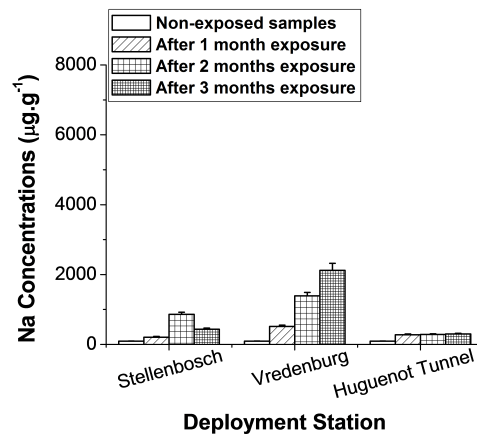
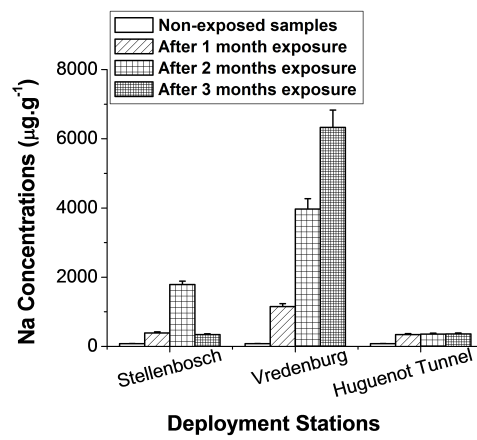
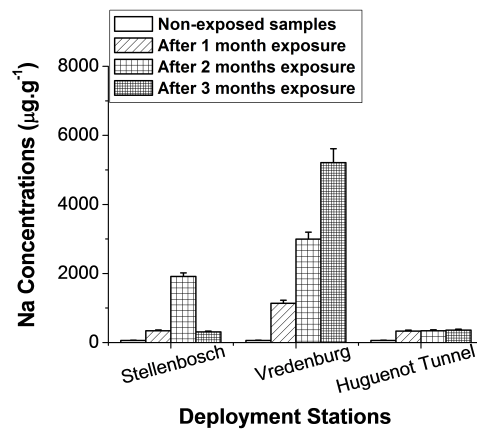


Figure 5.77: Na concentrations in *L. smithii*, *P. gracile* and *U. subflorida*; respectively

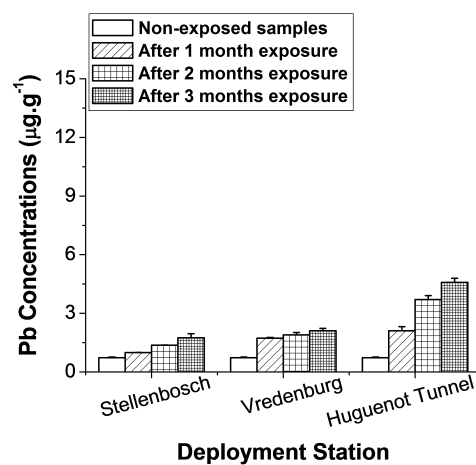
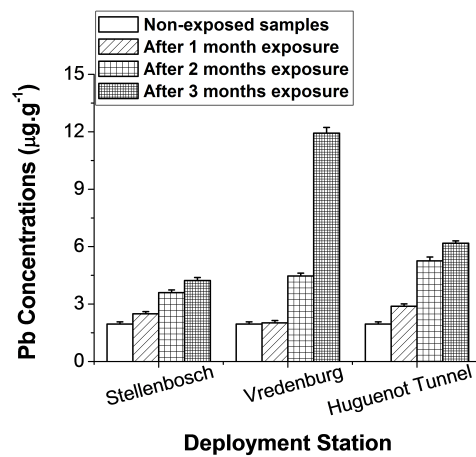
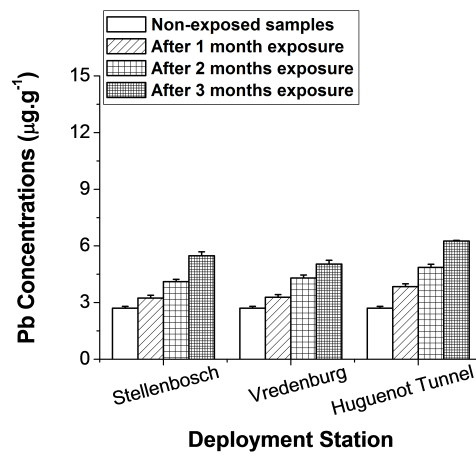


Figure 5.78: Pb concentrations in *L. smithii*, *P. gracile* and *U. subflorida*; respectively

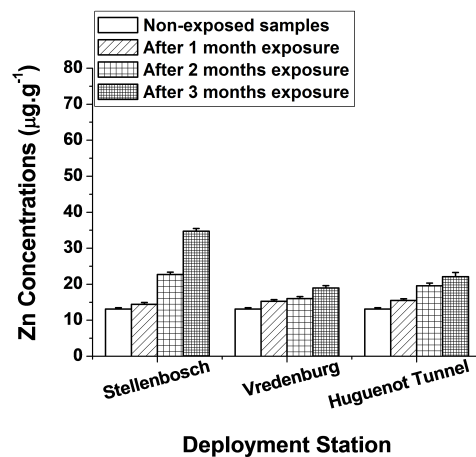
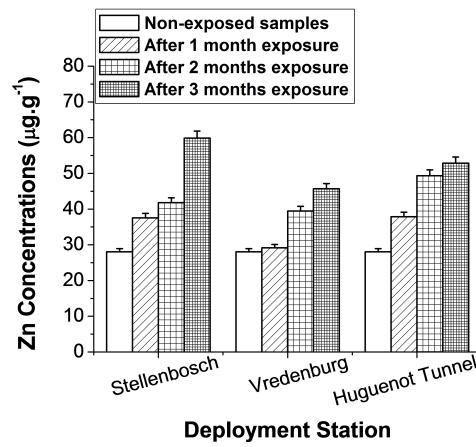
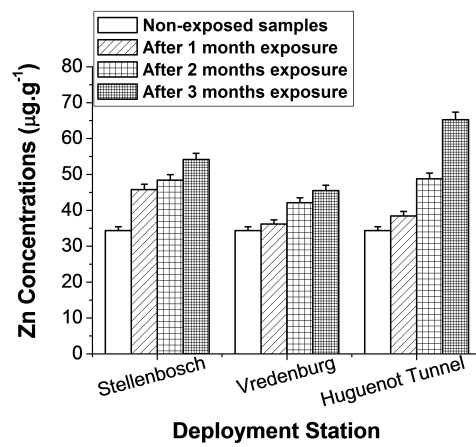


Figure 5.79: Zn concentrations in *L. smithii*, *P. gracile* and *U. subflorida*; respectively

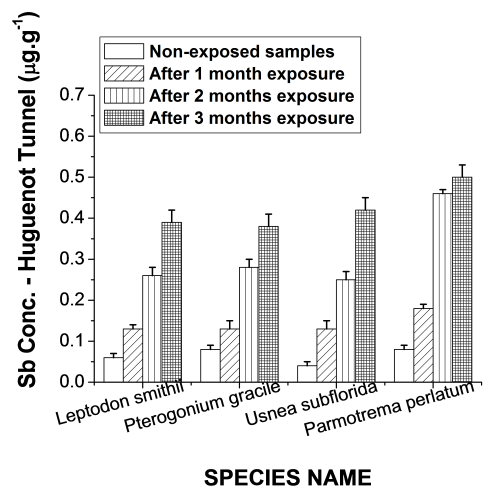
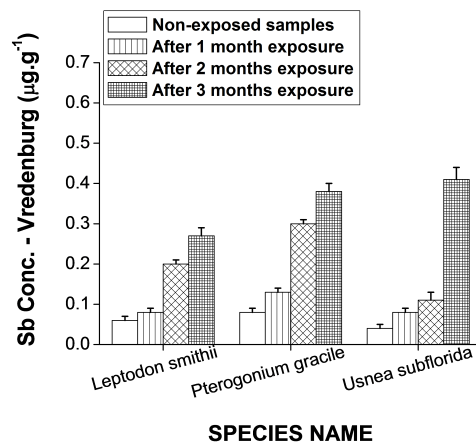
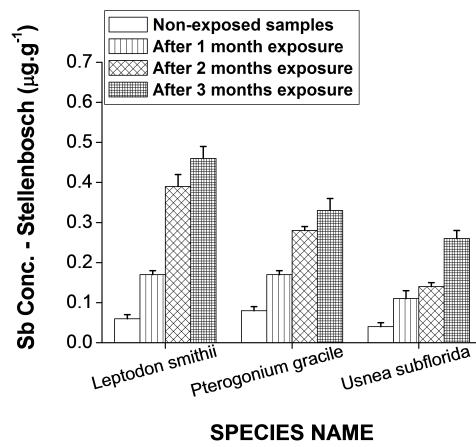


Figure 5.80: *Sb* concentrations in the samples from Stellenbosch, Vredenburg and Huguenot tunnel; respectively

It has to be taken into account that in active biomonitoring, the accumulated element concentration values over time are usually affected by initial element content in biomonitors before the exposure. This total element uptake by mosses or lichens (after exposure) as well as the influence of their initial content (before exposure) may be expressed by relative accumulation factor (RAF). RAF is presented as a percentage and mathematically determined using equation 5.2.2 [26, 184, 187].

$$\text{RAF} = \frac{C_{\text{exposed}} - C_{\text{non-exposed}}}{C_{\text{non-exposed}}} \quad (5.2.2)$$

According to previous active biomonitoring studies by Aničić *et al.* and Culicov *et al.* [102, 184, 188], RAF values tend to differ from study to study. Therefore, there cannot be any direct comparison of RAF values as they largely depend on the transplanted biomonitor type and species, study sites, exposure period, as well as the initial concentrations of elements in biomonitors before exposure. Nevertheless, it has been observed that higher element concentration values in mosses/lichens before exposure are likely to lead to lower RAF levels [184]. In this study, negative RAF values for certain elements were consistently obtained during all exposure periods, for all species of biomonitors used and at all studied sites. This decrease in concentrations of elements observed in our results in all species of biomonitors used, leading to negative RAF values, is likely to be caused by leaching.

According to Gailey and Lloyd [189], some trace elements (especially heavy metals) entrapped by biomonitors can be leached out of the nylon net of the suspended bags, leading to a decrease in contents of trace elements in biomonitors. This happens when biomonitors are adjusting to toxic conditions of the new environment in which they have been trans-located to. Once they have reached equilibrium level with the new environment, the biomonitors' accumulation capacity for metals becomes more efficient. Moreover, leaching of heavy metals is likely to also occur when biomonitors approach their saturation level. Moreover, Aničić *et al.* and Culicov *et al.* [102, 184, 188] are in agreement that the damage caused by intensity of air pollution on the cell membranes of the biomonitors often leads to leakage of elements from the suspended bags. In both studies mentioned above, the depletion of Cl, K, Rb and Cs from the exposed moss-bags was observed. Chemical elements may also get depleted in dry moss-bags during exposure as humidity is not continuously maintained throughout the exposure period. It is believed that the accumulation capacity of mosses for elements like Al, Cr, Fe, Ca, Zn, Sr, Pb and Cd can be improved by continuous irrigation of the exposed bags [187]. In one of their active biomonitoring studies using wet and dry moss-bags, Aničić *et al.* [26] observed a higher uptake for Al, Cr, Fe, Zn and Sr in the irrigated moss-bags as compared to dry moss-bags. Hence their conclusion that main-

taining humidity in biomonitors during the entire exposure period may lead to a less pronounced loss of elements. They also observed that for most elements, a clear accumulation trend was observed after 6 months as opposed to a 3 months exposure period.

Descriptive statistics per element for all active biomonitoring results are given in Appendix F.

5.3 General discussion of results

As mentioned earlier in this chapter, passive biomonitoring results have only 6 elements (out of 15 elements) with linear correlation coefficients of 80 % and above. Moreover, active biomonitoring results have only 7 elements (out of 19 elements) with linear correlation coefficients of 80 % and above. Due to these facts, it can be deduced that INAA and ICP-MS results have some degree of discrepancy in the results.

For comparison purposes, concentrations of elements obtained from this study were compared to those obtained from related studies elsewhere, even though different species were used [64, 178]. This is because we could not find any study using exactly the same species with the same techniques as the ones used here. Firstly, we compared compared the lichen results for active biomonitoring from this study with the results obtained from Pretoria [64].

For the Pretoria study, the lichen species used was *Parmelia sulcata*, while *Usnea subfloridana* and *Parmotrema perlatum* were used in this study. The Pretoria study was an active biomonitoring study, where lichens were exposed in different areas (e.g. the Limpopo University campus, an industrial area, a high traffic center, etc.) for three months. Hence, a sensible comparison of the results obtained from that study with the results obtained from this study could be made. The results from the Limpopo University campus were compared with those from the Stellenbosch University campus (see Figure 5.81). The results from an industrial area were compared with those from the Vredenburg (see Figure 5.82). Finally, the results from a high traffic center were compared with those from the Huguenot tunnel Figure 5.83). For both studies, the lichen samples were analysed by ICP-MS. The results from all three compared areas indicated that the concentrations of elements accumulated from the Pretoria sites over the exposure period of three months were generally higher than those accumulated from the Western Cape site, for the same exposure period. Concentration levels of Pb, Zn, Cu, Cr and Mn from the Pretoria study were clearly higher compared to the levels obtained from the Western Cape areas, while for the concentrations of Sb, Cd and Ni from both studies were almost the same.

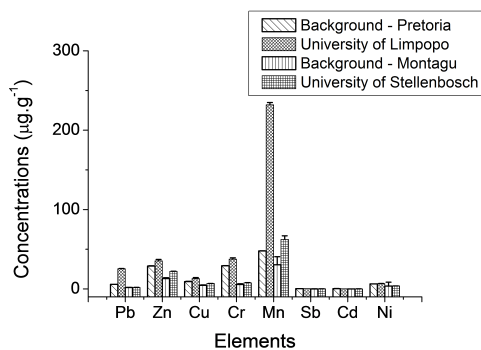


Figure 5.81: Comparison of the Stellenbosch University campus ICP-MS results with the Limpopo University campus results (3 months exposure).

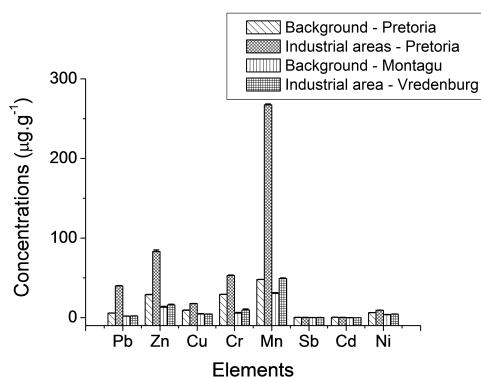


Figure 5.82: Comparison of the ICP-MS results from an industrial area in Pretoria with the results from Vredenburg (3 months exposure).

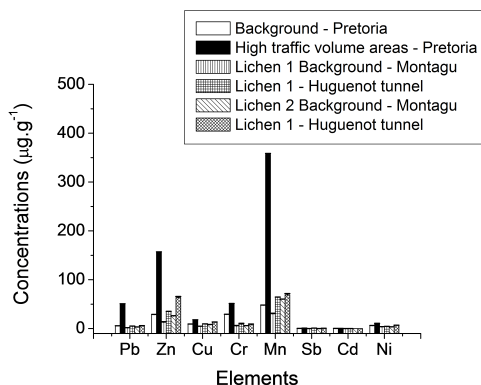


Figure 5.83: Comparison of the ICP-MS results from a high traffic center in Pretoria with the results from Huguenot tunnel (3 months exposure).

Another study that allowed a sensible comparison with the results obtained from this study was performed in Vienna, Austria [178]. Similar to the current study, the Austrian study comprised both active and passive biomonitoring using mosses. For active biomonitoring in the Vienna study, the samples of moss species (*Hylocomium splendens*) were exposed in the Laaer Berg tunnel for four weeks. These were then compared with the moss samples from this study (*Leptodon smithii* and *Pterogonium gracile*) that were exposed in the Huguenot Tunnel for four weeks. The results of this comparison are shown in Figure 5.84. As shown, the accumulated concentrations of As, Co, Mo, Ni, Sb, V, Ba, Cu and Zn from the Laaer Berg tunnel are higher than those accumulated inside Huguenot tunnel over the same exposure period. On the other hand, the moss samples for the passive biomonitoring in the Austria study were collected along five major roads distributed all over Austria [178]. The moss samples for passive biomonitoring in the current study were collected along Victoria Road in Stellenbosch. The moss species from Austria (used in passive biomonitoring) was the same as the one used in passive biomonitoring. However, a non-identified species was used in passive biomonitoring for the current study. As shown by Figure 5.85; As, Co, V, Ba, Cr, Ni and Pb concentration levels were higher from Austria. While only Cu and Zn concentration levels were higher from Stellenbosch.

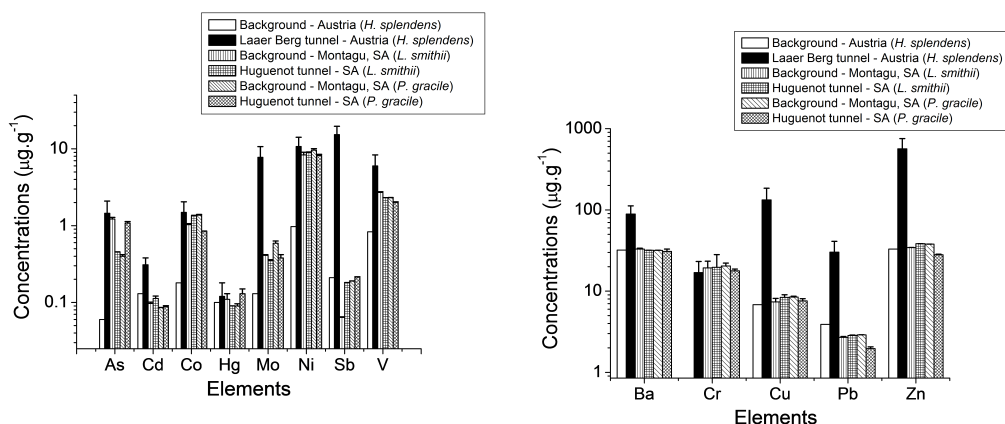


Figure 5.84: Concentrations of elements from moss samples exposed in tunnels (Stellenbosch (ICP-MS data) and Vienna (ICP-AES) data).

Finally, the metal median concentrations (from passive) in mosses from the Western Cape region of South Africa were plotted and compared with the corresponding values from the European data [62]. The results are presented in Figures 5.86 → 5.87 (Cd, Hg and Pb data from ICP-MS analyse and remaining data from INAA analysis).

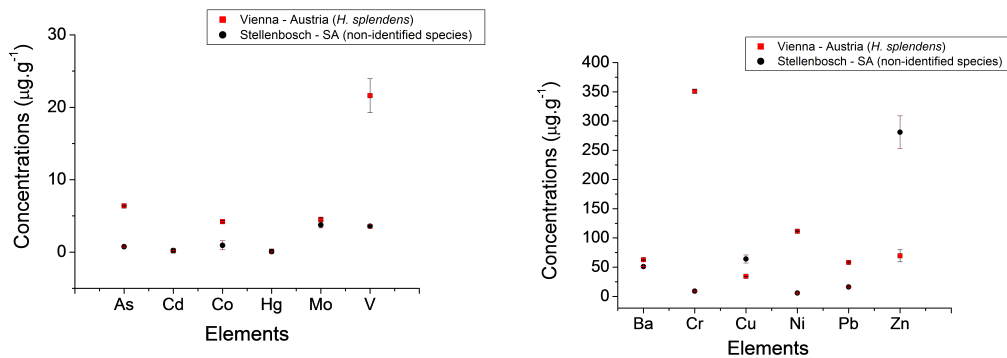


Figure 5.85: Concentrations of elements from moss samples collected along the roads (Stellenbosch data vs. Vienna data) for 1 month exposure.

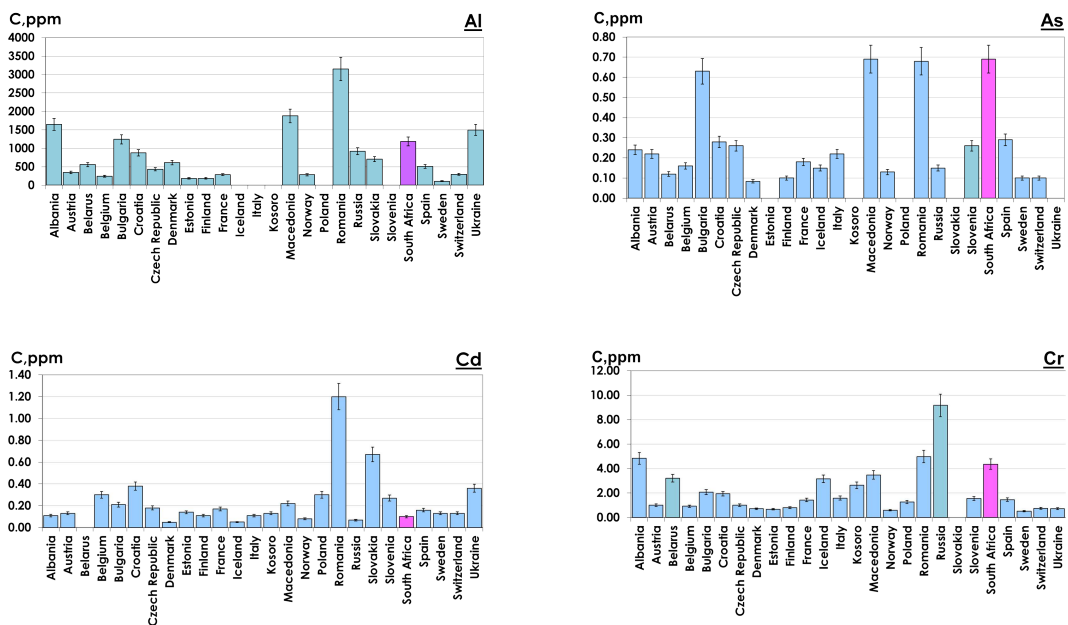


Figure 5.86: Comparing median concentrations of Al, As, Cd, Cr, Cu, Fe, Hg, Ni in moss from the Western Cape, South Africa with corresponding European data [62].

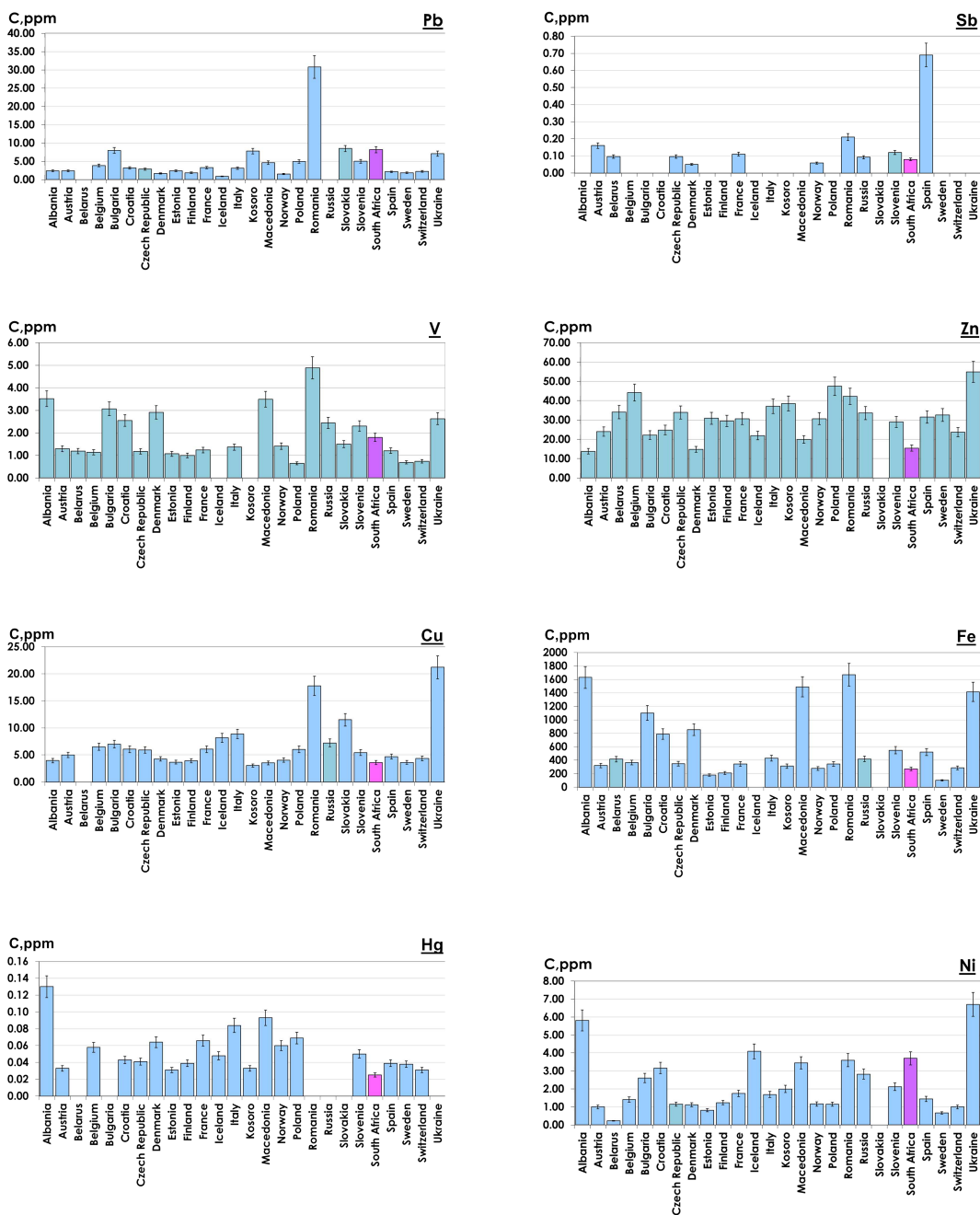


Figure 5.87: Comparing median concentrations of Pb, Sb in moss from the Western Cape, South Africa with corresponding European data [62].

Descriptive statistical analyses of the results were performed on the elemental concentrations of the 64 samples from both passive and active biomonitoring (mosses and lichens) analysed in this study. The main features measured for the acquired data include; minimum (min), maximum (max), mean, median, standard deviation (Stdev) and the coefficient of variation (CV). The results of the descriptive statistics for all analysed elements in moss and lichen samples are presented in Tables C.1 → F.2 in the Appendices. Multivariate statistical analysis (factor analysis) was also performed on the results using StatSoft STATISTICA (8.0.550 version). Factor analysis is used to facilitate the identification and characterization of different pollution sources [183]. Factor analysis results for this study are shown by the matrix of Varimax normalised factor loadings and presented in Table 5.6, where var (%) is the percentage measure of variability among presented variables under the same factor. All the treated elements had a 77% variability that could be explained by five identified factors. The com (%) is the communality of the variable in the identified factors.

Table 5.6: Matrix of varimax normalised factor loadings for $n=64$, 37 elements and factor loadings 55

Variable	Factor 1	Factor 2	Factor 3	Factor 4	Factor 5	Com, %
Al	0.92	0.05	0.07	0.23	0.08	93
B	0.71	0.14	0.18	0.48	0.29	62
Ca	0.48	0.77	0.15	0.46	0.07	70
Fe	0.78	0.17	0.36	0.31	0.18	74
K	0.15	0.84	0.13	0.28	0.21	84
Mg	0.45	0.78	0.33	0.11	0.09	87
Na	0.11	0.83	0.03	0.13	0.44	91
P	0.20	0.74	0.01	0.19	0.21	63
Si	0.71	0.41	0.13	0.25	0.01	80
Ti	0.87	0.08	0.10	0.18	0.03	66
V	0.92	0.04	0.01	0.28	0.78	92
Cr	0.47	0.03	0.23	0.90	0.18	88
Ni	0.46	0.06	0.15	0.79	0.18	66
Cu	0.32	0.02	0.12	0.02	0.65	80
Zn	0.44	0.01	0.13	0.01	0.77	90
As	0.28	0.04	0.13	0.88	0.08	73
Cd	0.17	0.10	0.31	0.15	0.66	76
Sn	0.16	0.19	0.29	0.84	0.01	65
Sb	0.34	0.01	0.05	0.80	0.13	69
Ba	0.76	0.08	0.06	0.12	0.58	87
Hg	0.34	0.32	0.06	0.0.73	0.08	66
Pb	0.31	0.10	0.15	0.31	0.72	83
Cl	0.03	0.11	0.82	0.11	0.07	94

Continued on next page

Variable	Factor 1	Factor 2	Factor 3	Factor 4	Factor 5	Com, %
I	0.16	0.19	0.92	0.08	0.15	81
Br	0.23	0.23	0.84	0.36	0.11	77
La	0.56	0.17	0.67	0.27	0.32	65
Sm	0.90	0.02	0.17	0.16	0.01	85
W	0.90	0.03	0.13	0.18	0.04	83
Sc	0.57	0.28	0.04	0.02	0.05	60
Rb	0.88	0.13	0.15	0.20	0.01	82
Ce	0.89	0.11	0.18	0.21	0.03	85
Nd	0.82	0.08	0.07	0.16	0.09	76
Gd	0.67	0.36	0.32	0.21	0.21	62
Tb	0.76	0.24	0.06	0.01	0.18	72
Tm	0.87	0.12	0.14	0.23	0.07	84
Th	0.80	0.09	0.27	0.10	0.01	73
U	0.80	0.25	0.31	0.28	0.15	74
Var (%)	17.95	4.69	2.47	7.75	2.34	77

The strongest factor loadings are presented by Factor1, containing Al, B, Fe, La, Sm, W, Sc, Rb, Ce, Nd, Gd, Tb, Tm, Th and U, with nearly 20% of total variability. This group represents chemical elements that are mostly naturally distributed. In mosses and lichens, content of these elements is significantly influenced by natural sources relative to any anthropogenic activities. These include REE and other elements which come from mineral particles released into the atmosphere by wind erosion of local sources or particles attached to the biomonitors when soil surface is covered by water [1, 183]. Factor 2 (K, Ca, Mg, Na, P) with total variability of 4.69% represent anthropogenic geochemical association of elements. High contents of these elements are usually found in agricultural land due to intensive use of organic fertilizers like potassium and phosphorus fertilizers [183, 190]. This group is associated with agricultural activities happening on various farms (mostly wine farms) around the Western Cape region. Factor 3 (Cl, I, Br) represents elements that are associated with elements from marine sources [1]. High values of halogens are likely to be found in regions closer to the oceans. Factor 4 (Cr, Ni, As, Sn, Sb, Hg) is highly influenced by soil contamination with mixed (geogenic-anthropogenic) activities. Even though anthropogenic activities affect concentrations of these elements in air, their high contents are mainly influenced by natural factors like lithological background [183, 191]. Factor 5 (V, Cu, Zn, Cd, Ba, Pb), explaining 2.34% of the total variability represents another group of anthropogenic geochemical association [1, 183], which is highly connected with the industrial activities around the Western Cape region, especially along the West Coast.

Chapter 6

Conclusion and Recommendations for Further Work

The purpose of this work was to monitor the elemental content of native and transplanted mosses and lichens (i.e. passive and active biomonitoring) in selected areas of the Western Cape area. This was done in order to indirectly assess atmospheric pollution caused by heavy metals and other trace elements.

Mosses and lichens were selected owing to their ability to accumulate and retain elements as a result of wet and dry deposition. These plants can therefore be thought of as the analogues of air filters that have the ability to reflect environmental conditions, including atmospheric pollution levels [1]. The elemental content of the biomonitors were measured using two techniques; INAA and ICP-MS, thus facilitating an intercomparison of selected results obtained from these measurements.

Using passive biomonitoring, a maximum of 44 elements (Na, Mg, Al, Cl, K, Ca, Sc, Ti, V, Cr, Mn, Fe, Co, Zn, As, Se, Br, Rb, Sb, I, Cs, La, Ce, Nd, Sm, Tb, Hf, Ta, W, Th, U, Ni, Cu, Sr, Mo, Cd, Sn, Ba, Hg, Pb, B, Li, P, Si) were identified and quantified using INAA and ICP-MS.

From active biomonitoring, a maximum of 47 elements (Al, Ca, Fe, K, Mg, Na, Ti, V, Cr, Mn, Co, Ni, Zn, As, Se, Sr, Mo, Sb, Ba, Cl, I, Br, La, Sm, W, U, Sc, Rb, Zr, Cs, Ce, Nd, Gd, Tb, Tm, Hf, Th, B, P, Si, Li, Be, Cu, Cd, Sn, Hg, Pb) were identified and quantified.

A comparison of INAA and ICP-MS results for elements that were obtained using both techniques indicated that discrepancies (low correlation coefficients) exist for some elements. Overall, only a few major and essential elements (Na, Ca, Mg, K, Mn, Sr, Al, V, Ba, Zn) showed satisfactory linear correlations, $R \geq 80\%$. In order to further study these discrepancies, manual calculations of elemental concentrations (INAA) were made for two samples using the relative method which makes use of irradiated standard reference material (SRM). The manual results were consistent with the INAA results obtained using

the automated concentration program used at the JINR in Dubna (Russia). This provided some level of confidence in the INAA results. However, the ICP-MS results were nonetheless important since certain elements cannot be measured using INAA (e.g. Pb, Cu, Cd, Hg). Hence, it is useful to use two complementary techniques when performing monitoring studies, so as to overcome the limitations of each.

The active biomonitoring results from this study generated more questions than answers. The accumulation rates of elements by the exposed samples over the 0 to 3 month period were not consistent for the monitored stations (Stellenbosch, Vredenburg, Huguenot Tunnel). The highest accumulated elemental concentrations were found for Vredenburg, for the elements Fe, Al, Hg, As, Cd, Pb, Ba and Na. These elements are the fingerprints of a combination of potential air-pollution sources around Vredenburg and the surrounding Saldanha Bay area. These sources are; an oil rig facility, steel plant, heavy mineral plant, galvanising plant and an oil storage facility.

For Stellenbosch, higher concentration levels of V, Ba, Cr, Cu, Ti and Zn were found. These elements are mainly associated with emissions from dust re-suspension of soil mixed with traffic-related particles, as well as vehicle exhaust emissions [1, 26, 183].

For the Huguenot tunnel the maximum accumulated elemental concentrations were for Sb, Ni, Cr, Zn and Al which are also indicators of vehicle exhaust emissions and dust re-suspension of soil mixed with traffic-related particles.

The active biomonitoring results for some elements indicate negative accumulation factors (i.e. there is loss of element content relative to initial values). There are a number of factors that could have contributed to this Aničić *et al.* [26, 187, 188]. Gailey and Lloyd [189] and Culicov [102] provide a list of causes that may hinder the accumulation capacity of biomonitors during the exposure period, leading to a decrease in trace elements. These are:

1. when biomonitors are adjusting to toxic conditions of the new environment in which they have been trans-located to, some trace elements might be leached out of the nylon net of the suspended bags. However, it is important to note that once the biomonitors have reached equilibrium level with the new environment, their accumulation capacity for metals becomes even more efficient.
2. biomonitors are likely to undergo leaching of heavy metals when they are approaching their saturation level.
3. the leakage of elements from the suspended bags may be caused by the high intensity of air pollution on the cell membranes of the biomonitor.
4. when humidity is not continuously maintained throughout the exposure period, i.e. when dry moss- bags are being used (as in this study) instead of wet moss-bags, elements may also get depleted during exposure. This means that, maintaining humidity in biomonitors during the entire exposure period by continuous irrigation of the exposed bags may lead to a less pronounced

loss of elements.

5. depending on the type of the biomonitor and the pollution levels of the environment, a clear accumulation trend might not be accomplished over a 3 month exposure period and a 6 month exposure period (or more) is then preferred.

Based on the five points listed above, it is recommended to use wet-moss bags (via continuous irrigation) in parallel with dry-moss bags when conducting active biomonitoring in order to also maintain humidity in biomonitors during the entire exposure period. It is also recommended to extend the exposure period to 6 months or even a year, so one can monitor the changes in the biomonitors' accumulation capacity as a function of season.

In this study, mosses proved themselves to be more efficient at accumulating major, minor and trace elements. Moreover, both moss species displayed a generally higher bioaccumulation capacity for metals and a more linear trend of element accumulation than lichens. In lichens, *Usnea subfloridana* indicated a better bioaccumulation capacity as compared to the *Parmotrema perlatum*. Overall, both lichens were more efficient in accumulating halogens as compared to mosses.

However, complementary results were achieved by using both mosses and lichens. The results of this study have also indicated the significance of using different kinds and/or species of biomonitors when performing biomonitoring studies as this may assist in overcoming some bioaccumulation capacity limitations. The comparison of median heavy metal concentrations (which are the most toxic air pollutants) in biomonitors from the Western Cape region with those from Europe, revealed lower concentrations for the Western Cape.

Appendices

Appendix A

Sample data

A.1 Sampling, sample preparation, irradiation and counting data

Table A.1: *Passive biomonitoring sample preparation data. Victoria Street, Jan Marais Nature Reserve, Coetzenburg sports grounds and Coetzenburg Mountain are in Stellenbosch.*

Sampling Location	Sample ID	Sample Prep. Date	JINR Sample ID
Victoria Street	MS2	06/06/2012	k01
Victoria Street	MS3	06/06/2012	k02
Jan Marais Nature Reserve	LS4	06/06/2012	k03
Jan Marais Nature Reserve	LS5	06/06/2012	k04
Coetzenburg sports grounds	MS4	06/06/2012	k05
Jan Marais Nature Reserve	LS6	06/06/2012	k06
Jan Marais Nature Reserve	LS3	06/06/2012	k07
Jan Marais Nature Reserve	LS2	06/06/2012	k08
Victoria Street	LS1(a)	06/06/2012	k09
Coetzenburg Mountain	CLS3	06/06/2012	k11
Coetzenburg Mountain	CMS4(a)	06/06/2012	k12
Coetzenburg Mountain	CLS1	06/06/2012	k14
Coetzenburg Mountain	CMS2	06/06/2012	k15
Coetzenburg Mountain	CMS3	06/06/2012	k16
Coetzenburg Mountain	CMS1	06/06/2012	k17
Coetzenburg Mountain	CLS2	06/06/2012	k18
Coetzenburg Mountain	CMS5	06/06/2012	k20
Coetzenburg Mountain	CLS4	06/06/2012	k21

Continued on next page

Table A.1 –continued from previous page			
Sampling Location	Sample ID	Sample Prep. Date	JINR Sample ID
Franschoek	F-L1	06/06/2012	k22
Franschoek	F-M1	06/06/2012	k23
False Bay	FBMS1	06/06/2012	k24
False Bay	FBMS1(b)	06/06/2012	k25
False Bay	FBL1	06/06/2012	k26
Betty's Bay	BBM1	06/06/2012	k27
Betty's Bay	BBM2	06/06/2012	k28
Betty's Bay	BBL1	06/06/2012	k29
Betty's Bay	BBM3	06/06/2012	k30
Signal Hill	TML1	06/06/2012	k31
Signal Hill	TML2	06/06/2012	k32

Table A.2: *Passive biomonitoring sample irradiation data (duration given in seconds).*

JINR Sample ID	Short-lived Isotopes		Long-lived Isotopes		
	Date	Duration	Start Date	End Date	Duration
k01	19/06/2012	180	02/10/2012	06/10/2012	309700
k02	19/06/2012	180	02/10/2012	06/10/2012	309700
k03	19/06/2012	180	02/10/2012	06/10/2012	309700
k04	19/06/2012	180	02/10/2012	06/10/2012	309700
k05	19/06/2012	180	02/10/2012	06/10/2012	309700
k06	19/06/2012	180	02/10/2012	06/10/2012	309700
k07	19/06/2012	156	02/10/2012	06/10/2012	309700
k08	19/06/2012	180	02/10/2012	06/10/2012	309700
k09	19/06/2012	180	02/10/2012	06/10/2012	309700
k11	19/06/2012	180	02/10/2012	06/10/2012	309700
k12	19/06/2012	180	02/10/2012	06/10/2012	309700
k14	19/06/2012	180	02/10/2012	06/10/2012	309700
k15	19/06/2012	180	02/10/2012	06/10/2012	309700
k16	19/06/2012	180	02/10/2012	06/10/2012	309700
k17	19/06/2012	180	02/10/2012	06/10/2012	309700
k18	19/06/2012	180	02/10/2012	06/10/2012	309700
k20	19/06/2012	180	02/10/2012	06/10/2012	309700
k21	19/06/2012	180	02/10/2012	06/10/2012	309700
k22	19/06/2012	180	02/10/2012	06/10/2012	309700
k23	19/06/2012	180	02/10/2012	06/10/2012	309700
k24	19/06/2012	180	02/10/2012	06/10/2012	309700
k25	19/06/2012	180	02/10/2012	06/10/2012	309700
k26	19/06/2012	180	02/10/2012	06/10/2012	309700
k27	19/06/2012	180	02/10/2012	06/10/2012	309700
k28	19/06/2012	180	02/10/2012	06/10/2012	309700
k29	19/06/2012	180	02/10/2012	06/10/2012	309700
k30	20/06/2012	180	02/10/2012	06/10/2012	309700
k31	20/06/2012	180	02/10/2012	06/10/2012	309700
k32	20/06/2012	180	02/10/2012	06/10/2012	309700

Table A.3: *Passive biomonitoring counting data for short-lived isotopes (duration given in seconds).*

JINR Sample ID	Date	Duration	Spectra ID
k01	19/06/2012	900	6000543
k02	19/06/2012	900	6000545
k03	19/06/2012	757	6000547
k04	19/06/2012	900	6000549
k05	19/06/2012	876	6000551
k06	19/06/2012	882	6000553
k07	19/06/2012	574	6000555
k08	19/06/2012	170	6000556
k09	19/06/2012	803	6000558
k11	19/06/2012	717	6000562
k12	19/06/2012	541	6000564
k14	19/06/2012	487	6000588
k15	19/06/2012	642	6000570
k16	19/06/2012	900	6000572
k17	19/06/2012	541.8	6000574
k18	19/06/2012	559.6	6000576
k20	19/06/2012	825.6	6000580
k21	19/06/2012	742.3	6000582
k22	19/06/2012	889.5	6000584
k23	19/06/2012	900	6000586
k24	19/06/2012	900	6000588
k25	19/06/2012	774.9	6000590
k26	19/06/2012	747.5	600592
k27	19/06/2012	778.1	000594
k28	19/06/2012	738.2	6000596
k29	19/06/2012	900	6000598
k30	20/06/2012	770.2	6000601
k31	20/06/2012	812.6	6000603
k32	20/06/2012	726.9	6000605

Table A.4: *Passive biomonitoring counting data for the 1st long-lived isotopes (duration given in seconds).*

JINR Sample ID	Long-lived 1 Isotopes		
	Date	Duration	Spectra ID
k01	09/10/2012	1800	5100306
k02	09/10/2012	1800	5100308
k03	09/10/2012	1800	5100310
k04	09/10/2012	1800	5100312
k05	09/10/2012	1800	5100314
k06	09/10/2012	1800	5100316
k07	09/10/2012	1800	5100318
k08	09/10/2012	1800	5100320
k09	09/10/2012	1800	5100322
k11	09/10/2012	1800	6100302
k12	09/10/2012	1800	6100304
k14	09/10/2012	1800	6100306
k15	09/10/2012	1800	6100308
k16	09/10/2012	1800	6100310
k17	09/10/2012	1800	6100312
k18	09/10/2012	1800	6100314
k20	09/10/2012	1800	6100316
k21	09/10/2012	1800	6100318
k22	09/10/2012	1800	6100320
k23	09/10/2012	1800	7100306
k24	09/10/2012	1800	7100308
k25	09/10/2012	1800	7100310
k26	09/10/2012	1800	7100312
k27	10/10/2012	1800	7100314
k28	10/10/2012	1800	7100316
k29	10/10/2012	1800	7100318
k30	10/10/2012	1800	7100320
k31	10/10/2012	1800	7100322
k32	10/10/2012	1800	7100324

Table A.5: *Passive biomonitoring counting data for the 2nd long-lived isotopes (duration given in seconds).*

Sample ID	Long-lived 2 Isotopes		
	Date	Duration	Spectra ID
k01	25/10/2012	5400	5200275
k02	25/10/2012	5400	5200276
k03	25/10/2012	5400	5200277
k04	25/10/2012	5400	5200278
k05	25/10/2012	5400	5200279
k06	25/10/2012	5400	5200280
k07	25/10/2012	5400	5200281
k08	25/10/2012	5400	5200282
k09	25/10/2012	5400	5200289
k11	25/10/2012	5400	6200273
k12	25/10/2012	5400	6200274
k14	25/10/2012	5400	6200275
k15	25/10/2012	5400	6200276
k16	25/10/2012	5400	6200277
k17	25/10/2012	5400	6200278
k18	25/10/2012	5400	6200279
k20	25/10/2012	5400	6200280
k21	25/10/2012	5400	6200281
k22	25/10/2012	5400	6200282
k23	25/10/2012	5400	7200275
k24	25/10/2012	5400	7200276
k25	25/10/2012	5400	7200277
k26	25/10/2012	5400	7200278
k27	25/10/2012	5400	7200279
k28	25/10/2012	5400	7200280
k29	25/10/2012	5400	7200281
k30	26/10/2012	5400	7200282
k31	26/10/2012	5400	7200289
k32	26/10/2012	5400	7200290

Table A.6: *Active biomonitoring sample preparation data.*

Location	Sample ID	Exposure Period	Sample Prep. Date
Montagu	CMLS	non-exposed	14/05/2014
Montagu	CMPG	non-exposed	14/05/2014
Montagu	CLPP	non-exposed	14/05/2014
Montagu	CLUS	non-exposed	14/05/2014
Stellenbosch	NRML1	1 month	14/05/2014
Stellenbosch	NRMP1	1 month	14/05/2014
Stellenbosch	NRLU1	1 month	14/05/2014
Stellenbosch	NRML2	2 months	14/05/2014
Stellenbosch	NRMP2	2 months	14/05/2014
Stellenbosch	NRLU2	2 months	14/05/2014
Stellenbosch	NRML3	3 months	14/05/2014
Stellenbosch	NRMP3	3 months	14/05/2014
Stellenbosch	NRLU3	3 months	14/05/2014
Vredenburg	SVML1	1 month	14/05/2014
Vredenburg	SVMP1	1 month	14/05/2014
Vredenburg	SVLU1	1 month	14/05/2014
Vredenburg	SVML2	2 months	14/05/2014
Vredenburg	SVMP2	2 months	14/05/2014
Vredenburg	SVLU2	2 months	14/05/2014
Vredenburg	SVML3	3 months	14/05/2014
Vredenburg	SVMP3	3 months	14/05/2014
Vredenburg	SVLU3	3 months	14/05/2014
Huguenot tunnel	HTML1	1 month	14/05/2014
Huguenot tunnel	HTMP1	1 month	14/05/2014
Huguenot tunnel	HTLU1	1 month	14/05/2014
Huguenot tunnel	HTLP1	1 month	14/05/2014
Huguenot tunnel	HTML2	2 months	14/05/2014
Huguenot tunnel	HTMP2	2 months	14/05/2014
Huguenot tunnel	HTLU2	2 months	14/05/2014
Huguenot tunnel	HTLP2	2 months	14/05/2014
Huguenot tunnel	HTML3	3 months	14/05/2014
Huguenot tunnel	HTMP3	3 months	14/05/2014
Huguenot tunnel	HTLU3	3 months	14/05/2014
Huguenot tunnel	HTLP3	3 months	14/05/2014

Table A.7: *Active biomonitoring sample irradiation data for short-lived isotopes, (duration given in seconds).*

Sample ID	JINR Sample ID	Date	Duration
CMLS	h05	14/05/2014	180
CMPG	h04	14/05/2014	180
CLPP	h07	14/05/2014	180
CLUS	h06	14/05/2014	180
NRML1	h09	14/05/2014	180
NRMP1	h08	14/05/2014	180
NRLU1	h10	14/05/2014	180
NRML2	h12	14/05/2014	180
NRMP2	h11	14/05/2014	180
NRLU2	h13	14/05/2014	180
NRML3	h15	14/05/2014	180
NRMP3	h14	14/05/2014	180
NRLU3	h16	14/05/2014	180
SVML1	h18	14/05/2014	180
SVMP1	h17	14/05/2014	180
SVLU1	h19	14/05/2014	180
SVML2	h21	14/05/2014	180
SVMP2	h20	14/05/2014	180
SVLU2	h22	14/05/2014	180
SVML3	h24	14/05/2014	180
SVMP3	h23	14/05/2014	180
SVLU3	h25	14/05/2014	180
HTML1	h27	14/05/2014	180
HTMP1	h26	14/05/2014	180
HTLU1	h28	14/05/2014	180
HTLP1	h29	14/05/2014	180
HTML2	h31	14/05/2014	180
HTMP2	h30	14/05/2014	180
HTLU2	h32	14/05/2014	180
HTLP2	h33	14/05/2014	180
HTML3	h35	14/05/2014	180
HTMP3	h34	14/05/2014	180
HTLU3	h36	14/05/2014	180
HTLP3	h37	14/05/2014	180

Table A.8: Active biomonitoring sample irradiation data for the 1st and 2nd long-lived isotopes (duration given in seconds).

Sample ID	JINR Sample ID	Start Date	End Date	Duration
CMLS	h43	23/09/2014	26/09/2014	277260
CMPG	h42	23/09/2014	26/09/2014	277260
CLPP	h45	23/09/2014	26/09/2014	277260
CLUS	h44	23/09/2014	26/09/2014	277260
NRML1	h47	23/09/2014	26/09/2014	277260
NRMP1	h46	23/09/2014	26/09/2014	277260
NRLU1	h48	23/09/2014	26/09/2014	277260
NRML2	h50	23/09/2014	26/09/2014	277260
NRMP2	h49	23/09/2014	26/09/2014	277260
NRLU2	h51	23/09/2014	26/09/2014	277260
NRML3	h53	23/09/2014	26/09/2014	277260
NRMP3	h52	23/09/2014	26/09/2014	277260
NRLU3	h54	23/09/2014	26/09/2014	277260
SVML1	h56	23/09/2014	26/09/2014	277260
SVMP1	h55	23/09/2014	26/09/2014	277260
SVLU1	h57	23/09/2014	26/09/2014	277260
SVML2	h59	23/09/2014	26/09/2014	277260
SVMP2	h58	23/09/2014	26/09/2014	277260
SVLU2	h60	23/09/2014	26/09/2014	277260
SVML3	h62	23/09/2014	26/09/2014	277260
SVMP3	h61	23/09/2014	26/09/2014	277260
SVLU3	h63	23/09/2014	26/09/2014	277260
HTML1	h65	23/09/2014	26/09/2014	277260
HTMP1	h64	23/09/2014	26/09/2014	277260
HTLU1	h66	23/09/2014	26/09/2014	277260
HTLP1	h67	23/09/2014	26/09/2014	277260
HTML2	h69	23/09/2014	26/09/2014	277260
HTMP2	h68	23/09/2014	26/09/2014	277260
HTLU2	h70	23/09/2014	26/09/2014	277260
HTLP2	h71	23/09/2014	26/09/2014	277260
HTML3	h73	23/09/2014	26/09/2014	277260
HTMP3	h72	23/09/2014	26/09/2014	277260
HTLU3	h74	23/09/2014	26/09/2014	277260
HTLP3	h75	23/09/2014	26/09/2014	277260

Table A.9: *Active biomonitoring counting data for short-lived isotopes (duration given in seconds).*

. JINR Sample ID	Date	Duration	Spectra ID
h05	14/05/2014	180	7002702
h04	14/05/2014	180	7002701
h07	14/05/2014	180	7002704
h06	14/05/2014	180	7002703
h09	14/05/2014	180	7002706
h08	14/05/2014	180	7002705
h10	14/05/2014	180	7002707
h12	14/05/2014	180	7002700
h11	14/05/2014	180	1002699
h13	14/05/2014	180	1002701
h15	14/05/2014	180	1002703
h14	14/05/2014	180	1002702
h16	14/05/2014	180	1002704
h18	14/05/2014	180	1002706
h17	14/05/2014	180	1002705
h19	14/05/2014	180	1002707
h21	14/05/2014	180	1002708
h20	14/05/2014	180	7002708
h22	14/05/2014	180	1002709
h24	14/05/2014	180	7002711
h23	14/05/2014	180	7002710
h25	14/05/2014	180	7002712
h27	14/05/2014	180	7002714
h26	14/05/2014	180	7002713
h28	14/05/2014	180	7002713
h29	14/05/2014	180	7002715
h31	14/05/2014	180	7002716
h30	14/05/2014	180	7002732
h32	14/05/2014	180	1002709
h33	14/05/2014	180	1002710
h35	14/05/2014	180	1002712
h34	14/05/2014	180	1002711
h36	14/05/2014	180	1002713
h37	14/05/2014	180	1002714

Table A.10: Active biomonitoring counting data for the 1st long-lived isotopes (duration given in seconds).

JINR Sample ID	Long-lived 1 Isotopes		
	Date	Duration	Spectra ID
h43	30/09/2014	1800	5102198
h42	30/09/2014	1800	5102197
h45	30/09/2014	1800	5102203
h44	30/09/2014	1800	5102202
h47	30/09/2014	1800	5102205
h46	30/09/2014	1800	5102204
h48	30/09/2014	1800	1102194
h50	30/09/2014	1800	1102196
h49	30/09/2014	1800	1102195
h51	30/09/2014	1800	1102197
h53	30/09/2014	1800	1102202
h52	30/09/2014	1800	1102198
h54	30/09/2014	1800	1102203
h56	30/09/2014	1800	1102205
h55	30/09/2014	1800	1102204
h57	30/09/2014	1800	7102194
h59	30/09/2014	1800	7102196
h58	30/09/2014	1800	7102195
h60	30/09/2014	1800	7102197
h62	30/09/2014	1800	7102202
h61	30/09/2014	1800	7102198
h63	30/09/2014	1800	7102203
h65	30/09/2014	1800	7102205
h64	30/09/2014	1800	7102204
h66	30/09/2014	1800	5102210
h67	30/09/2014	1800	5102211
h69	01/10/2014	1800	5102213
h68	30/09/2014	1800	5102212
h70	01/10/2014	1800	5102214
h71	01/10/2014	1800	5102218
h73	01/10/2014	1800	5102220
h72	01/10/2014	1800	5102219
h74	30/09/2014	1800	1102210
h75	30/09/2014	1800	1102211

Table A.11: Active biomonitoring counting data for the 2nd long-lived isotopes (duration given in seconds).

JINR Sample ID	Long-lived 2 Isotopes		
	Date	Duration	Spectra ID
h43	16/10/2014	5400	5201885
h42	16/10/2014	5400	5201884
h45	16/10/2014	5400	5201890
h44	16/10/2014	5400	5201889
h47	16/10/2014	5400	5201892
h46	16/10/2014	5400	5201891
h48	15/10/2014	5400	1201881
h50	16/10/2014	5400	1201883
h49	16/10/2014	5400	1201882
h51	16/10/2014	5400	1201884
h53	16/10/2014	5400	1201889
h52	16/10/2014	5400	1201885
h54	16/10/2014	5400	1201890
h56	16/10/2014	5400	1201892
h55	16/10/2014	5400	1201891
h57	15/10/2014	5400	7201881
h59	16/10/2014	5400	7201883
h58	15/10/2014	5400	7201882
h60	16/10/2014	5400	7201884
h62	16/10/2014	5400	7201889
h61	16/10/2014	5400	7201885
h63	16/10/2014	5400	7201890
h65	16/10/2014	5400	7201892
h64	16/10/2014	5400	7201891
h66	16/10/2014	5400	5201893
h67	16/10/2014	5400	5201894
h69	16/10/2014	5400	5201896
h68	16/10/2014	5400	5201895
h70	16/10/2014	5400	5201897
h71	17/10/2014	5400	5201901
h73	17/10/2014	5400	5201903
h72	17/10/2014	5400	5201902
h74	16/10/2014	5400	1201893
h75	16/10/2014	5400	1201894

Appendix B

Standard reference material (SRM) elemental concentrations: certified and measured (analysis of passive biomonitors)

Table B.1: Comparison of the SRM measured values with values listed in the certificates (short-lived isotopes). A "*" indicates a non-certified value in the certificates. The uncertainties in the concentrations are indicated at the 1σ (standard deviation) level.

Ref. Mat.	Element	Cert. Conc., ppm	Meas. Conc., ppm	% Dev.
2710	Al	64400 \pm 800	63600 \pm 740	1.2
1571	Ca	20900 \pm 300	20600 \pm 120	1.4
1575a	Cl	421 \pm 7	414 \pm 5	1.7
1515	I*	0.3	0.21 \pm 0.02	30
1547	Mg	4300 \pm 80	4200 \pm 60	1.9
2710	Mn	10100 \pm 400	9700 \pm 300	4.0
2710	V	80 \pm 2	70 \pm 2	3.0

APPENDIX B. STANDARD REFERENCE MATERIAL (SRM) ELEMENTAL CONCENTRATIONS: CERTIFIED AND MEASURED (ANALYSIS OF PASSIVE BIOMONITORS)

161

Table B.2: Comparison of the SRM measured values with values listed in the certificates (long-lived 1 isotopes). A "*" indicates a non-certified value in the certificates. The uncertainties in the concentrations are indicated at the 1σ (standard deviation) level.

Ref. Mat.	Element	Cert. Conc., ppm	Meas. Conc., ppm	% Dev.
1633b	As	136 ± 3	133 ± 2	2.0
2710	Br*	6	4.2 ± 1.3	30
1633b	K	19500 ± 300	19200 ± 200	1.5
1633b	La*	94	70 ± 4	30
2709	Na	11600 ± 300	11300 ± 300	2.6
1633b	Sm*	20.0	14.0 ± 2.3	30
1633b	Np (U)	8.8 ± 0.4	8.4 ± 0.3	4.1
2710	W*	93	70 ± 3	30

Table B.3: Comparison of the SRM measured values with values listed in the certificates (long-lived 2 isotopes). A "*" indicates a non-certified value in the certificates. The uncertainties in the concentrations are indicated at the 1σ (standard deviation) level.

Ref. Mat.	Element	Cert. Conc., ppm	Meas. Conc., ppm	% Dev.
1633b	Ba	710 ± 30	680 ± 30	3.8
1633b	Ce*	190	130 ± 40	30
1633b	Co*	120	119 ± 14	30
1633b	Cr	198 ± 5	193 ± 3	2.4
2710	Cs*	107	75 ± 11	30
1633b	Fe	17800 ± 2300	17300 ± 2200	3.0
2709	Hf*	3.7	2.6 ± 0.2	30
1633b	Nd*	85	59 ± 3	30
1633b	Pa (Th)	25.7 ± 1.3	24.4 ± 0.3	5.1
2710	Rb*	120	84 ± 12	30.0
2710	Sb	38 ± 3	35.4 ± 1.8	7.8
2709	Sc*	12	8.40 ± 0.04	30
1633b	Se	10.3 ± 0.2	10.1 ± 0.1	1.7
1633b	Sr	1040 14	1030 ± 12	1.3
1633b	Ta*	1.8	1.26 ± 0.06	30
1633b	Tb*	2.6	1.82 ± 0.02	30
2710	Zn	7000 ± 90	6700 ± 60	1.3

Appendix C

Descriptive statistics: passive biomonitoring

C.1 Moss Data

Table C.1: *Descriptive statistical analysis for passive biomonitoring moss data. The uncertainties in the concentrations are indicated at the 1σ (standard deviation) level. Where relevant, sample IDs are indicated.*

Statistics	INAA Data	ICP-MS Data
	<u>Na</u>	<u>Na</u>
Min (ppm)	414 ± 12 (BBM3)	270 ± 20 (MS3)
Max (ppm)	3700 ± 100 (FBMS1)	3400 ± 300 (FBMS1)
Mean (ppm)	1000	900
Median (ppm)	754	630
Stdev ⁴ (ppm)	800	1000
CV ⁵ (%)	83	110
	<u>Mg</u>	<u>Mg</u>
Min (ppm)	374 ± 30 (CMS5)	660 ± 70 (MS4)
Max (ppm)	2100 ± 90 (FBMS1)	4500 ± 300 (FBMS1)
Mean (ppm)	1200	2100
Median (ppm)	1160	1750
Stdev (ppm)	500	1200
CV (%)	50	60
	<u>Al</u>	<u>Al</u>
Min (ppm)	1490 ± 40 (BBM3)	1290 ± 50 (BBM3)
Max (ppm)	26100 ± 700 (CMS5)	10200 ± (CMS3)
Continued on next page		

⁴ σ

⁵The ratio of the standard deviation (σ) to the mean (\bar{x}). It is a useful statistic tool for comparing the degree of variation from one data point to another

APPENDIX C. DESCRIPTIVE STATISTICS: PASSIVE BIOMONITORING 163

Table C.1 –continued from previous page		
Statistics	INAA Data	ICP-MS Data
Mean (ppm)	7100	5600
Median (ppm)	5680	5600
Stdev(ppm)	6000	3000
CV (%)	80	50
	<u>K</u>	<u>K</u>
Min (ppm)	1300 ± 200 (BBM3)	800 ± 30 (BBM3)
Max (ppm)	11300 ± 800 (MS2)	7800 ± 700 (MS2)
Mean (ppm)	4400	3600
Median (ppm)	3500	2850
Stdev (ppm)	2900	2300
CV (%)	70	60
	<u>Ca</u>	<u>Ca</u>
Min (ppm)	1600 ± 100 (F-M1)	2500 ± 300 (BBM3)
Max (ppm)	11800 ± 800 (CMS2)	11700 ± 1300 (FBMS4)
Mean (ppm)	4000	6300
Median (ppm)	3000	5100
Stdev (ppm)	3000	3600
CV (%)	70	60
	<u>V</u>	<u>V</u>
Min (ppm)	3.1 ± 0.2 (BBM3)	3.4 ± 0.1 (CMS4)
Max (ppm)	18.4 ± 0.9 (CMS5)	25.9 ± 1.8 (CMS3)
Mean (ppm)	9	12
Median (ppm)	7.4	10
Stdev (ppm)	5	9
CV (%)	60	70
	<u>Cr</u>	<u>Cr</u>
Min (ppm)	4 ± 1 (CMS2)	21.6 ± 0.2 (MS4)
Max (ppm)	16 ± 2 (MS2)	2380 ± 40 (FBMS1)
Mean (ppm)	8	680
Median (ppm)	6	148
Stdev (ppm)	3	1000
CV (%)	40	150
	<u>Mn</u>	<u>Mn</u>
Min (ppm)	590 ± 50 (BBM1)	560 ± 60 (BBM2)
Max (ppm)	8200 ± 600 (MS2)	8300 ± 700 (MS2)
Mean (ppm)	2060	2210
Median (ppm)	1410	1210
Stdev (ppm)	2100	2610
CV (%)	100	118
	<u>Fe</u>	<u>Fe</u>
Continued on next page		

APPENDIX C. DESCRIPTIVE STATISTICS: PASSIVE BIOMONITORING 164

Table C.1 –continued from previous page		
Statistics	INAA Data	ICP-MS Data
Min (ppm)	1000 ± 73 (BBM3)	1630 ± 30 (BBM3)
Max (ppm)	11000 ± 600 (MS2)	18300 ± 300 (CMS3)
Mean (ppm)	4000	7500
Median (ppm)	2955	5200
Stdev (ppm)	2700	6600
CV (%)	70	90
	<u>Co</u>	<u>Co</u>
Min (ppm)	0.16 ± 0.02 (BBM3)	0.47 ± 0.02 (CMS3)
Max (ppm)	1.8 ± 0.1 (MS2)	15.1 ± 0.4 (FBMS1)
Mean (ppm)	0.7	6
Median (ppm)	0.5	2.5
Stdev (ppm)	0.5	6
CV (%)	70	110
	<u>Zn</u>	<u>Zn</u>
Min (ppm)	10.4 ± 0.6 (BBM3)	10.7 ± 0.1 (BBM3)
Max (ppm)	80.7 ± 1.6 (MS2)	85 ± 7 (MS2)
Mean (ppm)	35	37
Median (ppm)	34	34
Stdev (ppm)	19	22
CV (%)	54	60
	<u>As</u>	<u>As</u>
Min (ppm)	10.76 ± 0.02 (BBM3)	0.59 ± 0.03 (BBM3)
Max (ppm)	11.5 ± 0.3 (MS2)	3.69 ± 0.01 (MS2)
Mean (ppm)	3	2.0
Median (ppm)	1.8	1.9
Stdev (ppm)	3	1.0
CV (%)	92	47
	<u>Se</u>	<u>Se</u>
Min (ppm)	0.08 ± 0.09 (MS4)	0.49 ± 0.03 (MS4)
Max (ppm)	7.3 ± 0.7 (F-M1)	4.31 ± 0.2 (CMS3)
Mean (ppm)	1.4	1.8
Median (ppm)	0.8	1.6
Stdev (ppm)	1.9	1.2
CV (%)	129	68
	<u>Sr</u>	<u>Sr</u>
Min (ppm)	0.01 ± 0.001 (F-M1)	23.8 ± 0.7 (BBM3)
Max (ppm)	122 ± 8 (FBMS1)	111 ± 3 (FBMS1)
Mean (ppm)	50	50
Median (ppm)	41	35
Stdev (ppm)	30	30

Continued on next page

APPENDIX C. DESCRIPTIVE STATISTICS: PASSIVE BIOMONITORING 165

Table C.1 –continued from previous page		
Statistics	INAA Data	ICP-MS Data
CV (%)	58	63
	Ba	Ba
Min (ppm)	10.7 ± 1.2 (BBM3)	12.7 ± 0.5 (BBM3)
Max (ppm)	177 ± 9 (MS2)	160 ± 2 (MS2)
Mean (ppm)	50	50
Median (ppm)	37	41
Stdev (ppm)	50	50
CV (%)	88	90
	Br	Mo
Min (ppm)	5.7 ± 1.7 (CMS2)	1.5 ± 0.2 (BBM3)
Max (ppm)	90 ± 30 (FBMS1)	26 ± 3 (CMS3)
Mean (ppm)	20	8
Median (ppm)	21	2.6
Stdev (ppm)	20	10
CV (%)	83	130
	Rb	Cd
Min (ppm)	3 ± 1 (BBM3)	0.04 ± 0.001 (BBM3)
Max (ppm)	42 ± 14 (MS2)	0.53 ± 0.01 (MS2)
Mean (ppm)	14	0.2
Median (ppm)	8	0.1
Stdev (ppm)	12	0.2
CV (%)	88	106
	Sb	Sn
Min (ppm)	0.19 ± 0.02 (BBM3)	0.4 ± 0.001 (BBM3)
Max (ppm)	1.3 ± 0.1 (CMS1)	3.93 ± 0.02 (CMS3)
Mean (ppm)	0.5	1.6
Median (ppm)	0.4	1.02
Stdev (ppm)	0.3	1.3
CV (%)	67	80
	I	Hg
Min (ppm)	2.01 ± 0.6 (FBMS1(b))	0.07 ± 0.001 (FBMS1 & BBM1)
Max (ppm)	19 ± 3 (F-M1)	0.2 ± (MS2)
Mean (ppm)	9	0.12
Median (ppm)	7	0.12
Stdev (ppm)	6	0.05
CV (%)	63	40
	Cs	Pb
Min (ppm)	0.1 ± 0.01 (BBM1)	4.7 ± 0.1 (BBM3)
Max (ppm)	2 ± 0.6 (MS2)	80 ± 2 (BBM2)
Mean (ppm)	0.7	30
Continued on next page		

APPENDIX C. DESCRIPTIVE STATISTICS: PASSIVE BIOMONITORING 166

Table C.1 –continued from previous page		
Statistics	INAA Data	ICP-MS Data
Median (ppm)	0.4	27
Stdev (ppm)	0.6	30
CV (%)	90	80
	<u>Cl</u>	<u>B</u>
Min (ppm)	263 ± 20 (BBM3)	0.98 ± 0.07 (BBM3)
Max (ppm)	3100 ± 200 (FBMS1)	69 ± 5 (FBMS1)
Mean (ppm)	1000	18
Median (ppm)	700	12
Stdev (ppm)	800	22
CV (%)	84	119
	<u>Sc</u>	<u>Li</u>
Min (ppm)	0.3 ± 0.1 (BBM3)	0.5 ± 0.001 (BBM3)
Max (ppm)	2.7 ± 0.8 (MS2)	4.6 ± 0.7 (MS2)
Mean (ppm)	1.1	2.4
Median (ppm)	0.8	2.3
Stdev (ppm)	0.8	1.2
CV (%)	68	53
	<u>Ti</u>	<u>P</u>
Min (ppm)	140 ± 30 (BBM3)	246 ± 5 (BBM3)
Max (ppm)	1800 ± 200 (CMS5)	2600 ± 100 (MS3)
Mean (ppm)	600	1500
Median (ppm)	456	1319
Stdev (ppm)	500	1000
CV (%)	78	66
	<u>La</u>	<u>Ni</u>
Min (ppm)	1.4 ± 0.4 (BBM3)	23.3 ± 0.1 (MS4)
Max (ppm)	15 ± 5 (CMS5)	649 ± 3 (CMS3)
Mean (ppm)	6	200
Median (ppm)	5	45
Stdev (ppm)	4	300
CV (%)	68	139
	<u>Ce</u>	<u>Si</u>
Min (ppm)	2.78 ± 1.04 (BBM3)	510 ± 30 (MS3)
Max (ppm)	33 ± 10 (CMS5)	930 ± 40 (BBM2)
Mean (ppm)	13	700
Median (ppm)	8.8	793
Stdev (ppm)	10	200
CV (%)	75	25
	<u>Nd</u>	<u>Cu</u>
Min (ppm)	0.1 ± 0.001 (BBM1)	7.8 ± 0.6 (BBM3)
Continued on next page		

APPENDIX C. DESCRIPTIVE STATISTICS: PASSIVE BIOMONITORING 167

Table C.1 –continued from previous page		
Statistics	INAA Data	ICP-MS Data
Max (ppm)	13 ± 4 (CMS5)	40 ± 3 (CMS3)
Mean (ppm)	5	21
Median (ppm)	4	15
Stdev (ppm)	4	12
CV (%)	77	60
	<u>Sm</u>	-
Min (ppm)	0.2 ± 0.06 (CMS4(a))	
Max (ppm)	2.5 ± 0.7 (MS2)	
Mean (ppm)	1.0	
Median (ppm)	0.8	
Stdev (ppm)	0.7	
CV (%)	75	
	<u>Tb</u>	-
Min (ppm)	0.03 ± 0.01 (BBM3)	
Max (ppm)	0.3 ± 0.1 (MS2)	
Mean (ppm)	0.13	
Median (ppm)	0.11	
Stdev (ppm)	0.09	
CV (%)	69	
	<u>Hf</u>	-
Min (ppm)	0.3 ± 0.1 (BBM2)	
Max (ppm)	4.5 ± 1.4 (MS2)	
Mean (ppm)	1.5	
Median (ppm)	1.2	
Stdev (ppm)	1.2	
CV (%)	83	
	<u>Ta</u>	-
Min (ppm)	0.01 ± 0.001 (BBM2 & BBM3)	
Max (ppm)	0.6 ± 0.2 (MS2)	
Mean (ppm)	0.2	
Median (ppm)	0.19	
Stdev (ppm)	0.2	
CV (%)	80	
	<u>W</u>	-
Min (ppm)	0.08 ± (0.03 BBM3)	
Max (ppm)	0.9 ± (0.3 CMS5)	
Mean (ppm)	0.3	
Median (ppm)	0.3	
Stdev (ppm)	0.2	
CV (%)	71	

Continued on next page

APPENDIX C. DESCRIPTIVE STATISTICS: PASSIVE BIOMONITORING 168

Table C.1 –continued from previous page		
Statistics	INAA Data	ICP-MS Data
	<u>Th</u>	-
Min (ppm)	0.53 ± 0.03 (BBM3)	
Max (ppm)	7.3 ± 0.4 (MS2)	
Mean (ppm)	2.4	
Median (ppm)	1.9	
Stdev (ppm)	1.9	
CV (%)	77	
	<u>U</u>	-
Min (ppm)	0.14 ± 0.01 (BBM3)	
Max (ppm)	1.53 ± 0.06 (MS2)	
Mean (ppm)	0.6	
Median (ppm)	0.6	
Stdev (ppm)	0.4	
CV (%)	63	

C.2 Lichen Data

Table C.2: Descriptive statistical analysis for passive biomonitoring lichen data. The uncertainties in the concentrations are indicated at the 1σ (standard deviation) level.

Statistics	INAA Data	ICP-MS Data
	<u>Na</u>	<u>Na</u>
Min (ppm)	417 ± 12 (CLS4)	260 ± 20 (LS4)
Max (ppm)	1270 ± 40 (CLS2)	1130 ± 100 (TML2)
Mean (ppm)	800	700
Median (ppm)	804	609
Stdev (ppm)	300	300
CV (%)	38	43
	<u>Mg</u>	<u>Mg</u>
Min (ppm)	190 ± 10 (LS6)	540 ± 30 (F-L1)
Max (ppm)	2080 ± 90 (CLS1)	2400 ± 300 (LS4)
Mean (ppm)	1100	14000
Median (ppm)	850	1128
Stdev (ppm)	600	700
CV (%)	48	49
	<u>Al</u>	<u>Al</u>
Min (ppm)	15.5 ± 0.5 (LS6)	1480 ± 50 (LS6)
Max (ppm)	13400 ± 85 (CLS1)	7900 ± 300 (CLS1)
Mean (ppm)	5400	3600
Median (ppm)	4470	2800
Stdev (ppm)	3200	2100
CV (%)	59	57
	<u>K</u>	<u>K</u>
Min (ppm)	3200 ± 200 (F-L1)	2800 ± 100 (F-L1)
Max (ppm)	7000 ± 500 (LS1(a))	6200 ± 500 (LS1(a))
Mean (ppm)	4600	3900
Median (ppm)	4200	3700
Stdev (ppm)	1200	900
CV (%)	25	24
	<u>Ca</u>	<u>Ca</u>
Min (ppm)	193 ± 1 (F-L1)	650 ± 70 (F-L1)
Max (ppm)	27600 ± 1900 (LS5)	36900 ± 5200 (LS4)
Mean (ppm)	11100	13400
Median (ppm)	8000	7650
Stdev (ppm)	9800	11300
CV (%)	88	85
	<u>V</u>	<u>V</u>
Continued on next page		

APPENDIX C. DESCRIPTIVE STATISTICS: PASSIVE BIOMONITORING 170

Table C.2 –continued from previous page		
Statistics	INAA Data	ICP-MS Data
Min (ppm)	0.17 ± 0.02 (LS6)	2.64 ± 0.03 (LS6)
Max (ppm)	18.1 ± 0.8 (FBL1)	15.2 ± 1.1 (CLS1)
Mean (ppm)	8	6
Median (ppm)	6.2	5.96
Stdev (ppm)	5	4
CV (%)	64	59
	<u>Cr</u>	<u>Cr</u>
Min (ppm)	2.5 ± 0.8 (LS6)	12.6 ± 0.1 (LS2)
Max (ppm)	17 ± 2 (FBL1)	305 ± 5 (CLS1)
Mean (ppm)	8	70
Median (ppm)	6.9	19.9
Stdev (ppm)	4	90
CV (%)	50	144
	<u>Mn</u>	<u>Mn</u>
Min (ppm)	600 ± 50 (F-L1)	640 ± 50 (F-L1)
Max (ppm)	3800 ± 300 (LS1(a))	3400 ± 200 (ls6)
Mean (ppm)	1800	1700
Median (ppm)	1300	1300
Stdev (ppm)	1100	1100
CV (%)	63	63
	<u>Fe</u>	<u>Fe</u>
Min (ppm)	1500 ± 80 (LS6)	1367 ± 11 (LS6)
Max (ppm)	9100 ± 500 (FBL1)	7200 ± 100 (CLS1)
Mean (ppm)	3700	2900
Median (ppm)	3300	2700
Stdev (ppm)	1900	1700
CV (%)	52	60
	<u>Co</u>	<u>Co</u>
Min (ppm)	0.31 ± 0.02 (LS2)	0.39 ± 0.01 (LS2)
Max (ppm)	1.05 ± 0.06 (LS1(a))	3.01 ± 0.08 (CLS1)
Mean (ppm)	0.7	0.9
Median (ppm)	0.74	0.65
Stdev (ppm)	0.2	0.8
CV (%)	29	85
	<u>Zn</u>	<u>Zn</u>
Min (ppm)	39.3 ± 1.0 (CLS2)	25.3 ± 0.2 (F-L1)
Max (ppm)	99 ± 2 (FBL1)	66.8 ± 0.5 (CLS1)
Mean (ppm)	54	46
Median (ppm)	45	42.9
Stdev (ppm)	17	12
Continued on next page		

APPENDIX C. DESCRIPTIVE STATISTICS: PASSIVE BIOMONITORING 171

Table C.2 –continued from previous page		
Statistics	INAA Data	ICP-MS Data
CV (%)	33	25
	<u>As</u>	<u>As</u>
Min (ppm)	1.68 ± 0.04 (TML1)	1.37 ± 0.07 (CLS2)
Max (ppm)	6.4 ± 0.2 (FBL1)	3.01 ± 0.14 (CLS1)
Mean (ppm)	3.4	2.04
Median (ppm)	2.9	1.8
Stdev (ppm)	1.4	0.6
CV (%)	43	30
	<u>Se</u>	<u>Se</u>
Min (ppm)	0.28 ± 0.09 (LS1(a))	0.15 ± 0.01 (LS5)
Max (ppm)	6.3 ± 0.3 (F-L1)	3.99 ± 0.2 (F-L1)
Mean (ppm)	1.3	1.5
Median (ppm)	0.8	1.2
Stdev (ppm)	1.5	1.1
CV (%)	118	72
	<u>Sr</u>	<u>Sr</u>
Min (ppm)	6.9 ± 0.8 (F-L1)	19 ± 1.4 (F-L1)
Max (ppm)	151 ± 10 (LS4)	73 ± 4 (LS1(a))
Mean (ppm)	50	40
Median (ppm)	43	43
Stdev (ppm)	40	30
CV (%)	67	69
	<u>Ba</u>	<u>Ba</u>
Min (ppm)	19 ± 1.4 (F-L1)	12.4 ± 0.5 (F-L1)
Max (ppm)	73 ± 3.4 (LS1(a))	69.7 ± 1.0 (LS2)
Mean (ppm)	44	34
Median (ppm)	42	30
Stdev (ppm)	16	18
CV (%)	36	69
	<u>Br</u>	<u>Mo</u>
Min (ppm)	8 ± 3 (F-L1)	0.5 ± 0.05 (F-L1)
Max (ppm)	90 ± 30 (FBL1)	3.9 ± 0.4 (CLS1)
Mean (ppm)	30	1.3
Median (ppm)	19.7	1.03
Stdev (ppm)	20	1
CV (%)	82	77
	<u>Rb</u>	<u>Cd</u>
Min (ppm)	6 ± 2 (F-L1)	0.06 ± 0.001 (TML2)
Max (ppm)	16 ± 6 (LS6)	0.19 ± 0.02 (CLS1)
Mean (ppm)	11	0.13
Continued on next page		

APPENDIX C. DESCRIPTIVE STATISTICS: PASSIVE BIOMONITORING 172

Table C.2 –continued from previous page		
Statistics	INAA Data	ICP-MS Data
Median (ppm)	10.2	0.12
Stdev (ppm)	3	0.05
CV (%)	25	42
	<u>Sb</u>	<u>Sn</u>
Min (ppm)	0.27 ± 0.03 (BBL1)	0.77 ± 0.001 (F-L1)
Max (ppm)	1.67 ± 0.13 (LS3)	2.05 ± 0.01 (TML2)
Mean (ppm)	0.7	1.4
Median (ppm)	0.6	1.27
Stdev (ppm)	0.4	0.4
CV (%)	58	32
	<u>I</u>	<u>Hg</u>
Min (ppm)	4.8 ± 0.9 (LS6)	0.1 ± 0.001 (LS1(a))
Max (ppm)	25.4 ± 4.6 (BBL1)	0.25 ± 0.001 (LS3)
Mean (ppm)	11	0.18
Median (ppm)	9	0.18
Stdev (ppm)	6	0.04
CV (%)	55	23
	<u>Cs</u>	<u>Pb</u>
Min (ppm)	0.28 ± 0.08 (LS2)	2.23 ± 0.06 (F-L1)
Max (ppm)	0.82 ± 0.19 (BBL1)	59.9 ± 1.5 (CLS1)
Mean (ppm)	0.48	24
Median (ppm)	0.47	22.9
Stdev (ppm)	0.14	16
CV (%)	28	64
	<u>Cl</u>	<u>B</u>
Min (ppm)	600 ± 40 (CLS3)	1.93 ± 0.14 (CLS2)
Max (ppm)	3200 ± 200 (LS2)	12.3 ± 0.9 (TML2)
Mean (ppm)	1500	9
Median (ppm)	1520	9.6
Stdev (ppm)	700	4
CV (%)	50	41
	<u>Sc</u>	<u>Li</u>
Min (ppm)	0.3 ± 0.1 (LS2)	0.01 ± 0.001 (LS5, LS6, LS3)
Max (ppm)	1.6 ± 0.5 (FBL1)	3.26 ± 0.001 (CLS1)
Mean (ppm)	0.9	1.23
Median (ppm)	0.8	1.27
Stdev (ppm)	0.3	1.06
CV (%)	40	86
	<u>Ti</u>	<u>P</u>
Min (ppm)	35 ± 13 (LS3)	652 ± 13 (F-L1)
Continued on next page		

APPENDIX C. DESCRIPTIVE STATISTICS: PASSIVE BIOMONITORING 173

Table C.2 –continued from previous page		
Statistics	INAA Data	ICP-MS Data
Max (ppm)	1000 ± 100 (CLS1)	1630 ± 80 (LS3)
Mean (ppm)	400	1100
Median (ppm)	257	1056
Stdev (ppm)	300	300
CV (%)	76	27
	<u>La</u>	<u>Ni</u>
Min (ppm)	1.5 ± 0.4 (LS6)	4.75 ± 0.03 (CLS6)
Max (ppm)	9 ± 3 (FBL1)	93.3 ± 0.4 (CLS1)
Mean (ppm)	4	20
Median (ppm)	3.6	7.5
Stdev (ppm)	2	30
CV (%)	49	145
	<u>Ce</u>	<u>Si</u>
Min (ppm)	3.12 ± 1.02 (LS2)	440 ± 20 (LS6)
Max (ppm)	18 ± 5 (FBL1)	1070 ± 40 (TML2)
Mean (ppm)	8	700
Median (ppm)	8.1	536
Stdev (ppm)	4	300
CV (%)	50	39
	<u>Nd</u>	<u>Cu</u>
Min (ppm)	0.4 ± 0.06 (F-L1)	9.9 ± 0.7 (F-L1)
Max (ppm)	7 ± 3 (LS1(a))	24 ± 1.8 (CLS1)
Mean (ppm)	3.2	14
Median (ppm)	3.3	13
Stdev (ppm)	4	5
CV (%)	51	33
	<u>Sm</u>	-
Min (ppm)	0.28 ± 0.09 (LS6)	
Max (ppm)	1.31 ± 0.4 (FBL1)	
Mean (ppm)	0.7	
Median (ppm)	0.7	
Stdev (ppm)	0.3	
CV (%)	43	
	<u>Tb</u>	-
Min (ppm)	0.04 ± 0.01 (LS2)	
Max (ppm)	0.19 ± 0.06 (FBL1)	
Mean (ppm)	0.10	
Median (ppm)	0.09	
Stdev (ppm)	0.04	
CV (%)	45	

Continued on next page

APPENDIX C. DESCRIPTIVE STATISTICS: PASSIVE BIOMONITORING 174

Table C.2 –continued from previous page		
Statistics	INAA Data	ICP-MS Data
	<u>Hf</u>	-
Min (ppm)	0.23 ± 0.07 (LS6)	
Max (ppm)	2.44 ± 0.7 (FBL1)	
Mean (ppm)	0.9	
Median (ppm)	0.67	
Stdev (ppm)	0.7	
CV (%)	80	
	<u>Ta</u>	-
Min (ppm)	0.01 ± 0.001 (TML2)	
Max (ppm)	0.29 ± 0.1 (LS1(a))	
Mean (ppm)	0.13	
Median (ppm)	0.11	
Stdev (ppm)	0.08	
CV (%)	63	
	<u>W</u>	-
Min (ppm)	0.09 ± 0.03 (LS6)	
Max (ppm)	0.6 ± 0.2 (FBL1)	
Mean (ppm)	0.24	
Median (ppm)	0.23	
Stdev (ppm)	0.12	
CV (%)	49	
	<u>Th</u>	-
Min (ppm)	0.68 ± 0.04 (LS6)	
Max (ppm)	2.76 ± 0.14 (LS1(a))	
Mean (ppm)	1.7	
Median (ppm)	1.75	
Stdev (ppm)	0.7	
CV (%)	42	
	<u>U</u>	-
Min (ppm)	0.16 ± 0.01 (LS2)	
Max (ppm)	0.78 ± 0.03 (FBL1)	
Mean (ppm)	0.4	
Median (ppm)	0.38	
Stdev (ppm)	0.2	
CV (%)	45	

Appendix D

Standard reference material (SRM) elemental concentrations: certified and measured (analysis of active biomonitors)

Table D.1: Comparison of the SRM measured values with values listed in the certificates (short-lived isotopes). A "*" indicates a non-certified value in the certificates. The uncertainties in the concentrations are indicated at the 1σ (standard deviation) level.

Ref. Mat.	Element	Cert. Conc., ppm	Meas. Conc., ppm	% Dev.
2709	Al	75000 \pm 600	74400 \pm 500	0.8
1572	Ca	31500 \pm 1000	30500 \pm 900	3.2
1549	Cl	10900 \pm 200	10700 \pm 200	1.8
1549	I	3.38 \pm 0.02	3.36 \pm 0.02	0.6
2711	Mg	10500 \pm 300	10200 \pm 200	2.9
2711	Mn	640 \pm 30	610 \pm 20	4.4
2709	V	112 \pm 5	107 \pm 3	4.5

APPENDIX D. STANDARD REFERENCE MATERIAL (SRM) ELEMENTAL CONCENTRATIONS: CERTIFIED AND MEASURED (ANALYSIS OF ACTIVE BIOMONITORS) 176

Table D.2: Comparison of the SRM measured values with values listed in the certificates (long-lived 1 isotopes). A "*" indicates a non-certified value in the certificates. The uncertainties in the concentrations are indicated at the 1σ (standard deviation) level.

Ref. Mat.	Element	Cert. Conc., ppm	Meas. Conc., ppm	% Dev.
1632b	As	3.7 ± 0.1	3.4 ± 0.1	2.4
1632b	*Br	17	11.9 ± 0.2	30
2711	K	24500 ± 800	23700 ± 700	3.3
690CC	La	24.4 ± 1.7	22.7 ± 1.3	7
2711	*Mo	1.6	1.12 ± 0.02	30
2711	Na	11400 ± 300	11100 ± 200	2.6
690CC	Sm	3.5 ± 0.4	3.1 ± 0.3	11.4
1632b	Np (U)	0.44 ± 0.01	0.42 ± 0.03	2.8
2711	*W	3	2.10 ± 0.04	30

Table D.3: Comparison of the SRM measured values with values listed in the certificates (long-lived 2 isotopes). A "*" indicates a non-certified value in the certificates. The uncertainties in the concentrations are indicated at the 1σ (standard deviation) level.

Ref. Mat.	Element	Cert. Conc., ppm	Meas. Conc., ppm	% Dev.
1632b	Ba	68 ± 2	65 ± 2	3.1
690CC	Ce	49 ± 3	46 ± 2	5.1
2711	Co*	10	20 ± 4	30
2711	Cr*	47	2.4 ± 0.7	30
2711	Cs*	6.1	4.3 ± 0.2	30
2711	Fe	28900 ± 600	28300 ± 600	2.1
690CC	Gd	3.2 ± 0.4	2.8 ± 0.2	12.5
2711	Hf*	7.3	5.1 ± 0.2	30
2711	Nd*	31	21 ± 2	30
1632b	Pa (Th)	1.34 ± 0.04	1.30 ± 0.03	2.7
1632b	Rb	5.1 ± 0.1	4.9 ± 0.1	2.2
2711	Sb	19.4 ± 1.8	17.6 ± 1.7	9.3
690CC	Sc	7.9 ± 0.9	7.0 ± 0.9	1.4
1632b	Se	1.3 ± 0.1	1.2 ± 0.1	8.5
2711	Sr	2.5 ± 0.7	2.4 ± 0.7	0.3
690CC	Tb	0.5 ± 0.1	0.4 ± 0.1	14
690CC	Tm	1.6 ± 0.2	1.4 ± 0.2	11.2
2711	Zn	350 ± 5	345 ± 3	1.4
2711	Zr*	230	160 ± 30	30

Appendix E

Elemental concentrations in Montagu (pristine) samples

Table E.1: Average background concentrations of elements in biomonitors collected from Montagu (INAA data). The uncertainties in the concentrations are indicated at the 1σ (standard deviation) level.

Element	<i>L. smithii</i>	<i>P. gracile</i>	<i>U. subflorida</i>	<i>P. perlatum</i>
Al	2000 ± 50	3300 ± 90	990 ± 30	1930 ± 50
Ca	4900 ± 400	5050 ± 500	1720 ± 200	10300 ± 900
Fe	400 ± 40	1100 ± 100	310 ± 30	430 ± 40
K	8700 ± 1700	9300 ± 1900	2600 ± 500	5400 ± 1100
Mg	1860 ± 80	2040 ± 90	520 ± 30	620 ± 30
Na	410 ± 20	387 ± 19	152 ± 8	340 ± 17
Ti	117 ± 18	290 ± 30	75 ± 12	170 ± 30
V	3.0 ± 0.2	4.2 ± 0.3	1.3 ± 0.1	2.6 ± 0.2
Cr	2.0 ± 0.6	2.01 ± 0.6	1.9 ± 0.6	2.4 ± 0.7
Mn	186 ± 13	282 ± 19	41 ± 3	53 ± 4
Co	0.12 ± 0.02	0.5 ± 0.1	0.20 ± 0.03	0.3 ± 0.1
Ni	1.0 ± 0.3	1.7 ± 0.4	2.5 ± 0.6	2.7 ± 0.7
Zn	12.9 ± 0.7	36.3 ± 1.8	13.3 ± 0.7	12.9 ± 0.7
As	0.30 ± 0.03	0.5 ± 0.1	0.35 ± 0.04	0.35 ± 0.04
Se	0.12 ± 0.04	0.3 ± 0.1	0.09 ± 0.02	0.14 ± 0.04
Sr	11.7 ± 1.8	46 ± 7	10.7 ± 1.1	14.8 ± 2.2
Mo	0.04 ± 0.01	0.09 ± 0.01	0.03 ± 0.01	0.1 ± 0.01
Sb	0.08 ± 0.01	0.06 ± 0.01	0.04 ± 0.01	0.08 ± 0.01
Ba	7.7 ± 0.7	31.3 ± 3.1	7.1 ± 0.7	9.1 ± 0.9
La	0.6 ± 0.1	1.4 ± 0.1	0.5 ± 0.1	0.7 ± 0.1
Ce	0.8 ± 0.2	2.2 ± 0.4	0.8 ± 0.2	0.9 ± 0.2
Nd	0.7 ± 0.2	1.8 ± 0.5	1.7 ± 0.4	0.9 ± 0.2
Sm	0.08 ± 0.01	0.25 ± 0.04	0.07 ± 0.01	0.09 ± 0.01

APPENDIX E. ELEMENTAL CONCENTRATIONS IN MONTAGU
(PRISTINE) SAMPLES

178

Table E.1 cont...				
Tb	0.010 ± 0.002	0.04 ± 0.01	0.010 ± 0.003	0.010 ± 0.002
Cl	390 ± 30	590 ± 40	192 ± 14	500 ± 30
Br	6.3 ± 1.9	18.8 ± 5.6	5.4 ± 1.6	7.0 ± 2.1
I	4.2 ± 0.6	5.7 ± 0.9	1.8 ± 0.3	5.0 ± 0.8
Sc	0.10 ± 0.01	0.4 ± 0.1	0.11 ± 0.02	0.17 ± 0.03
Rb	1.70 ± 0.34	8.6 ± 1.7	1.3 ± 0.3	1.9 ± 0.4
Cs	0.06 ± 0.02	0.3 ± 0.1	0.04 ± 0.01	0.07 ± 0.02
Hf	0.05 ± 0.01	0.3 ± 0.1	0.03 ± 0.01	0.06 ± 0.02
Tm	0.010 ± 0.004	0.020 ± 0.004	0.010 ± 0.003	0.010 ± 0.004
Zr	2.7 ± 0.8	3.0 ± 0.9	1.8 ± 0.5	2.2 ± 0.7
Gd	0.02 ± 0.01	0.15 ± 0.04	0.010 ± 0.004	0.03 ± 0.01
W	0.04 ± 0.01	0.07 ± 0.02	0.03 ± 0.01	0.07 ± 0.02
Th	0.13 ± 0.01	0.46 ± 0.05	0.12 ± 0.01	0.16 ± 0.02
U	0.040 ± 0.004	0.12 ± 0.01	0.030 ± 0.003	0.050 ± 0.005

Table E.2: Average background concentrations of elements in biomonitors collected from Montagu (ICP-MS data). The uncertainties in the concentrations are indicated at the 1σ (standard deviation) level.

Element	<i>L. smithii</i>	<i>P. gracile</i>	<i>U. subflorida</i>	<i>P. perlatum</i>
Al	1450 ± 30	2092 ± 17	936 ± 10	2188 ± 9
B	16.56 ± 0.001	17 ± 0.001	3.78 ± 0.001	10.10 ± 0.002
Ca	5768 ± 3	6277 ± 0.6	2005 ± 5	7117 ± 11
Fe	840 ± 4	1237 ± 1.5	241 ± 0.6	1364 ± 1.4
K	5488 ± 9.2	6142 ± 9.2	2117 ± 12.9	3373 ± 0.7
Mg	2893 ± 0.7	3058 ± 0.3	868 ± 0.8	1060 ± 0.04
Na	77.6 ± 0.4	63 ± 0.3	92.5 ± 7.8	2.1 ± 0.1
P	3023 ± 3	2666 ± 1.6	678.3 ± 1.5	1459 ± 0.5
Si	986.2 ± 0.7	1002 ± 1.5	883.4 ± 2.7	983.3 ± 2.9
Li	0.58 ± 0.01	1.010 ± 0.001	0.48 ± 0.01	1.28 ± 0.01
Be	0.030 ± 0.001	0.060 ± 0.001	0.0100 ± 0.0001	0.060 ± 0.001
Ti	24.7 ± 1.8	33.2 ± 2.1	18.2 ± 2.0	37.2 ± 0.3
V	2.010 ± 0.003	2.70 ± 0.01	1.290 ± 0.004	2.890 ± 0.004
Cr	17.8 ± 0.1	19.33 ± 0.04	5.52 ± 0.01	5.98 ± 0.01
Mn	162.5 ± 0.4	227.4 ± 0.5	30.4 ± 0.1	60.01 ± 0.02
Co	0.850 ± 0.003	1.030 ± 0.003	1.340 ± 0.002	0.610 ± 0.001
Ni	8.18 ± 0.03	8.32 ± 0.01	3.6 ± 0.1	3.36 ± 0.01
Cu	7.6 ± 0.1	7.37 ± 0.01	4.5 ± 0.1	7.96 ± 0.01
Zn	28.3 ± 0.1	34.35 ± 0.01	13.1 ± 0.1	25.69 ± 0.01
As	1.08 ± 0.01	1.22 ± 0.01	1.09 ± 0.01	1.40 ± 0.01
Se	2.27 ± 0.01	1.50 ± 0.02	1.21 ± 0.01	1.34 ± 0.02
Sr	47.2 ± 0.2	51.2 ± 0.1	17.4 ± 0.1	42.8 ± 0.1

APPENDIX E. ELEMENTAL CONCENTRATIONS IN MONTAGU
(PRISTINE) SAMPLES

179

Table E.1 cont...				
Mo	0.38 ± 0.01	0.41 ± 0.01	0.120 ± 0.001	0.120 ± 0.001
Cd	0.088 ± 0.001	0.097 ± 0.001	0.016 ± 0.001	0.027 ± 0.001
Sn	0.054 ± 0.001	0.060 ± 0.001	0.010 ± 0.001	0.01100 ± 0.0001
Sb	0.010 ± 0.001	0.064 ± 0.001	0.005 ± 0.001	0.199 ± 0.001
Ba	30.80 ± 0.21	32.93 ± 0.01	7.78 ± 0.03	22.79 ± 0.02
Hg	0.130 ± 0.002	0.110 ± 0.002	0.140 ± 0.002	0.150 ± 0.001
Pb	2.70 ± 0.01	0.73 ± 0.03	3.13 ± 0.13	2.490 ± 0.003

Appendix F

Descriptive statistics: active biomonitoring

F.1 Moss Data

Table F.1: *Descriptive statistical analysis for active biomonitoring moss data. The uncertainties in the concentrations are indicated at the 1σ (standard deviation) level. Where relevant, sample IDs are indicated.*

Statistics	INAA Data	ICP-MS Data
	<u>Na</u>	<u>Na</u>
Min (ppm)	390 ± 20 (HTMP1)	310 ± 20 (NRMP3)
Max (ppm)	5400 ± 300 (SVMP3)	6300 ± 500 (SVML3)
Mean (ppm)	1500	1600
Median (ppm)	627	376
Stdev (ppm)	1600	1900
CV (%)	103	120
	<u>Mg</u>	<u>Mg</u>
Min (ppm)	1410 ± 50 (HTML2)	3040 ± 50 (NRML1)
Max (ppm)	2400 ± 100 (SVMP3)	4030 ± 60 (SVML3)
Mean (ppm)	1900	3400
Median (ppm)	1850	3300
Stdev (ppm)	300	300
CV (%)	16	9
	<u>Al</u>	<u>Al</u>
Min (ppm)	1400 ± 40 (HTML2)	1300 ± 200 (SVML3)
Max (ppm)	4000 ± 100 (NRMP1)	2600 ± 300 (NRMP3)
Mean (ppm)	2300	1700
Median (ppm)	2135	1600
Stdev(ppm)	800	400
Continued on next page		

APPENDIX F. DESCRIPTIVE STATISTICS: ACTIVE BIOMONITORING 181

Table F.1 –continued from previous page		
Statistics	INAA Data	ICP-MS Data
CV (%)	32	24
	<u>K</u>	<u>K</u>
Min (ppm)	1200 ± 200 (NRMP3)	1300 ± 100 (NRML3)
Max (ppm)	6800 ± 1400 (HTML2)	6500 ± 500 (HTML3)
Mean (ppm)	3900	4300
Median (ppm)	3550	4900
Stdev (ppm)	2100	2000
CV (%)	45	48
	<u>Ca</u>	<u>Ca</u>
Min (ppm)	4400 ± 400 (HTML1)	5600 ± 200 (HTML3)
Max (ppm)	7600 ± 600 (NRMP3)	7100 ± 300 (NRMP3)
Mean (ppm)	5900	6300
Median (ppm)	5800	6250
Stdev (ppm)	800	500
CV (%)	14	7
	<u>V</u>	<u>V</u>
Min (ppm)	2.3 ± 0.7 (HTML2)	1.98 ± 0.05 (SVML1)
Max (ppm)	5.4 ± 0.3 (NRMP1)	4.0 ± 0.1 (NRMP3)
Mean (ppm)	3.48	2.7
Median (ppm)	3.21	2.6
Stdev (ppm)	1.01	0.5
CV (%)	29	19
	<u>Cr</u>	<u>Cr</u>
Min (ppm)	2.0 ± 0.6 (NRML1)	10.4 ± 0.3 (SVMP2)
Max (ppm)	6.6 ± 2.0 (NRMP3)	29.8 ± 1.0 (SVMP3)
Mean (ppm)	3.8	20
Median (ppm)	3.6	19.6
Stdev (ppm)	1.3	5
CV (%)	34	26
	<u>Mn</u>	<u>Mn</u>
Min (ppm)	147 ± 10 (HTML2)	165 ± 6 (NRML3)
Max (ppm)	361 ± 24 (NRMP1)	318 ± 12 (SVMP3)
Mean (ppm)	240	210
Median (ppm)	241	201
Stdev (ppm)	70	209
CV (%)	28	20
	<u>Fe</u>	<u>Fe</u>
Min (ppm)	760 ± 80 (SVML1)	900 ± 20 (NRML1)
Max (ppm)	2100 ± 200 (SVMP3)	1800 ± 50 (SVMP3)
Mean (ppm)	1200	1300
Continued on next page		

APPENDIX F. DESCRIPTIVE STATISTICS: ACTIVE BIOMONITORING 182

Table F.1 –continued from previous page		
Statistics	INAA Data	ICP-MS Data
Median (ppm)	1100	1274
Stdev (ppm)	400	300
CV (%)	30	21
	<u>Co</u>	<u>Co</u>
Min (ppm)	0.32 ± 0.01 (SVML1)	0.58 ± 0.02 (SVML1)
Max (ppm)	0.73 ± 0.01 (SVMP3)	2.14 ± 0.06 (SVMP3)
Mean (ppm)	0.5	1.2
Median (ppm)	0.5	1.2
Stdev (ppm)	0.1	0.4
CV (%)	22	32
	<u>Zn</u>	<u>Zn</u>
Min (ppm)	25.9 ± 1.3 (SVML1)	29 ± 1.0 (SVML1)
Max (ppm)	63.2 ± 3.2 (NRMP3)	65 ± 2 (HTMP3)
Mean (ppm)	41	45
Median (ppm)	38	46
Stdev (ppm)	10	9
CV (%)	25	20
	<u>As</u>	<u>As</u>
Min (ppm)	0.35 ± 0.03 (HTML1)	0.4 ± 0.01 (HTML1)
Max (ppm)	1.5 ± 0.2 (SVMP3)	7.1 ± 0.3 (SVMP3)
Mean (ppm)	0.8	1.4
Median (ppm)	0.7	1.1
Stdev (ppm)	0.4	1.5
CV (%)	49	109
	<u>Se</u>	<u>Se</u>
Min (ppm)	0.21 ± 0.01 (HTMP2)	0.25 ± 0.01 (NRMP1)
Max (ppm)	0.45 ± 0.01 (SVMP3)	2.91 ± 0.07 (NRMP3)
Mean (ppm)	0.33	1.7
Median (ppm)	0.33	1.6
Stdev (ppm)	0.07	0.6
CV (%)	22	37
	<u>Sr</u>	<u>Sr</u>
Min (ppm)	38 ± 6 (NRML2)	45 ± 5 (HTML2)
Max (ppm)	63 ± 10 (SVMP3)	59 ± 6 (SVMP3)
Mean (ppm)	50	51
Median (ppm)	52	52
Stdev (ppm)	6	4
CV (%)	13	8
	<u>Ti</u>	<u>Ti</u>
Min (ppm)	73 ± 14 (HTML2)	23 ± 12 (NRML1)
Continued on next page		

APPENDIX F. DESCRIPTIVE STATISTICS: ACTIVE BIOMONITORING 183

Table F.1 –continued from previous page		
Statistics	INAA Data	ICP-MS Data
Max (ppm)	280 ± 30 (NRMP1)	49 ± 30 (NRMP3)
Mean (ppm)	170	35
Median (ppm)	156	35
Stdev (ppm)	60	7
CV (%)	33	20
	<u>Mo</u>	<u>Mo</u>
Min (ppm)	0.05 ± 0.02 (SVMP3)	0.26 ± 0.01 (SVML2)
Max (ppm)	0.28 ± 0.08 (NRMP2)	0.78 ± 0.03 (HTML3)
Mean (ppm)	0.16	0.5
Median (ppm)	0.16	0.43
Stdev (ppm)	0.06	0.2
CV (%)	39	33
	<u>Sb</u>	<u>Sb</u>
Min (ppm)	0.08 ± 0.01 (SVMP1)	0.01 ± 0.00004 (SVMP1)
Max (ppm)	0.46 ± 0.01 (NRMP3)	0.64 ± 0.004 (HTML3)
Mean (ppm)	0.3	0.4
Median (ppm)	0.27	0.4
Stdev (ppm)	0.1	0.2
CV (%)	41	51
	<u>Ba</u>	<u>Ba</u>
Min (ppm)	24.2 ± 0.2 (SVML1)	27.3 ± 1.3 (SVML1)
Max (ppm)	42.8 ± 0.4 (SVMP3)	42 ± 2 (NRMP3)
Mean (ppm)	35	34
Median (ppm)	35	35
Stdev (ppm)	5	4
CV (%)	14	11
	<u>Ci</u>	<u>Cu</u>
Min (ppm)	260 ± 20 (NRMP3)	8.36 ± 0.07 (HTMP1)
Max (ppm)	13600 ± 900 (SVMP3)	20.04 ± 0.02 (NRML3)
Mean (ppm)	2400	11
Median (ppm)	569	10.11
Stdev (ppm)	3500	3
CV (%)	137	30
	<u>I</u>	<u>Cd</u>
Min (ppm)	3.2 ± 0.5 (HTML1)	0.08 ± 0.0002 (HTMP3)
Max (ppm)	8.5 ± 1.3 (NRMP3)	0.18 ± 0.001 (NRMP3)
Mean (ppm)	6.0	0.12
Median (ppm)	6.2	0.12
Stdev (ppm)	1.6	0.03
CV (%)	25	26
Continued on next page		

APPENDIX F. DESCRIPTIVE STATISTICS: ACTIVE BIOMONITORING 184

Table F.1 –continued from previous page		
Statistics	INAA Data	ICP-MS Data
	<u>Br</u>	<u>Sn</u>
Min (ppm)	9.7 ± 2.9 (NRML1)	0.09 ± 0.003 (NRMP1)
Max (ppm)	36 ± 11 (SVMP3)	0.7 ± 0.1 (HTML3)
Mean (ppm)	17	0.3
Median (ppm)	15.8	0.2
Stdev (ppm)	7	0.2
CV (%)	43	67
	<u>Rb</u>	<u>Hg</u>
Min (ppm)	4.1 ± 0.8 (NRML1)	0.07 ± 0.001 (HTMP3)
Max (ppm)	7.8 ± 1.6 (NRMP2)	0.6 ± 0.0002 (NRML1)
Mean (ppm)	6.4	0.1
Median (ppm)	6.6	0.09
Stdev (ppm)	0.9	0.02
CV (%)	13	19
	<u>Sc</u>	<u>Pb</u>
Min (ppm)	0.22 ± 0.03 (SVML1)	0.99 ± 0.02 (NRMP1)
Max (ppm)	0.6 ± 0.1 (NRMP2)	6.3 ± 0.3 (HTML3)
Mean (ppm)	0.4	3.4
Median (ppm)	0.38	3.5
Stdev (ppm)	0.1	1.6
CV (%)	26	46
	<u>Cs</u>	<u>B</u>
Min (ppm)	0.12 ± 0.03 (SVML1)	19.36 ± 0.03 (NRML1)
Max (ppm)	0.31 ± 0.09 (NRMP2)	46 ± 5 (HTML3)
Mean (ppm)	0.19	29
Median (ppm)	0.18	26.3
Stdev (ppm)	0.05	8
CV (%)	26	26
	<u>La</u>	<u>Li</u>
Min (ppm)	1.0 ± 0.1 (HTML1)	0.47 ± 0.01 (SVML1)
Max (ppm)	2.4 ± 0.2 (NRMP2)	6.81 ± 0.02 (SVMP3)
Mean (ppm)	1.5	3
Median (ppm)	1.4	3.9
Stdev (ppm)	0.4	2
CV (%)	28	61
	<u>Ce</u>	<u>P</u>
Min (ppm)	1.6 ± 0.3 (SVML1)	1400 ± 200 (NRMP2)
Max (ppm)	5.06 ± 1.01 (NRMP2)	2900 ± 100 (HTML3)
Mean (ppm)	2.8	2300
Median (ppm)	2.9	2370
Continued on next page		

APPENDIX F. DESCRIPTIVE STATISTICS: ACTIVE BIOMONITORING 185

Table F.1 –continued from previous page		
Statistics	INAA Data	ICP-MS Data
Stdev (ppm)	0.9	500
CV (%)	31	22
	<u>Nd</u>	<u>Si</u>
Min (ppm)	0.9 ± 0.2 (SVML1)	552 ± 60 (SVMP1)
Max (ppm)	3.3 ± 0.8 (SVMP2)	1214 ± 14 (NRMP3)
Mean (ppm)	1.72	1000
Median (ppm)	1.65	1004
Stdev (ppm)	0.6	200
CV (%)	35	19
	<u>Sm</u>	<u>Be</u>
Min (ppm)	0.16 ± 0.02 (HTML3)	0.03 ± 0.003 (NRML1)
Max (ppm)	0.38 ± 0.06 (NRMP3)	0.3 ± 0.02 (SVMP3)
Mean (ppm)	0.25	0.11
Median (ppm)	0.24	0.08
Stdev (ppm)	0.07	0.09
CV (%)	27	82
	<u>Tb</u>	-
Min (ppm)	0.02 ± 0.004 (SVML1)	
Max (ppm)	0.06 ± 0.01 (NRMP2)	
Mean (ppm)	0.03	
Median (ppm)	0.03	
Stdev (ppm)	0.01	
CV (%)	26	
	<u>Hf</u>	-
Min (ppm)	0.1 ± 0.03 (SVML1)	
Max (ppm)	0.5 ± 0.1 (NRMP2)	
Mean (ppm)	0.2	
Median (ppm)	0.19	
Stdev (ppm)	0.09	
CV (%)	42	
	<u>Gd</u>	-
Min (ppm)	0.03 ± 0.01 (HTML1)	
Max (ppm)	0.4 ± 0.1 (NRMP2)	
Mean (ppm)	0.2	
Median (ppm)	0.13	
Stdev (ppm)	0.1	
CV (%)	74	
	<u>Tm</u>	-
Min (ppm)	0.01 ± 0.004 (HTML1)	
Max (ppm)	0.05 ± 0.02 (NRMP2)	
Continued on next page		

APPENDIX F. DESCRIPTIVE STATISTICS: ACTIVE BIOMONITORING 186

Table F.1 –continued from previous page		
Statistics	INAA Data	ICP-MS Data
Mean (ppm)	0.03	
Median (ppm)	0.03	
Stdev (ppm)	0.01	
CV (%)	41	
	Zr	-
Min (ppm)	3.59 ± 1.08 (NRML1)	
Max (ppm)	11.2 ± 3.4 (SVMP3)	
Mean (ppm)	6.1	
Median (ppm)	5.4	
Stdev (ppm)	1.9	
CV (%)	31	
	W	-
Min (ppm)	0.04 ± 0.01 (HTML1)	
Max (ppm)	0.28 ± 0.08 (NRMP2)	
Mean (ppm)	0.11	
Median (ppm)	0.1	
Stdev (ppm)	0.05	
CV (%)	48	
	Th	-
Min (ppm)	0.2 ± 0.02 (SVML1)	
Max (ppm)	0.65 ± 0.07 (SVMP3)	
Mean (ppm)	0.4	
Median (ppm)	0.41	
Stdev (ppm)	0.1	
CV (%)	28	
	U	-
Min (ppm)	0.06 ± 0.01 (SVML1)	
Max (ppm)	0.16 ± 0.02 (SVMP3)	
Mean (ppm)	0.11	
Median (ppm)	0.1	
Stdev (ppm)	0.03	
CV (%)	27	

F.2 Lichen Data

Table F.2: Descriptive statistical analysis for active biomonitoring lichen data. The uncertainties in the concentrations are indicated at the 1σ (standard deviation) level.

Statistics	INAA Data	ICP-MS Data
	<u>Na</u>	<u>Na</u>
Min (ppm)	240 ± 12 (HTLU2)	200 ± 60 (NRLU1)
Max (ppm)	1430 ± 70 (SVLU3)	2100 ± 200 (SVLU3)
Mean (ppm)	600	600
Median (ppm)	429	291
Stdev (ppm)	400	600
CV (%)	63	101
	<u>Mg</u>	<u>Mg</u>
Min (ppm)	408 ± 17 (HTLU2)	974 ± 15 (NRLU1)
Max (ppm)	900 ± 40 (HTLP2)	1800 ± 30 (SVLU2)
Mean (ppm)	600	1200
Median (ppm)	581	1197
Stdev (ppm)	200	200
CV (%)	25	19
	<u>Al</u>	<u>Al</u>
Min (ppm)	1400 ± 40 (HTML2)	1300 ± 200 (SVML3)
Max (ppm)	4000 ± 100 (NRMP1)	2600 ± 300 (NRMP3)
Mean (ppm)	2300	1700
Median (ppm)	2135	1600
Stdev(ppm)	800	400
CV (%)	32	24
	<u>K</u>	<u>K</u>
Min (ppm)	1800 ± 200 (SVLU3)	2000 ± 200 (NRLU2)
Max (ppm)	4800 ± 1000 (HTLPL2)	4100 ± 300 (HTLP3)
Mean (ppm)	2800	2900
Median (ppm)	2500	2800
Stdev (ppm)	1000	800
CV (%)	36	27
	<u>Ca</u>	<u>Ca</u>
Min (ppm)	1100 ± 100 (HTLP3)	2000 ± 80 (NRLU1)
Max (ppm)	6200 ± 500 (HTLP2)	7200 ± 300 (HTLP2)
Mean (ppm)	2500	3700
Median (ppm)	2300	2700
Stdev (ppm)	1300	1900
CV (%)	52	51
	<u>V</u>	<u>V</u>
Min (ppm)	0.52 ± 0.05 (HTLU2)	0.8 ± 0.02 (NRLU1)
Continued on next page		

APPENDIX F. DESCRIPTIVE STATISTICS: ACTIVE BIOMONITORING 188

Table F.2 –continued from previous page		
Statistics	INAA Data	ICP-MS Data
Max (ppm)	4.9 ± 0.3 (HTLP2)	3.22 ± 0.08 (HTLP2)
Mean (ppm)	1.7	1.53
Median (ppm)	1.29	1.01
Stdev (ppm)	1.2	0.96
CV (%)	72	63
	<u>Cr</u>	<u>Cr</u>
Min (ppm)	1.4 ± 0.4 (HTLU1)	3.4 ± 0.1 (NRLU2)
Max (ppm)	4.1 ± 1.2 (HTLP2)	14.4 ± 0.5 (HTLP2)
Mean (ppm)	9	8
Median (ppm)	2.87	8.14
Stdev (ppm)	1.1	3
CV (%)	38	42
	<u>Mn</u>	<u>Mn</u>
Min (ppm)	26.4 ± 1.9 (HTLU3)	34.9 ± 1.3 (NRLU2)
Max (ppm)	145 ± 10 (HTLU1)	87.1 ± 3.2 (HTLP2)
Mean (ppm)	60	62
Median (ppm)	44.3	63
Stdev (ppm)	30	17
CV (%)	59	28
	<u>Fe</u>	<u>Fe</u>
Min (ppm)	310 ± 30 (HTLU2)	342 ± 9 (NRLU1)
Max (ppm)	1400 ± 200 (HTLP3)	1700 ± 40 (HTLP2)
Mean (ppm)	700	800
Median (ppm)	517	700
Stdev (ppm)	400	400
CV (%)	60	55
	<u>Co</u>	<u>Co</u>
Min (ppm)	0.16 ± 0.02 (NRLU1)	0.31 ± 0.01 (NRLU2)
Max (ppm)	0.61 ± 0.01 (HTLP2)	1.34 ± 0.04 (HTLU3)
Mean (ppm)	0.3	0.7
Median (ppm)	0.21	0.65
Stdev (ppm)	0.2	0.3
CV (%)	58	45
	<u>Zn</u>	<u>Zn</u>
Min (ppm)	11.6 ± 0.6 (SVLU3)	14.4 ± 0.5 (HTLU1)
Max (ppm)	45.1 ± 2.3 (HTLP2)	63.4 ± 2.1 (HTLP3)
Mean (ppm)	19	28
Median (ppm)	14.2	20.8
Stdev (ppm)	12	17
CV (%)	59	59

Continued on next page

APPENDIX F. DESCRIPTIVE STATISTICS: ACTIVE BIOMONITORING 189

Table F.2 –continued from previous page		
Statistics	INAA Data	ICP-MS Data
	<u>As</u>	<u>As</u>
Min (ppm)	0.3 ± 0.03 (HTLU2)	0.37 ± 0.01 (HTLU2)
Max (ppm)	0.64 ± 0.01 (HTLP3)	1.23 ± 0.04 (NRLU1)
Mean (ppm)	0.48	0.8
Median (ppm)	0.48	0.78.1
Stdev (ppm)	0.11	0.3
CV (%)	24	34
	<u>Se</u>	<u>Se</u>
Min (ppm)	0.09 ± 0.003 (HTLP3)	0.44 ± 0.01 (NRLU1)
Max (ppm)	0.43 ± 0.01 (HTLP1)	2.54 ± 0.06 (HTLP1)
Mean (ppm)	0.2	1.4
Median (ppm)	0.19	1.36
Stdev (ppm)	0.09	0.5
CV (%)	46	37
	<u>Sr</u>	<u>Sr</u>
Min (ppm)	11.7 ± 1.8 (NRML1)	16.0 ± 1.6 (HTLU2)
Max (ppm)	38 ± 6 (HTLP2)	48 ± 5 (HTLP2)
Mean (ppm)	22	27
Median (ppm)	20.8	21.7
Stdev (ppm)	8	12
CV (%)	36	45
	<u>Ti</u>	<u>Ti</u>
Min (ppm)	30 ± 8 (HTLU2)	9 ± 5 (NRLU1)
Max (ppm)	330 ± 30 (HTLP2)	45 ± 20 (HTLP3)
Mean (ppm)	90	22
Median (ppm)	62	17
Stdev (ppm)	80	12
CV (%)	89	56
	<u>Mo</u>	<u>Mo</u>
Min (ppm)	0.03 ± 0.01 (SVLU1)	0.08 ± 0.002 (SVLU2)
Max (ppm)	0.32 ± 0.0003 (HTLP3)	0.51 ± 0.02 (HTLP3)
Mean (ppm)	0.12	0.23
Median (ppm)	0.09	0.18
Stdev (ppm)	0.09	0.14
CV (%)	73	62
	<u>Sb</u>	<u>Sb</u>
Min (ppm)	0.08 ± 0.01 (SVLU1)	0.1 ± 0.0006 (SVLU2)
Max (ppm)	0.5 ± 0.01 (HTLP3)	0.78 ± 0.005 (HTLU3)
Mean (ppm)	0.25	0.4
Median (ppm)	0.21	0.34
Continued on next page		

APPENDIX F. DESCRIPTIVE STATISTICS: ACTIVE BIOMONITORING 190

Table F.2 –continued from previous page		
Statistics	INAA Data	ICP-MS Data
Stdev (ppm)	0.2	0.2
CV (%)	62	60
	<u>Ba</u>	<u>Ba</u>
Min (ppm)	7.13 ± 0.07 (SVLU1)	8.6 ± 0.4 (NRLU1)
Max (ppm)	35 ± 0.4 (HTLP2)	35.6 ± 1.7 (HTLP3)
Mean (ppm)	15	17
Median (ppm)	10.2	11.1
Stdev (ppm)	10	10
CV (%)	65	61
	<u>Ci</u>	<u>Cu</u>
Min (ppm)	219 ± 16 (HTLU1)	3.8 ± 0.0002 (NRLU1)
Max (ppm)	3700 ± 200 (SVLU3)	13.34 ± 0.003 (HTLP3)
Mean (ppm)	1100	7
Median (ppm)	724	6.3
Stdev (ppm)	1000	3
CV (%)	92	45
	<u>I</u>	<u>Cd</u>
Min (ppm)	1.42 ± 0.23 (HTLU2)	0.01 ± 0.0001 (HTLU1)
Max (ppm)	5.73 ± 0.89 (HTLP2)	0.05 ± 0.00006 (HTLP2)
Mean (ppm)	2.8	0.03
Median (ppm)	2.4	0.04
Stdev (ppm)	1.4	0.01
CV (%)	51	42
	<u>Br</u>	<u>Sn</u>
Min (ppm)	5.3 ± 1.6 (NRLU1)	0.05 ± 0.0005 (SVLU3)
Max (ppm)	17 ± 5 (HTLP1)	0.69 ± 0.04 (HTLU3)
Mean (ppm)	9	0.3
Median (ppm)	7.9	0.2
Stdev (ppm)	4	0.2
CV (%)	42	84
	<u>Rb</u>	<u>Hg</u>
Min (ppm)	1.3 ± 0.3 (HTLU2)	0.06 ± 0.001 (HTLU2, HTLU3)
Max (ppm)	4.9 ± 1.0 (HTLP1)	0.12 ± 0.0002 (SVLU1)
Mean (ppm)	2.6	0.09
Median (ppm)	2.1	0.09
Stdev (ppm)	1.3	0.02
CV (%)	50	18
	<u>Sc</u>	<u>Pb</u>
Min (ppm)	0.1 ± 0.01 (HTLU2)	2.02 ± 0.001 (SVLU1)
Max (ppm)	0.5 ± 0.07 (HTLP1)	11.93 ± 0.96 (SVLU3)

Continued on next page

APPENDIX F. DESCRIPTIVE STATISTICS: ACTIVE BIOMONITORING 191

Table F.2 –continued from previous page		
Statistics	INAA Data	ICP-MS Data
Mean (ppm)	0.2	4.9
Median (ppm)	0.16	4.5
Stdev (ppm)	0.1	2.6
CV (%)	63	53
	Cs	B
Min (ppm)	0.04 ± 0.01 (HTLU2)	3.64 ± 0.005 (NRLU1)
Max (ppm)	0.23 ± 0.07 (HTLP3)	19.4 ± 0.4 (HTLP3)
Mean (ppm)	0.11	11
Median (ppm)	0.07	8.9
Stdev (ppm)	0.07	6
CV (%)	65	50
	La	Li
Min (ppm)	0.35 ± 0.03 (HTLU2)	0.1 ± 0.0001 (NRLU2)
Max (ppm)	2.0 ± 0.2 (HTLP3)	5.18 ± 0.09 (HTLP2)
Mean (ppm)	0.9	2.7
Median (ppm)	0.6	2.8
Stdev (ppm)	0.4	1.7
CV (%)	67	64
	Ce	P
Min (ppm)	0.8 ± 0.2 (SVLU2)	584.1 ± 0.6 (SVLU3)
Max (ppm)	4.54 ± 1.91 (HTLP1)	1627.18 ± 0.09 (HTLP2)
Mean (ppm)	1.8	1000
Median (ppm)	1.4	1002
Stdev (ppm)	1.2	300
CV (%)	69	31
	Nd	Si
Min (ppm)	0.7 ± 0.2 (HTLU2)	439.1 ± 0.9 (SVLU1)
Max (ppm)	1.8 ± 0.5 (HTLP1)	1147 ± 0.5 (HTLP1)
Mean (ppm)	1.1	800
Median (ppm)	0.99	712
Stdev (ppm)	0.3	200
CV (%)	30	28
	Sm	Be
Min (ppm)	0.06 ± 0.01 (HTLU2)	0.01 ± 0.00007 (NRLU2)
Max (ppm)	0.33 ± 0.05 (HTLP3)	0.3 ± 0.002 (HTLU3)
Mean (ppm)	0.2	0.1
Median (ppm)	0.1	0.08
Stdev (ppm)	0.1	0.1
CV (%)	67	90
	Tb	-
Continued on next page		

APPENDIX F. DESCRIPTIVE STATISTICS: ACTIVE BIOMONITORING 192

Table F.2 –continued from previous page		
Statistics	INAA Data	ICP-MS Data
Min (ppm)	0.01 ± 0.003 (HTLU3)	
Max (ppm)	0.04 ± 0.01 (HTLP3)	
Mean (ppm)	0.02	
Median (ppm)	0.01	
Stdev (ppm)	0.01	
CV (%)	71	
	Hf	-
Min (ppm)	0.03 ± 0.01 (SVLU2)	
Max (ppm)	0.29 ± 0.09 (HTLP3)	
Mean (ppm)	0.11	
Median (ppm)	0.07	
Stdev (ppm)	0.09	
CV (%)	84	
	Gd	-
Min (ppm)	0.01 ± 0.004 (SVLU2)	
Max (ppm)	0.23 ± 0.07 (HTLP3)	
Mean (ppm)	0.08	
Median (ppm)	0.06	
Stdev (ppm)	0.08	
CV (%)	94	
	Tm	-
Min (ppm)	0.01 ± 0.003 (SVLU1, SVLU3)	
Max (ppm)	0.04 ± 0.01 (HTLP2)	
Mean (ppm)	0.02	
Median (ppm)	0.02	
Stdev (ppm)	0.01	
CV (%)	44	
	Zr	-
Min (ppm)	1.8 ± 0.5 (SVLU1)	
Max (ppm)	7.6 ± 2.3 (HTLP3)	
Mean (ppm)	5.0	
Median (ppm)	5.8	
Stdev (ppm)	1.9	
CV (%)	38	
	W	-
Min (ppm)	0.03 ± 0.01 (SVLU2)	
Max (ppm)	0.15 ± 0.05 (HTLP3)	
Mean (ppm)	0.08	
Median (ppm)	0.08	
Stdev (ppm)	0.04	
Continued on next page		

APPENDIX F. DESCRIPTIVE STATISTICS: ACTIVE BIOMONITORING 193

Table F.2 –continued from previous page		
Statistics	INAA Data	ICP-MS Data
CV (%)	43	
	<u>Th</u>	-
Min (ppm)	0.12 ± 0.01 (NRLU2)	
Max (ppm)	0.49 ± 0.05 (HTLP1)	
Mean (ppm)	0.2	
Median (ppm)	0.17	
Stdev (ppm)	0.1	
CV (%)	57	
	<u>U</u>	-
Min (ppm)	0.02 ± 0.002 (HTLU2)	
Max (ppm)	0.13 ± 0.1 (HTLP3)	
Mean (ppm)	0.06	
Median (ppm)	0.04	
Stdev (ppm)	0.04	
CV (%)	67	

Appendix G

Sample elemental concentrations (measured by INAA and ICP-MS)

G.1 Passive biomonitoring

APPENDIX G. SAMPLE ELEMENTAL CONCENTRATIONS (MEASURED BY INAA AND ICP-MS)

195

SAMPLE CODE	Na				Mg			
	NAA		ICP-MS		NAA		ICP-MS	
	Conc. (ppm)	Error (ppm)	Conc. (ppm)	Error (ppm)	Conc. (ppm)	Error (ppm)	Conc. (ppm)	Error (ppm)
MS2	971	28	311	27	2050	89	1900	200
MS3	653	19	271	23	905	42	1600	200
LS1(a)	481	14	262	22	1420	60	2400	300
LS4	635	18	347	30	647	32	810	90
LS5	614	18	691	59	605	29	659	73
LS6	428	13	414	35	189	10	943	79
LS3	1240	36	838	71	806	39	877	98
LS2	1070	31	908	77	677	43	1300	100
MS4	940	27	673	57	1820	78	2300	300
CLS1	1090	31	874	74	2080	88	2086	100
CMS3	1050	29	729	62	1440	60	1400	85
CLS2	1270	36	544	46	1350	59	1039	65
F-L1	460	13	524	44	539	26	538	34
FBMS1	3700	100	3400	300	2100	87	4500	300
BBM1	534	16	637	54	1250	54	2200	100
BBM2	554	17	630	53	1400	60	2900	200
BBM3	414	12	401	34	657	30	1305	82
TML2	1140	33	1127	96	820	37	1217	76

SAMPLE CODE	Al				K			
	NAA		ICP-MS		NAA		ICP-MS	
	Conc. (ppm)	Error (ppm)	Conc. (ppm)	Error (ppm)	Conc. (ppm)	Error (ppm)	Conc. (ppm)	Error (ppm)
MS2	8600	300	8800	300	11300	800	7800	700
MS3	6200	200	5200	200	7300	500	5700	500
LS1(a)	5000	100	5100	200	3800	300	3500	300
LS4	3500	99	2581	82	3400	300	3300	300
LS5	3110	84	2033	65	4300	300	4300	400
LS6	15.5	0.5	1484	47	4200	300	3900	300
LS3	4000	100	2190	70	4400	300	4300	400
LS2	3400	85	1875	60	4400	300	4100	300
MS4	6600	200	6000	200	7000	500	6200	500
CLS1	13400	300	7900	300	5000	400	3500	200
CMS3	8900	200	10200	400	3300	300	2900	100
CLS2	8300	200	3000	100	3800	300	3200	100
F-L1	3100	78	2600	100	3200	200	2800	100
FBMS1	4600	100	6200	200	3700	400	2500	100
BBM1	4600	100	4700	200	2000	200	1900	84
BBM2	3820	99	6000	200	2900	300	2800	100
BBM3	1490	40	1295	51	1300	200	801	35
TML2	4000	100	3278	130	3800	400	4000	200

Figure G.1: Concentrations of Na, Mg, Al, K. "Error" represents the standard deviation at 1σ level.

APPENDIX G. SAMPLE ELEMENTAL CONCENTRATIONS (MEASURED BY INAA AND ICP-MS)

196

SAMPLE CODE	Ca				V			
	NAA		ICP-MS		NAA		ICP-MS	
	Conc. (ppm)	Error (ppm)	Conc. (ppm)	Error (ppm)	Conc. (ppm)	Error (ppm)	Conc. (ppm)	Error (ppm)
MS2	5600	400	6900	1000	18.0	1.0	11.5	0.2
MS3	4800	400	5900	800	5.2	0.4	6.2	0.1
LS1(a)	21100	1400	36900	5200	6.4	0.3	7.2	0.1
LS4	27600	1900	25100	3500	4.8	0.4	4	0.1
LS5	3700	300	11700	1600	3.7	0.3	3.4	0.1
LS6	1600	100	7000	1000	0.2	0.1	2.6	0
LS3	6000	500	6700	900	5.8	0.4	3.7	0.1
LS2	24500	1700	22100	3100	4.0	0.3	2.7	0.1
MS4	8000	600	8300	1200	6.2	0.6	7.8	0.1
CLS1	1500	200	5900	700	18	0.7	15.2	1.1
CMS3	1900	200	3200	400	9.9	0.4	26	2
CLS2	1600	200	15500	1800	8.7	1.1	6.2	0.4
F-L1	<193	*	646	74	5.5	0.3	5.7	0.4
FBMS1	7300	500	11700	1300	5.6	0.3	24	2
BBM1	2700	200	4300	500	7.8	0.4	8	0.6
BBM2	3200	300	4100	500	8.9	0.4	14.1	1.0
BBM3	2000	200	2500	300	3.1	0.2	4	0.3
TML2	5900	400	5800	700	8.2	0.4	8.8	0.6

SAMPLE CODE	Cr				Mn			
	NAA		ICP-MS		NAA		ICP-MS	
	Conc. (ppm)	Error (ppm)	Conc. (ppm)	Error (ppm)	Conc. (ppm)	Error (ppm)	Conc. (ppm)	Error (ppm)
MS2	16	2	74.4	0.7	8200	600	8300	700
MS3	5.1	1.4	146.3	1.4	3900	300	3100	100
LS1(a)	9	2	34	0.3	1270	98	1300	100
LS4	7.2	1.2	19	0.2	1300	100	1300	100
LS5	6.4	1.3	21.6	0.2	729	57	730	94
LS6	2.5	0.8	16.9	0.2	3400	300	3400	300
LS3	12	2	13.1	0.1	892	71	826	82
LS2	3.5	1.0	12.6	0.1	3500	300	3100	200
MS4	6.4	1.4	65.2	0.6	3800	300	3200	200
CLS1	6	1.3	305	5	1700	100	1600	100
CMS3	6.4	1.4	2200	38	2100	200	2000	100
CLS2	10.3	1.5	156	3	1200	91	1100	92
F-L1	5.8	1.1	16	0.3	603	48	640	52
FBMS1	7	2	2383	42	1600	100	1600	100
BBM1	6	2	149	3	590	47	820	69
BBM2	6	2	362	6	608	48	560	60
BBM3	<6,49	*	111	2	625	49	590	52
TML2	5	2	20.7	0.4	705	56	800	63

Figure G.2: Concentrations of Ca, V, Cr, Mn. "Error" represents the standard deviation at 1σ level.

APPENDIX G. SAMPLE ELEMENTAL CONCENTRATIONS (MEASURED BY INAA AND ICP-MS)

197

SAMPLE CODE	Fe				Co			
	NAA		ICP-MS		NAA		ICP-MS	
	Conc. (ppm)	Error (ppm)	Conc. (ppm)	Error (ppm)	Conc. (ppm)	Error (ppm)	Conc. (ppm)	Error (ppm)
MS2	11000	600	6195	52	1.8	0.1	7.6	0.3
MS3	3100	200	4052	34	1.1	0.1	1.9	0.1
LS1(a)	3900	200	3935	33	0.74	0.04	0.97	0.04
LS4	2700	100	2138	18	0.52	0.03	0.43	0.02
LS5	2200	100	1752	15	0.45	0.03	0.47	0.02
LS6	1500	84	1367	11	0.37	0.02	0.44	0.02
LS3	5200	300	1878	16	0.8	0.1	0.4	0
LS2	1600	90	1443	12	0.31	0.02	0.39	0.01
MS4	3400	200	2911	24	1.1	0.1	1.17	0.04
CLS1	3300	200	7200	100	0.8	0.1	3.0	0.1
CMS3	6300	300	18300	300	1.0	0.1	15.1	0.4
CLS2	5300	300	3074	50	0.8	0.1	1.3	0.04
F-L1	2900	200	2492	41	0.56	0.03	0.48	0.01
FBMS1	2600	200	17100	281	0.44	0.04	14.4	0.4
BBM1	2000	100	4113	67	0.23	0.02	1.3	0.04
BBM2	2100	100	6600	108	0.29	0.03	3.0	0.1
BBM3	1000	73	1628	27	0.16	0.02	0.86	0.02
TML2	2200	100	2848	47	0.52	0.04	0.82	0.02

SAMPLE CODE	Zn				As			
	NAA		ICP-MS		NAA		ICP-MS	
	Conc. (ppm)	Error (ppm)	Conc. (ppm)	Error (ppm)	Conc. (ppm)	Error (ppm)	Conc. (ppm)	Error (ppm)
MS2	81	2	85	7	11.5	0.3	3.69	0.01
MS3	39.2	0.9	37	2	1.8	0.1	1.35	0.01
LS1(a)	59.4	1.3	50	2	5.1	0.3	2.99	0.01
LS4	39.4	0.9	41	2	3.3	0.2	1.81	0.01
LS5	43.6	1.0	42	2	3.3	0.2	1.81	0.01
LS6	41	0.9	42	2	2.9	0.2	1.66	0.01
LS3	75	2	60	3	6.2	0.3	2.45	0.01
LS2	42.3	1.0	43	2	2.8	0.1	1.48	0.01
MS4	40.7	1.0	40	2	3.0	0.2	2.27	0.01
CLS1	66.8	1.4	66.8	0.5	3.3	0.2	3.0	0.1
CMS3	45.5	1.1	42.4	0.3	3.5	0.2	2.7	0.1
CLS2	39.3	1.0	51.9	0.4	2.8	0.2	1.4	0.1
F-L1	46.8	1.1	25.3	0.2	2.7	0.2	1.7	0.1
FBMS1	28.2	1.0	30.7	0.2	1.7	0.1	2.5	0.1
BBM1	13.7	0.7	19.3	0.1	1.4	0.04	1.5	0.1
BBM2	23.8	0.9	28.6	0.2	1.4	0.04	1.9	0.1
BBM3	10.4	0.6	10.7	0.1	0.8	0.02	0.59	0.03
TML2	40.4	1.2	42.9	0.3	2.0	0.1	1.7	0.1

Figure G.3: Concentrations of Fe, Co, Zn, As. "Error" represents the standard deviation at 1σ level.

APPENDIX G. SAMPLE ELEMENTAL CONCENTRATIONS (MEASURED BY INAA AND ICP-MS)

198

SAMPLE CODE	Se				Sr			
	NAA		ICP-MS		NAA		ICP-MS	
	Conc. (ppm)	Error (ppm)	Conc. (ppm)	Error (ppm)	Conc. (ppm)	Error (ppm)	Conc. (ppm)	Error (ppm)
MS2	0.5	0.1	1.6	0.1	45	3	33.3	0.4
MS3	0.1	0.1	1.6	0.1	40	3	28	0.4
LS1(a)	0.29	0.03	0.75	0.04	151	10	110.1	1.4
LS4	0.4	0.1	0.15	0.01	53	3	45.4	0.6
LS5	0.7	0.1	0.49	0.03	39	3	34.4	1.0
LS6	0.4	0.1	1.1	0.1	27	2	22.6	0.3
LS3	0.8	0.1	2.1	0.1	40	3	17.2	0.2
LS2	0.4	0.1	0.9	0.1	43	3	43.3	0.6
MS4	0.3	0.1	1.1	0.1	64	4	50.7	0.7
CLS1	1.7	0.1	2.5	0.1	38	3	47.2	1.3
CMS3	1.5	0.1	4.3	0.2	34	2	34.8	1.0
CLS2	1.0	0.1	1.3	0.1	29	2	43	1.2
F-L1	6.3	0.3	4.0	0.2	6.9	0.8	5.9	0.2
FBMS1	0.5	0.2	1.9	0.1	122	8	112	3
BBM1	0.8	0.2	1.5	0.1	47	3	46.7	1.3
BBM2	1.6	0.2	2.8	0.1	56	4	47.3	1.3
BBM3	1.1	0.2	0.51	0.03	33	2	23.9	0.7
TML2	1.2	0.2	1.4	0.1	32	2	25.4	0.7

SAMPLE CODE	Ba			
	NAA		ICP-MS	
	Conc. (ppm)	Error (ppm)	Conc. (ppm)	Error (ppm)
MS2	177	9	161	2
MS3	85	4	53.3	0.7
LS1(a)	72	4	49.5	0.7
LS4	60	3	34.3	1.0
LS5	51	3	50.7	0.7
LS6	34	2	25.5	0.4
LS3	58	3	22.5	0.3
LS2	44	2	69.6	1.0
MS4	73	4	51.8	0.7
CLS1	32	2	40	2
CMS3	59	3	53	2
CLS2	42	2	15.4	0.7
F-L1	19	1.4	12.4	0.5
FBMS1	33	2	30.9	1.3
BBM1	16.6	1.4	18.3	0.8
BBM2	23	2	26.6	1.1
BBM3	10.7	1.2	12.6	0.5
TML2	28	2	20.2	0.9

Figure G.4: Concentrations of Se, Sr, Ba. "Error" represents the standard deviation at 1σ level.

G.2 Active biomonitoring

SAMPLE CODE	Al				Ca			
	NAA		ICP-MS		NAA		ICP-MS	
	Conc. (ppm)	Error (ppm)	Conc. (ppm)	Error (ppm)	Conc. (ppm)	Error (ppm)	Conc. (ppm)	Error (ppm)
CMPG	2000	53	1500	200	4900	400	5800	200
CMLS	3310	87	2100	300	5100	500	6300	300
CLUS	990	27	900	100	1700	200	2000	80
CLPP	1930	51	2200	300	10300	900	7100	300
NRMP 1	1910	50	1400	200	5400	500	6100	200
NRML 1	4000	100	2100	200	6200	600	6800	300
NRLU 1	541	15	500	63	2200	200	2000	80
NRMP 2	2030	54	1400	200	5600	500	6200	200
NRML 2	3500	92	2500	300	7000	600	6800	300
NRLU 2	692	19	700	89	2400	200	2200	88
NRMP 3	2680	70	1700	200	6800	600	6500	300
NRML 3	3510	92	2600	300	7600	600	7100	300
NRLU 3	946	25	800	93	1800	200	2400	96
SVMP 1	1610	42	1400	200	4900	400	5700	200
SVML 1	1980	52	2500	300	5900	500	6400	300
SVLU 1	825	22	800	91	2600	200	2700	100
SVMP 2	1740	46	1400	200	5600	500	6000	200
SVML 2	3150	83	1900	200	6600	600	6800	300
SVLU 2	537	15	600	68	2500	200	4200	200
SVMP 3	2620	69	1300	200	5800	500	6300	300
SVML 3	2500	66	1800	200	6700	600	7000	300
SVLU 3	811	22	600	74	2200	200	2600	100
HTMP 1	1470	39	1400	200	4400	400	6100	200
HTML 1	2240	59	1500	200	5800	500	5900	200
HTLU 1	552	15	600	76	2400	200	2700	100
HTLP 1	2020	56	1800	200	3100	300	6700	300
HTMP 2	1400	37	1500	200	4600	400	5700	200
HTML 2	2010	53	1700	200	5400	500	6400	300
HTLU 2	319	9	600	70	2000	200	2700	100
HTLP 2	3790	99	2100	300	6200	500	7200	300
HTMP 3	1660	44	1400	200	6100	500	5600	200
HTML 3	2240	58	1700	200	5700	500	6200	200
HTLU 3	1410	38	800	91	1400	200	3100	100
HTLP 3	2090	55	2100	300	1100	100	6300	300

Figure G.5: Concentrations of Al and Ca. "Error" represents the standard deviation at 1 σ level.

APPENDIX G. SAMPLE ELEMENTAL CONCENTRATIONS (MEASURED BY INAA AND ICP-MS)

200

SAMPLE CODE	Fe				K			
	NAA		ICP-MS		NAA		ICP-MS	
	Conc. (ppm)	Error (ppm)	Conc. (ppm)	Error (ppm)	Conc. (ppm)	Error (ppm)	Conc. (ppm)	Error (ppm)
CMPG	407	41	840	22	8700	1700	5500	400
CMLS	1100	100	1237	33	9300	1900	6100	500
CLUS	311	31	241	6	2600	500	2100	200
CLPP	431	43	1364	36	5400	1100	3400	300
NRMP 1	845	85	877	23	2700	500	2000	200
NRML 1	1300	100	1273	34	2000	400	1500	100
NRLU 1	339	34	342	9	2000	400	2100	200
NRMP 2	1300	100	936	25	2600	500	2100	200
NRML 2	1700	200	1554	41	1700	300	1300	100
NRLU 2	407	41	424	11	2300	500	2000	200
NRMP 3	1200	100	1271	34	2200	400	1300	100
NRML 3	1600	200	1726	46	1200	200	1500	100
NRLU 3	542	54	554	15	2300	500	2100	200
SVMP 1	760	76	940	25	6000	1200	4500	400
SVML 1	982	98	1379	36	5100	1000	4000	300
SVLU 1	383	38	541	14	2700	500	2400	200
SVMP 2	1100	100	1276	34	3700	700	5700	500
SVML 2	1800	200	1522	40	3600	700	4800	400
SVLU 2	556	56	620	16	1800	400	3200	300
SVMP 3	1400	100	1531	40	3500	700	5600	500
SVML 3	2100	200	1800	48	3000	600	5000	400
SVLU 3	492	49	708	19	1800	400	2300	200
HTMP 1	852	85	989	26	4100	800	6500	500
HTML 1	1100	100	1001	26	3500	700	6400	500
HTLU 1	431	43	683	18	2800	600	3200	300
HTLP 1	1200	100	1312	35	3900	800	3900	300
HTMP 2	1100	100	1272	34	6800	1400	6300	500
HTML 2	1100	100	1381	36	6300	1300	6100	500
HTLU 2	311	31	567	15	2100	400	2500	200
HTLP 2	1300	100	1672	44	4800	1000	4000	300
HTMP 3	942	94	1140	30	6400	1300	6500	500
HTML 3	1000	100	1292	34	5700	1100	5800	500
HTLU 3	637	64	748	20	3200	600	3100	200
HTLP 3	1400	100	1583	42	4400	900	4100	300

Figure G.6: Concentrations of Fe and K. "Error" represents the standard deviation at 1σ level.

APPENDIX G. SAMPLE ELEMENTAL CONCENTRATIONS (MEASURED BY INAA AND ICP-MS)

201

SAMPLE CODE	Mg				Na			
	NAA		ICP-MS		NAA		ICP-MS	
	Conc. (ppm)	Error (ppm)	Conc. (ppm)	Error (ppm)	Conc. (ppm)	Error (ppm)	Conc. (ppm)	Error (ppm)
CMPG	1860	78	2893	43	411	21	78	6
CMLS	2040	86	3059	46	387	19	63	5
CLUS	518	25	868	13	152	8	93	7
CLPP	616	29	1060	16	340	17	2	0
NRMP 1	1790	75	3044	45	656	33	390	29
NRML 1	2160	91	3166	47	556	28	342	25
NRLU 1	603	28	974	15	416	21	206	15
NRMP 2	1790	66	3224	48	1830	92	1800	100
NRML 2	2370	87	3359	50	2100	100	1900	100
NRLU 2	551	23	989	15	864	43	860	64
NRMP 3	1870	68	3137	47	598	30	341	25
NRML 3	2120	78	3406	51	432	22	308	23
NRLU 3	520	21	1191	18	669	33	434	32
SVMP 1	1540	57	3111	47	1170	59	1151	86
SVML 1	1880	69	3286	49	1080	54	1139	85
SVLU 1	530	22	1022	15	1060	53	515	38
SVMP 2	1880	80	3673	55	3620	200	4000	300
SVML 2	2360	99	3798	57	3310	200	3000	200
SVLU 2	657	30	1804	27	888	44	1400	100
SVMP 3	2090	88	4031	60	4300	200	6300	500
SVML 3	2400	100	4006	60	5400	300	5200	400
SVLU 3	741	34	1358	20	1430	72	2100	200
HTMP 1	1520	65	3270	49	392	20	343	26
HTML 1	1820	76	3247	49	391	20	334	25
HTLU 1	855	38	1133	17	243	12	285	21
HTLP 1	744	36	1430	21	327	16	236	18
HTMP 2	1410	52	3104	46	430	22	361	27
HTML 2	1830	67	3242	48	470	24	361	27
HTLU 2	408	17	1164	17	240	12	278	21
HTLP 2	899	36	1382	21	338	17	223	17
HTMP 3	1570	58	3103	46	421	21	356	26
HTML 3	1710	63	3349	50	423	21	341	25
HTLU 3	430	19	1324	20	328	16	298	22
HTLP 3	559	23	1203	18	441	22	214	16

Figure G.7: Concentrations of Mg and Na. "Error" represents the standard deviation at 1σ level.

APPENDIX G. SAMPLE ELEMENTAL CONCENTRATIONS (MEASURED BY INAA AND ICP-MS)

202

SAMPLE CODE	Ti				V			
	NAA		ICP-MS		NAA		ICP-MS	
	Conc. (ppm)	Error (ppm)	Conc. (ppm)	Error (ppm)	Conc. (ppm)	Error (ppm)	Conc. (ppm)	Error (ppm)
CMPG	117	18	25	13	3	0.2	2	0.1
CMLS	294	33	33	17	4.2	0.3	2.7	0.1
CLUS	75	12	18	9	1.3	0.1	1.29	0.03
CLPP	173	27	37	19	2.6	0.2	2.9	0.1
NRMP 1	163	22	23	12	3.1	0.2	2.1	0.1
NRML 1	281	33	35	18	5.4	0.3	2.9	0.1
NRLU 1	43	11	9	5	1	0.1	0.8	0.02
NRMP 2	150	24	26	13	3.4	0.3	2.4	0.1
NRML 2	213	31	48	24	4.9	0.4	3.6	0.1
NRLU 2	52	10	14	7	1	0.1	1.01	0.03
NRMP 3	236	27	37	19	4.3	0.3	3.1	0.1
NRML 3	280	33	49	25	5.2	0.3	4	0.1
NRLU 3	75	12	18	9	1.4	0.1	1.22	0.03
SVMP 1	160	23	29	15	2.4	0.2	2	0.1
SVML 1	157	25	38	19	2.9	0.2	3.1	0.1
SVLU 1	62	19	14	7	1.2	0.1	0.98	0.03
SVMP 2	148	24	38	19	3.1	0.3	2.4	0.1
SVML 2	229	28	45	23	4.4	0.3	3	0.1
SVLU 2	48	9	16	8	1	0.1	0.97	0.03
SVMP 3	154	22	33	17	3.7	0.3	2.3	0.1
SVML 3	197	29	39	20	3.8	0.3	2.9	0.1
SVLU 3	62	12	17	9	1.4	0.1	1.02	0.03
HTMP 1	105	17	28	14	2.3	0.2	2.3	0.1
HTML 1	141	19	29	15	3.3	0.2	2.3	0.1
HTLU 1	49	14	12	6	0.7	0.1	0.95	0.02
HTLP 1	97	17	38	19	2.6	0.2	2.9	0.1
HTMP 2	73	14	34	17	2.3	0.2	2.6	0.1
HTML 2	146	22	39	20	2.6	0.2	2.8	0.1
HTLU 2	30	7	15	8	0.5	0.1	0.87	0.02
HTLP 2	333	34	42	21	4.9	0.3	3.2	0.1
HTMP 3	122	18	31	16	2.3	0.2	2.3	0.1
HTML 3	142	20	34	17	3.2	0.2	2.6	0.1
HTLU 3	116	15	24	12	2	0.2	1.22	0.03
HTLP 3	171	20	45	23	3	0.2	3.2	0.1

Figure G.8: Concentrations of Ti and V. "Error" represents the standard deviation at 1σ level.

APPENDIX G. SAMPLE ELEMENTAL CONCENTRATIONS (MEASURED BY INAA AND ICP-MS)

203

SAMPLE CODE	Cr				Mn			
	NAA		ICP-MS		NAA		ICP-MS	
	Conc. (ppm)	Error (ppm)	Conc. (ppm)	Error (ppm)	Conc. (ppm)	Error (ppm)	Conc. (ppm)	Error (ppm)
CMPG	2	0.6	17.8	0.6	186	13	162	6
CMLS	2.1	0.6	19.3	0.6	282	19	227	8
CLUS	1.9	0.6	5.5	0.2	41	3	30.4	1.1
CLPP	2.4	0.7	6	0.2	53	4	60	2
NRMP 1	2	0.6	16.1	0.5	187	13	174	6
NRML 1	4.1	1.2	20.4	0.7	361	24	277	10
NRLU 1	3.7	1.1	5	0.2	35	2	45	2
NRMP 2	5	2	19	0.6	192	13	194	7
NRML 2	6	2	14.7	0.5	330	22	245	9
NRLU 2	3.5	1.1	3.4	0.1	41	3	34.8	1.3
NRMP 3	5	2	19.5	0.6	247	16	165	6
NRML 3	7	2	22.8	0.7	328	22	271	10
NRLU 3	4	1.2	7.7	0.2	65	4	62	2
SVMP 1	4.3	1.3	15.4	0.5	175	12	170	6
SVML 1	4.5	1.3	20.6	0.7	259	17	235	9
SVLU 1	2	0.6	4.2	0.1	48	3	44	2
SVMP 2	3	0.9	14	0.4	192	13	194	7
SVML 2	3.8	1.1	10.4	0.3	268	18	245	9
SVLU 2	1.9	0.6	5.1	0.2	41	3	75	3
SVMP 3	3	0.9	15	0.5	249	17	186	7
SVML 3	5	1.5	29.9	1.0	277	19	318	12
SVLU 3	1.9	0.6	9.6	0.3	55	4	49	2
HTMP 1	2.4	0.7	20.4	0.7	151	10	211	8
HTML 1	2.8	0.8	19.6	0.6	235	16	207	8
HTLU 1	1.4	0.4	11.5	0.4	145	10	53	2
HTLP 1	2.2	0.7	12.9	0.4	91	6	80	3
HTMP 2	2.5	0.7	29.2	0.9	147	10	173	6
HTML 2	2.9	0.9	15	0.5	348	23	222	8
HTLU 2	1.8	0.5	7.2	0.2	32	2	86	3
HTLP 2	4.1	1.2	14.4	0.5	68	5	87	3
HTMP 3	3.3	1.0	21.1	0.7	183	12	165	6
HTML 3	2.7	0.8	23.1	0.7	216	14	217	8
HTLU 3	4.1	1.2	9.1	0.3	26	2	64	2
HTLP 3	4.1	1.2	8.6	0.3	36	2	69	3

Figure G.9: Concentrations Cr and Mn. "Error" represents the standard deviation at 1σ level.

APPENDIX G. SAMPLE ELEMENTAL CONCENTRATIONS (MEASURED BY INAA AND ICP-MS)

204

SAMPLE CODE	Co				Zn			
	NAA		ICP-MS		NAA		ICP-MS	
	Conc. (ppm)	Error (ppm)	Conc. (ppm)	Error (ppm)	Conc. (ppm)	Error (ppm)	Conc. (ppm)	Error (ppm)
CMPG	0.12	0.02	0.85	0.03	12.9	0.6	28	0.9
CMLS	0.54	0.01	1.03	0.03	36	2	34.4	1.1
CLUS	0.2	0.03	1.34	0.04	13.3	0.7	13.1	0.4
CLPP	0.319	0.005	0.61	0.02	12.9	0.6	25.7	0.8
NRMP 1	0.46	0.01	0.73	0.02	36	2	37.6	1.2
NRML 1	0.61	0.01	1.08	0.03	36	2	45.8	1.5
NRLU 1	0.16	0.02	0.43	0.01	15	0.8	15.5	0.5
NRMP 2	0.6	0.01	0.79	0.02	39	2	41.8	1.4
NRML 2	0.71	0.01	0.96	0.03	50	2	48	2
NRLU 2	0.22	0.03	0.31	0.01	14.2	0.7	19.6	0.6
NRMP 3	0.46	0.01	1.16	0.04	52	3	60	2
NRML 3	0.7	0.01	1.71	0.05	63	3	54	2
NRLU 3	0.2	0.03	0.55	0.02	12.9	0.6	22.1	0.7
SVMP 1	0.32	0.01	0.58	0.02	25.9	1.3	29.1	1.0
SVML 1	0.47	0.01	0.92	0.03	33	2	36.2	1.2
SVLU 1	0.2	0.03	0.31	0.01	14.1	0.7	15.2	0.5
SVMP 2	0.48	0.01	0.94	0.03	37	2	39.5	1.3
SVML 2	0.65	0.1	1.68	0.05	45	2	42.1	1.4
SVLU 2	0.2	0.03	0.6	0.02	12.9	0.6	16	0.5
SVMP 3	0.46	0.07	1.3	0.04	52	3	45.7	1.5
SVML 3	0.73	0.01	2.14	0.06	57	3	45.5	1.5
SVLU 3	0.21	0.03	0.75	0.02	11.6	0.6	19	0.6
HTMP 1	0.39	0.01	1.12	0.03	28.1	1.4	37.9	1.2
HTML 1	0.58	0.01	1.24	0.04	32	2	38.4	1.3
HTLU 1	0.22	0.03	0.59	0.02	13.3	0.7	14.4	0.5
HTLP 1	0.52	0.01	0.83	0.03	19.8	1.0	42.3	1.4
HTMP 2	0.42	0.01	1.37	0.04	37	2	49	2
HTML 2	0.54	0.01	1.34	0.04	38	2	49	2
HTLU 2	0.16	0.02	0.7	0.02	12.9	0.6	22.7	0.7
HTLP 2	0.61	0.01	0.89	0.03	45	2	54	2
HTMP 3	0.41	0.01	1.59	0.05	33	2	53	2
HTML 3	0.53	0.01	1.39	0.04	39	2	65	2
HTLU 3	0.31	0.01	1.34	0.04	19.6	1.0	34.7	1.1
HTLP 3	0.61	0.01	1.15	0.04	42	2	63	2

Figure G.10: Concentrations of Co and Zn "Error" represents the standard deviation at 1 σ level.

APPENDIX G. SAMPLE ELEMENTAL CONCENTRATIONS (MEASURED BY INAA AND ICP-MS)

205

SAMPLE CODE	As				Se			
	NAA		ICP-MS		NAA		ICP-MS	
	Conc. (ppm)	Error (ppm)	Conc. (ppm)	Error (ppm)	Conc. (ppm)	Error (ppm)	Conc. (ppm)	Error (ppm)
CMPG	0.302	0.003	1.08	0.04	0.12	0.04	2.27	0.06
CMLS	0.48	0.01	1.22	0.04	0.3	0.01	1.5	0.04
CLUS	0.35	0.03	1.09	0.04	0.09	0.03	1.21	0.03
CLPP	0.35	0.04	1.4	0.05	0.14	0.04	1.34	0.03
NRMP 1	0.41	0.04	1.12	0.04	0.24	0.01	0.91	0.02
NRML 1	0.9	0.1	1.49	0.05	0.38	0.01	0.25	0.01
NRLU 1	0.39	0.04	1.23	0.04	0.14	0.04	0.44	0.01
NRMP 2	0.7	0.1	1.11	0.04	0.34	0.01	1.5	0.04
NRML 2	0.8	0.1	1.47	0.05	0.42	0.01	2.39	0.06
NRLU 2	0.5	0.1	0.86	0.03	0.25	0.01	1.31	0.03
NRMP 3	0.8	0.1	0.8	0.03	0.33	0.01	1.31	0.03
NRML 3	1.4	0.1	2.02	0.07	0.44	0.01	2.91	0.07
NRLU 3	0.5	0.1	0.64	0.02	0.13	0.04	1.33	0.03
SVMP 1	0.9	0.1	1.54	0.05	0.31	0.01	2.44	0.06
SVML 1	0.6	0.1	1.29	0.04	0.27	0.01	2.21	0.06
SVLU 1	0.5	0.1	1	0.03	0.19	0.01	1.02	0.03
SVMP 2	1	0.1	1.08	0.04	0.34	0.01	1.72	0.04
SVML 2	1.1	0.1	1.03	0.04	0.32	0.01	1.63	0.04
SVLU 2	0.6	0.1	0.6	0.02	0.19	0.01	1.42	0.04
SVMP 3	1.5	0.1	1.46	0.05	0.4	0.01	1.35	0.03
SVML 3	1.5	0.2	7.14	0.25	0.45	0.01	1.39	0.04
SVLU 3	0.5	0.1	0.77	0.03	0.22	0.01	1.3	0.03
HTMP 1	0.35	0.03	0.4	0.01	0.35	0.01	2.01	0.05
HTML 1	0.44	0.04	0.45	0.02	0.26	0.01	1.8	0.05
HTLU 1	0.35	0.04	0.38	0.01	0.2	0.01	0.99	0.03
HTLP 1	0.6	0.1	0.79	0.03	0.43	0.01	2.54	0.06
HTMP 2	0.38	0.04	0.56	0.02	0.24	0.01	1.22	0.03
HTML 2	0.5	0.01	0.67	0.02	0.21	0.01	1.62	0.04
HTLU 2	0.3	0.03	0.37	0.01	0.14	0.04	1.81	0.05
HTLP 2	0.63	0.01	0.95	0.03	0.29	0.01	1.38	0.04
HTMP 3	0.46	0.01	0.61	0.02	0.28	0.01	1.45	0.04
HTML 3	0.49	0.01	0.57	0.02	0.28	0.01	1.59	0.04
HTLU 3	0.39	0.04	0.53	0.02	0.121	0.004	1.42	0.04
HTLP 3	0.64	0.01	0.9	0.03	0.089	0.003	2.01	0.05

Figure G.11: Concentrations of As and Se. "Error" represents the standard deviation at 1σ level.

APPENDIX G. SAMPLE ELEMENTAL CONCENTRATIONS (MEASURED BY INAA AND ICP-MS)

206

SAMPLE CODE	Sr				Mo			
	NAA		ICP-MS		NAA		ICP-MS	
	Conc. (ppm)	Error (ppm)	Conc. (ppm)	Error (ppm)	Conc. (ppm)	Error (ppm)	Conc. (ppm)	Error (ppm)
CMPG	12	2	47	5	0.04	0.01	0.38	0.01
CMLS	46	7	51	5	0.09	0.03	0.41	0.01
CLUS	10.7	1.1	17	2	0.03	0.01	0.122	0.004
CLPP	15	2	43	4	0.05	0.01	0.124	0.004
NRMP 1	47	5	52	5	0.1	0.03	0.31	0.01
NRML 1	51	8	55	6	0.13	0.04	0.47	0.02
NRLU 1	12	2	19	2	0.09	0.03	0.126	0.005
NRMP 2	38	6	53	5	0.176	0.001	0.38	0.01
NRML 2	59	9	57	6	0.3	0.1	0.4	0.01
NRLU 2	16	2	18	2	0.07	0.02	0.088	0.003
NRMP 3	53	8	52	5	0.175	0.001	0.4	0.01
NRML 3	54	8	58	6	0.225	0.001	0.46	0.02
NRLU 3	15	2	18	2	0.12	0.03	0.121	0.004
SVMP 1	44	7	49	5	0.11	0.03	0.31	0.01
SVML 1	46	7	53	5	0.207	0.001	0.45	0.02
SVLU 1	18	3	21	2	0.03	0.01	0.103	0.004
SVMP 2	52	8	51	5	0.07	0.02	0.26	0.01
SVML 2	54	8	58	6	0.24	0.01	0.27	0.01
SVLU 2	22	3	23	2	0.09	0.03	0.082	0.003
SVMP 3	56	8	53	5	0.12	0.04	0.29	0.01
SVML 3	63	9	59	6	0.05	0.02	0.46	0.02
SVLU 3	18	3	28	3	0.05	0.01	0.18	0.01
HTMP 1	45	7	47	5	0.1	0.03	0.59	0.02
HTML 1	53	8	47	5	0.219	0.001	0.41	0.01
HTLU 1	19	3	22	2	0.056	0.002	0.19	0.01
HTLP 1	28	4	47	5	0.081	0.002	0.32	0.01
HTMP 2	45	7	45	5	0.125	0.004	0.7	0.03
HTML 2	55	8	50	5	0.152	0.001	0.54	0.02
HTLU 2	24	4	16	2	0.092	0.003	0.3	0.01
HTLP 2	38	6	48	5	0.18	0.001	0.38	0.01
HTMP 3	45	7	45	5	0.187	0.001	0.78	0.03
HTML 3	45	7	49	5	0.224	0.001	0.66	0.02
HTLU 3	23	3	22	2	0.24	0.001	0.39	0.01
HTLP 3	35	5	45	5	0.325	0.0003	0.51	0.02

Figure G.12: Concentrations of Sr and Mo. "Error" represents the standard deviation at 1σ level.

APPENDIX G. SAMPLE ELEMENTAL CONCENTRATIONS (MEASURED BY INAA AND ICP-MS)

207

SAMPLE CODE	Sb				Ba			
	NAA		ICP-MS		NAA		ICP-MS	
	Conc. (ppm)	Error (ppm)	Conc. (ppm)	Error (ppm)	Conc. (ppm)	Error (ppm)	Conc. (ppm)	Error (ppm)
CMPG	0.08	0.01	0.01	0.0001	7.7	0.1	30.8	1.5
CMLS	0.06	0.01	0.0641	0.0004	31.3	0.03	32.9	1.6
CLUS	0.04	0.01	0.0553	0.0004	7.1	0.1	7.8	0.4
CLPP	0.08	0.01	0.199	0.001	9	0.1	22.8	1.1
NRMP 1	0.27	0.04	0.369	0.002	30.2	0.3	31.5	1.5
NRML 1	0.17	0.02	0.502	0.003	39.1	0.4	35.2	1.7
NRLU 1	0.11	0.02	0.384	0.003	8.7	0.1	8.6	0.4
NRMP 2	0.28	0.04	0.571	0.004	35	0.4	33.4	1.6
NRML 2	0.39	0.06	0.612	0.004	41	0.4	37.5	1.8
NRLU 2	0.14	0.02	0.301	0.002	7.7	0.1	9.5	0.5
NRMP 3	0.33	0.05	0.439	0.003	35.1	0.4	35.4	1.7
NRML 3	0.46	0.01	0.327	0.002	41.1	0.4	42	2
NRLU 3	0.26	0.04	0.181	0.001	11	0.1	10.3	0.5
SVMP 1	0.13	0.02	0.075	0.001	24.2	0.2	27.3	1.3
SVML 1	0.08	0.01	0.006	0.00004	31.4	3.1	35	1.7
SVLU 1	0.08	0.01	0.502	0.003	7.1	0.1	9.5	0.5
SVMP 2	0.4	0.01	0.424	0.003	32.4	0.3	29.5	1.4
SVML 2	0.27	0.04	0.236	0.002	37.5	0.4	34.7	1.7
SVLU 2	0.11	0.01	0.103	0.001	8.8	0.1	11.1	0.5
SVMP 3	0.37	0.01	0.247	0.002	32.5	0.3	28.3	1.4
SVML 3	0.25	0.04	0.352	0.002	42.8	0.4	33.7	1.6
SVLU 3	0.41	0.01	0.112	0.001	9	0.1	9.8	0.5
HTMP 1	0.13	0.02	0.194	0.001	30.4	0.3	31.7	1.5
HTML 1	0.13	0.02	0.176	0.001	35.8	0.4	32.9	1.6
HTLU 1	0.13	0.02	0.152	0.001	9.8	0.1	11.1	0.5
HTLP 1	0.18	0.03	0.301	0.002	22.7	0.2	31.1	1.5
HTMP 2	0.28	0.04	0.574	0.004	32	0.3	36.6	1.8
HTML 2	0.26	0.04	0.502	0.003	40.6	0.4	37	1.8
HTLU 2	0.25	0.04	0.448	0.003	10.5	0.1	13.3	0.6
HTLP 2	0.46	0.01	0.507	0.003	35	0.4	33.5	1.6
HTMP 3	0.38	0.01	0.645	0.004	31.9	0.3	38.4	1.8
HTML 3	0.39	0.01	0.627	0.004	37	0.4	38.1	1.8
HTLU 3	0.42	0.01	0.784	0.005	15.1	0.2	19.4	0.9
HTLP 3	0.5	0.01	0.707	0.005	30.4	0.3	35.6	1.7

Figure G.13: Concentrations of Sb and Ba. "Error" represents the standard deviation at 1σ level.

List of References

- [1] Frontasyeva M.V. Neutron Activation Analysis in the Life Sciences. *Physics of Particles and Nuclei*, 42(2):332–378, 2011.
- [2] World Health Organisation Working Group. Health Aspects of Air Pollution with Particulate Matter, Ozone and Nitrogen Dioxide. Technical report, World Health Organisation (WHO) Regional Office for Europe, 2003.
- [3] Lilley J.S. Nuclear Physics: principles and applications. John Wiley & Sons, Ltd, England, 2001.
- [4] Bode P. Instrumental and Organizational Aspects of a Neutron Activation Analysis Laboratory. PhD thesis, Delft University of Technology, The Netherlands, December 1996.
- [5] Bode P., Greenberg R.R., and De Nadai Fernandes E.A. Neutron Activation Analysis: a primary (ratio) method to determine SI-traceable values of element content in complex samples. *Metrology in Chemistry*, 63(10):1–3, 2009.
- [6] Berlizov A. Presentation on Neutron Activation Analysis., September 2006.
- [7] Pavlov S.S. Radioanalytical Complex REGATA At IBR-2 Reactor In Dubna: project REGATA. Technical report, Joint Institute of Nuclear Research, April 2008.
- [8] Baechler S. Two Non-Destruction Neutron Inspection Techniques: prompt gamma-ray activation analysis and cold neutron tomography. PhD thesis, University of Fribourg, Switzerland, July 2002.
- [9] Daud M. Use of Various Plants as Biomonitors to Estimate Atmospheric Pollution. PhD thesis, University of the Punjab, Pakistan, January 2009.
- [10] Modern Trends in Neutron Activation Analysis. Application to some African environmental samples., Egypt, February 2008. Proceedings of the 3rd Environmental Physics Conference.
- [11] Peetermans S. Neutron Activation Analysis. Trainingship notes, Nuclear Physics Institute, Czech Republic, Summer 2009.
- [12] Glascock M.D. An Overview of Neutron Activation Analysis. Technical report, University of Missouri Research Reactor, Columbia, 2006.

- [13] Frontasyeva M.V. Neutron Activation Analysis for the Life Sciences and Material Sciences., July 2011.
- [14] Agilent Technologies. ICP-MS: Inductively Coupled Plasma Mass Spectrometry : a primer. Technical report, 2005.
- [15] Rosen A.L. and Hieftje G.M. Inductively Coupled Plasma Mass Spectrometry and Electrospray Mass Spectrometry for Speciation Analysis: applications and instrumentation. *Spectrochimica Acta Part B: Atomic Spectroscopy*, 59(2):135–146, 2004.
- [16] Revel G. and Ayrault S. Comparative Use of INAA and ICP-MS Methods for Environmental Studies. *Journal of Radioanalytical and Nuclear Chemistry*, 244(1):73–80, 2000.
- [17] Ammann A.A. Inductively Coupled Plasma Mass Spectrometry (ICP MS): a versatile tool. *Journal of Mass Spectrometry*, 42(4):419–427, 2007.
- [18] Sutton K.L. and Caruso J.A. Liquid Chromatography–Inductively Coupled Plasma Mass Spectrometry. *Journal of Chromatography A*, 856(1–2):243–258, 1999.
- [19] Smodiš B., editor. Biomonitoring of Atmospheric Pollution (WITH EMPHASIS ON TRACE ELEMENTS)–BioMAP II., Austria, January 2003. International Atomic Energy Agency, IAEA.
- [20] Ganbold G., Gerbish S., Gundorina S.F., Frontasyeva M.V., Ostrovnaya T.M., Pavlov S.S., and Tsendeekhuu T. Atmospheric Deposition of Trace Elements Around Ulan-Bator City studied by Moss and Lichen Biomonitoring Technique and INAA. Technical report, Joint Inst. Nucl. Res., Dubna, July 2005.
- [21] Department of Environmental Affairs and Tourism. National Environmental Management: Air Quality Act (39/2004), 2005.
- [22] Department of Environmental Affairs and Tourism. Integrated Pollution and Waste Management for South Africa: a policy on pollution prevention, waste minimisation, impact management and remediation., 2000.
- [23] De Bruin D. Applying Biological Monitors and Neutron Activation Analysis in Studies of Heavy-Metal Air Pollution. In *IAEA Bulletin*, pages 22–27. IAEA, Austria, April 1990.
- [24] Rühling Å. and Tyler G. An Ecological Approach to the Lead Problem. *Botaniska Notiser*, 121:321–342, 1968.
- [25] Rühling Å and Tyler A. Regional Differences in the Deposition of Heavy Metals over Scandinavia. *Journal of Applied Ecology*, 8(2):497–507, Aug. 1971.
- [26] Aničić M., Tasić M., Frontasyeva M.V., Tomašević M., Rajšić S., Strelkova L.P., Popović A., and Steinnes E. Active Biomonitoring with Wet and Dry Moss: a case study in an urban area. *Environmental Chemistry Letters*, 7(1):55–60, 2009.

- [27] Markert B., Wuenschmann S., Fraenzle S., Wappelhorst O., and Weckert V. On the Road from Environmental Biomonitoring to Human Health Aspects: Monitoring Atmospheric Heavy Metal Deposition by Epiphytic/Epigeic Plants: present status and future needs. *International Journal of Environment and Pollution*, 32:486–498, 2008.
- [28] Martin M.H. and Coughtrey P.J. Biological Monitoring of Heavy Metal Pollution: land and air. Applied Science Publisher, London and New York, 1982.
- [29] Steinnes E. Biomonitoring of Air Pollution by Heavy Metals, pages 321–338. Kluwer Academic Publishers, 1989.
- [30] G. T. Goodman and T. M. Roberts. Plants and Soil as Indicators of Metals in the Air. *Nature*, 231:287–292, 1971.
- [31] Little P. and Martin M.H. Biological Monitoring of Heavy Metal Pollution. *Environmental Pollution*, 6(1):1–19, 1974.
- [32] Cao T., Wang M., An L., Yu Y., Lou Y., Guo S., Zuo B., Liu Y., Wu J., Cao Y., and Zhu Z. Air Quality for Metals and Sulfur in Shanghai, China, Determined with Moss Bags. *Environmental Pollution*, 157(4):1270–1278, 2009.
- [33] Steinnes E. Monitoring of Trace Element Deposition by Means of Mosses. *Fresenius Zeitschrift für analytische Chemie*, 317(3–4):350–350, 1984.
- [34] Steinnes E., Johansen O., Røyset O., and Ødegård M. Comparison of different multielement techniques for analysis of mosses used as biomonitors. *Environmental Monitoring and Assessment*, 25(2):87–97, 1993.
- [35] Namieśnik J. Trace Analysis - challenges and problems. *Critical Reviews in Analytical Chemistry*, 32(4):271–300, 2002.
- [36] Nielsen F.H. Essential and Toxic Trace Elements in Human Health and Disease: an update. *Hyper-trace elements and disease*, 101:1–7, 2008.
- [37] Iyengar G.V. Human Health and Trace Element Research: problems and prospects. *Science of the Total Environment*, 19(2):105–109, June 1981.
- [38] Kabata-Pendias A. and Mukherjee A.B. Trace Elements from Soil to Human. Springer-Verlag Berlin Heidelberg, New York, 2007.
- [39] Kalra Y.P. Handbook of Reference Methods for Plant Analysis. Taylor and Francis Group, LLC, USA, 1998.
- [40] Mertz W. The Essential Trace Elements. *American Association for the Advancement of Science*, 213(4514):1332–1338, September 1981.
- [41] Tangahu B.V., Rozaimah S., Abdullah S., Basri H., Idris M., Anuar N., and Mukhlisin M. A Review on Heavy Metals (As, Pb, and Hg) Uptake by Plants through Phytoremediation. *International Journal of Chemical Engineering*, 2011:1–31, June 2011.

- [42] Appenroth K.J. Definition of "Heavy Metals" and their Roles in Biological Systems., volume 19 of *Soil Biology*, chapter 2, pages 19–29. Springer Berlin Heidelberg, 2010.
- [43] Steinnes E., Berg T., and Uggerud H.T. Three Decades of Atmospheric Metal Deposition in Norway as Evident from Analysis of Moss Samples. *Science of The Total Environment*, 412–413(0):351–358, 2011.
- [44] Greenberg R.R. Pushing The Limits Of NAA: accuracy, uncertainty and detection limits. *Journal of Radioanalytical and Nuclear Chemistry*, 278(2):231–240, 2008.
- [45] Frontasyeva M.V., Pavlov S.S., and Shvetsov V.N. NAA for Applied Investigations at FLNP JINR: present and future. *Journal of Radioanalytical and Nuclear Chemistry*, 286(2):519–524, 2010.
- [46] Frontasyeva M.V. NAA For Life Sciences at Frank Laboratory of Neutron Physics, Joint Institute for Nuclear Research in Dubna. *Ecological Chemistry and Engineers*, 18(3):281–304, 2011.
- [47] Cenci R.M. Guidelines for the Use of Native Mosses, Transplanted Mosses and Soils in Assessing Organic and Inorganic Contaminant Fallout. Guidelines, European Commission's Joint Research Centre, Italy, 2008.
- [48] Marinova S., Yurukova L., Frontasyeva M.V., Steinnes E., Strelkova L.P., Marinov A., and Karadzhinova A.G. Air Pollution Studies in Bulgaria using the Moss Biomonitoring Technique. *Ecological Chemistry and Engineers*, 17(1):37–52, 2010.
- [49] Harmens H., Norris D., and the Participants of the Moss Survey. Spatial and Temporal Trends in Heavy Metal Accumulation in Mosses in Europe (1990–2005). Technical report, Centre for Ecology and Hydrology, United Kingdom, July 2008.
- [50] Ares A., Aboal J.R., Carballeira A., Giordano S., Adamo P., and Fernández J.A. Moss Bag Biomonitoring: a methodological review. *Science of The Total Environment*, 432(0):143–158, 2012.
- [51] Department of Environmental Affairs and Tourism. National Environmental Management Act (107/1998), 1998.
- [52] Department of Environmental Affairs. National Ambient Air Quality Standards, 2009.
- [53] Cairncross E.K., John J., and Zunckel M. A Novel Air Pollution Index based on the Relative Risk of Daily Mortality Associated with Short-term Exposure to Common Air Pollutants. *Atmospheric Environment*, 41(38):8442–8454, 2007.
- [54] Department of Environmental Affairs and Development Planning. Air Quality Management Plan for the Western Cape Province: final draft. Technical report, Western Cape Province, 2010.

- [55] Department of Environmental Affairs and Development Planning. Air Quality Management Plan Clears the Air. Technical report, Western Cape Province, 2011.
- [56] Department of Environmental Affairs and Development Planning. State of Environment Outlook Report for the Western Cape Province: air quality chapter - for public comment. Technical report, Western Cape Government, 2013.
- [57] Department of Environmental Affairs and Development Planning. Air Quality Management Plan for the Western Cape Province. Technical report, Provincial Government of the Western Cape, 2010.
- [58] Linde H. Monitoring Campaigns and Emission Inventories - The Western Cape Cooperative Governance Experience, 2007.
- [59] Linde H. Progress Report on Air Quality Management in the Western Cape., 2008.
- [60] Sowden M., Cairncross E., Wilson G., Zunckel M., Kirillova E., Reddy V., and Hietkamp S. Developing a Spatially and Temporally Resolved Emission Inventory for Photochemical Modeling in the City of Cape Town and Assessing its Uncertainty. *Atmospheric Environment*, 42(30):7155–7164, 2008.
- [61] Van Rensburg C. and Snow N. Ambient Air Quality Monitoring Report for the Provincial Government of the Western Cape Department of Environmental Affairs and Development Planning. Technical report, Western Cape Province, 2012.
- [62] Harmens H. and Norris D., Mills G., and the participants of the moss survey. Heavy Metals and Nitrogen in Mosses: spatial patterns in 2010/2011 and long-term temporal trends in Europe. Technical report, ICP Vegetation Programme Coordination Centre, Centre for Ecology and Hydrology, Bangor, United Kingdom, 2013.
- [63] Olowoyo J.O., van Heerden E., Fischer J.L., and Baker C. Trace metals in soil and leaves of *Jacaranda mimosifolia* in Tshwane area, South Africa. *Atmospheric Environment*, 44(14):1826 – 1830, 2010.
- [64] Olowoyo J.O., Van Heerden E., and Fischer J.L. Trace element concentrations from lichen transplants in Pretoria, South Africa. *Environmental Science and Pollution Research*, 18(4):663–668, 2011.
- [65] Olowoyo J.O., Odiwe A.I., Mkolo N.M., and Macheke L. Investigating the Concentrations of Different Elements in Soil and Plant Composition from a Mining Area. *Polish Journal of Environmental Studies*, 22(4):1135 – 1141, 2013.
- [66] City of Cape Town. Monitoring Sites, 2012.
- [67] Bertulani C.A. Nuclear Physics in a Nutshell. Princeton University Press, New Jersey, 2007.

- [68] Krane K.S. *Introductory Nuclear Physics*. John Wiley & Sons, Inc., USA, 1988.
- [69] Mokaleng R. *A Database Development For Multi-Element Concentrations Of Medicinal Plants Using Instrumental Neutron Activation Analysis (INAA) And Inductively Coupled Plasma Mass Spectrometry (ICP-MS)*. Masters thesis, North West University, South Africa, November 2008.
- [70] Hassan M.M.Z. *Identification Of Platinum Ores via Trace Element Signatures*. PhD thesis, University of Cape Town, South Africa, May 2011.
- [71] Singo T.D. *Development of a High Flux Neutron Radiation Detection System for In-Core Temperature Monitoring*. PhD thesis, Stellenbosch University, South Africa, March 2012.
- [72] Severo M.I.G., Barbier F., De Oliveira A.H., Loustalot M.F.G., Carneiro C.G., and Silva M.R.S. INAA and ICP-MS Methods for Biological Tissues Studies. *Revista de Física Aplicada e Instrumentação*, 17(3):110–115, Setembro 2004.
- [73] Maleka P.P. *In-situ Element Analysis from Gamma-Ray And Neutron Spectra Using a Pulsed-Neutron Source*. PhD thesis, University of Groningen, The Netherlands, 2010.
- [74] Chaplin R.A. Nuclear Interactions, in *Nuclear Energy Materials and Reactors.*, chapter Sample Chapter. *Encyclopedia of Life Support Systems*, Oxford, UK., 2007.
- [75] United States Nuclear Regulatory Commission. Neutron Flux. Online [Downloaded - 24/04/2015], April 2014.
- [76] Filby R.H. *Isotopic and Nuclear Analytical Techniques in Biological Systems: a critical study - PART IX. NEUTRON ACTIVATION ANALYSIS*. Technical report, IUPAC, Great Britain, 1995.
- [77] OECD-NEA. *JANIS 4.0 USER'S GUIDE*. Nuclear Energy Agency, France, revision 1 edition, October 2013.
- [78] Knoll G.F. *Radiation Detection and Measurement*. John Wiley & Sons, Inc., USA, 3rd edition (ebook) edition, 1999.
- [79] L'Annunziata M.F. *Handbook of Radioactivity Analysis*. Elsevier, USA, 2nd edition edition, 2003.
- [80] Murray R.L. and Holbert K.E. *Nuclear Energy: an introduction to the concepts, systems, and applications of nuclear processes*. Elsevier, USA, 7th edition edition, 2015.
- [81] *Electropaedia*. Nuclear Energy - the theory. Online, 2005.
- [82] Hammouda B. Chapter 3 - Neutron Sources. *Distance Learning - Electronic Course Content*, 2013.

- [83] Koelzer W. Glossary of Nuclear Terms., 2008.
- [84] U.S. Department of Energy. Nuclear Physics and Reactor Theory., 1993.
- [85] Stratton G. Comparison of a High Purity Germanium Gamma Ray Spectrometer and a Multidimensional NaI(Tl) Scintillation Gamma Ray Spectrometer., July 2009.
- [86] Pillalamarri I. Trace Element Analysis of Geological, Biological and Environmental Materials By Neutron Activation Analysis: an exposure. Electronic, 2005.
- [87] Weisshaar D. Gamma-ray Spectroscopy. Online [Downloaded - 29/12/2013], 2011.
- [88] Knoll G.F. Radiation Detection And Measurement. Wiley & Sons, Incorporated, John, USA, 2nd edition edition, 1989.
- [89] Park C.S., Sun G.M., and Choi H.D. Determination of Single Escape and Double Escape Peak Efficiency for a HPGe Detector. *Journal of the Korean Nuclear Society*, 35(6):532–528, December 2003.
- [90] Rittersdorf I. Gamma Ray Spectroscopy. Technical report, University of Michigan, USA, 2007.
- [91] Potts P.J. A Handbook Of Silicate Rock Analysis. Chapman and Hall, New York, 1987.
- [92] De Villiers D. Characterisation of Heavy Mineral Sands and Soils by Radiometry and its Use in Mineral Beneficiation and Agriculture. PhD thesis, Stellenbosch University, South Africa, March 2011.
- [93] ORTEC. Experiment 7: High-Resolution Gamma-Ray Spectroscopy. Online [Downloaded - 02/01/2014], May 2012.
- [94] Chakraborty S. and Paratkar G.T. Biomonitoring of Trace Element Air Pollution Using Mosses. *Aerosol and Air Quality Research*, 6(3):247–258, 2006.
- [95] Nali C. and Lorenzini G. Air Quality Survey Carried Out by School Children: an innovative tool for urban planning. *Environmental Monitoring and Assessment*, 131(1–3):201–210, 2007.
- [96] Wolterbeek H.T. and Bode P. Strategies in Sampling and Sample Handling in the Context of Large-scale Plant Biomonitoring Surveys of Trace Element Air Pollution. *Science of The Total Environment*, 176(1–3):33–43, 1995.
- [97] Wolterbeek B. Biomonitoring Of Trace Element Air Pollution: principles , possibilities and perspectives. *Environmental Pollution*, 120(1):11–21, 2002.
- [98] Smodiš B. and Parr R.M. Biomonitoring of Air Pollution as exemplified by Recent IAEA Programs. *Biological Trace Element Research*, 71–72(1):257–266, 1999.

- [99] Basile A., Sorbo S., Aprile G., Conte B., and Castaldo-Cobianchi R. Comparison of the Heavy Metal Bioaccumulation Capacity of an Epiphytic Moss and an Epiphytic Lichen. *Environmental Pollution*, 151(2):401–407, 2008.
- [100] Grodzińska K., Frontasyeva M., Szarek-Lukaszewska G., Klich M., Kucharska fabiś A., Gundorina S.F., and Ostrovnaya T.M. Trace Element Contamination in Industrial Regions of Poland studied by Moss Monitoring. *Environmental Monitoring and Assessment*, 87(3):255–270, 2003.
- [101] Steinnes E., Rambæk J.P., and Hanssen J.E. Large Scale Multi-Element Survey of Atmospheric Deposition using Naturally Growing Moss as Biomonitor . *Chemosphere*, 25(5):735–752, 1992.
- [102] Culicov O.A., Mocanu R., Frontasyeva M.V., Yurukova L., and Steinnes E. Active Moss Biomonitoring Applied To An Industrial Site In Romania: Relative Accumulation of 36 Elements in Moss-Bags. *Environmental Monitoring and Assessment*, 108(1–3):229–240, 2005.
- [103] Godinho R.M., Freitas M.C., and Wolterbeek H.T. Assessment of Lichen Vitality during a Transplantation Experiment to a Polluted Site. *Journal of Atmospheric Chemistry*, 49(1–3):355–361, 2004.
- [104] Godinho R.M., Verburg T.G., Freitas M.C., and Wolterbeek H.T. Accumulation of Trace Elements in the Peripheral and Central Parts of two Species of Epiphytic Lichens Transplanted to a Polluted Site in Portugal. *Environmental Pollution*, 157(1):102–109, 2009.
- [105] Saitanis C.J., Frontasyeva M.V., Steinnes E., Palmer M.W., Ostrovnaya T.M., and Gundorina S.F. Spatiotemporal Distribution of Airborne Elements Monitored with the Moss Bags Technique in the Greater Thriasion Plain, Attica, Greece. *Environmental Monitoring and Assessment*, 185(1):955–968, 2013.
- [106] Culicov O.A. and Yurukova L. Comparison of Element Accumulation of Different Moss and Lichen-Bags Exposed in the City of Sofia (Bulgaria). *Journal of Atmospheric Chemistry*, 55(1):1–12, 2006.
- [107] Aničić M., Tomašević M., Tasić M., Rajšić S., Popović A., Frontasyeva M.V., Lierhagen S., and Steinnes E. Monitoring of Trace Element Atmospheric Deposition Using Dry and Wet Moss Bags: accumulation capacity versus exposure time. *Journal of Hazardous Materials*, 171(1–3):182–188, 2009.
- [108] Conti M.E. and Cecchetti G. Biological Monitoring: lichens as bioindicators of air pollution assessment - a review. *Environmental Pollution*, 114(3):471–492, 2001.
- [109] Wolterbeek H.T., Bode P., and Verburg T.G. Assessing the Quality of Biomonitoring via Signal-to-Noise Ratio Analysis. *Science of The Total Environment*, 180(2):107–116, 1996.

- [110] Harmens H. United Nations Economic Commission For Europe Convention On Long-Range Transboundary Air Pollution: monitoring of atmospheric deposition of heavy metals, nitrogen and POPs in Europe using bryophytes. ICP Vegetation Coordination Centre, United Kingdom, 2010.
- [111] Bates A.W. Mineral Nutrition, Substratum Ecology, and Pollution. pages 248–311. Cambridge University Press, 2000.
- [112] Bargagli R., Monaci F., Borghini F., Bravi F., and Agnorelli C. Mosses and Lichens as Biomonitors of Trace Metals: a comparison study on *Hypnum cupressiforme* and *Parmelia caperata* in a former mining district in Italy. *Environmental Pollution*, 116(2):279–287, 2002.
- [113] Krmar M., Wattanavatee K., Radnović D., Slivka J., Bhongsuwan T., Frontasyeva M.V., and Pavlov S.S. Airborne Radionuclides in Mosses Collected at Different Latitudes. *Journal of Environmental Radioactivity*, 117(0):45–48, 2013.
- [114] Harmens H. ICP Vegetation - background. Online, December 2009.
- [115] Samecka-Cymerman A. and Kempers A.J. Differences in Concentrations of Heavy Metals Between Native And Transplanted *Pohlia Nutans* (Hedw.) Lindb.– a case study from a dump exposed to industrial emissions in Poland. *Polish Journal of Environmental Studies*, 16(2):251–258, 2007.
- [116] Saxena D.K., Srivastava K., and Singh S. Biomonitoring of Metal Deposition by using Moss Transplant Method Through *Hypnum Cupressiforme* (Hedw.) in Mussoorie. *Journal of Environmental Biology*, 29(5):683–688, September 2008.
- [117] Stark L. Leptodon. Bryophyte Flora of North America - Provisional Publication (Online), 2000.
- [118] Bourell M. Pterogonium. Bryophyte Flora of North America - Provisional Publication (Online), 2001.
- [119] Boamponsem L. K., Adam J.I., Dampare S.B., Nyarko B.J.B., and Essumang D.K. Assessment of Atmospheric Heavy Metal Deposition in the Tarkwa Gold Mining Area of Ghana using Epiphytic Lichens. *Nuclear Instruments and Methods in Physics Research Section B: Beam Interactions with Materials and Atoms.*, 268(9):1492–1501, 2010.
- [120] Purvis O.W. and Pawlik-Skowrońska B. Chapter 12 - Lichens and Metals. In M. Stratford S. V. Avery and P. Van West, editors, *Stress in Yeast and Filamentous Fungi*, volume 27 of *British Mycological Society Symposia Series*, pages 175–200. Academic Press, 2008.
- [121] Purvis W. Lichens. Natural History Museum, London, 2010.

- [122] Bettinelli M., Perotti M., Spezia S., Baffi C., Beone G.M., Alberici F., Bergonzi S., Bettinelli C., Cantarini P., and Mascetti L. The Role of Analytical Methods for the Determination of Trace Elements in Environmental Biomonitors. *Microchemical Journal*, 73(1–2):131–152, 2002.
- [123] Wolterbeek H.T., Garty J., Reis M.A., and Freitas M.C. Chapter 11–Biomonitoring in use: lichens and metal air pollution. In A. M. Breure, B. A. Markert and H.G. Zechmeister, editors, *Bioindicators and Biomonitors—Principles, Concepts and Applications.*, volume 6 of *Trace Metals and other Contaminants in the Environment.*, pages 377–419. Elsevier, 2003.
- [124] Garty J. Biomonitoring Atmospheric Heavy Metals with Lichens: theory and application. *Critical Reviews in Plant Sciences*, 20(4):309–371, 2001.
- [125] Light K.H. Lichens. American Museum of Science and Energy - Nature Reporters Blog (Online), 2012.
- [126] Budka D., Przybyłowicz W.J., Mesjasz-Przybyłowicz J., and Sawicka-Kapusta K. Elemental Distribution in Lichens Transplanted to Polluted Forest Sites Near Kraków (Poland). *Nuclear Instruments and Methods in Physics Research Section B: Beam Interactions with Materials and Atoms*, 189(1–4):499–505, 2002.
- [127] Budka D., Mesjasz-Przybyłowicz J., and Przybyłowicz W.J. Environmental Pollution Monitoring using Lichens As Bioindicators: a micro-PIXE study. *Radiation Physics and Chemistry*, 71(3–4):783–784, 2004.
- [128] Branquinho C., Catarino F., Brown D.H., Pereira M.J., and Soares A. Improving the use of Lichens as Biomonitors of Atmospheric Metal Pollution. *Science of The Total Environment*, 232(1–2):67–77, 1999.
- [129] South Carolina Department of Natural Resources. Old Man’s Beard. Online [Downloaded - 12/12/2013], 2006.
- [130] Brown R.J.C. and Milton M.J.T. Analytical Techniques for Trace Element Analysis: an overview. *TrAC Trends in Analytical Chemistry*, 24(3):266–274, 2005.
- [131] Frontasyeva M.V. Nuclear and Related Analytical Techniques for Life Sciences. *Ovidius University Annals of Chemistry*, 20(1):11–18, 2009.
- [132] Papaefthymiou H. and Papatheodorou G. A Comparison between INAA and ICP-MS for the Determination of Element Concentrations in Marine Sediments. *Journal of Radioanalytical and Nuclear Chemistry*, 289(3):679–688, 2011.
- [133] Frontasyeva M.V., Nazarov V.M., and Steinnes E. Moss as Monitor of Heavy Metal Deposition: comparison of different multi-element analytical techniques. *Journal of Radioanalytical and Nuclear Chemistry*, 181(2):363–371, 1994.

- [134] Kamitakahara B. Nuclear Analytical Methods. Online [Downloaded - 18/08/2015], 2002.
- [135] Nageswara Rao R. and Kumar Talluri M.V.N. An Overview of Recent Applications of Inductively Coupled Plasma-Mass Spectrometry (ICP-MS) in Determination of Inorganic Impurities in Drugs and Pharmaceuticals. *Journal of Pharmaceutical and Biomedical Analysis*, 43(1):1–13, 2007.
- [136] IAEA. Quality Aspects of Research Reactor Operations for Instrumental Neutron Activation Analysis. Technical Report 1011–4289, International Atomic Energy Agency, Austria, May 2001.
- [137] Alagarsamy R., You C.F., Nath B.N., and Sijin-Kumar A.V. Determination of Rare Earth, Major and Trace Elements in Authigenic Fraction of Andaman Sea (Northeastern Indian Ocean) Sediments by Inductively Coupled Plasma-Mass Spectrometry. *Microchemical Journal*, 94(1):90–97, 2010.
- [138] Freitas M.C., Pacheco A.M.G., Dionísio I., Sarmento S., Baptista M.S., Vasconcelos M.T.S.D., and Cabral J.P. Multianalytical Determination of Trace Elements in Atmospheric Biomonitoring by k_0 -INAA, ICP-MS and AAS. *Nuclear Instruments and Methods in Physics Research Section A: Accelerators, Spectrometers, Detectors and Associated Equipment*, 564(2):733–742, 2006.
- [139] Marqués M.J., Salvador A., Morales-Rubio A.E., and De la Guardia M. Trace Element Determination in Sediments: a comparative study between neutron activation analysis (NAA) and inductively coupled plasma-mass spectrometry (ICP-MS). *Microchemical Journal*, 65(2):177–187, 2000.
- [140] Ellison S.L.R. and Williams A. Quantifying Uncertainty in Analytical Measurement. EURACHEM/CITAC, United Kingdom, 3rd edition edition, 2012.
- [141] IAEA. Quantifying Uncertainty in Nuclear Analytical Measurements. Technical Report IAEA-TECDOC-1401, IAEA, Vienna, July 2004.
- [142] Greenberg R.R., Bode P., and De Nadai-Fernandes E.A. Neutron Activation Analysis: a primary method of measurement. *Spectrochimica Acta Part B: atomic spectroscopy*, 66(3–4):193–241, 2011.
- [143] Google Earth: Software Version 7.1.5.1557.
- [144] Wikipedia. Western Cape. Online [Downloaded - 14/01/2014], December 2013.
- [145] Government of South Africa Department of Communications. About SA. Online, 2014.
- [146] T.A. Hedderson. University of Cape Town, Private Communication (02/April/2013).
- [147] Wikipedia. Huguenot Tunnel. Online [Accessed - 02/04/2013].
- [148] Bullock P.J. Online [Downloaded - 01/04/2013].

- [149] Ananiev V.D., Vinogradov A.V., Dolgikh A.V., and Yu. N. Pepelyshev Yu.N. Physical and Power Start-up of the modernized IBR-2M Research Reactor. In *RRFM 2013 Transactions*, ISBN 978-92-95064-18-8, pages 16–21, Russia, April 2013. European Nuclear Society, European Nuclear Society.
- [150] Frontasyeva M.V., Dmitriev A.Y., and Pavlov S.S. Automation of Reactor Neutron Activation Analysis: contract no. 17363. Delft, The Netherlands, 2012.
- [151] JINR University Centre. Fast Pulsed Reactor IBR-2. Online [Downloaded - 10/02/2014], 2014.
- [152] Frontasyeva M.V. Radioanalytical Investigations at IBR-2 reactor, FLNP, JINR. Pretoria, September 2010. South African Institute of Physics.
- [153] Frontasyeva M.V. and Pavlov S.S. Analytical Investigations at the IBR-2 reactor in Dubna. Online [Downloaded - 03/02/2014], 2000.
- [154] Canberra. Genie 2000 Gamma Analysis Software., October 2013.
- [155] Haigh S. Thorium, LFTR, Future Energy. Online, August 2013.
- [156] Machine-History. Breeder Reactor. Online [Downloaded - 31/07/2014], 2010.
- [157] Luca A., Neacsu B., Antohe A., and Sahagia M. Calibration of the High and Low Resolution Gamma-ray Spectrometers. *Romanian Reports in Physics*, 64(4):968–976, March 2010.
- [158] Osvath I. Basic Hands-on Gamma Calibration for Low Activity Environmental Levels. Technical report, IAEA Environment Laboratories, Austria, 2011.
- [159] Agarwal C., Chaudhury S., Goswami A., and Gathibandhe M. Full Energy Peak Efficiency Calibration of HPGe Detector for Point and Extended Sources using Monte Carlo Code. *Journal of Radioanalytical and Nuclear Chemistry*, 287(3):701–708, 2011.
- [160] Zahn G.S., Genezini F.A., and Morales M. Evaluation of Peak-fitting Software for Gamma Spectrum Analysis. In *2009 International Nuclear Atlantic Conference*, volume 41 of 27, Brazil, 2009. International Atomic Energy Agency.
- [161] Dmitriev A.Y. and Pavlov S.S. Automation of the Quantitative Determination of Elemental Content in Samples Using Neutron Activation Analysis on the IBR 2 Reactor at the Frank Laboratory for Neutron Physics, Joint Institute for Nuclear Research. *Physics of Particles and Nuclei Letters*, 10(1):33–36, 2013.
- [162] Zinicovscaia I. Study of the Interaction of Metals (Hg, Cr, Zn, Ag, Au) with *Arthrobacter* Genera and *Spirulina Platensis*. PhD thesis, Institute of Chemistry of the Academy of Science of Moldova - Joint Institute of Nuclear Research, Dubna, Russia., Chisinau, 2013.

- [163] Canberra. Genie 2000 Spectroscopy Software: customization tools. AREVA Company, USA, 9233653h v3.3 edition, March 2013.
- [164] Canberra. Model S506 Interactive Peak Fit: user's manual. AREVA Company, USA, 9230873e v1.3 edition, April 2003.
- [165] Canberra. Genie 2000 Spectroscopy Software: operations manual. AREVA Company, USA, 9233652h v3.3 edition, April 2003.
- [166] Låg J. and Steinnes E. Regional Distribution of Halogens in Norwegian Forest Soils. *Geoderma*, 16:317–325, 1976.
- [167] Correns C.W. The Geochemistry of the Halogens. *Physics and Chemistry of the Earth.*, 1:18–233, 1956.
- [168] Frontasyeva M.V. and Steinnes E. Marine Gradients of halogens in Moss Studies by Epithermal Neutron Activation Analysis. *Journal of Radioanalytical and Nuclear Chemistry.*, 261(1):101–106, 2004.
- [169] Papastergios G., Filippidis A., Fernandez-Turiel J., Gimeno D., and Sikalidis C. Distribution of Potentially Toxic Elements in Sediments of an Industrialized Coastal Zone of the Northern Aegean Sea. *Environmental Forensics.*, 11:282–292, 2010.
- [170] IAEA. Use of Nuclear Related Analytical Techniques in Studying Human Health Impacts of Toxic Elements Consumed Through Food Stuffs Contaminated by Industrial Activities. Technical Report NAHRES-75, IAEA, Vienna, March 2003.
- [171] Steinnes E. Human Health Problems Related to Trace Element Deficiencies in Soil. In *19th World Congress of Soil Science, Soil Solutions for a Changing World*, Australia, 1–6 August 2010.
- [172] Blett T., Geiser L., Porter E.M., U.S. Department of the Interior, and U.S. Department of Agriculture. Air Pollution-related Lichen Monitoring in National Parks, Forests, and Refuges: Guidelines for Studies Intended for Regulatory and Management Purposes. National Park Service Air Resources Division, United States, 2003.
- [173] Easton R.M. Lichens and Rocks. *Geoscience Canada*, 21(2):59–76, 1995.
- [174] UK Air Pollution Information System. Impacts of Air Pollution on Lichens and Bryophytes (Mosses and Liverworts). Electronic Article [Downloaded - 03/10/2014], 2014.
- [175] Liu X., Sun L., Li D., and Wang Y. Rare Earth Elements in the Ornithogenic Sediments from the Maritime Antarctic: a potential new palaeoecology proxy. *Geochemical Journal*, 45:15–26, 2011.

- [176] Chellam S, Kulkarni P., and Fraser M. Emissions of Organic Compounds and Trace Metals in Fine Particulate Matter from Motor Vehicles: a tunnel study in Houston, Texas. *Air & Waste Management Association.*, 55:60–72, 2005.
- [177] Almeida-Silva M., Canha N., Freitas M.C., Dung H.M., and Dionísio I. Air Pollution at an Urban Traffic Tunnel in Lisbon, Portugal—an INAA Study. *Applied Radiation and Isotopes*, 69(11):1586–1591, 2011.
- [178] Zechmeister H.G., Dullinger S., Hohenwallner D., Riss A., Hanus-Illyar A., and Scharf S. Pilot Study on Road Traffic Emissions (PAHs, Heavy Metals) Measured by Using Mosses in a Tunnel Experiment in Vienna, Austria. *Environmental Science and Pollution Research International*, 13(6):398–405, 2006.
- [179] Kucuksezgin F., Kontas A., Altay O., Uluturhan E., and Darilmaz E. Assessment of Marine Pollution in Izmir Bay: nutrient, heavy metal and total hydrocarbon concentrations. *Environment International*, 32:41–51, 2006.
- [180] Ramessur R.T. Statistical Comparison and Correlation of Zinc and Lead in Estuarine Sediments along the Western Coast of Mauritius. *Environment International*, 30:1039–1044, 2004.
- [181] Grigoriadou A., Schwarzbauer J., and Georgakopoulos A. Molecular Indicators for Pollution Source Identification in Marine and Terrestrial Water of the Industrial Area of Kavala City, North Greece. *Environmental Pollution*, 151:231–242, 2008.
- [182] Grigoriadou A., Schwarzbauer S.J., and Georgakopoulos A. Organic Geochemical Parameters for Estimation of Petrogenic Inputs in the Coastal Area of Kavala City, Greece. *J. Soils Sediments*, 8:253–262, 2008.
- [183] Barandovski L., Trajče S., Šajn R., Frontasyeva M.V., and Bačeva K. Air Pollution Study in Macedonia Using Moss Biomonitoring Technique, ICP-AES and AAS. *Macedonian Journal of Chemistry and Chemical Engineering*, 32(1):89–107, 2013.
- [184] Aničić M., Tasić M., Frontasyeva M.V., Tomašević M., Rajšić S., Mijić Z., and Popović A. Active moss biomonitoring of trace elements with *Sphagnum girgensohnii* moss bags in relation to atmospheric bulk deposition in Belgrade, Serbia. *Environmental Pollution*, 157(2):673 – 679, 2009.
- [185] Botha R. and Jili T., editors. Proceedings of SAIP2013: the 58th annual conference of the South African Institute of Physics, number 978-0-620-62819-8, Richards Bay, July 2013. SAIP.
- [186] Vuković G., Aničić Urošević M., Tomašević M., Samson R., and Popović A. Biomagnetic Monitoring of Urban Air Pollution Using Moss Bags (*Sphagnum girgensohnii*). *Ecological Indicators*, 52:40–47, 2015.

- [187] Aničić M., Tasić M., Frontasyeva M.V., Tomašević M., Rajšić S., Strelkova L.P., and Steinnes E. Active Moss Biomonitoring of Atmospheric Trace Element Deposition in Belgrade Urban Area using ENAA and AAS. In *AIP Conference Proceedings*, volume 958, pages 222–223, Czech Republic, 2007. Association of Independent Publishers.
- [188] Aničić M., Spasić T., Tomašević M., Rajšić S., and Tasić M. Trace Elements Accumulation and Temporal Trends in Leaves of Urban Deciduous Trees (*Aesculus Hippocastanum* and *Tilia* spp.). *Ecological Indicators*, 11(3):824–830, 2011.
- [189] F.A.Y. Gailey and O. Ll. Lloyd. Methodological Investigations into Low Technology Monitoring of Atmospheric Metal Pollution: Part 2 - the effects of length of exposure on metal concentrations. *Environmental Pollution Series B, Chemical and Physical*, 12(1):61–74, 1986.
- [190] Balabanova B., Stafilov T., and Bačeva K. Bioavailability and Bioaccumulation Characterization of Essential and Heavy Metals Contents in *R. acetosa*, *S. oleracea* and *U. dioica* from Copper Polluted and Referent Areas. *Journal of Environmental Health Science and Engineering*, 13(1):1–22, 2015.
- [191] Bačeva K., Stafilov T., and Matevski V. Distribution and mobility of toxic metals in *Thymus alsarensis* Ronniger in Allchar As-Sb-Tl mine, Republic of Macedonia. *Plant Biosystems - An International Journal Dealing with all Aspects of Plant Biology*, pages 1–10, 2014.